THE UNIVERSITY OF HULL

Aspects of Automation in the Shoe Industry

being a Thesis submitted for

Doctor of Philosophy

in the University of Hull

by

Frederick Mark Hudman, B. Eng (Hons.)

March 1997

Contents.

Appendices

Figures.

Chapter 1

Chapter 2

Chapter 3

Chapter 4

Chapter 5

Chapter 6

Plates.

Abstract.

The shoe manufacturing industry has undergone a revolution during the last 50 years, due to the introduction of task specific machinery. Great technological strides have been made in the areas of shoe manufacture prior to actual component assembly. Computer systems are now becoming the norm for the design of shoes for today's market place. Technological innovations have also started to be applied in the assembly and construction processes of modern shoes. Computer controlled cutting machines calculate the optimum usage of leather from any given hide, new machines allow decorative stitch patterns to be associated with a given shape and size of component and automatically stitched on to the presented workpiece. However the majority of assembly operations have remained predominantly manual with technology playing a secondary role to the human operator due to complexities either in manipulation, control or sensing. In these machines electronic and mechanical innovations have been used to add new features to often simple machines and in some cases to simplify some of the more complex operations, thus increasing productivity but reducing the required dexterity and knowledge of an operator. Modern preferences in industry are to utilise fully automated machines, that are as operator independent as possible, thus improving quality, consistency and production speed whilst at the same time reducing production costs.

Due to the nature of the shoe manufacturing industry and the complex operations that have to be performed in order to construct a shoe, machinery manufacturers who have ventured into this field of automation have generally struggled to gain acceptance

from the shoe makers as the machinery is generally complex and slow in operation. This together with the fact that a large proportion of the world's main footwear production is centred in the far east, with their correspondingly low labour costs, has held back the automation of the shoe manufacturing industry.

This thesis examines a selection of operations encountered in the construction of a typical shoe. These include operations for processing single flat component parts as well as more complex three-dimensional operations encountered when lasting and soling a shoe. The aim of the research was to develop an understanding of processes encountered in specific areas within the shoe manufacturing industry in order to identify areas where further advances in automation could be achieved. This understanding has been applied to produce proposals and in some cases hardware, to allow for the development of working systems.

Acknowledgements

I would like to take this opportunity to recognise the considerable support offered by a number of individuals over the period for which this research has extended.

To Mr. D.C. Reedman who instigated the original research contract at Hull University and whose boundless enthusiasm and support has resulted in a number of successes to emerge from this research in the form of patents and new contracts for further research.

To Mr. D.L. Evans and Mr. M.Q. Blatherwick of B.U.S.M lasting department for their "vision" of future automated shoe machinery and for their understanding during the period in which this thesis was written.

Recognition must be paid to Prof. G.E. Taylor formerly of Hull, and now of Leeds Metropolitan University and Prof. P.M. Taylor of Hull University for their guidance both during the period of the research and in the compilation of this thesis.

Thanks go to Mr. D. Wildbore for his hardworking contribution in the area of materials handling whilst working on a final year degree project and to Mr. J. Hodgson and Mr. D. Joyce of Hull University's mechanical workshop whose skill was able to turn ideas into working realities.

Finally, I must thank my wife who offered support and understanding during the traumatic times experienced during the writing of this thesis.

Mark Hudman

Abbreviations.

2-D	Two dimensional.
2.5-D	Parts that have significant variations in thickness, but that can still be treated as flat.
3-D	Three dimensional.
ASCII	American standard code for information interchange.
B.U.S.M	British United Shoe Machinery Ltd.
CAD	Computer aided design.
CAM	Computer aided manufacture.
CCD	Charge Coupled Device.
DSP	Digital signal processing.
EPDM	Ethylene-Propylene.
LED	Light Emitting Diode.
LSH	Acronym for a particular class of lasting machine.
LSI	Large scale integration.
LTL	Acronym for a particular class of lasting machine.
M.P.C.S	Micro-Processor Controlled Stitching.
PVC	Poly vinyl chloride.
PCD	Pitch circle diameter.
RAM	Random access (read/write) memory.
S.E.M.	Scanning electron microscope.
TSM320C30	Texas Instruments C30 digital signal processor.
TTL	Transistor-transistor logic.
VRAM	Video RAM.
Z8000	16-bit microprocessor manufactured by Zilog.

Chapter 1

Introduction

1.0 Introduction.

As the shoe making process is not generally understood and consists of numerous operations. This chapter begins with a brief description of the practices and terminology used within the industry. The chapter concludes with a resume of the thesis history and its significance within a larger area of ongoing research.

1.1 The shoe making process.

The shoe making process can be subdivided into four distinct stages from the point where the hide has been prepared and tanned. However the operations that can take place at any stage are numerous and those that are performed on any given shoe will vary greatly from style to style. Some shoes are complex in construction, being made up of a considerable number of components, Figure 1.1, others such as a lady's court shoe are comparatively simple and require fewer operations. The following is intended to give the reader an insight into the main operations performed in the construction of a typical shoe. It is in no way intended to offer a comprehensive guide to shoe making. Figure 1.2 shows a summary of the operations performed during shoe making.

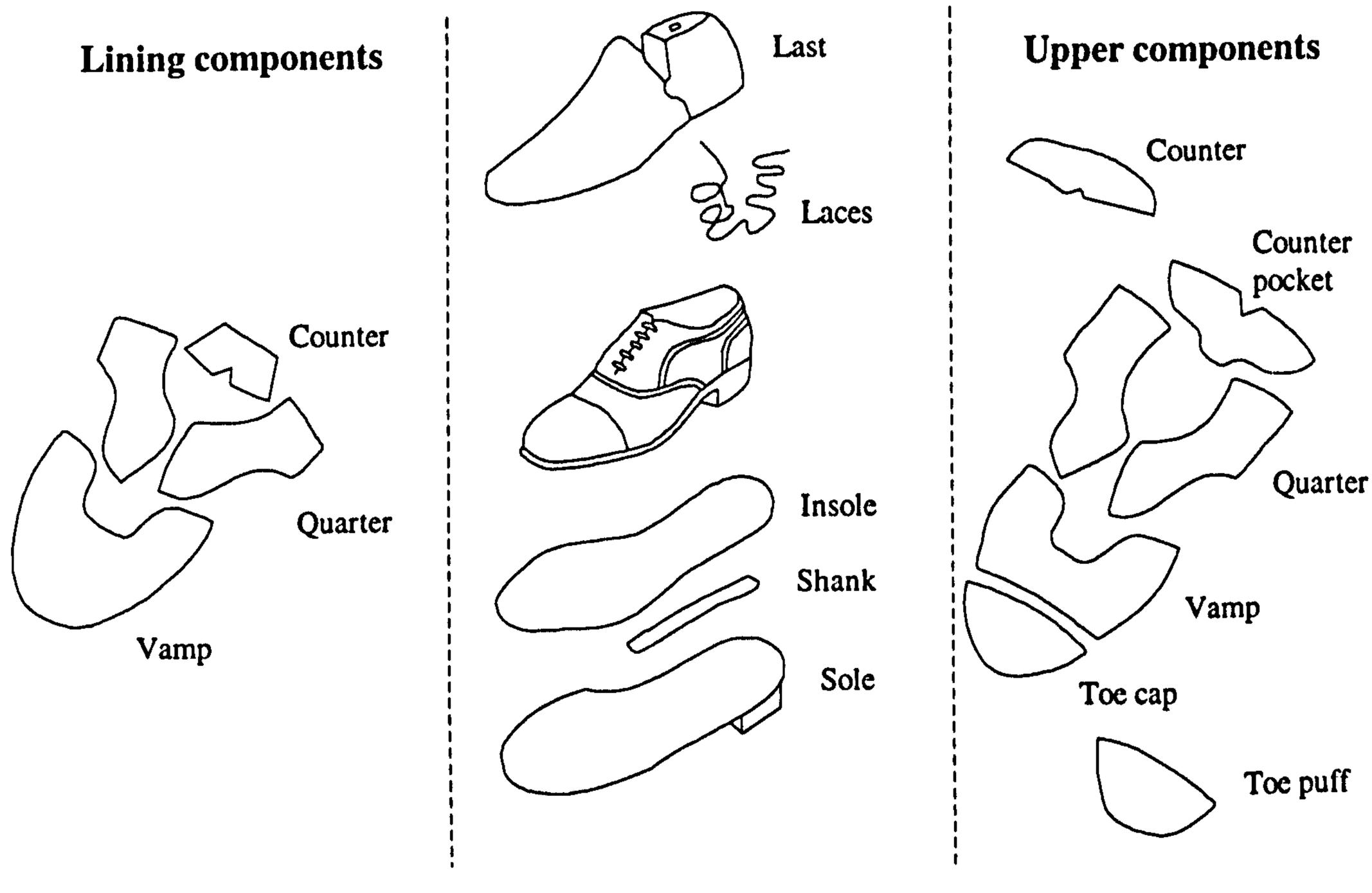

Figure 1.1 Component parts that can be found in the construction of a typical shoe.

'Clicking'

:- Component parts are prepared

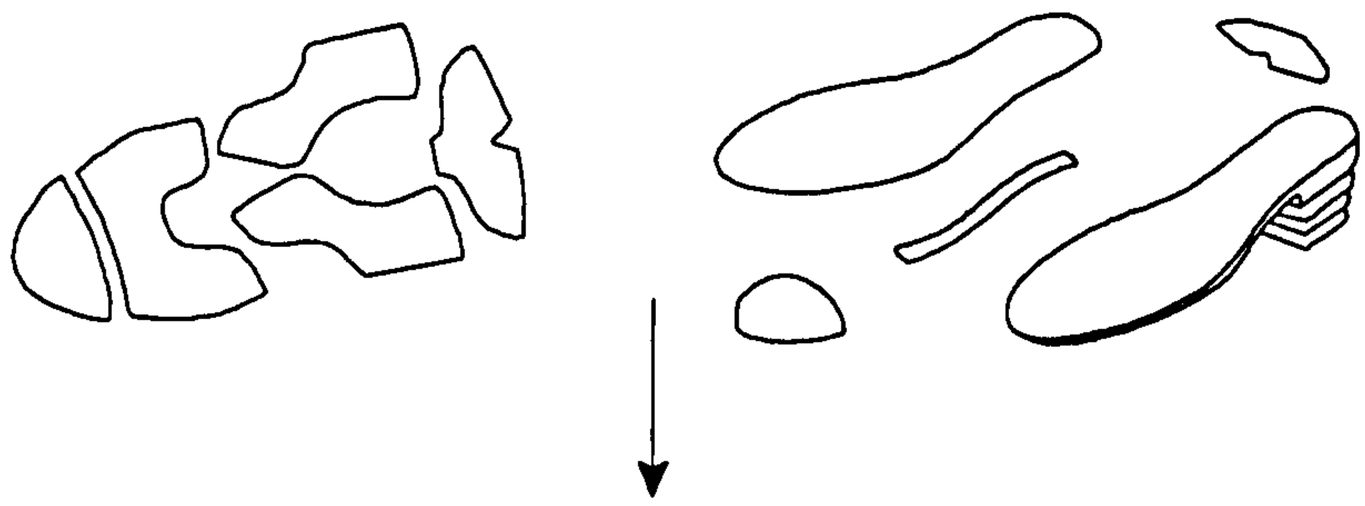

'Preparation'

:- Application of stitch marking
Parts are skived
Decorative stitching

'Closing'

:- Components stitched together
Linings and stiffeners are sewn in.
Upper is closed resulting in a 3-D part.

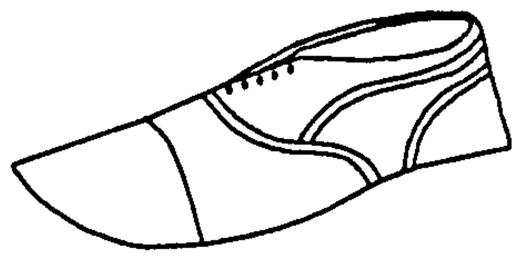

'Making'

:- Upper is Lasted, Roughed and soled.

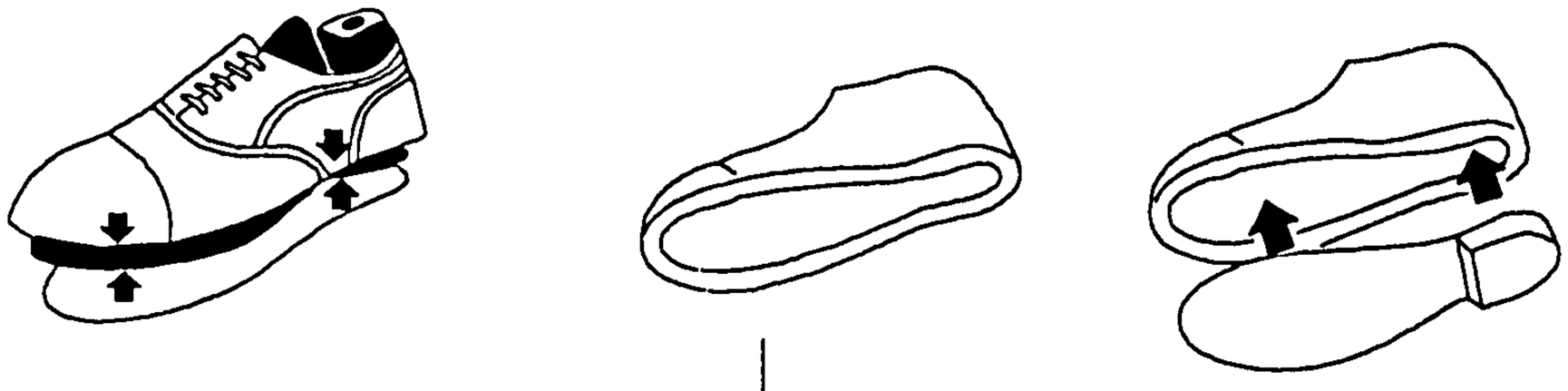

'Finishing'

:- Polishing and inspection.

Figure 1.2 Flow chart summary of the shoe making process.

1.1.1 'Clicking'

The first operations in shoe making take place in the 'Clicking Room'. Here the individual shoe components are cut from the basic materials that will make up the shoe. Traditionally this was performed manually by cutting around the edge of a template with a scalpel. Although there are now some automated systems that implement high pressure water cutting methods, these are expensive and limited in the materials they can cut. Consequently the majority of component cutting is now achieved by the use of pre-formed dice. Each die is made from a steel strip that has a ground, hardened edge and has been formed in to the shape of the shoe component required. Support plates, or cross-members are then welded into place resulting in a strong, sharp device capable of cutting cleanly through the materials. The material is laid out on the flat bed of a high pressure press, the die is placed onto its surface and the press activated, forcing the knife through the material. For man-made materials often multiple thickness can be cut in one stroke without any degradation in component quality. In addition to cutting the components from the material, holes can be punched to assist in their alignment during further processes, or simply to give a decorative appearance. For synthetic materials the cutting pattern can be arranged in such a manner as to optimise the material usage by ensuring the shapes to be punched are arranged so that they inter-lock. For hides the 'clickers' need to be very skilled in order to maintain the quality of the leather from which individual parts of the shoe are cut. The best parts of the hide, around the butt region, are generally reserved for the forepart of the shoe, whilst less critical parts can be cut from the poorer quality leather at the neck and belly, Figure 1.3.

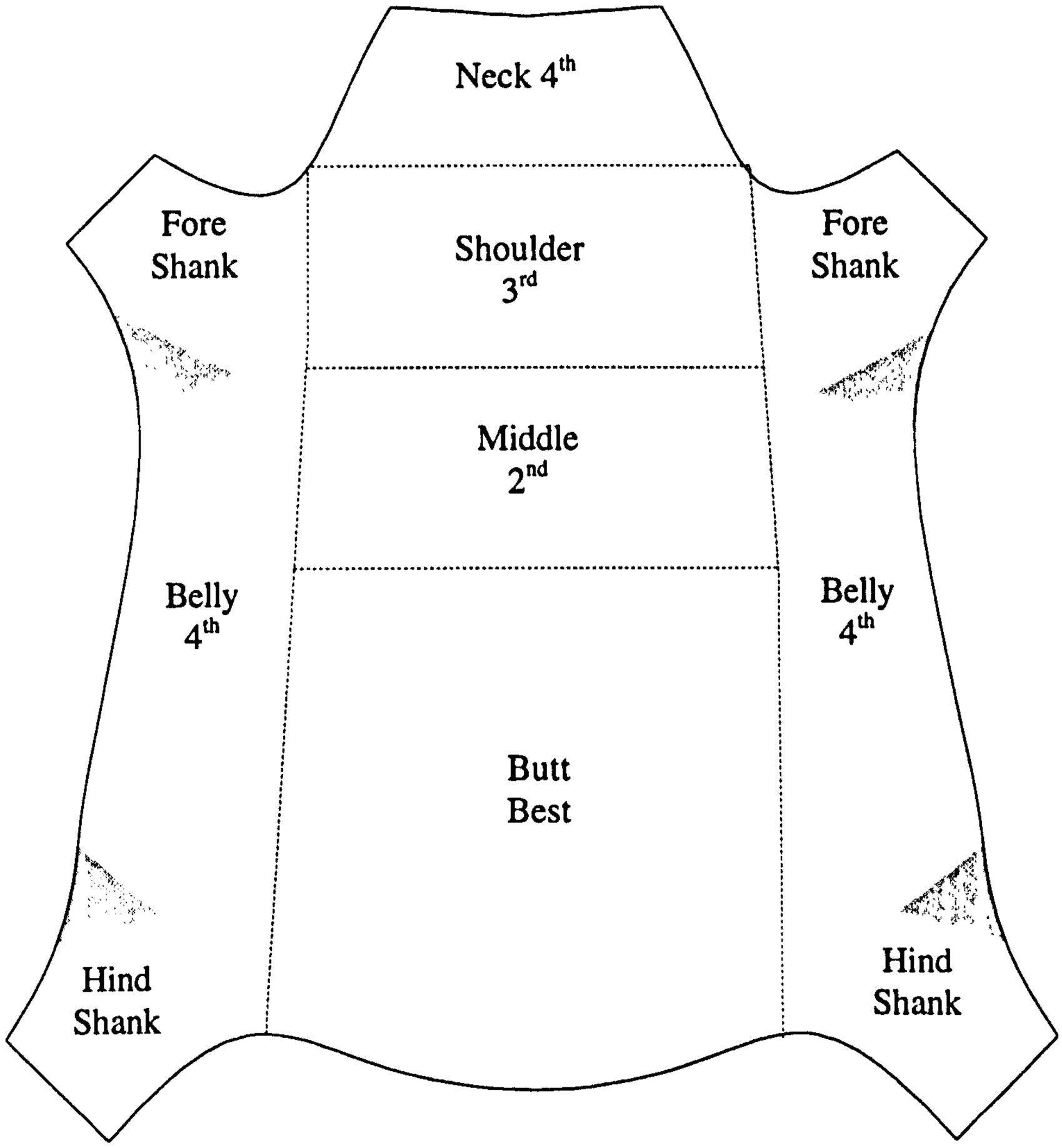

Figure 1.3 Schematic showing the variation in leather quality across a typical hide

1.1.2 'Preparation'

After 'Clicking' comes preparation, this includes such operations as marking and skiving. Marking is performed for a variety of reasons which play an important role in ensuring the quality of the final shoe. Parts may be temporarily marked to indicate stitching lines, alignment or ornamentation. Additional permanent markings are made to convey size and style. Skiving is the removal of a wedge of leather from the flesh, nap, side of a leather component either by a band-knife or a rotating cutter. This is generally performed for two reasons. The 'underlay skive' is performed so as to remove step edges resulting on the inside of the upper after closing. An example being on the tongue where a ridge would make the final shoe uncomfortable to wear. The second type of skive is the 'turning-in skive', here the edge of the leather is rolled over and glued in place, after skiving, by a subsequent operation called folding.

This type of skive is implemented generally around the top-line of the upper as it allows for the fixing of reinforcing tape whilst resulting in a pleasant and smooth edge not much broader than the thickness of the leather itself. In addition, other operations that are based on 2-D workpieces can be performed. These include joining and decorative stitching, which is analogous to embroidery, although in certain factories these may be done in the 'closing room'

1.1.3 'Closing'

In the 'closing room', the flat component parts that will make up the shoe upper are taken and sewn together in such a manner as to produce a three-dimensional part called the 'Closed Upper'. Closing also covers the stitching and attaching of the shoe lining, which can consist of facings, stiffeners, backstraps and other components. Before final closing the shoe upper is essentially flat and as such is still relatively simple to manipulate. This then allows for operations such as top-line stitching to be carried out with comparative ease thus finishing off the earlier turned-in skive. This operation has had to wait until this point as the complete top-line encompasses several components which would not have been assembled together until closing.

The closing operation itself is generally performed by sewing along the line of disparate curves at the heel[15]. The main example of this is the closing of the heel which transforms the flat upper into a 3-D workpiece ready for lasting. This can either be performed by laying the two parts one on top of the other, grain sides together, and sewing along the curve in the flat, resulting in an tucked join once the closed upper has been turned right side out, or by using a machine similar to the Pfaff 418-49[13], where the sewing head zig-zags from one workpiece to another forming a 'butt' join.

1.1.4 'Making'

The final process in the construction of a shoe is that of 'making', this is where the closed upper is lasted and soled. Lasting is the complex task of deforming the closed upper around a former called a last and bonding it to an insole board. Lasting consists of

three operations, toe, side and seat and often includes tacking. In toe lasting the last which has the insole board attached to its base and the shoe upper on it is loaded into a machine by locating the margin around the perimeter of the upper into a series of pincers, typically seven or nine, which are then gripped. The leather is then tensioned by lifting the last against the pull of the pincers by a pneumatic ram called a last post. Additional support is then provided by another pneumatic ram which presses against the heel of the shoe. At this point an operator can adjust the position of the upper on the last by altering the height of the pincers by means of a series of levers. Once satisfied with the orientation of the upper, adhesive is applied to the insole board and a series of plates wipe the leather of the upper over the adhesive. In order to achieve this the pincers are released and retracted from the plane of the wipers in order to prevent any damage occurring to them. Once this process, known as over-wiping, is achieved, a high pressure is applied to the top of the last, forcing it down onto the wiper plates and thus ensuring a good bond between the material of the upper and the insole board. The seat and side lasting is achieved in a similar way, with adhesive being applied to the insole board and the upper material being rolled or wiped over the adhesive in order to form the bond. The shoe then passes on to a heat setter to set the upper material to the last form. Other operations that are common within lasting include tacking. This is where a series of tacks are driven through the highly tensioned upper into the base of the shoe for added strength. This has until recently been a subsidiary operation to side and seat lasting. A new family of B.U.S.M. machines implement individual pneumatic rams which are capable of driving in only a few pins each whilst performing the lasting operation. The length of the tack is crucial. The ideal tack will pass through both the upper and the

insole board and the tip of the tack upon hitting the metal underside of the last will bend over locking the tack tightly into place. If the tack is too short it will fail to reach the last and thus will not become locked in place. In certain circumstances, after some wear, the tacks can work loose and start to penetrate through the shoe inner lining and into the wearer's foot. If the tack is too long it will not bend correctly resulting in a loose tack.

Once the upper has been fully lasted the sole has to be attached. Before this can be achieved the bottom of the lasted upper has to be 'scoured' in order to flatten any pleats that have been introduced by the folding of the upper material around the curved profile of the last. In order to achieve a good bond surface for the cement the bottom is then 'roughed' by using abrasive wheels generally in the form of wire brushes rotating at high speeds. These brushes, when brought into contact, grind away any protrusions and the surface of the leather in order to produce a relatively flat surface for the sole to be bonded to. Adhesive is then applied to the base of the shoe and to the sole. This adhesive is generally of a reactivatable form and is often applied to the soles sometime in advance of actual bonding. The actual attaching of the sole involves a process known as 'spotting'. Once the adhesive has been reactivated the sole is presented to the bottom firstly at the toe and then at the heel as these are the most important areas from a cosmetic viewpoint. The shoe is then placed into a press which forces the sole onto the bottom of the shoe under high pressure. Finally the shoe is passed through a chiller in order to ensure a good bond.

1.1.5 'Finishing'

Before the shoes are packaged and sent to the retailers they are 'finished'. This process includes the removal of any loose threads that may have resulted from earlier stitching processes and the polishing of the shoes. The shoes are then inspected to ensure they are of sufficient quality and presentation.

1.2 Process automation.

Automation within the shoe manufacturing industry has been ongoing since the birth of the sewing machine itself. Indeed the introduction of the sewing machine greatly simplified the stitching process, but more importantly vastly increased the speed at which shoes could be made. This meant that the mass production of shoes, as with other sewn articles became a reality. The principle of the sewing machine has changed very little since its early days, except for the addition of motors to provide a constant and effortless source of needle actuation. In more recent years a major development in automated stitching came with the introduction of the M.P.C.S. [14,16], (Micro-Processor Controlled Stitching). The M.P.C.S. is a decorative stitching and joining mechanism for flat workpieces. It utilises a series of pallets to hold the workpieces whilst leaving the area to be stitched exposed. The pallets clamp the workpieces between them with workpiece alignment ensured by guide pins passing through punched holes. Stitching is accurate to within 0.06mm (0.002"), regardless of stitching speed. This machine can not be said to be fully automated as an operator is still required to both load and unload the palettes which hold the workpieces. The majority of machinery now taking its place on the shop floors

of the shoemakers factories, although often complex, can rarely be described as automated. Both the International Shoe Machine Corporation and B.U.S.M, for example, are major suppliers of shoe making machinery, but by far the majority of their machines still require an operator to load, manipulate and/or extract the part(s) from them. It is due to this factor that the 'Autoscan', a fully automated decorative stitching machine, is such an advance in automated shoe machinery. Here the workpieces are fed into the machine, via an automated device such as a conveyer belt, at any orientation. The component is then passed over a back-lit light source which is viewed by the line-scan camera system building up the shape of the part in a raster manner. The extracted shape is then compared against those in a data base, regardless of orientation. If the workpiece corresponds to a known part the associated stitch pattern is rotated in order to correctly align with the presented workpiece. The machine then has the ability to perform the required operations to produce the required stitch pattern by manipulating the workpiece with the rollers and base table under the needle. As a result the Autoscan, which, once it has been taught a shape and its associated stitch pattern, either by an operator or by down loading the information directly from a CAD package such as CRISPIN[14], can be regarded as fully automated.

Both Pfaff and B.U.S.M[31] have investigated the feasibility of producing a vectored stitching device, Figure 1.4. This is where the stitching head and bobbin are rotated to ensure a constant direction of stitching. This is desired to ensure a high quality of lock-stitch and prevent the bobbin mechanism introducing an extra twist in the upper thread if the material is fed in the opposite direction. This extra twist, called 'half-hitching', results in a visually unacceptable stitch.

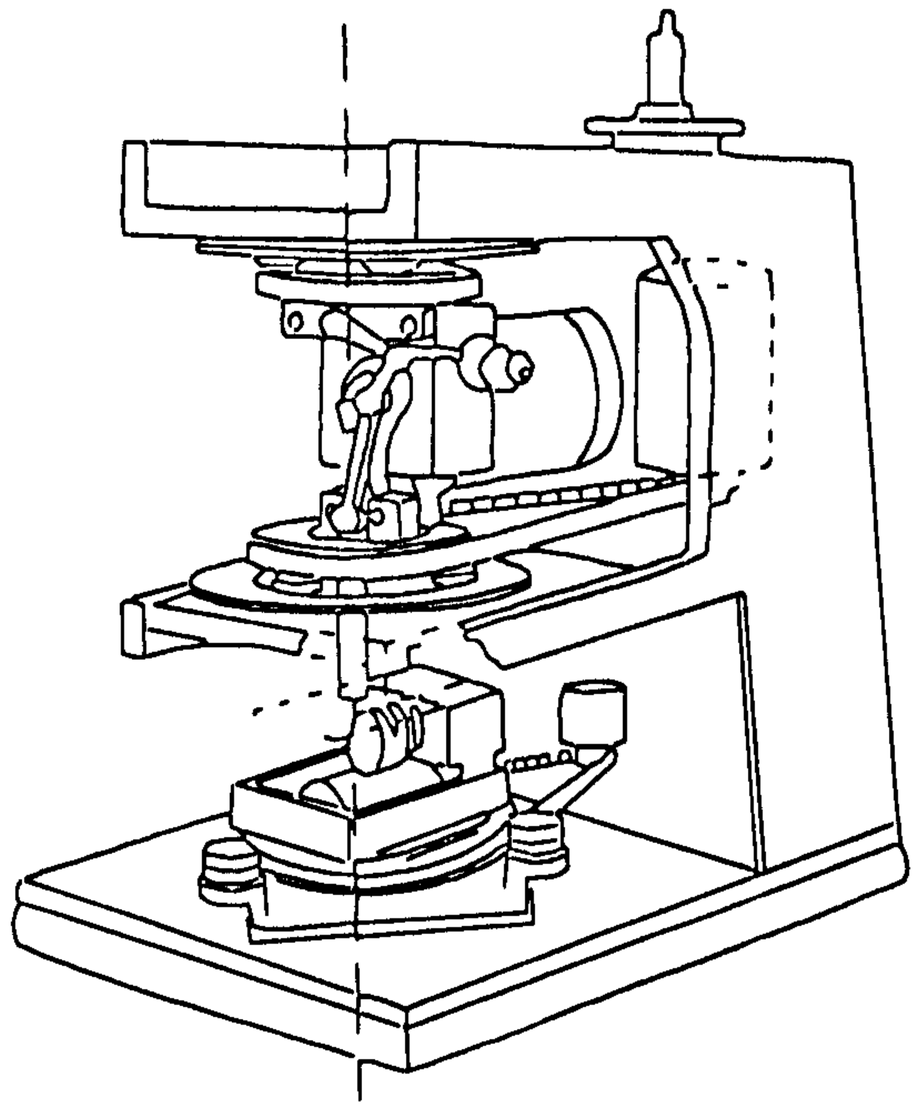

Figure 1.4 Schematic drawing of the B.U.S.M Vector stitcher.

In manual stitching operations the operator turns the workpiece as a curve or corner is encountered in order to ensure the material is correctly fed through the feed mechanism. However, in automated stitching such as the M.P.C.S. the palette is moved in pre-taught X and Y movements only, with no rotation of the workpiece, as a consequence half-hitching occurs when stitching at certain angles.

Early attempts employed a mechanical linkage to maintain the essential link between the needle mechanism and the bobbin but these were found to be complex and failed to produce commercial machines. In an attempt to overcome this problem B.U.S.M began a research programme jointly between the Universities of Hull and Durham to develop a vector stitcher where the bobbin and needle mechanism were individually driven by stepper motors under computer control[17]. To date this machine has not been adopted for the commercial market, but shows potential for the future.

Automation in the 'clicking room' has been achieved to a great extent with the implementation of computers, which are used to calculate cut-out orientations and for the control of punching machines. High powered computer systems are implemented throughout the industry by shoe designers to allow for ideas to be quickly transferred into 3-D computer models. These models can then be adjusted to cater for variations in style and size at a touch of a button. Once the design is complete the computer systems are able to generate information required to produce lasts, knives and the stitch patterns required to construct the shoe. Engineers at B.U.S.M have developed a computer aided design suite called CRISPIN which has the capability of producing a complete CAD-CAM system when coupled with semi-automated machinery such as the M.P.C.S.

It is in the areas of preparation, closing and finishing where automation can potentially provide the largest rewards. However these are also the areas where the greatest complications lie, the majority of parts during these stages are joined and/or in 3-D, as a consequence automation in these areas has been slow to develop. Developments have been made in the areas of stitch marking, electronic pulling, lasting, roughing, cementing, and automated stitching, however few have made it through to the market place due to their complexity and cost.

1.2.1 Vision systems for automation

A large number of automated machines have been developed for general purpose stitching. The majority of these operate in an open loop manner, once the part has been loaded into the machine. These typically are used where the edges of 2-D components

are to be stitched[33]. However a number of 3-D handling devices[34,35] have also been attempted over the years, but, due to their inherent complexity and slow operating speeds, these have failed to become commercial. Some effort has been made to close the loop on such machines and enable them to follow edges of flat parts and 3-D parts in an automated manner by implementing simple vision, (optical) techniques. These include the implementation of an LED and receiver to detect the edge of a workpiece[36] or, more recently, a low resolution line-scan camera and computer control[1].

Vision systems are generally expensive and require large amounts of computer processing power if the images are to be processed at speeds sufficient to be of practical value. The types of camera that can be used vary greatly depending on the function that they are being asked to perform, from the relatively simple charged coupled device (CCD), line-scan type to the more sophisticated high-resolution colour area cameras. Camera technology is generally not a problem as there is an extensive range to choose from. Problems are more likely to arise in dealing with the image once it has been captured and in the resources required in extracting as much information as possible within acceptable time scales. To this end a whole specialist area has developed, that of image processing.

Techniques have been developed which achieve edge detection, image enhancement[8,10], line thinning[11], shape recognition, and many more. Which techniques are implemented depends, like the use of lighting and camera type, on the specific aspects under investigation. This then has a tendency to lead to vary task specific systems[3,5,6,12].

With the introduction of automation into the shoe industry, a number of specific areas have been identified where the implementation of vision systems could prove beneficial. One such area that has been exploited is that of last digitisation. When a new shoe design is to be designed the working surface, (last), must be described within the CAD package being implemented. As it has proved difficult to create a last directly on CAD the lasts are generally hand made in the first instance and their topology then converted into CAD data. To this end a number of mechanisms have been developed to perform this digitisation process, generally through laser triangulation. This process allows existing lasts to be recreated accurately within the environment of a 3-D CAD package. Example manufacturers of such scanning systems include CY LAN 3-D[28] and Romans CAD[29]. Plate 1, shows the B.U.S.M last digitiser[14]. In this system two line-scan cameras are used to detect the apparent horizontal movement of a laser spot as the last is rotated through 360°. By altering the position of the last in the Z axis and repeating the procedure a 3-D representation of the last is obtained. Two cameras have to be used in order to reduce the risk of occlusion by protuberances on the last.

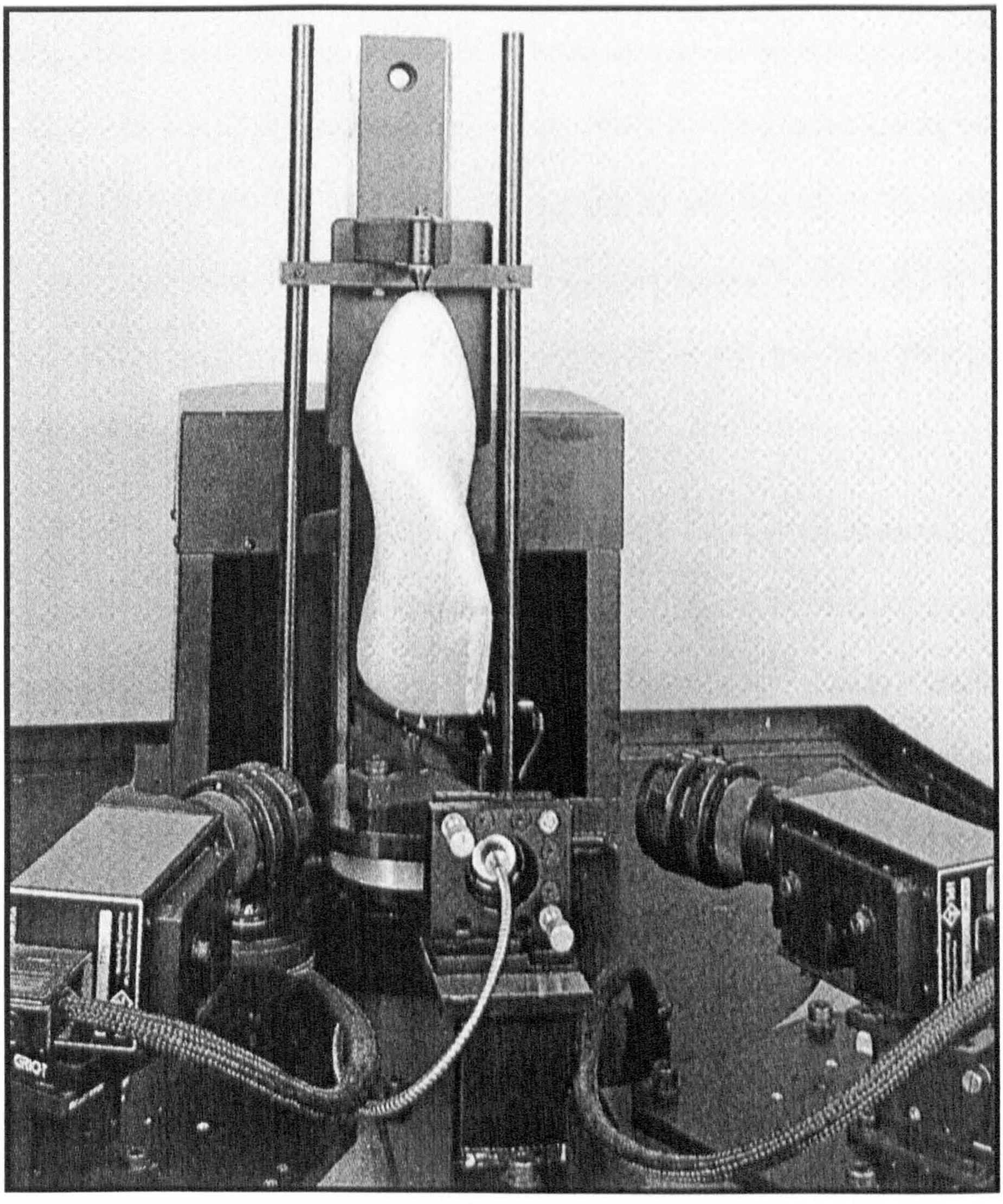

Plate 1. B.U.S.M last digitiser.

Camera systems have been used to monitor for missed stitches[6], inspect surface texture[12], or more commonly to determine the shape and orientation of a presented workpiece. Often in order to enhance the information that can be obtained by a camera structured lighting is used to illuminate the scene. The term 'structured lighting' covers a wide range of possible mechanisms, from daylight to infrared lasers or even more complicated mechanisms like those of colour fringe projection[5]. The type of lighting used depends on the characteristics of the subject to be viewed and what properties are to be observed.

A number of mechanisms have been investigated over the years for the purpose of edge following, all based on the same basic principle. If there is an edge to be followed as opposed to simply a line, there must be some physical characteristics that define the edge, generally this is a change in surface contour. The simplest mechanism for edge following is where the edge of a single part is to be followed, this can be achieved by using back lighting and a line-scan camera, the edge being defined by the point at which a light/dark transition occurs[1]. Most edges to be followed however, can be classed as internal, in that they lie within the body of a larger part and not at its perimeter. It is here where edge characteristics can be utilised to define an edge. Most systems for following internal edges use an angled light source behind the edge so that a shadow is produced which can be detected due to a light/dark(shadow)/light transition.

The B.U.S.M. line-scan system[14,37] for workpiece recognition has been implemented on a number of automated systems, however they are not alone in recognising the importance of vision in shoe manufacture. Orisol[16,32] of Israel, have

constructed a machine for the automatic sewing of 2-D parts by performing on-line vision analysis. The parts are held in a pallet during stitching, with the vision system only providing minor corrections to a previously taught stitch pattern. The system employs four light sources and twin area cameras so as to effectively see around the needle. By illuminating the light source that lies behind the edge, a shadow is produced which the cameras then detects. The images are processed and the information required to define the edge extracted. Torielli of Italy exhibited a vision controlled toe lasting machine at the SIMAC shoe fair, (Italy), in 1992. On this machine a CCD camera was used to look for a contrast change between the shoe upper and the last[30]. The contrast was created by high intensity light sources and selected uppers and lasts. Once the neckline of the upper was identified using image processing techniques, the computer issued commands to a series of actuators in order to correctly align the topline to a previously taught model. Due to the limitation of having to be able to see the last and the requirement that the last must have a significant contrast to the colour of the upper, only a small range of shoes could be successfully lasted.

1.3 Project background and historical development

The British United Shoe Machinery, the British subsidiary of the multi-national USM Texon, have been investigating automating aspects of shoe making machinery in conjunction with an expanding number of Universities for a number of years. B.U.S.M. started work in 1977 with a development project headed by Dr L. Norton-Wayne[21] at City University. This eventually led to a line-scan camera system for the recognition of flat components capable of pin pointing the edge of a scanned part to a precision of 125

microns. By 1982 the system was implemented on a PDP11 processor and initially took in the order of 20 minutes to produce the required data. By 1985 the processor had been exchanged for multiple Z8002 processors and was now capable of performing shape recognition within 2 seconds. It was at this time that research began at the Universities of Hull and Durham which would make use of this technology. Having achieved the ability to recognise the shape and orientation of a workpiece it became possible to automate a number of operations which are performed on flat shoe components.

At Durham the research was primarily concerned with operations on single flat components with the main research activities concentrating on stitch marking[22], and skiving[23], (Section 1.1.2). The work at Hull concentrated on automating stitching processes for both 2-D and 3-D workpieces as well as the construction of joined, (compound), components. Early work, E.Adams[2], looked at the construction of compound shoe components from several flat parts. This work combined the previously developed image recognition system and a dynamic store capable of holding all the component parts required for shoe assembly. Parts were retrieved from the dynamic store via a gantry and vacuum gripper. The final compound component was constructed from a number of flat components with orientation being ensured by repositioning the construction area in X, Y and θ. Each part would have been treated with an adhesive in order to produce a temporary join, resulting in a two-dimensional compound part which could be regarded as a single component during subsequent manual or automated operations. The primary area of research at Hull however, was concerned with generic research into the handling of flat leather shoe components for automated decorative stitching[1]. Building on work previously performed by B.U.S.M.[17] a machine capable of

stitching a taught pattern onto a flat leather shoe components was developed. The system scans the workpiece utilising the line-scan camera system previously developed by B.U.S.M and Dr L. Norton-Wayne in order to determine both the parts shape and orientation. The stitch pattern data is rotated to match that of the presented workpiece which is then guided about the stitching head, using rectangular positioning. The workpiece handling mechanism comprised a set of rollers either side of the needle, both above and below the workpiece, resulting in the workpiece being sandwiched between pairs of rollers. The rotation of the rollers provides movement in one axis, Y, with the motion of the roller table perpendicular to the roller rotation providing the X axis. Plate 2 shows the original Hull University decorative stitching mechanism that later evolved into the 'Autoscan'.

In addition to the work on two-dimensional workpieces an investigation was made into the handling of simple three-dimensional workpieces[1]. Both of the above will be discussed in greater detail in subsequent chapters as further research has been undertaken in these areas.

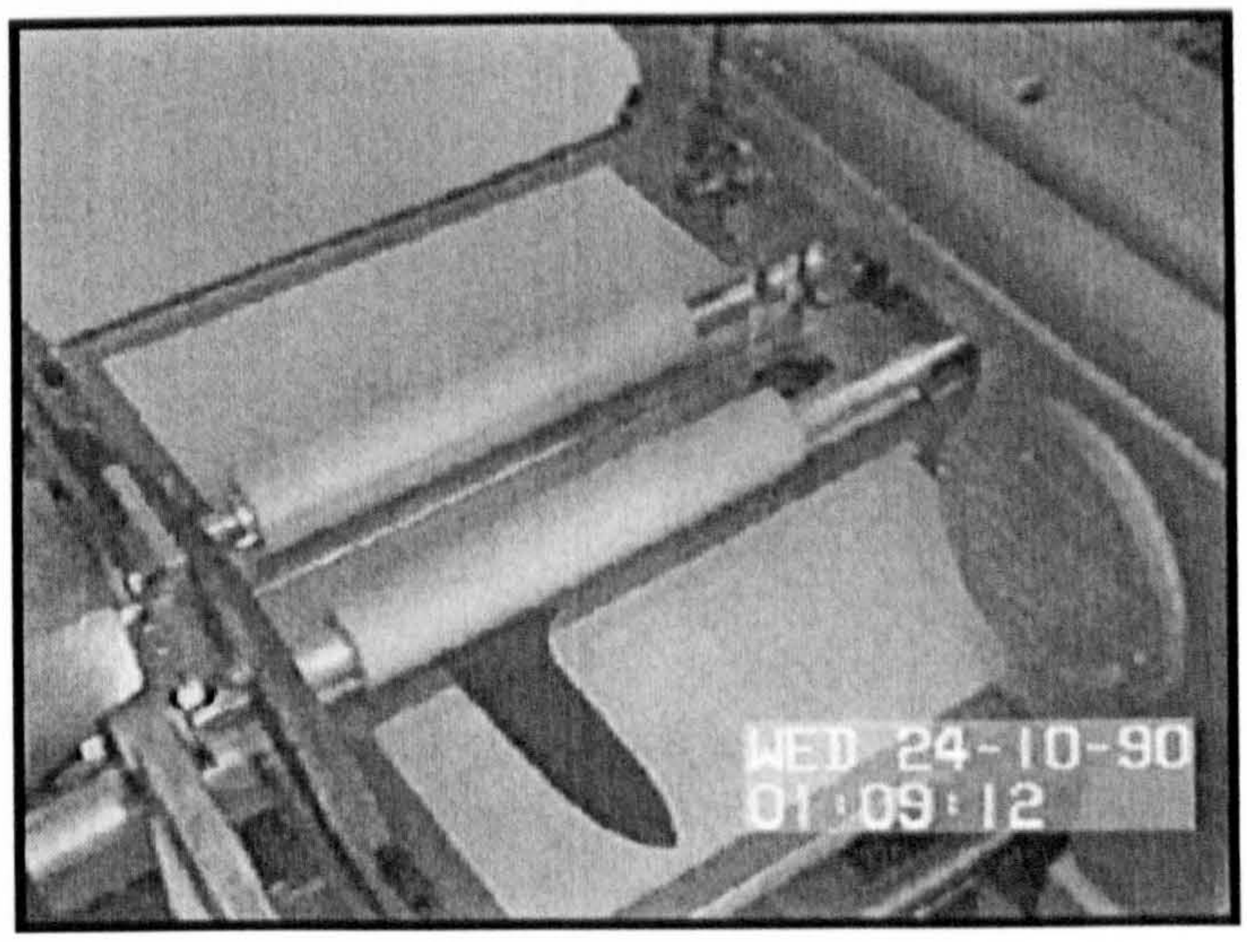

Plate 2. Prototype decorative stitching machine (Hull University 1990).

1.4 The research

The research described in this thesis formed part of a series of projects carried out jointly between B.U.S.M and the University of Hull. This work concentrated primarily on the automation of certain closing room operations beginning with decorative stitching and moving through flat constructional stitching to three dimensional construction and stitching.

The author's work was initially concentrated on aspects of both two and three dimensional constructive stitching. Building on a concept of pre-tacking to form a single, 2-D part, it was proposed to use the Autoscan approach, (developed for decorative stitching and described in Section 1.2 above), for flat constructional stitching. Pre-tacking being the temporary joining of multiple flat parts in order to produce a single, compound, workpiece and thus simplify subsequent handling operations. Initial investigation of this concept demonstrated the need for a better understanding of material behaviour during manipulation in the Autoscan system and hence an investigation was carried out into the morphological properties of leather.

Chapter 2 contains the results of the investigation into the morphological properties of this exceedingly complex and limp material whose structure varies not only from animal to animal but across a single hide. This chapter offers for the first time an understanding of why particular leather components behave during manipulation as they do. Consequently the knowledge gained offered pointers in how to overcome the material properties of a component in order to ensure correct handling.

Chapter 3 describes an implementation of the knowledge gained in Chapter 2, to manipulate flat workpieces made from both leathers and synthetic materials. This chapter covers an investigation into a surface capable of holding and manipulating these workpieces for the purpose of decorative and constructional stitching. A novel mechanism is proposed, tested and verified across a spectrum of the materials that can be expected to be encountered in the shoe industry.

Moving forward to 3-D operations, an investigation was carried out into the feasibility of using the pre-tack approach for these. Chapter 4 describes this novel approach and carries on from work undertaken by E. Adams[2].

Many of the operations carried out in the constructional stitching work highlighted the need for robust and reliable edge following techniques in order to ensure correct stitching lines are maintained. In Chapter 5 vision systems relevant to this are considered. This section moves on from the simple white light mechanisms evaluated by D.L.Smith[1] to investigations into laser triangulation methods. Mechanisms are proposed and investigated so as to determine the profile of an edge being followed.

Chapter 6 implements the knowledge gained in Chapter 5. This is clearly also of value in other areas where topographical information is required. A number of proposals were made and investigated including mechanisms for determining last profile and orientation in order to automate the complex 3-D making operations.

Chapter 7 concludes the thesis by examining the generic and industrial implications that have arisen from the work.

Chapter 2

The morphology and properties of skin and leather

2.0 Introduction.

Leather components, or workpieces as they are often termed, require numerous operations to be performed on them before they form part of a complete shoe. In order for these to be successfully carried out, the workpieces need to be manipulated in one of two ways.

The traditional method is to perform the tasks manually. This is both labour and time intensive. It does, however, allow for accurate manipulation of the workpiece during complex operations, as the operator can determine and correct for any small errors that may arise due to the material properties. Hand manipulation of components is something that industry in general has been trying to eliminate for a great many years through automation.

In areas of manufacture where the material properties of the workpiece need not be considered automated or semi-automated machines are becoming widely used. However, where complex materials such as those displaying limp properties are to be manipulated research is still continuing. Some successes have arisen where fabrics are to be handled, as their structure and properties are better understood. This in cloth is made simpler as it is made from a repetition of a basic number of operations, thus resulting in a regular and well understood weave. The nature of leather is far more complex as it has

been produced from the hide of a living beast. As a result its structure is non-uniform, leading to difficulties in predicting its behaviour under manipulation. If leather workpieces are to be manipulated in a fully automated fashion it is important to understand the basic components that make up the hide and the properties that they may exhibit.

What follows is a brief discussion of an investigation into the nature and properties of leather made by the author and makes significant references to work conducted in this region by Spearman[39], Wilson[40], Harrison & Korn[41], and Roberts, Worcester & Cuttiford[31]. It is not intended to provide the reader with a comprehensive biological understanding of the structure of leather.

2.1 Properties of skin.

Skin is a complex organ covering 100% of the body providing an elastic and compliant barrier against the hostilities of the outside world. It is equipped with a sensory structure which relays information on changes in the external and internal environment. This is achieved by a dense network of nerves which provide a sense of touch capable of detecting fine textures as well as temperature and pain. One of the most important functions of the skin is to maintain the body of its host at a near constant temperature. This is achieved by allowing evaporation of water from the surface in order to dissipate heat, should the body get to warm, and altering the blood supply to the surface should the need arise to preserve heat. In order for this to happen it has to be supplied with glands, ducts, muscles and blood vessels.

Variations in the properties of skin occur due to animal type, age and habitat but also across the body of a single animal. This is due to many individual and intricate parts being grouped together to form skin. These are exceedingly complex in structure and chemistry, in order to cater for the different demands made on particular regions of the body.

2.2 The structure of leather.

The major component of skin is protein. In forming leather, however, some of these proteins need to be removed in a series of treatments. These frequently include the use of alkali, enzymes, or bacteria, and the interaction of the remainder with the tanning materials, oils, soaps, emulsions, mordants, dyestuffs, gums, resins, and other complicated agents[40]. During these reactions the basic structure and property of the skin must be maintained, and if possible improved. The tanning process enhances the hydrothermal stability of the collagen by up to 100% for chrome tanned leather[40] as well as providing a resistance to bacterial attack. In addition lubricants, called fat liquors, are incorporated in order to replace the natural oils of the skin. These minimise the formation of 'inter-fibre'[43] adhesions that may occur during drying, ensuring that the leather remains supple. Figure 2.1 shows a labelled cross section of a typical calf hide and should be used for reference.

In crude terms the skin can be divided into two layers. A relatively thin layer of epithelial tissue, known as the ***epidermis***, and a much thicker layer of connective tissues called the ***derma*** or ***dermis***. The skin is a major organ for the storage of water, with the dermis containing up to a quarter of the body's water.

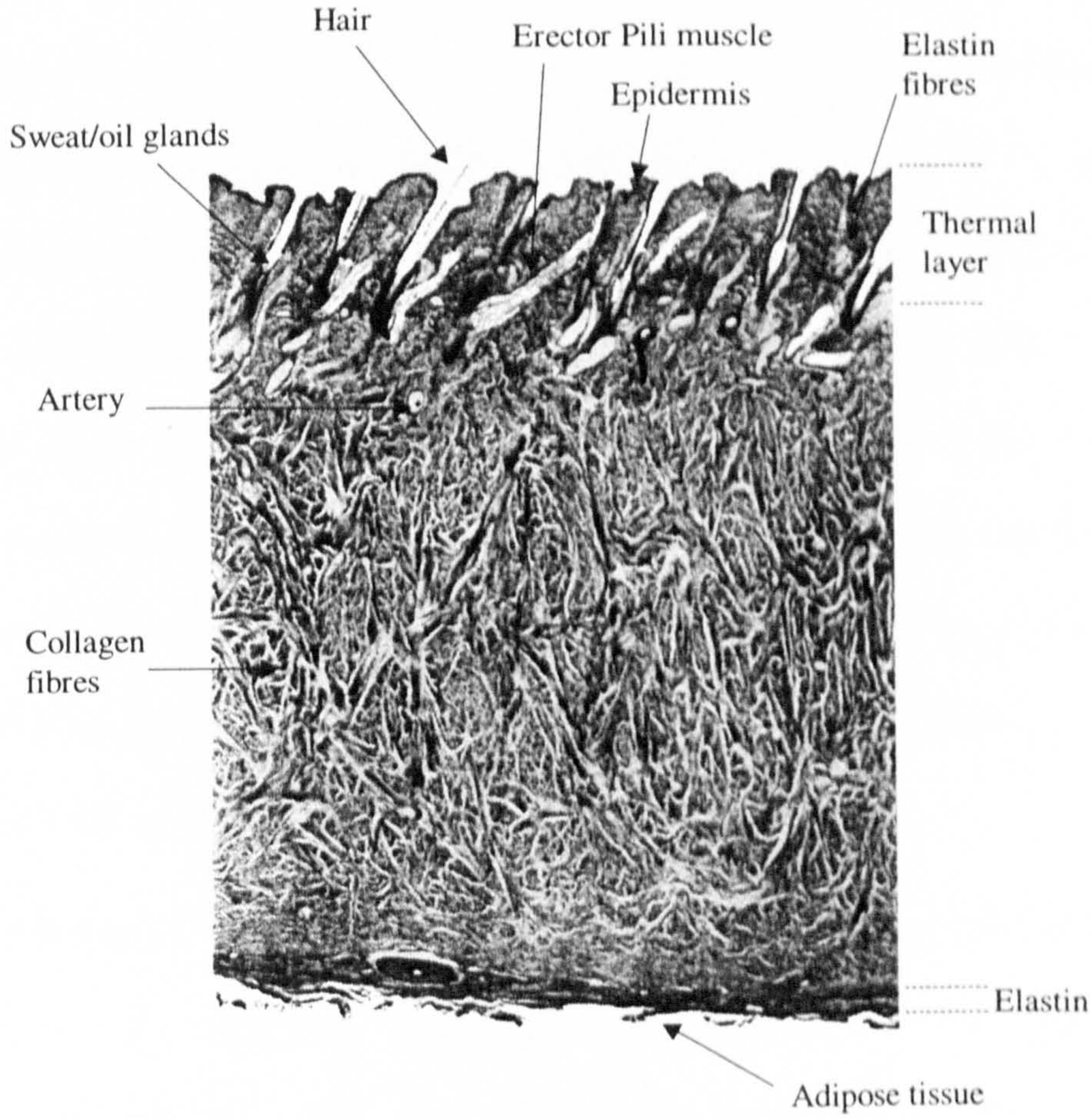

Figure 2.1 Cross-section of a typical calf hide

In between these two layers exists a thin interfacial region called the ***basal lamina*** which is rich in acid ***mucopolysaccharides*** and also contains a network of exceedingly fine ***collagen*** filaments[39]. Here, however, the author will restrict the investigation to the dominant layers of the skin, the epidermis and the dermis.

The epidermis is made up of a cellular structure with no blood vessels of its own and constitutes only about 1% of the total skin thickness. The chief constituent of the epidermal system including the epidermis, hair, and epithelial cells of the glands, is the protein known as ***keratin***. The portion of the epidermis in contact with the derma is a layer of living epithelial cells. In reproducing each of these cells splits into two, one above the other. The older cells are pushed outwards and eventually are unable to reproduce as they become dehydrated. These cells then die and can easily be dislodged from the surface of the skin. This layer also contains cells containing a pigment known as ***melanin***. This pigment is responsible for skin colour and changes in response to variations in the external environment.

Histological preparations have shown the dermis to be subdivided into two further layers, the ***superficial*** and deep (***reticular***) layers[39]. The superficial dermis contains more cells than the deep dermis and finer collagen fibres. Wilson[40] called this layer, when combined with the epidermis, the ***thermal*** layer due to one of its dominant functions. A network of ***elastin*** fibres which surround the hair follicles and glands are also present. Elastin always takes on the form of fine distinct fibres found beneath the epidermis and around the epidermal appendages. Elastin fibres exhibit both tensile strength and elasticity and, although they are predominantly located in the superficial dermis, they can also be found within the deep dermis. It should also be noted that the elastic properties of the elastin fibres are relatively unaltered by the tanning process.

Hair follicles appear to penetrate through the epidermis and the superficial dermis into the deep dermis, however they are always surrounded by a layer of superficial dermis. The dermis itself consists of broader diameter collagen fibres, (≈5μm Plate 3), and scattered elastin fibres. It also contains blood vessels, lymphatic vessels and nerve fibres. The dermis as a whole is often referred to as the true skin and it is this part of the skin that is used to make leather. The portion of the derma immediately in contact with the epidermis has been called the 'grain membrane', this is because it is this layer which forms the surface of the finished leather.

The dermis is chiefly made up of collagen fibres which form the connective tissue. The fibres of the connective tissue appear finer as they near the grain surface where they become extremely fine and generally run parallel to the surface. This effect can be seen in Plate 4. Quality leather can only be produced from hides where collagen fibres are well developed and abundant. A skin containing high levels of fat cells would produce a spongy leather as the fat would have been destroyed during the tanning processes leaving empty pockets forming a honeycomb structure. Beneath the deep dermis is the subcutaneous tissue called the ***hypodermis***. This layer is of variable depth and contains the collagen fibres known as the ***adipose*** tissue that bind the skin to the underlying muscle. It is here also that subcutaneous fat accumulates in order to store food and provide insulation. It should be noted that this layer is removed during the production of leather by processes known as fleshing and flaying.

Plate 3. SEM slide of dermis collagen fibres.
(some elastin fibres are also present)

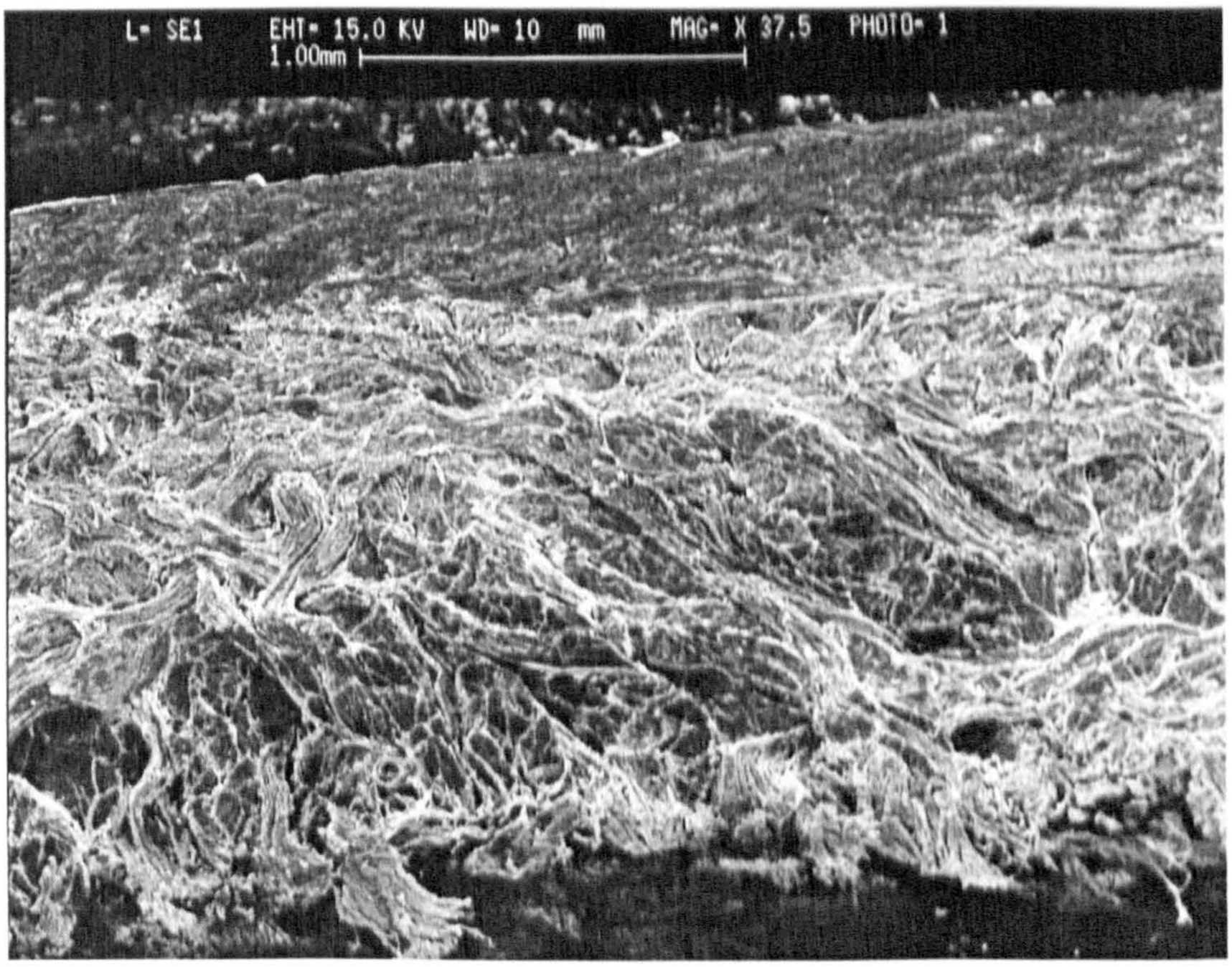

Plate 4. SEM slide of a vertical cross-section taken
from a vegetable tanned calf leather.

2.3 An investigation into the collagen structure of a typical calf hide.

The orientation, size and density of the collagen fibres within the dermis largely determines the leathers properties of stretch, strength and flexibility. In order to observe the dermis structure a typical vegetable tanned, buffalo calf hide, was divided in to 25 segments, Figure 2.2, and cross-section samples taken. The specimens were examined using a scanning electron microscope[45,47], (SEM). Appendix A.1, contains a brief description of SEM principles. Measurements of collagen bundle size and net orientation were then determined in an attempt to directly related these to the varying properties of leather over a typical hide.

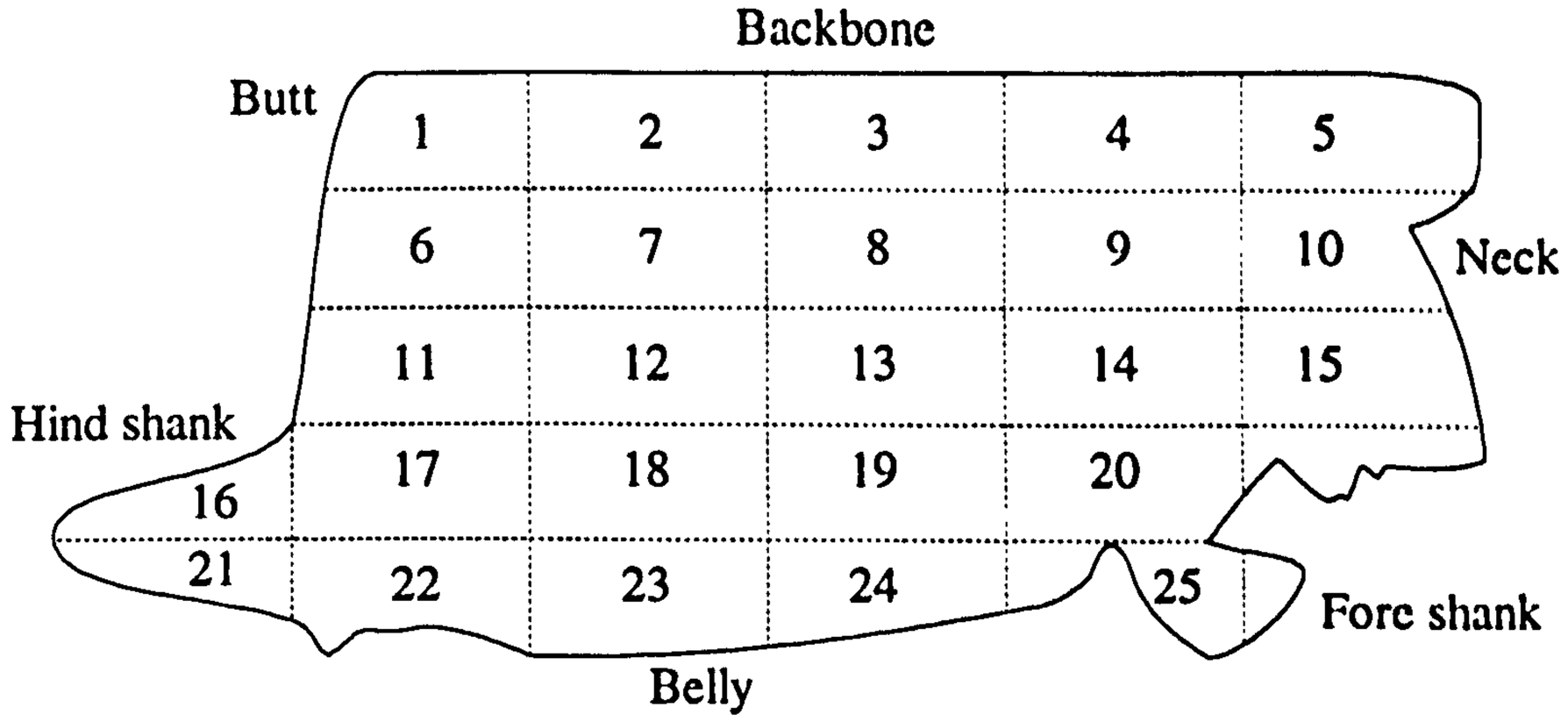

Figure 2.2 Location of samples taken for SEM observation

2.3.1 Variations in collagen bundle size.

The collagen fibres appeared to vary in size and group together to form bundles of fibres similar to that of rope, thus allowing for varying stretch and flexibility characteristics to exist. Figure 2.3 shows the results obtained from the SEM slides for the average bundle size within the dermis across the sample hide. Example slides can be seen in Appendix A.3.

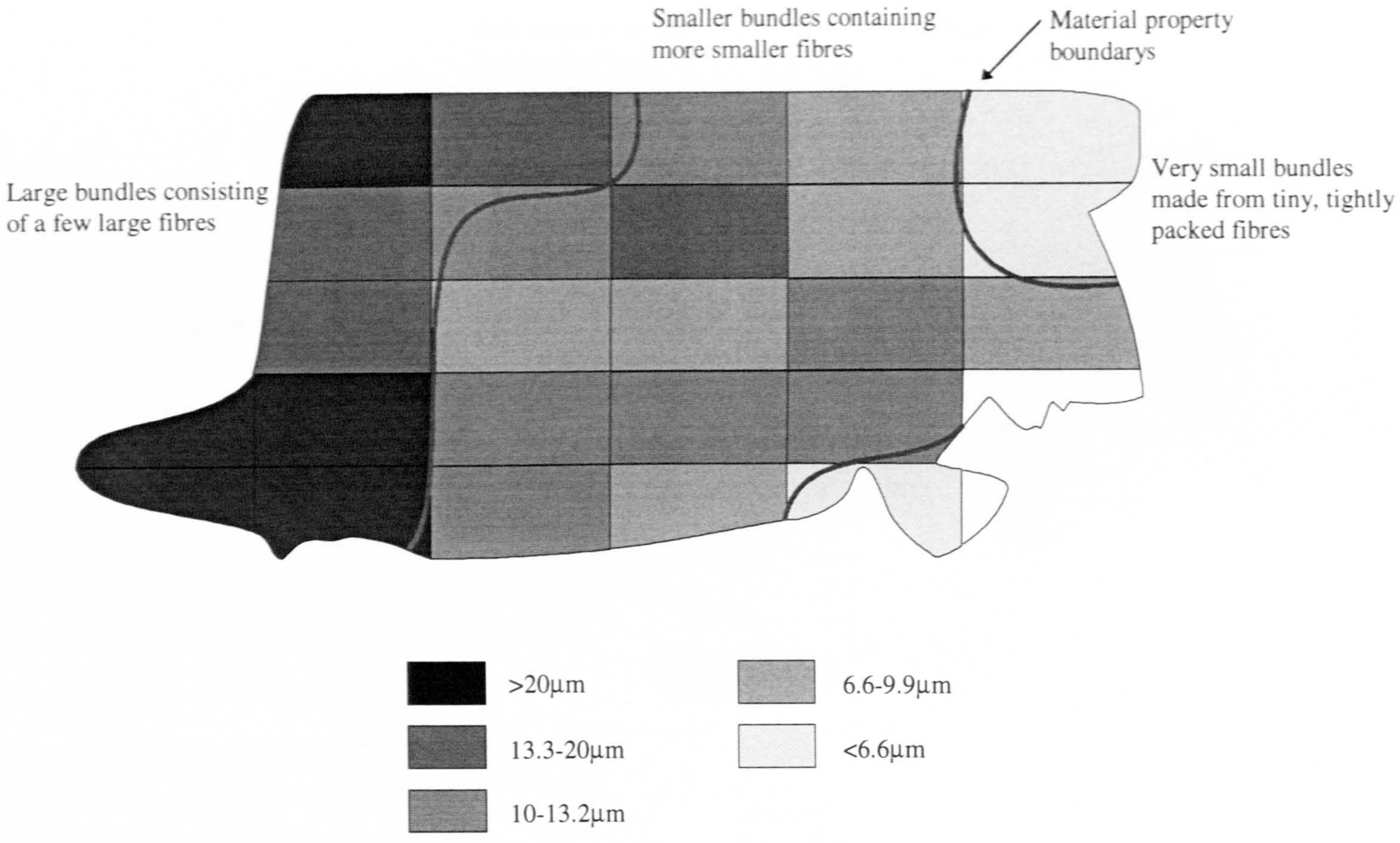

Figure 2.3 Results of SEM observations into collagen fibre bundle size

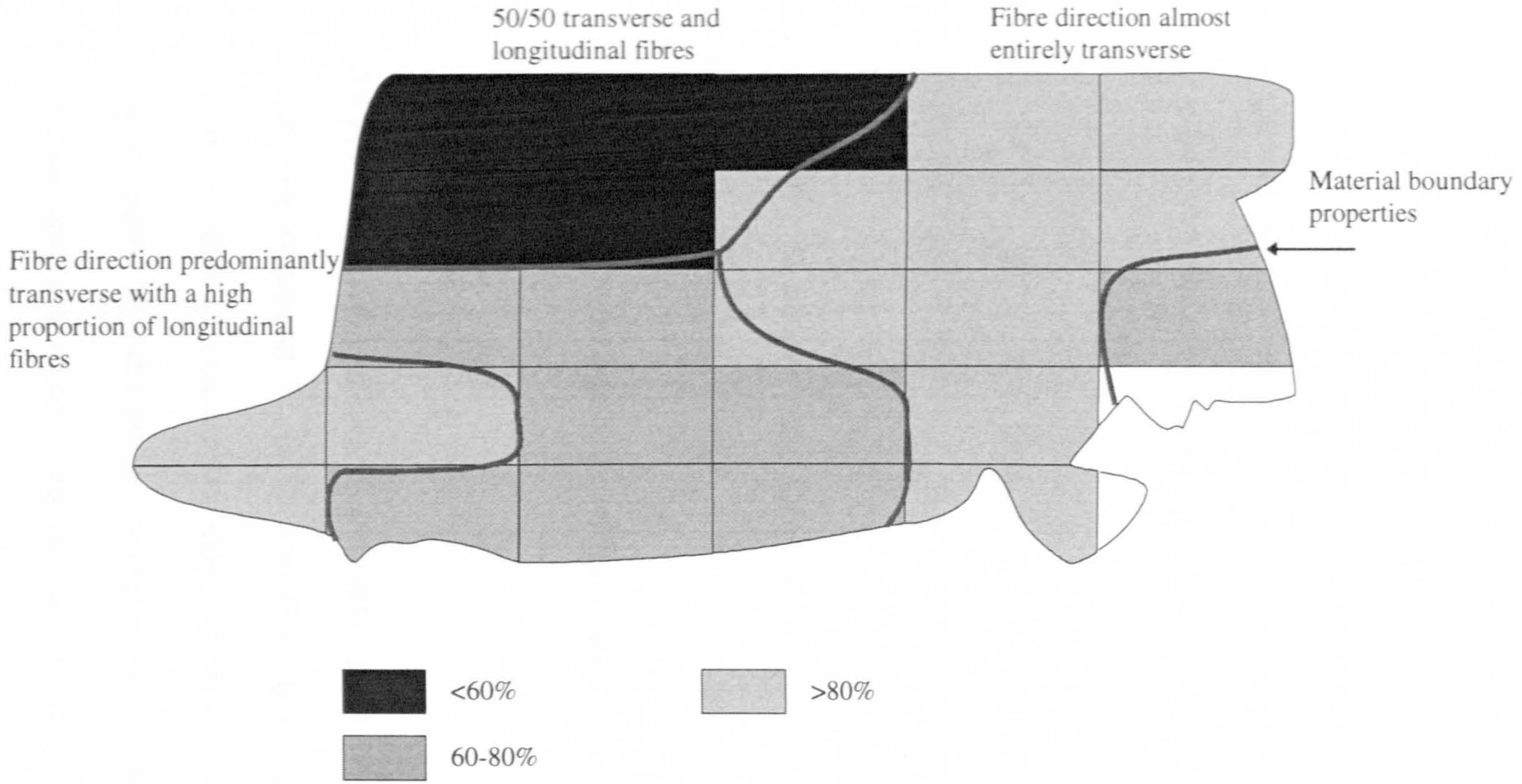

Figure 2.4 Results of SEM observations into net collagen fibre orientation

It can be seen from Figure 2.3 that the hide can be divided according to the bundle size in to three groups. Those fibre bundles around the hind quarters are generally large, (typically >14μm in diameter), and are made up from only a few large individual collagen fibres. Around the shoulders, flanks and belly region, these fibre bundles decrease in diameter but appear to contain a greater number of finer fibres. At the neck and fore shank area the fibre bundles become very small, (<7μm in diameter), with the individual collagen fibres greatly increasing in number and density. The mechanical properties of regions of a hide were investigated by D.L. Smith[1] and should be read for reference.

2.3.2 Variations in net collagen bundle orientation.

Figure 2.4 shows the results observed for net collagen fibre direction across the sample hide. The results demonstrate that a number of distinct regions exist. The fibre bundle directions can be divided in to two classes, transverse and longitudinal. Transverse fibres run around the girth of the animal, whilst the longitudinal fibre bundles run along the length of the animal from head to tail. Example slides can be seen in Appendix A.4.

Around the butt region of the hide there is approximately a 50/50 divide between the transverse and longitudinal fibres. Conversely around the neck and hind shanks the net fibre direction is dominantly transverse. Significantly, however, there is a region across the belly and up to the anus where although the net fibre direction remains transverse, a high proportion of longitudinal fibre bundles appear. It is hypothesised that these may have physiological significance.

2.4 Stretch and strength in relation to collagen structure.

Where the legs join the body a great deal of movement is demanded from the skin in order to facilitate walking. Consequently the skin has to exhibit considerable elastic properties both behind the forelegs and in front of the hind legs. Similarly flexibility is required in the regions of the neck and tail. In regions where little movement occurs, such as the butt, along the backbone and down the legs, there is very little stretch but a high degree of tensile strength. Wilson[40] showed that hide leather over the backbone exhibits a high tensile strength with elasticity remaining low until the hide reaches the side of the animal whilst the belly region is of high elasticity and low tensile strength.

The results obtained in Sections 2.3.1 and 2.3.2 correlate directly with this. The variation in the orientation of the collagen fibres results in differing stretch and strain characteristics for a given workpiece, depending where on the hide it was taken. Where flexibility is required, (eg, for upper components), the net fibre bundle direction is predominantly transverse with the bundle size becoming smaller where a degree of elasticity is also demanded. Across the butt where very little flexibility is required, (eg, for soling leather), the dermis is constructed from large bundles of crossing collagen fibres. This leads to a tough leather which exhibits little elastic ability.

In addition to the leathers structure, different tanning methods can effect the stretch and strain properties of a hide significantly. Certain tanning agents contain hardeners to reduce the elastic potential of the hide in order, for example, to make leather soles. Others contain little or no hardener resulting in a highly flexible, stretchy, leather.

2.5 Conclusions.

Although the prior discussion and measurement of the structure of skin and in particular leather, has only scratched the surface with regards to its structure, enough has been learnt to identify the chief components that will affect its handling. These are the collagen and elastin fibres which combine to provide the dermis with its tensile strength and elasticity. For any given hide the properties of the tanned skin or leather will vary greatly. The butt region is generally much thicker and has a greater solidity than any other part. The shanks, (top of the legs), are firm, but thin, whilst the flanks are typically thick, but spongy. The reticular layer at the butt can be three times thicker than in the hind shank, whilst the shoulder has a thinner layer than the butt and consists of finer fibres. In the belly region, the fibres run nearly parallel to the grain surface and offer little resistance to any vertical force. In contrast the fibres at the butt run both transversely and longitudinally with some randomly orientated, resulting in a region of hide very resistant to distortion. It should be noted, perhaps with surprise, that the thickness of the thermostat or superficial layer of the dermis remains roughly constant across a hide. As a consequence for finer grades of leather this region will occupy a greater proportion of the leather's thickness and have a greater effect on its handling properties. This is due to the high percentage of elastin fibres and the finer nature of the collagen fibres which appear to be broken up into individual fibrils. Thus thin leathers that have the thermal layer forming a high percentage of its thickness are often very elastic and limp in nature. This means that they are easily prone to stretching from a handling mechanism whilst at the same time unlikely to suffer greatly from compression problems. Conversely thicker leathers could suffer from both stretching and compression effects, depending on the net

direction and density of the now dominant collagen fibres. The thermal layer in this case will play a lesser role merely stretching or recovering to accommodate the effects of the collagen. This will if its elastic limit has not been exceeded resume its original state once the deforming force has been removed.

Consequently this highly complex natural structure is exceedingly hard to model due to is anisotropy, indeed the same component cut from the same place at a different orientation, were this possible, would exhibit different handling properties. Even so a number of models have been proposed[1]. These models possess a number of characteristics leather workpieces demonstrate when manipulated using a series of rollers. They do not however predict how a component cut from a given location on a hide will behave. Spearman[29], describes the dermis which is the component of skin used for making leather as 'behaving in life as a hydrated fibrous gel'. It will be seen in the following sections on leather handling that components when manipulated by a series of rollers or belts exhibit a number of fluid like characteristics.

These investigations have shown that a model capable of predicting the behaviour of a workpiece during handling, in addition to being complex, would require information about the hide and the location from which the part was cut. As this knowledge is not available the material characteristics need to be negated by the handling mechanism. This has been traditionally achieved by clamping devices or pallets, however having gained an insight into structure of leathers an alternative method will be discussed in the following chapter.

Chapter 3

Leather handling and manipulation

3.0 Introduction.

The following sections discuss the handling properties of the B.U.S.M 'Autoscan' decorative stitcher and its limitations. By considering the leather structure and its behaviour, when rolled, a mechanism to overcome these limitations will be proposed and verified.

The majority of handling tasks that take place on shoe uppers occur before the upper is closed. As a result the handling procedures are relatively simple as the parts are two dimensional. Two of these operations, decorative and constructional stitching, were to have been covered by the 'Autoscan'. Constructional stitching is the process of joining two or more flat parts together permanently by applying a series of stitches resulting in a 2.5-D compound part. This has previously either been performed by hand or by clamping the parts into pallets before stitching on an automated machine such as the M.P.C.S. The implementation of pallets unfortunately has high overheads both in operator time in loading and unloading, and for the need to manufacture, maintain and store the considerable number of pallets that are required for each style. With separate pallets being required for each foot, and with a pallet only catering for around two sizes, the desire for a palletless stitching device is clear. The 'Autoscan' however was unable to perform these operations successfully across a wide variety of leathers, both man-made

and synthetic due to effects known as 'drift' and 'slip'. An example of this effect could be seen if it was attempted to stitch a closed circle. The result may well appear slightly elliptical with the ends of the stitch line failing to meet. This effect becomes accentuated for composite components where there is a step variation in thickness over the surface. Consequently the Autoscan is unable to perform constructional stitching to a high degree of accuracy due to the ridges that occur when two or more components are joined.

3.1 The B.U.S.M 'Autoscan'.

The 'Autoscan' comprises a set of 16 rollers divided into two sets of four roller pairs either side of the needle. The workpiece is held between each set of roller pairs and fed through the system in the Y direction by the action of the rollers. Positioning in the X axis is achieved by the roller configuration being mounted on a carriage that can be moved along rails by a pair of DC servo motors. Figure 3.1, shows a schematic representation of the 'Autoscan'. Both the roller configuration and the position of the camera can be clearly seen, in addition the convention used to define the X and Y axis is labelled.

The Autoscan is based on the control system for the MPCS and the Intel 8086 micro-processor. In addition an SGS Thompson T800 transputer is used to perform the image analysis. In addition it incorporates a 80Mbyte hard disk to hold the shape recognition files and their associated stitch patterns. This depending on the part, and complexity of the stitch design, allows for approximately 300 separate styles to be stored at any time.

3.2 Types of movement.

During the manipulation of a workpiece through the rolling mechanism a number of types of undesired movement can be observed, include slip, drift and rotation. All of which are due to a combination of the material properties and the mechanical limitations of the handling system. It should be noted that the Autoscan stitcher, which will be considered here, operates as an open-loop system. Consequently once the reference position has been determined by the line scan camera system any subsequent movement of the workpiece will result in stitch position errors as there is no further positional sensing.

3.2.1 Drift.

Drift is the term used to describe the movement of a workpiece from a known reference position perpendicular to the direction of manipulation. This occurs due to the material properties and the forces acting upon it. Both D.L.Smith[1] and N.Tout[42] demonstrated drift characteristics of various leathers and synthetic materials by observing the movements of circular discs during their manipulation.

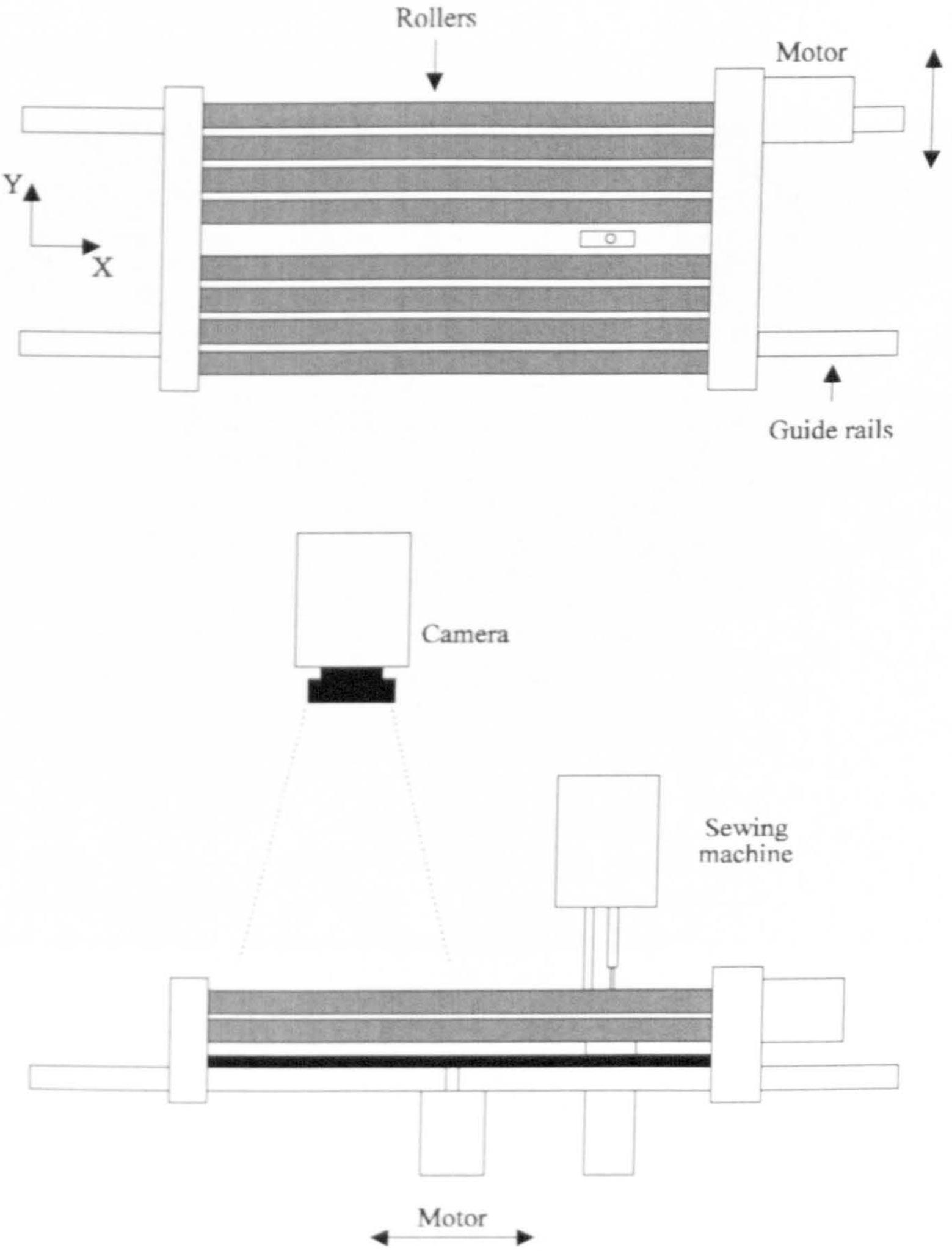

Figure 3.1 Schematic of the 'Autoscan'.

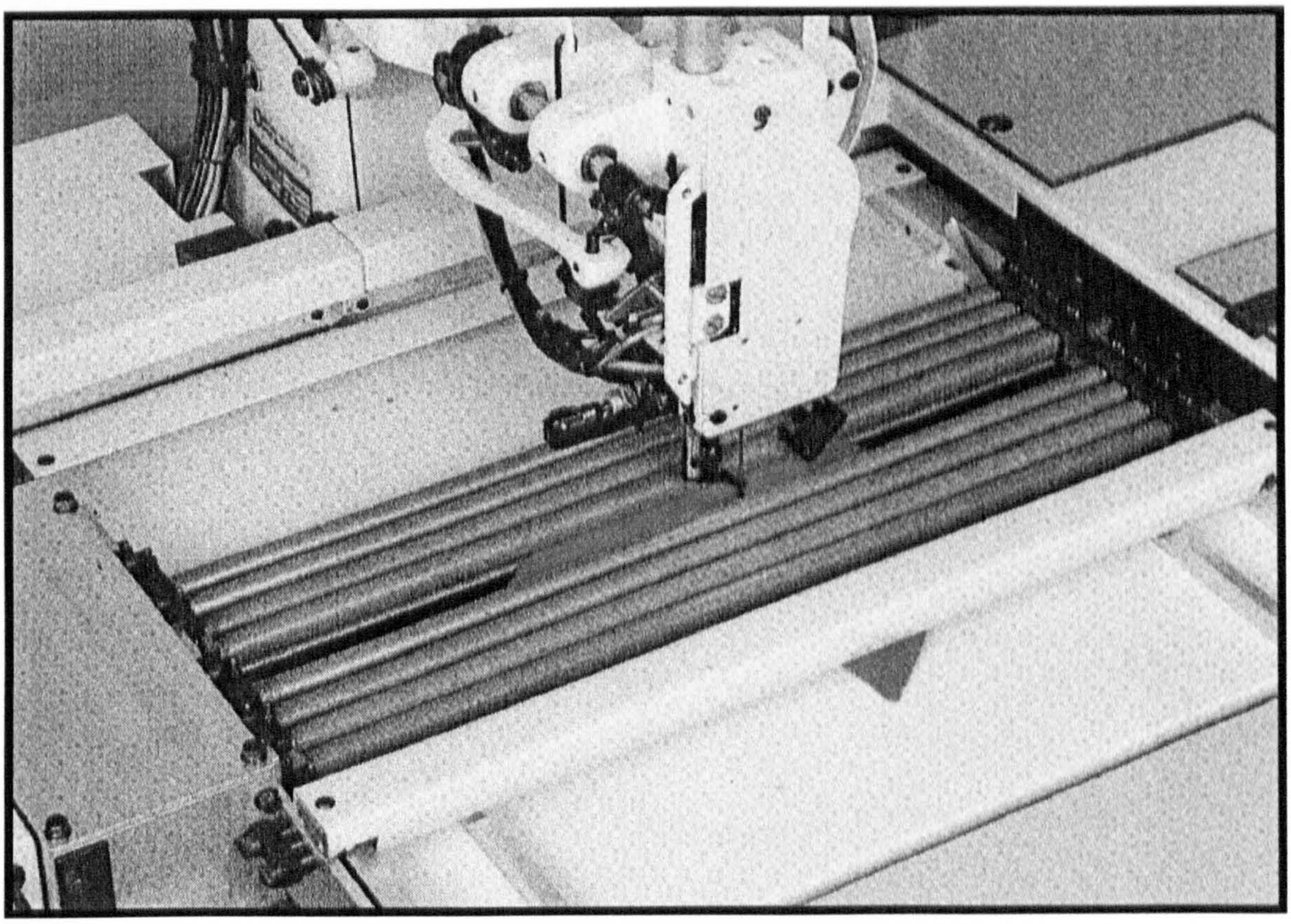

Plate 5. The B.U.S.M Autoscan, showing the rollers and a component during stitching.

The discs are divided into 22.5° segments by lines intersecting through the centre, with one line arbitrarily being chosen as a reference, (0°). The discs are then presented to the handling mechanism at each of the marked orientations and measurements of drift recorded whilst cycling the part backwards and forwards through the rollers. The results of these experiments showed that for the majority of samples the drift displayed a cyclical profile through a 360° rotation of the reference, Figure 3.2.

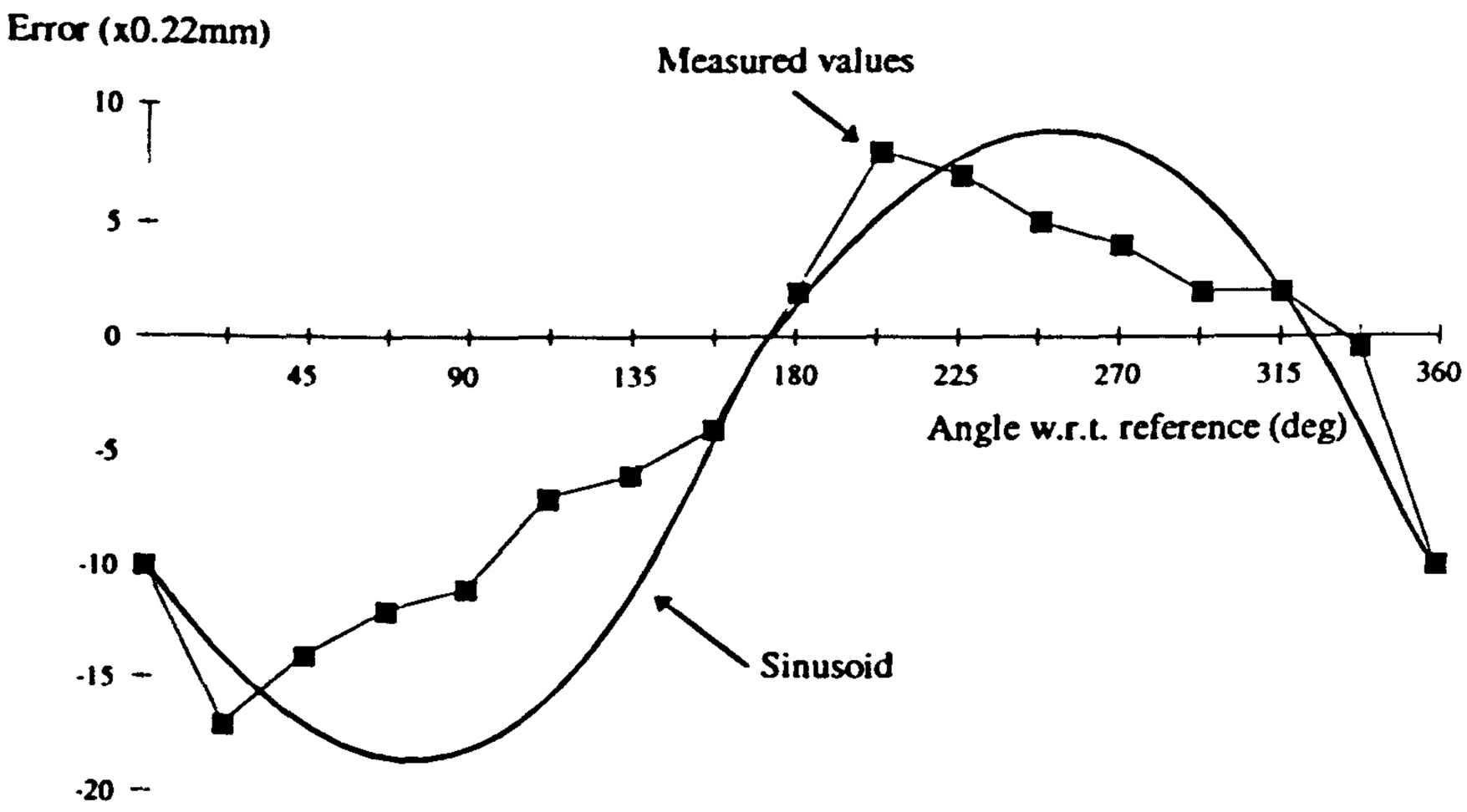

Figure 3.2. Typical result for a leather sample demonstrating a cyclical drift pattern as described by D.L.Smith[1].

This is as would be expected from the analysis of leather, providing that the net fibre direction was constant over the surface of the disc. In an attempt to reduce the drift to an acceptable level, a variety of roller coating materials were investigated resulting in a coarse 'Emery' type paper being wound around the rollers. This was later replaced by N.Tout with tungsten carbide particles heat bonded to a steel roller resulting in a

significant increase in performance. It was however in the former state that an Autoscan was returned to Hull for further research in 1992. Plate 5, shows the Autoscan fitted with tungsten carbide coated rollers.

When rolling a compliant or elastic material a compressive wave, or bulge, is induced behind the rollers, Figure 3.3a. This is due to the gap between the roller pair being less than the workpiece thickness in order to achieve grip. This effect can be seen more clearly and on a larger scale when pastry is being rolled. For rigid components, the trailing edge remains in plane as it passes between the rollers, however with elastic/compliant materials the trailing edge becomes heavily distorted. This is due to compressive forces being distributed over the remainder of the surface, due to the connecting material, following the path of least resistance. As a result, to some extent, this effect is shape as well as material dependant. Figure 3.3c shows the effects observed when rolling a simple vamp component. The workpiece has two side lobes, that extend from the body of the part, which distort during rolling. This effect is a direct result of the compressive force that is required in order to hold the workpiece during stitching and, within limits, increases with an increase in clamping force. The resulting localised distortion of the workpiece when combined with the induced material bulge, which offers an increase in resistance to the pull of the rollers, materialises in a complex drift effect.

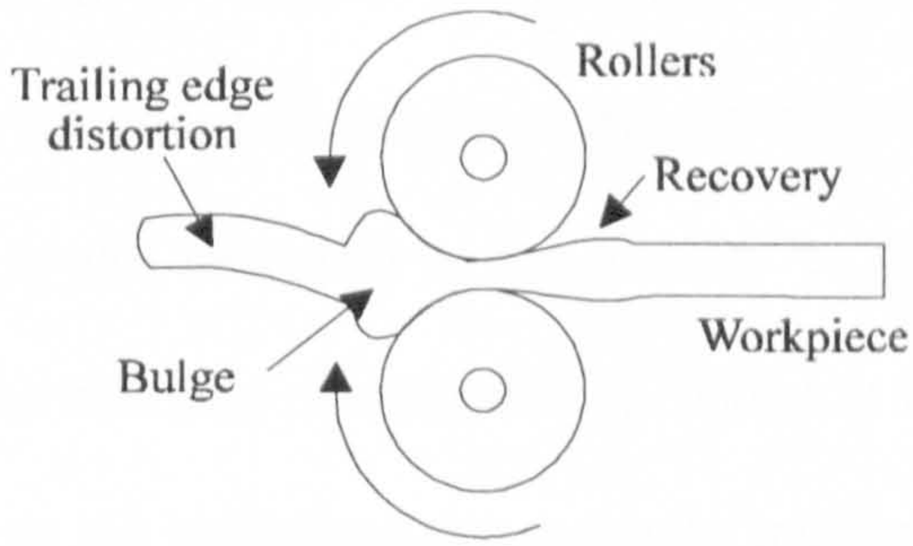

a) Compressive wave

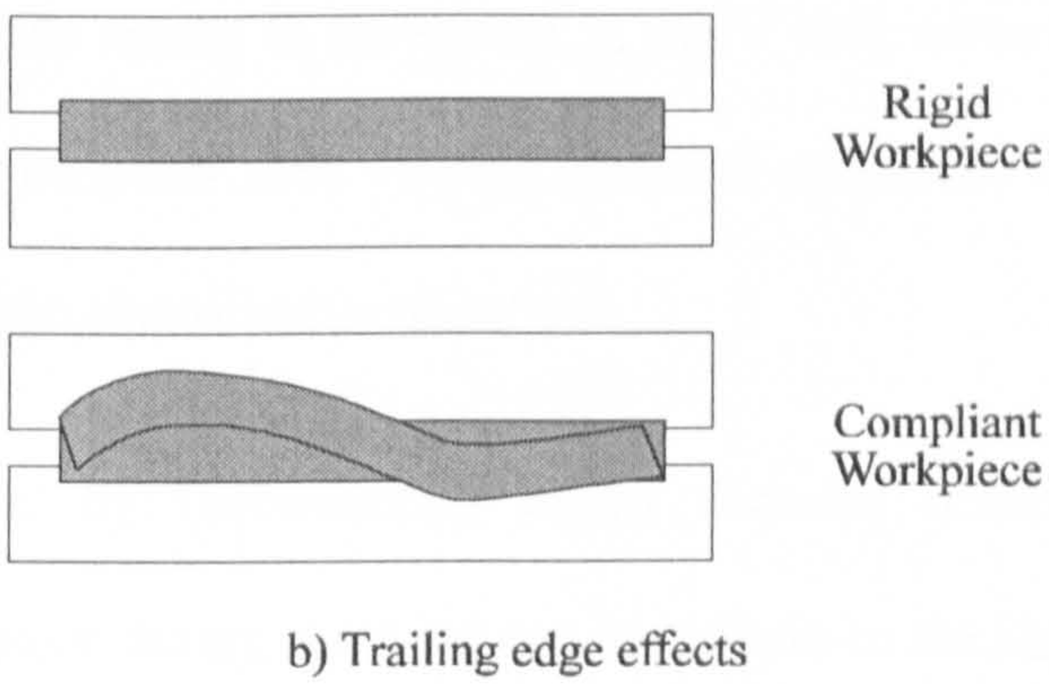

b) Trailing edge effects

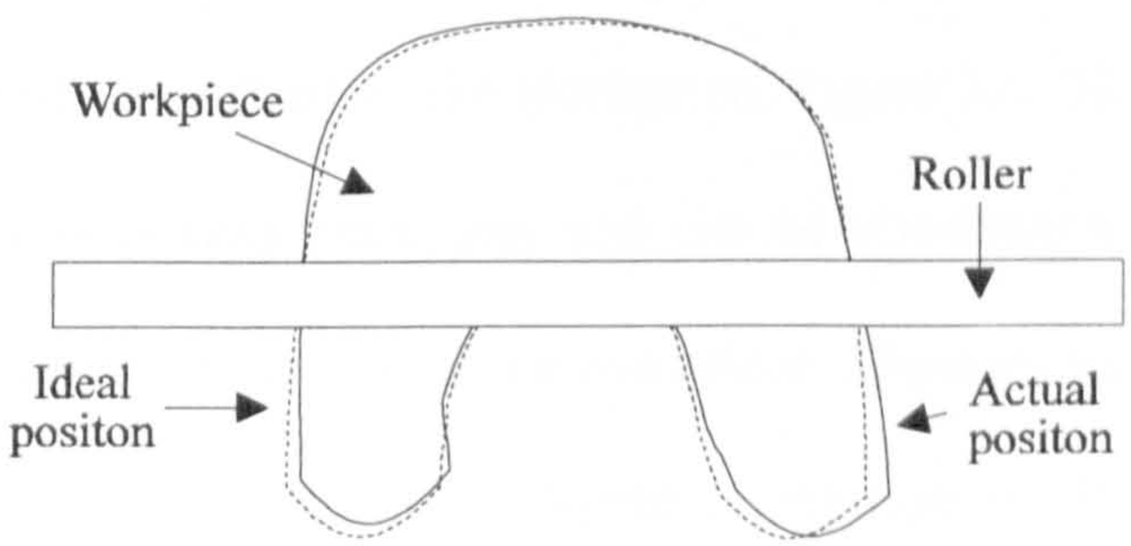

c) Observed drift

Figure 3.3 The effects of compression during manipulation on a compliant material.

3.2.2 Slip.

It has been shown that in order to reduce the drift caused by the rolling action, compressive forces need to be reduced. However, in so doing the possibility of slip increases. Slip being the undesired movement of the workpiece due to the inertial forces of the workpiece. This is also described as the inability of the handling mechanism to hold the workpiece in the direction of manipulation. This can manifest itself as a loss in positional accuracy due to the workpiece not correctly accelerating from rest, or due to overshoot where the workpiece continues to move after the driving force has stopped. Slip, therefore, generally results in movement in the Y axis, however as both the driving surface and the workpiece can have varying frictional properties across its surface some 'drift' and 'rotation' can also often be observed.

The 'Autoscan' by implementing highly abrasive rollers so as to grip and manipulate the workpiece during stitching can contribute to the slip effect at low holding pressures. The greater the abrasive characteristics the less surface contact area exists between the roller and the surface of the workpiece, Figure 3.4. This leads to a slip/grip effect occurring at low holding pressures, and can be observed on certain materials as small scratch marks on the grain side of the workpiece. Experiments have shown that for a single roller driving a flat workpiece a degree of rotation as well as drift occurs as a result of some net slip effect along a given axis. This is due to an uneven distribution of protruding particles over the length of the roller during manufacture. When this effect is expanded to a full roller configuration, it is proposed that at any given moment in time along a given line of drive, some of the rollers will be slipping whilst others will be

gripping the workpiece. This results in some parts of the workpiece being actively pulled through the rollers, whilst others will be dragged through by the connecting material. As a result, forces will be induced in the material other than along the desired line of drive. Consequently this will result in the workpiece trying to rotate in order to align itself with the acting force. Furthermore, due to variations in surface characteristics from roller to roller, the workpiece may stretch or become compressed between two or more consecutive roller pairs. This could then in itself, after a degree of rolling, compound to give small displacement errors.

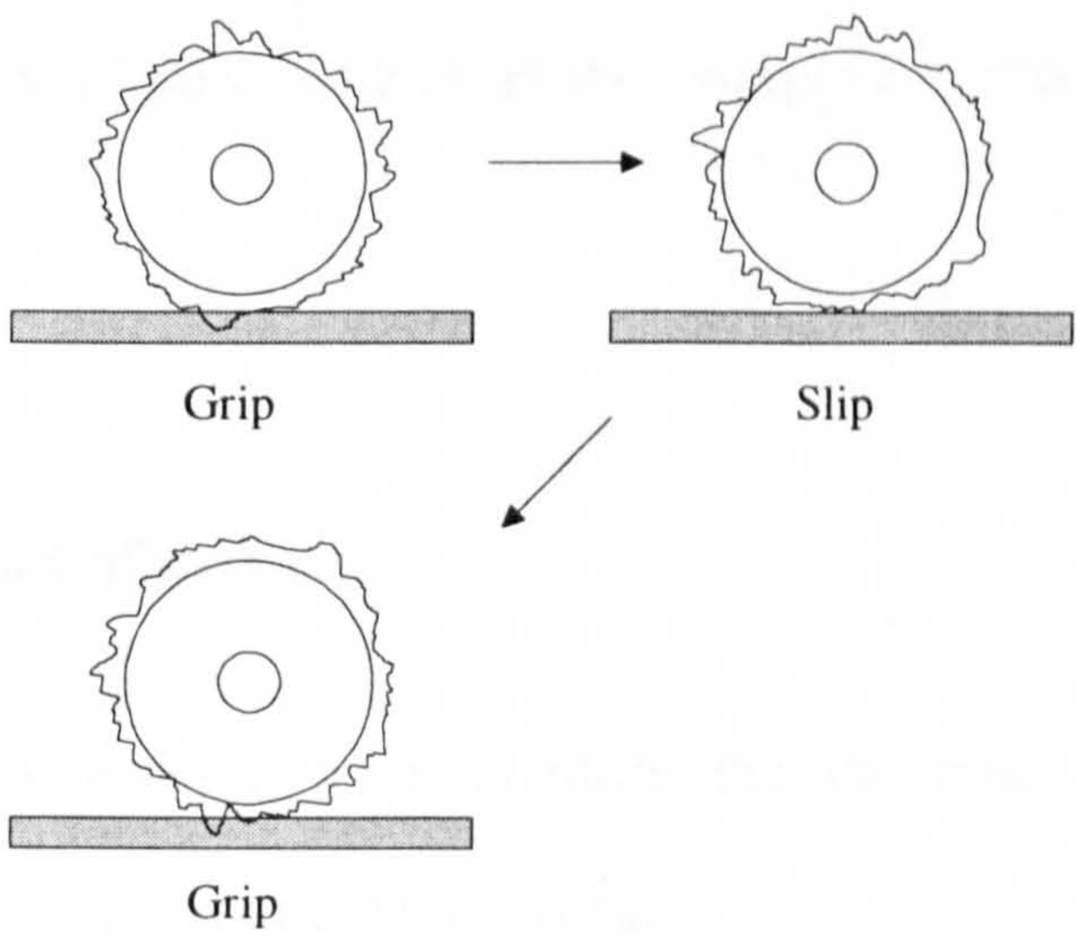

Figure 3.4 The effect of coarse rollers.

3.2.3 Rotation.

The previous consideration of drift and slip can, after a number of operations, compound to give small rotational errors, it is however, the mechanical properties of the handling device that predominantly cause rotation, the chief factor being that of roller deformation. When a workpiece enters the system it does so at a random orientation and anywhere within the cameras field of view, Figure 3.1. As a result the workpiece is generally some distance to the left of the centre of the rollers. The rollers are spring loaded so as to maintain pressure on the workpiece, but allow for a degree of vertical movement. The physical presence of the workpiece causes one end of the rollers to be deflected further than the other, with this displacement being dependant on the characteristics of the workpiece. As a result the workpiece is effectively being driven in an arc.

3.3 External causes of error.

There are two significant external effects that can result in the appearance of drift, these are needle drag and thread tensioning.

3.3.1 Needle drag.

The 'Autoscan' control system is based on the MPCS system mentioned in Chapter 1, as a result a number of its characteristics still remain. One such characteristic is that of needle dwell. The dwell, is how far into the workpiece the needle can be and

movement of the workpiece still be performed. On the MPCS the components to be stitched are clamped in pallets, so that they are unable to move. Consequently by having a dwell period, greater time is available to reposition the pallet during a stitch cycle allowing for higher stitching speeds. However on the 'Autoscan' the workpiece is held far less rigidly by the rollers and as a result any dwell will only act to retard the motion of the workpiece and is particularly noticeable when stitching close to an edge. The net effect can materialise as either drift or rotation with the needle acting as the focus.

3.3.2 Thread drag.

The second effect is similar to that of needle drag, but this time the thread itself acts to retard, or indeed accentuate the motion of the workpiece. The thread drag is most evident when the workpiece is being moved at the same time as the thread is being tensioned in order to complete a stitch. The force exerted by the tensioning cantilever is considerable as it has to pull the complete thread loop that was formed by the bobbin hook back through the workpiece. The resulting knot lying between the surfaces of the workpiece. Indeed for a standard Pfaff bobbin this can be as much as 39mm. This force at approximately 5N is quite considerable and as such deserves further consideration.

In a traditional sewing machine the workpiece is securely held between the dog and presser-foot during normal stitching operations. However, when this conventional advancement mechanism is replaced with the roller positioning system, the holding force is greatly reduced allowing the tensioning force to disrupt the workpieces positional accuracy. Two forms of tensioning mechanism are in common use. The first is the

implementation of a cam shaft, the rotation of which causes a cantilever to provide tensioning. The cam shaft has a profile cut into it which defines the profile of the tensioning cycle. This mechanism is generally employed in applications where the machines are to be used comparatively infrequently and under low load conditions. Where heavy materials are to be sewn in an industrial environment a 4-bar-link is preferred.

If we regard the needle position at any time to be describing a sinusoid ($y = \sin(x)$), with the plane of the workpiece lying at $^{dy}/_{dx} = max$, then the workpiece can only be moved when the needle position is in the positive cycle period. i. e. the needle is clear of the workpiece. Figure 3.5 shows the tensioner profile of a typical cantilever mechanism with respect to the needle position. It can be seen that the thread is being tensioned well into the workpiece movement phase, which can result in unwanted workpiece displacement in the direction of the applied tensioning force. In order to best understand the thread effects during stitching a computer simulation of the 4-bar-link employed on the 'Autoscan' was programmed. Figure 3.6 shows the 4-bar-link arrangement used in the simulation. The links that make up the 'four bars' of the 4-bar-link are shown as L_1-L_4, (Pfaff specification[13]), the other dimensions used in the simulation to calculate the thread tensioner profile are also shown. It can be seen from Figure 3.5b that the second half of the needle cycle, (needle in the workpiece), is unmodified. This is due to the complexity of the interaction between the needle and bobbin prohibiting the posibility of making simple modifications.

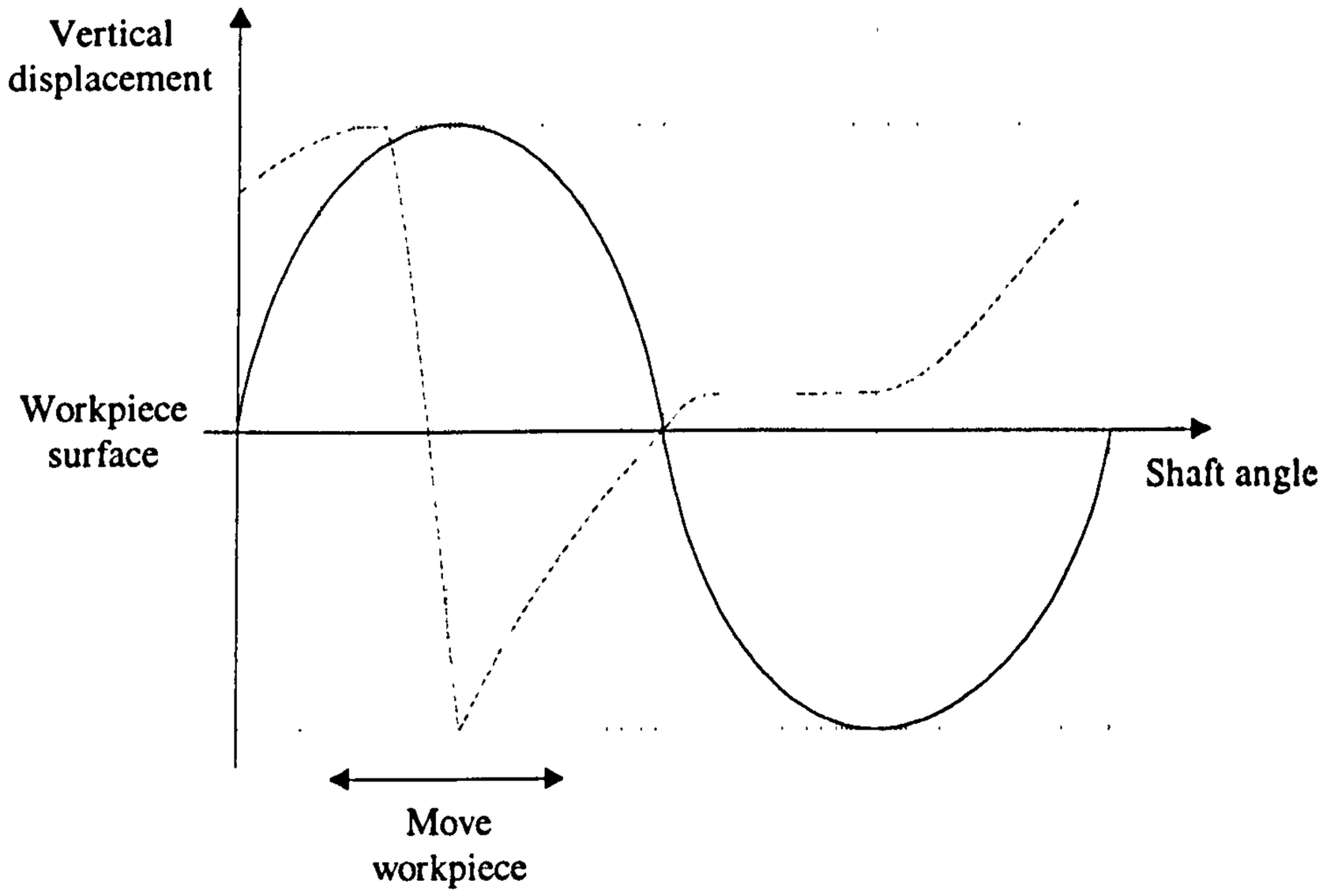

a) Cantilever thread tensioning cycle.

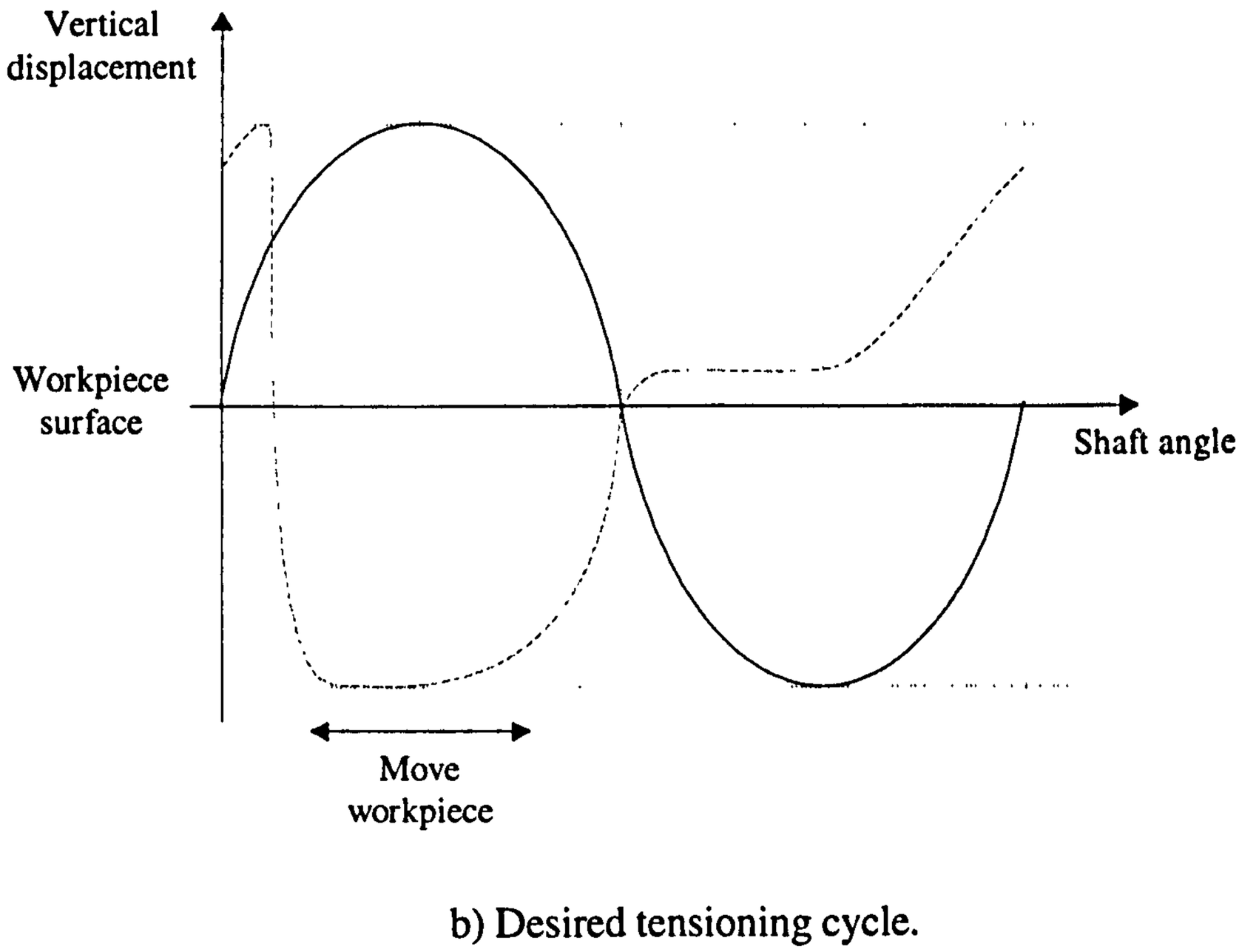

b) Desired tensioning cycle.

——— Needle profile - - - - - - - - - Tensioner profile

Figure 3.5 Thread tensioning cycles for a cantilever mechanism.

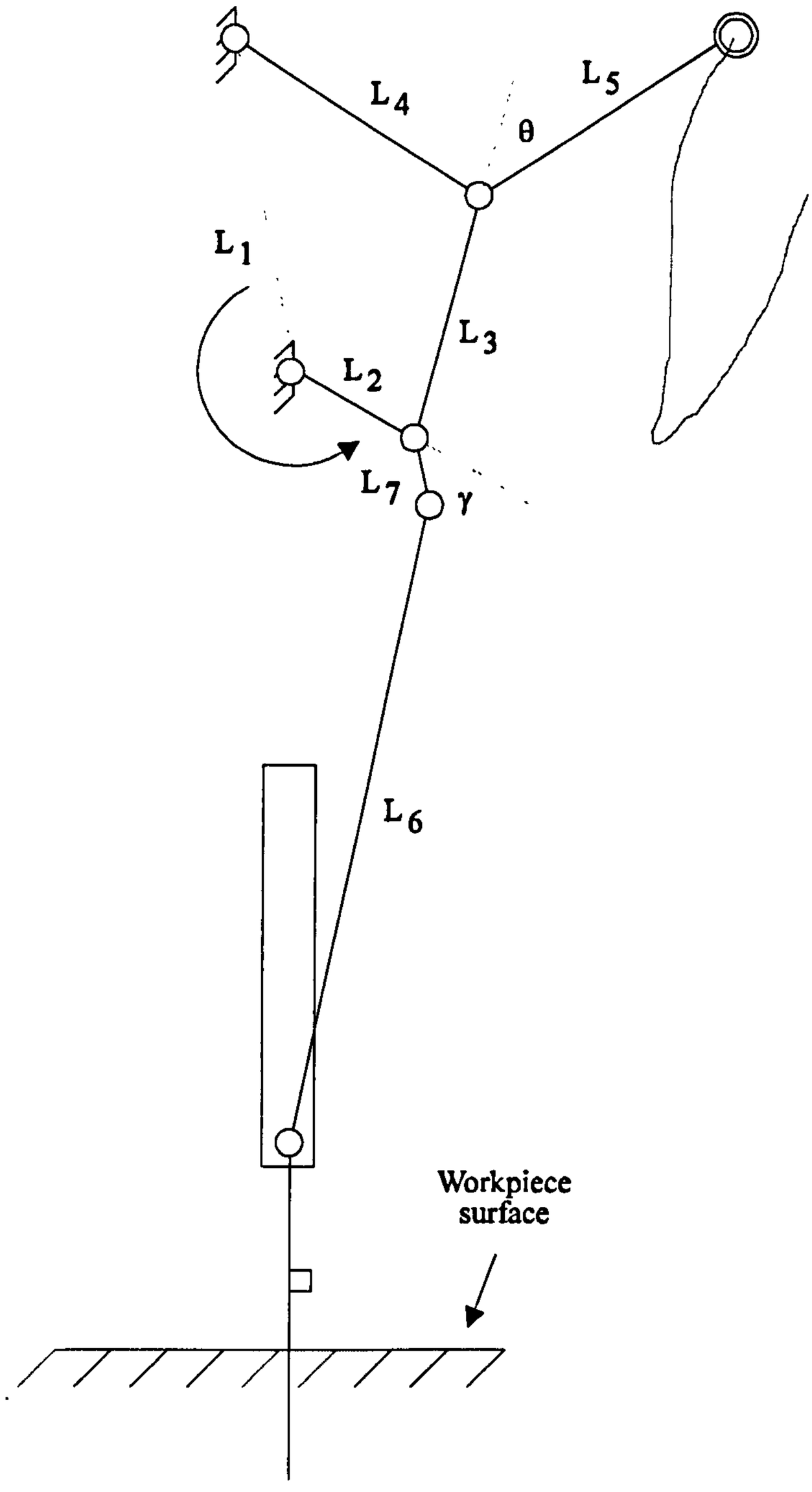

Typical Dimensions

L_1 = 35 - 38mm
L_2 = 16mm
L_3 = 28mm
L_4 = 32mm
L_5 = 34mm
L_6 = 70mm
L_7 = 3 - 4mm
$\theta \cong 45^o$
γ = Any

Figure 3.6 Typical 4-bar-link configuration.

If the thread tensioning phase could be adjusted so that minimal forces were exerted, or indeed slack created during the workpiece advancement phase, then the effects of thread drag could be vastly reduced or even eliminated. The desired tensioner cycle is shown in Figure 3.5b. Here it can be seen that the tensioning action in the negative part of the needles sinusoidal action need not be effected. However, during the positive needle cycle component the thread tensioning is altered so that the tensioning forces are nearly eliminated during the movement phase.

The ideal profile although achievable with the cam and cantilever mechanism is not obtainable for a 4-bar-link configuration. It is however possible to determine an optimum configuration for the mechanism from the results of the computer simulation, Appendix B. The results show that the thread tensioning forces can be reduced to a minimum by setting $\gamma = 90^{o}$, with further improvements occurring if L_7 is also increased.

3.4 Autoscan redevelopment.

The 'Autoscan' in its initial configuration consisted of the 8 roller pairs mounted as previously described, with all the rollers coated in a medium grade, abrasive, Emery paper type material. The rollers themselves were 12.4mm in diameter and made from carbon fibre. All the rollers were driven via a complex belt structure by a single DC servo motor with positional feedback. Due to an understanding of the effects of slip and compression on the degree of drift that a given workpiece exhibits when rolled an alternative mechanism implementing belts was considered. In so doing, the contacting surface between the drive mechanism and the workpiece increases from 8 linear lines to a

significant surface area, consequently the pressure on any point would be reduced for a given compressive force. Furthermore, the complexity of the drive system is reduced from having to actuate 16 rollers to a maximum of 8, or more conveniently to 4 central driving rollers. The penalty however for implementing a belt handling mechanism is in the increase in motor power required.

3.4.1 Types of belt mechanisms.

Two types of belt mechanism were investigated, firstly, wide belts replacing each bank of 4 rollers, and secondly the implementation of a series of narrow belts separated by small spacers. The former offers considerable resistance to being driven if belt tension is to be maintained across its surface, and also suffers from local surface deformations due to the way the belt material relaxes when removed from the mandrel on which it was formed. Consequently, a mechanism comprising of a number of narrow belts was selected for further investigation as they also significantly reduced the edge curling and tensioning problems.

3.4.2 Belt handling mechanism.

The prototype 'Autoscan' was to act as the base machine with the roller mechanism being directly replaced by belts. The belts themselves have to be positively driven so as to ensure that no positional errors occur. To this end Synchroflex[18] timing belts were selected as they suited the fixed dimensions and provided positive drive when

combined with pulleys of 11.13mm PCD. These belts are polyurethane based with steel wire reinforcement inserts offering a low degree of stretch under high loads. The belts themselves are 12mm wide and 138mm long, presenting a possible surface contact area of 6.18cm^2 per belt to the workpiece.

The handling mechanism consists of 80 belts mounted in banks of 20, each bank replacing 4 rollers.

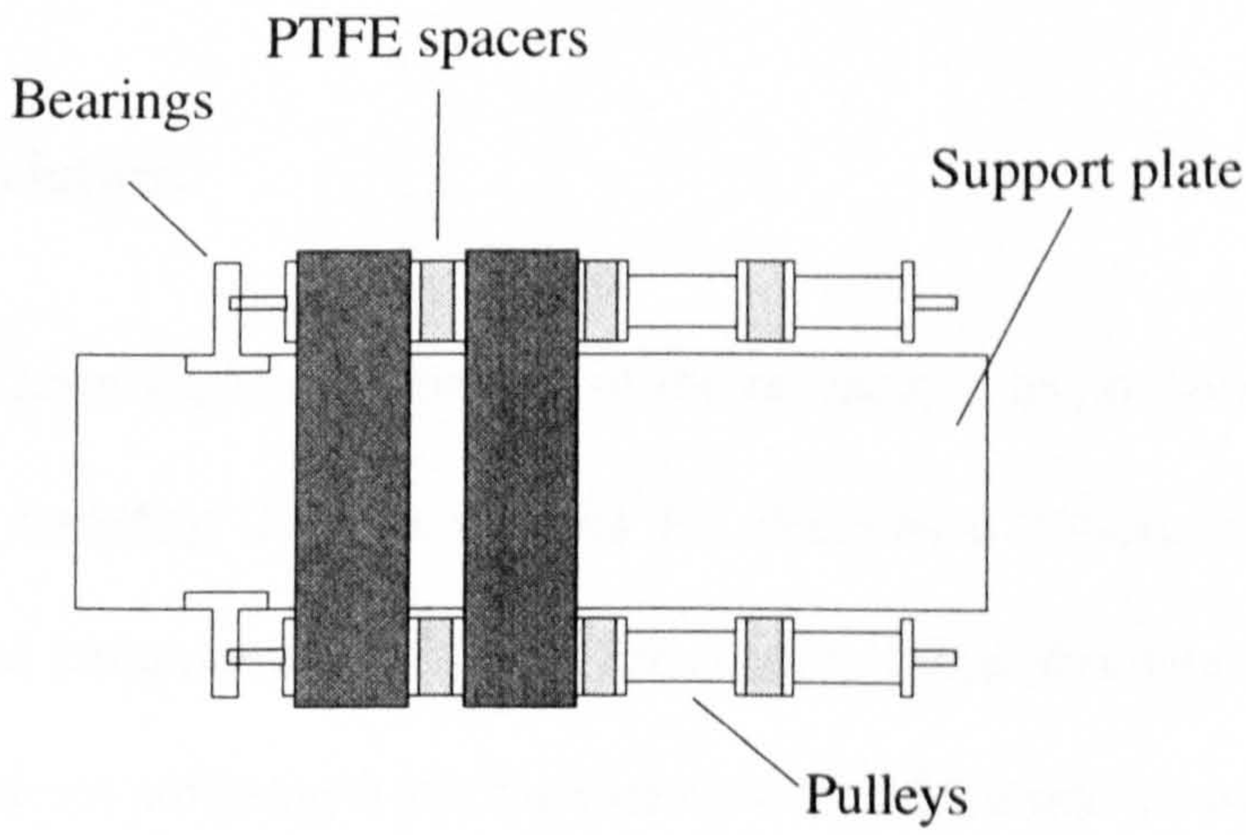

Figure 3.7 Belt handling mechanism.

Each of the belts are seated into pulleys fixed onto a drive shaft and separated by PTFE washers. The pulleys on the inner edge, nearest to the needle, are driven by a DC Servo motor with positional feedback, whilst the outer pulleys are free to rotate upon a support shaft. The shafts in turn are mounted in bearings to ensure as low a resistance to rotation as possible. In order to support the belts against the workpiece during manipulation a central support plate is included. This has an additional set of bearings to support the shafts and reduce the possibility of a variation in belt tension. The resultant system configuration can be seen below, Figure 3.8.

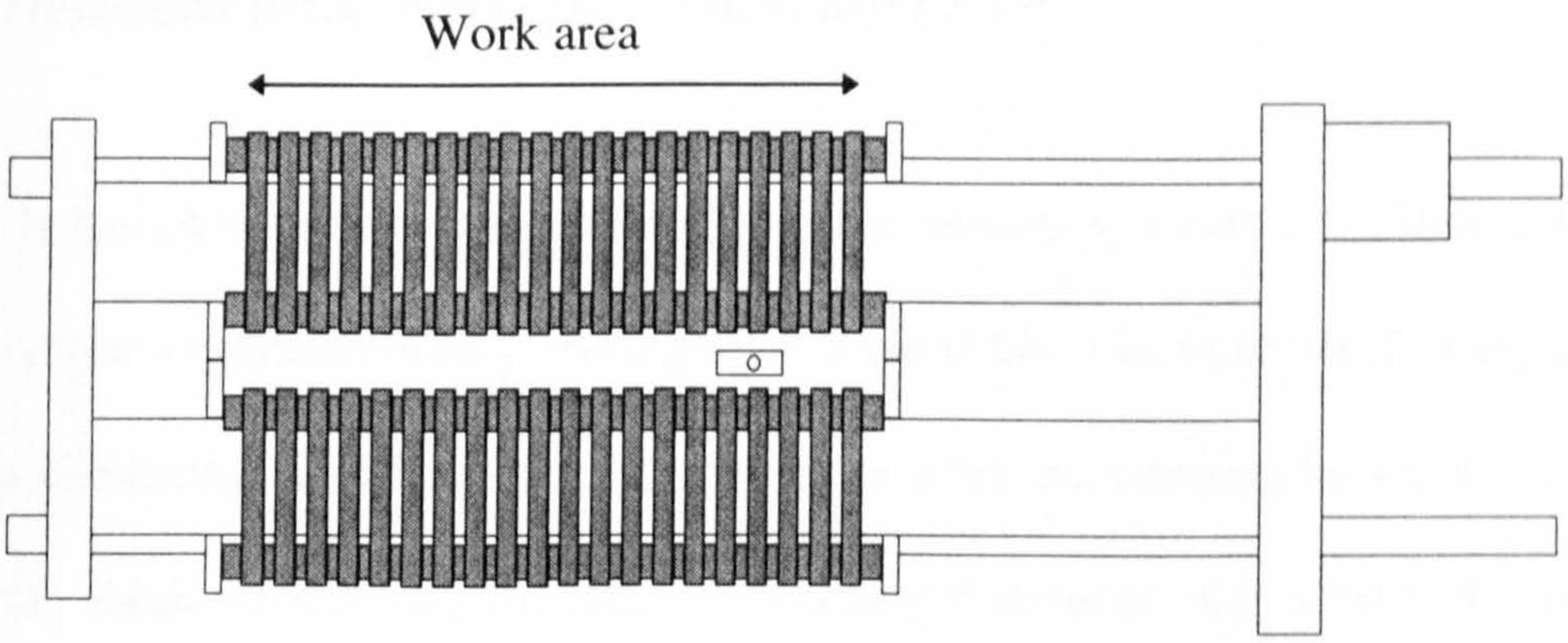

Figure 3.8 Schematic representation of complete belt handling mechanism.

3.5 Belt characteristics.

It has already been stated that the aim of the research is to produce a mechanism capable of not only handling 2-D workpieces for decorative stitching, but also, the handling of pre-tacked compound 2.5-D parts for constructional stitching. Both of these should be handled without suffering from the various drift effects and to a high degree of accuracy. An acceptable accuracy being loosely defined as, 'no stitch should be greater than 1mm from its ideal location, regardless of stitch pattern complexity, for the maximum number of materials'. In order to try and obtain this specification the lower pair of belt modules act as the drive surface, as rough handling of the nap, (flesh), side of a workpieces can soon recover, unlike the highly shiny and smooth grain surfaces of patent leathers. In contrast a compliant substrate forms the upper surface, this is due to its ability to cater for possible variations in the surface contour of a compound part.

3.5.1 Determination of required holding forces.

It has already been stated that the needle tensioning force is the dominant force acting on the workpiece during processing at around 5N. The other chief acting force, if dwell is eliminated, is that of the roller actuation when accelerating between stitches. In order for these effects not to cause mechanically induced slip effects the handling mechanism must be capable of withstanding the maximum resultant component of these two forces. Consequently the forces acting on a workpiece during manipulation need to be determined.

In order to determine this the control properties of the MPCS upon which the 'Autoscan' is based can be analysed. The acceleration/deceleration profile used to control the DC. servo motors for the MPCS is shown in Figure 3.9. M. Colls[44].

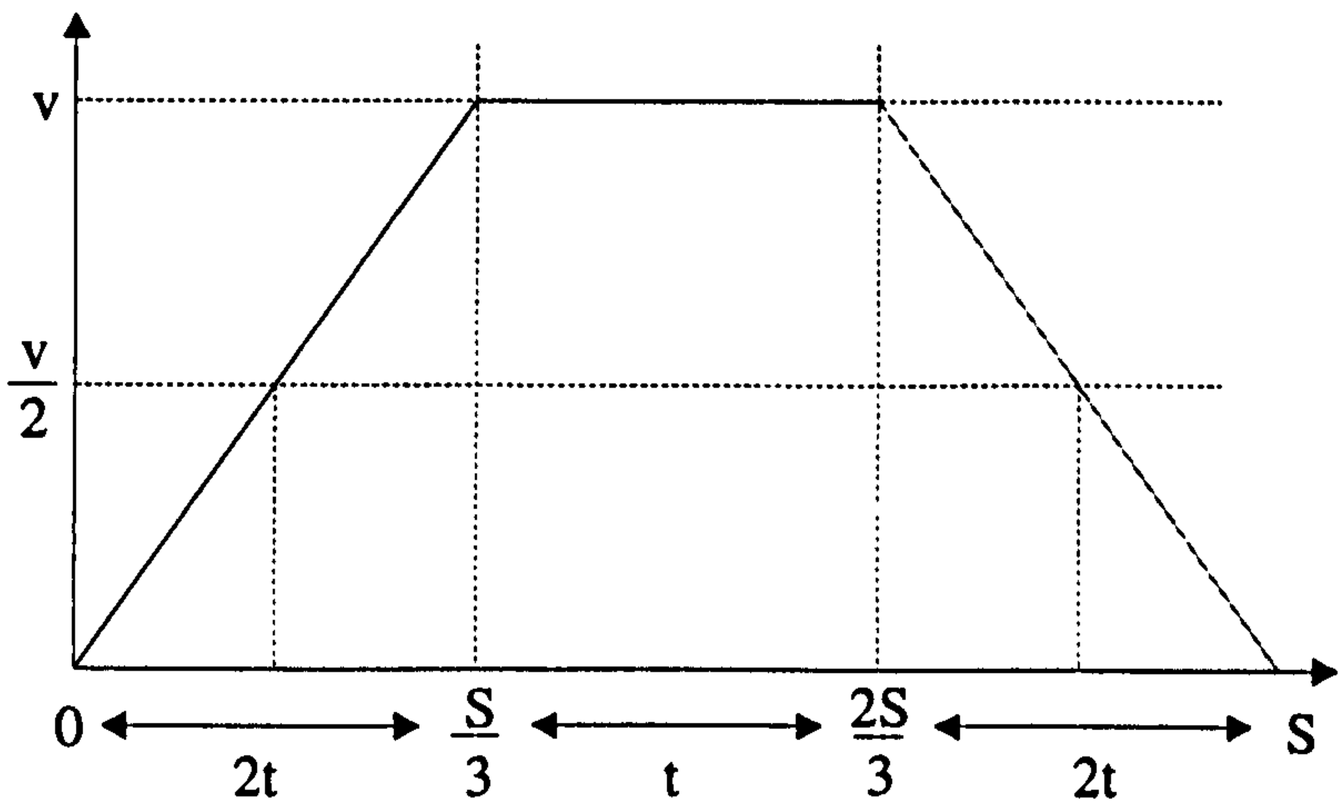

Figure 3.9 MPCS DC. Servo motor control profile.

The control system ramps up the servos to a maximum velocity over $^1/_3$ of the distance to be travelled, held constant for a further $^1/_3$ before ramping down over the remaining $^1/_3$. Of course motion does not occur instantaneously due to the static friction and masses involved. However for the purposes of this analysis the characteristics shown in the above figure will be considered as holding.

Total time taken to travel a distance *S*.

$$T = 2t + t + 2t = 5t$$

A cycle is defined as a 25mm movement forward followed by 25mm backwards, consequently the motors have to accelerate and decelerate twice in order to complete the action. Considering a half cycle and timing it to achieve a measure for *T*, *t* can also be found.

Total time for a half cycle, $T = 0.35\ seconds$.

Therefore,

$$t = \frac{0.35}{5} = 0.07\,\text{sec}\,onds$$

and

$$2t = 0.14\,\text{sec}\,onds$$

now, $v = \frac{distance}{time}$, and v_{max} occurs at $\frac{S}{3}$,

we have,

$$v_{max} = \frac{S}{6t}$$

hence,

$$v_{max} = \frac{S}{3} = \frac{25 \times 10^{-3}}{3 \times 0.14} \approx 0.06 mS^{-1}$$

Consequently for a large workpiece with a mass of 100 grams, the resultant force generated by the acceleration of the handling mechanism producing a change in workpiece momentum would be,

$$F = \frac{0.1 \times 0.06}{0.14} \approx 0.043 KgmS^{-2} \equiv 0.43 N$$

Consequently any handling mechanism would need to ensure that the workpiece remained stationary relative to the belt surface during manipulation. The resultant force of the combined thread tensioning, vertically up through the workfoot and component movement, Figure 3.10, show the thread tensioning effect to be the main consideration.

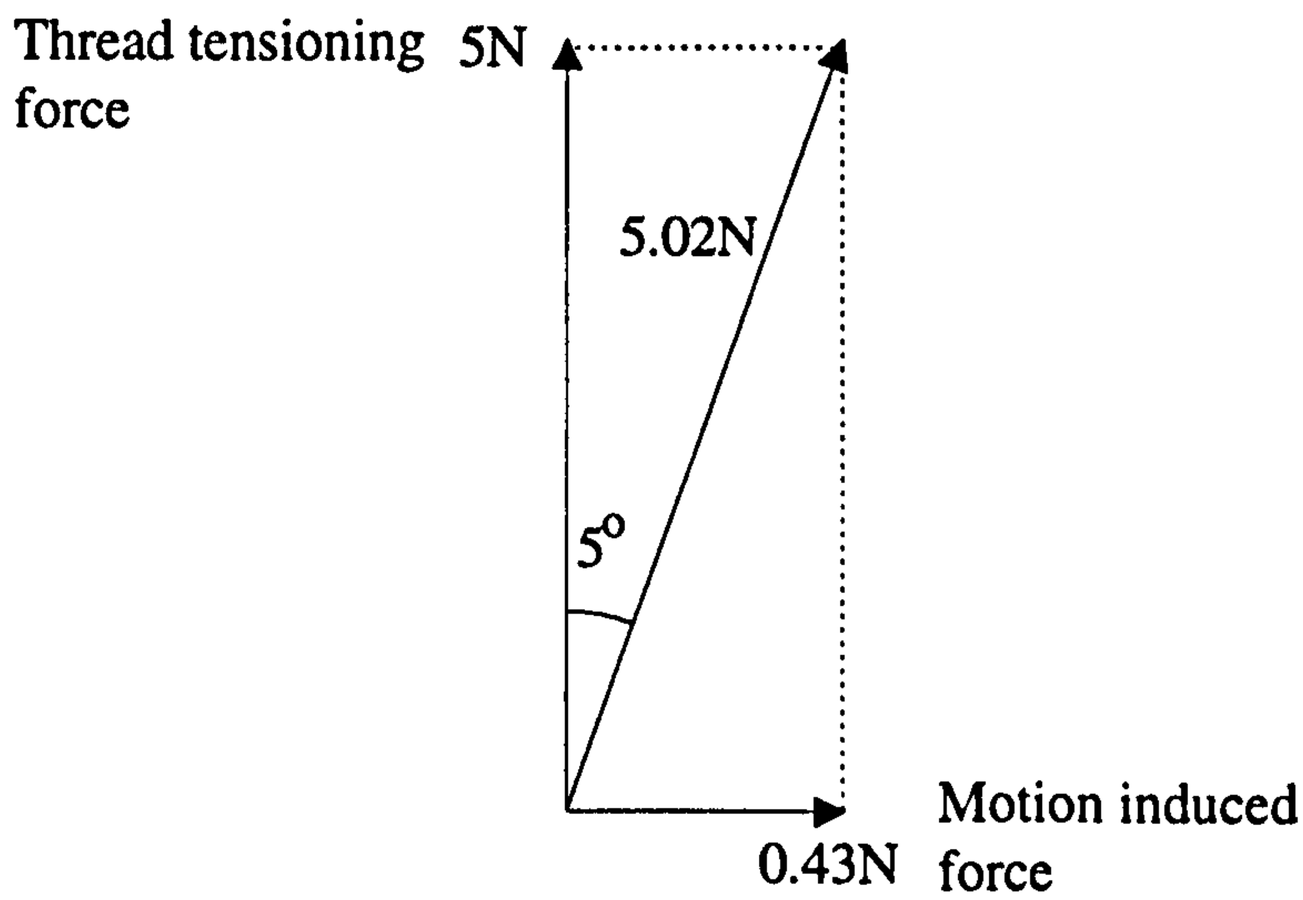

Figure 3.10 Resultant Force vector diagram of the forces exerted by the Autoscan during stitching.

3.5.2 Initial drive surface characteristics.

The choice of materials that could be bonded to the belts in order to provide characteristics capable of holding the workpiece during processing is potentially very large. This is due to the number of specialist manufacturers, such as Fenners[19], who deal with belting technology. However, many of the common belting materials are specifically designed for industrial conveyor systems and as such have physical properties that make them unsuitable for smaller scale work. As a result materials not normally associated with manipulation applications need to be considered. The roller system demonstrated that abrasive mechanisms could be implemented to hold the workpieces during stitching, without any deterioration in workpiece surface quality. Experiments were conducted using Emery cloths and papers to determine their suitability as a drive surface. The papers proved too brittle when negotiating the tight radius at the pulleys, however, the cloths returned more favourable results.

Fine abrasive surfaces produced poor drive properties due to the loose collagen fibres on the nap side of the leather acting as little rollers. Highly abrasive coatings tended to wear very quickly with the nodules forming the abrasive being dislodged due to insufficient bonding. As a compromise a medium grade cloth was initially selected to provide the grip for the driving surface.

A number of attempts were made at producing a continuous loop of abrasive material and bonding it to the polyurethane belt substrate, however these proved unsuccessful. Consequently 3M[20] were contacted, and agreed to supply continuous

samples of Carborundum coated cloth to a specification that would fit the dimensions of the belt substrate. The bonding of these abrasive material loops to the polyurethane substrate proved difficult due to the effective change in centres that arises when bonding one semi-rigid substrate to another. This effect can not be noticed until after the compound belt is rotated around the pulley radius, Figure 3.11a. A number of adhesives were investigated, most either dried hard producing a solid ridge at the bond or, were unable to form a successful join. The best results obtained from the implementation of adhesives came from a contact type capable of providing a partially elastic bond, with the bond only being made at a few points. This allowed for some relative movement to occur between the two belt materials. However even this type of bond soon failed under operation resulting in the need for an alternative bonding mechanism. This was achieved by making a physical link between the belt substrate and the material loop by stapling. Four staples, (size No. 10-1M), per belt were implemented and inserted between the teeth of the belt substrate. On the upper, or drive, surface the staples are flattened to reduce their effects on the handling properties. The resolution/spacing of the staples being defined by the pulley diameter in order to ensure that a maximum of only one staple can be affecting by the meshing properties of the belt and pulley at any point in time. This mechanism provided a reliable bond whilst allowing for a degree of flexibility.

3.5.3 Compliant surface construction.

The upper or supporting surface was selected to have a compliant nature so as to mould around any small fluctuations caused by the edges of overlaid parts. Again there

were a wide selection of materials available, with Neoprene, Nercoprene, EPDM and PVC foam being the ones selected for further investigation. The tight radius at the pulleys imposed a maximum compliance thickness of the order of 3mm, if the belts were to run smoothly. Figure 3.11b shows how, as the compliant material negotiates the radius it becomes stretched due to the increase in path length. This causes an inward force on the pulleys, resulting in a pinching action. In addition as the compliant surface is thicker than the abrasive surface, a differential velocity occurs between the upper and lower belts around the pulleys. The linear part of the belts which act to hold the workpiece during manipulation do not however suffer from this effect.

Figure 3.12 contains a summary of results obtained during an investigation into the compliant characteristics of selected foams, additional information is contained in Appendix C. The experiment measures the repulsive force generated by the foams for a given surface deflection. It can be seen from Figure 3.12 that the foams allow for deflections to be made close to the foam's actual thickness. The Nercoprene and Neoprene based foams offer an almost linear response over the first 1.75mm of deflection which relates approximately to a compressive force of 5N, (close to that of the maximum load exerted by the Autoscan calculated previously). The support surface was constructed using Nercoprene foam due to its extra thickness, which would allow for the better handling of compound parts in later experiments. It also had the benefit of a self-adhesive backing, making bonding to the Synchroflex belts particularly easy.

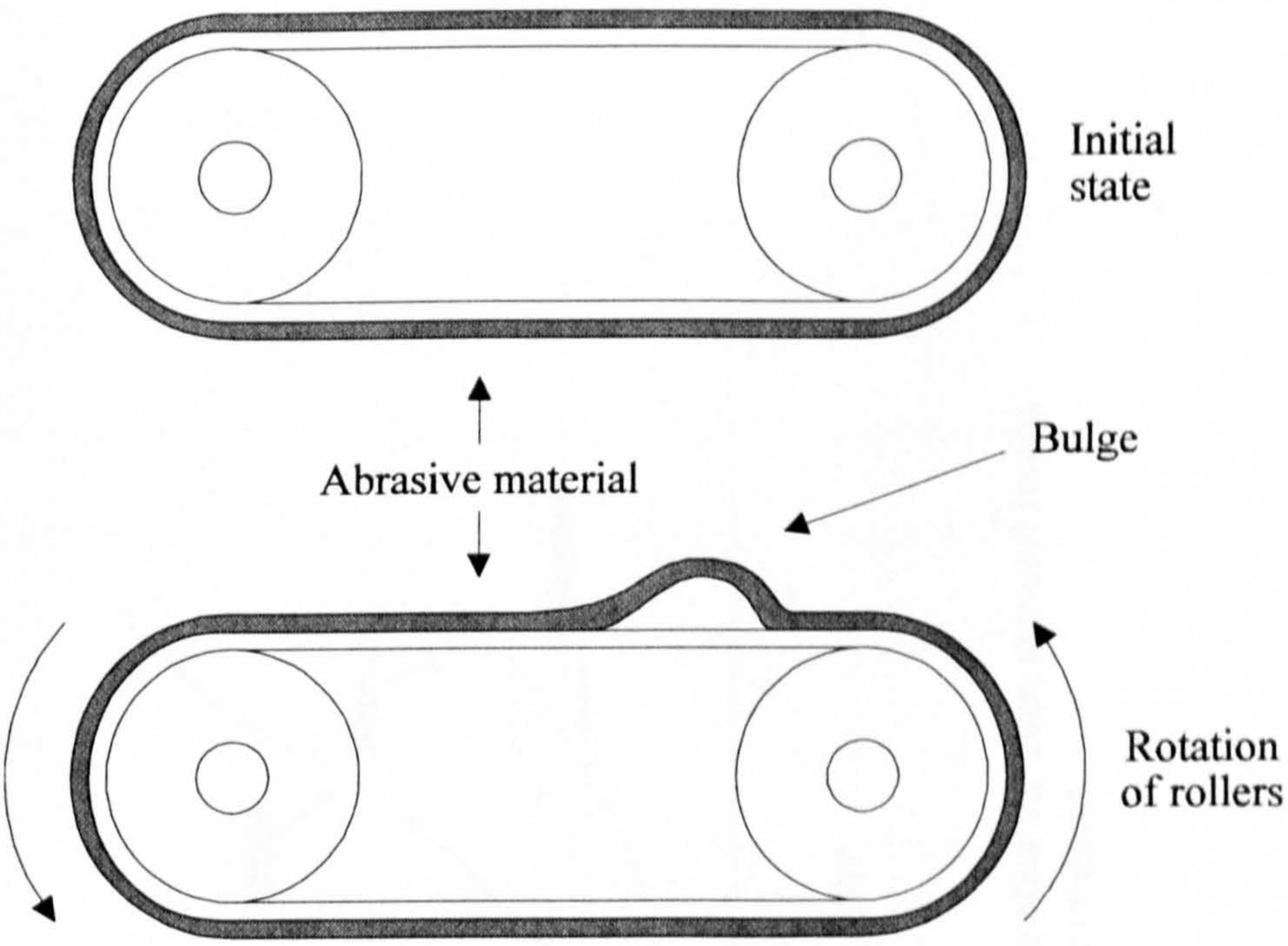

a) Substrate peeling

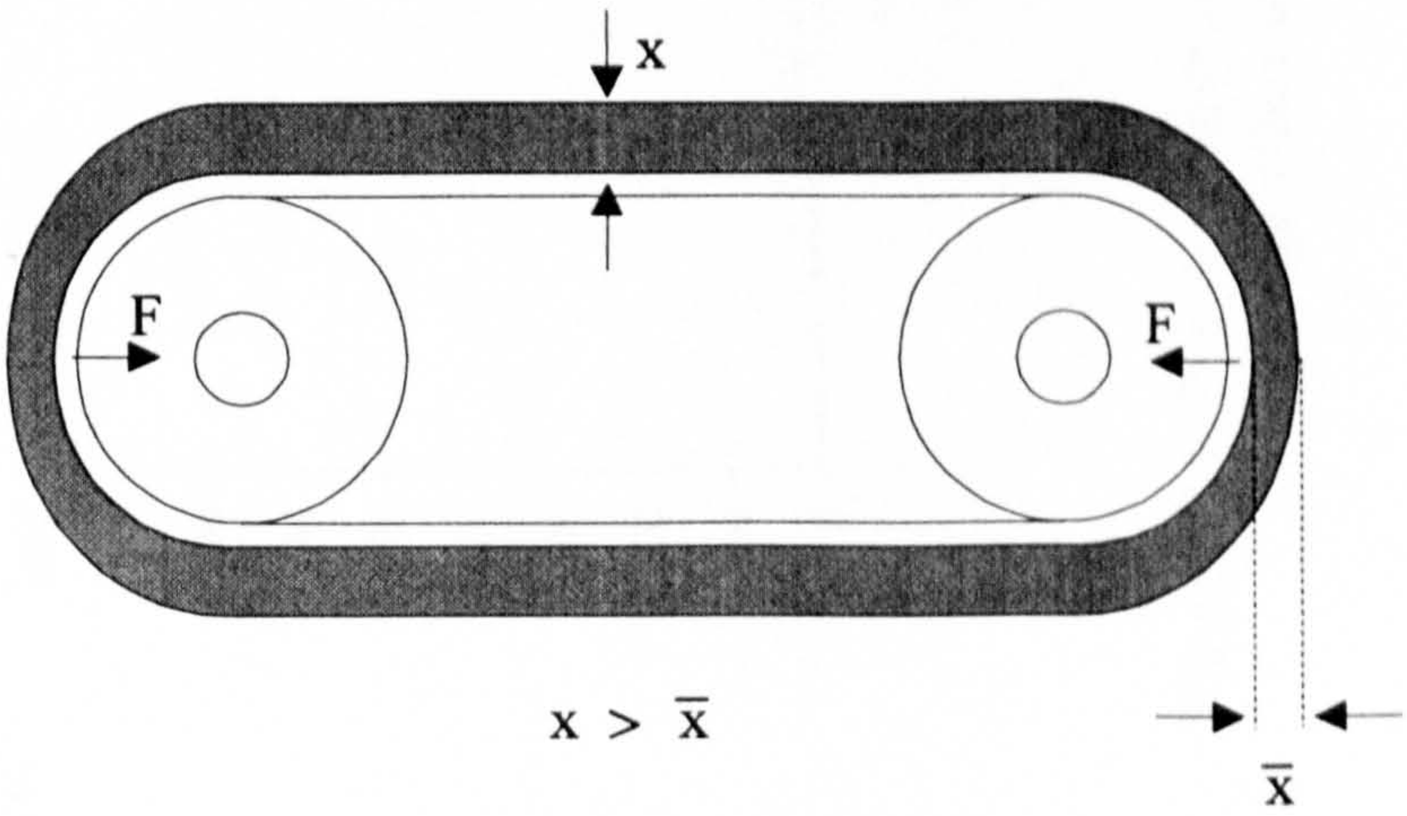

b) Effect of compliance

Figure 3.11. Effects of compound belt construction.

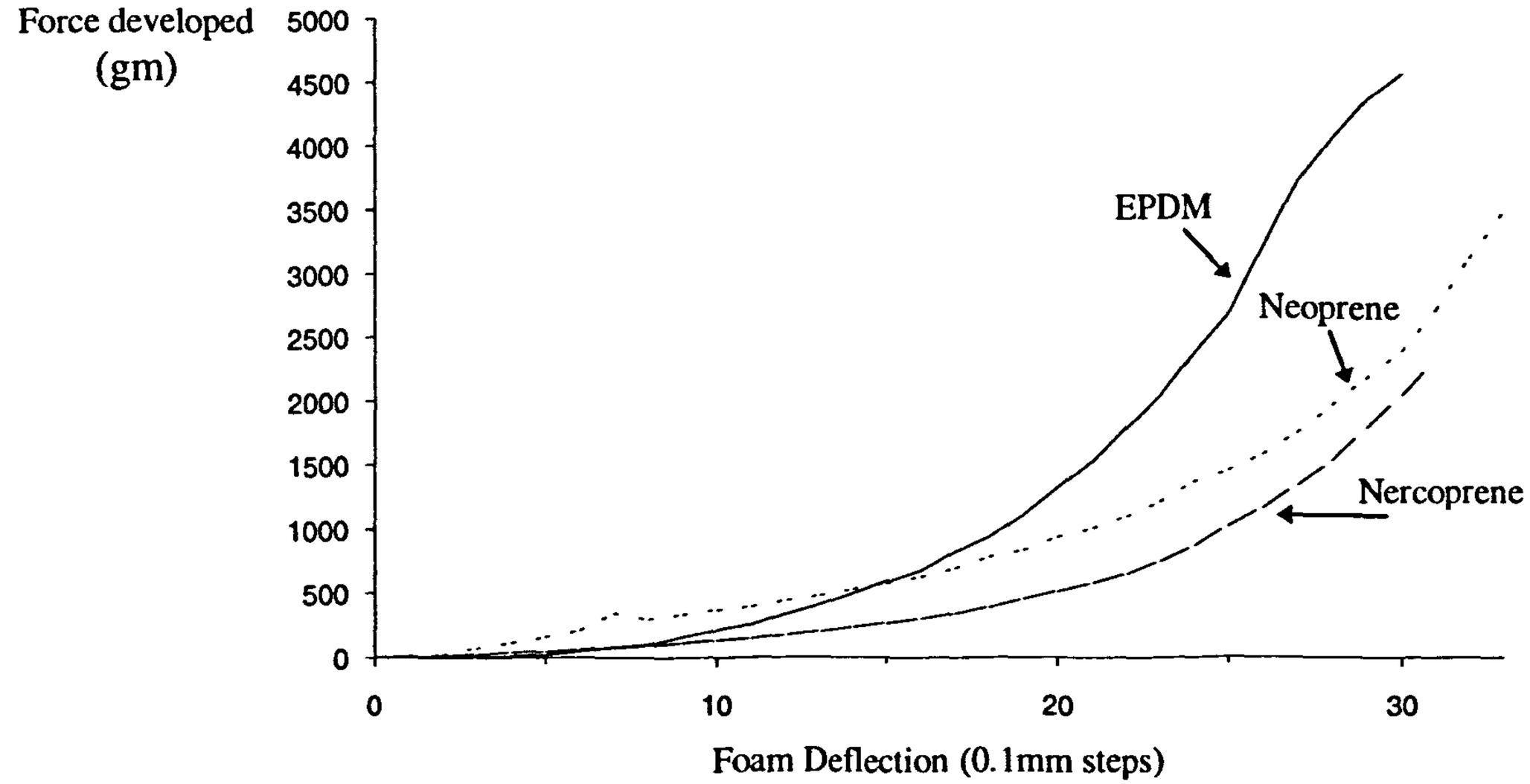

Figure 3.12 Plot showing the compression characteristics for three selected foams (average values obtained from 5 measurements).

3.5.4 Belt tensioning.

The Synchroflex timing belts used as the substrate for both the support and drive surfaces are made to within a circumference tolerance of ±0.4mm resulting in a possible error of 0.8mm between any two belts. To overcome this and ensure that no undesired movement can occur tensioning must be provided. Conventional tensioning mechanisms are cumbersome and would be difficult to apply to a situation where 80 belts are in close proximity to each other. As a result a mechanism of compliant tensioning was developed. This mechanism replaces the free pulleys with ones with a compliant material around their centre, Figure 3.13. The belt compresses the material, whose reaction forces pushes back, tensioning the belt. Positive drive is not lost as the belt is taunt at all times with the second pulley providing the belt rotational drive. Pulleys were constructed from a PTFE substrate with an EPDM foam providing the compliant medium.

The belts remain well tensioned even after considerable use as the belt teeth eventually bed into the compliant material forming a tooth gear of the ideal dimensions. A side effect of tensioning the belts is an increase in the power requirement needed to drive them successfully. To overcome this problem a second motor was modified so that it could be mechanically linked to the drive motor in order to provide the additional power required.

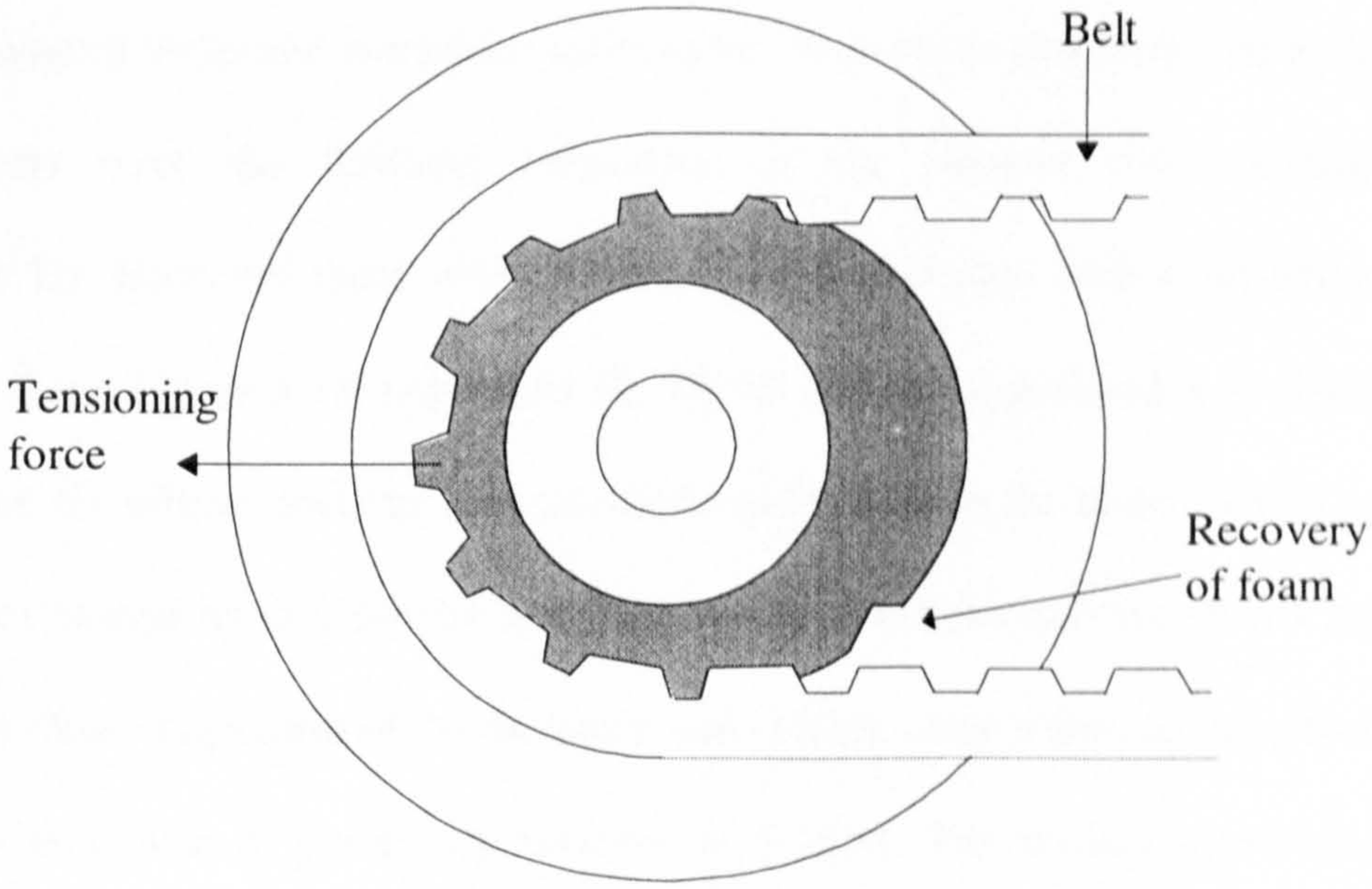

Figure 3.13 Cross-section through a compliant tensioned pulley.

3.6 System evaluation.

In order to evaluate the narrow belt configuration with an abrasive driving surface and a neoprene compliant upper support substrate the Autoscan was configured to enable a number of experiments to be performed. Appendix D, defines the methods used to measure undesired workpiece movement. These belts demonstrated a significant improvement over the handling properties of the original roller configuration, (Appendix E). However there were still significant positional errors occurring of the order of 1-2mm, Figure 3.14, (Appendix F). This is due to a combination of slip and drift effects. The slip effects could be seen as small scuff marks on the under side of a number of test discs caused by the abrasive action of the drive surface moving relative to that of the disc. A closer inspection of the carborundum surface using a microscope showed that it was not as coarse or potentially invasive as desired. The surface area between the carborundum particles was in fact filled with adhesive which had the effect of smoothing the surface. What is needed is a mechanism of penetrating the fleshy nap side of the leather without damaging the cosmetic characteristics of the grain surface. In order to achieve this a redesign using a pin array is to be considered.

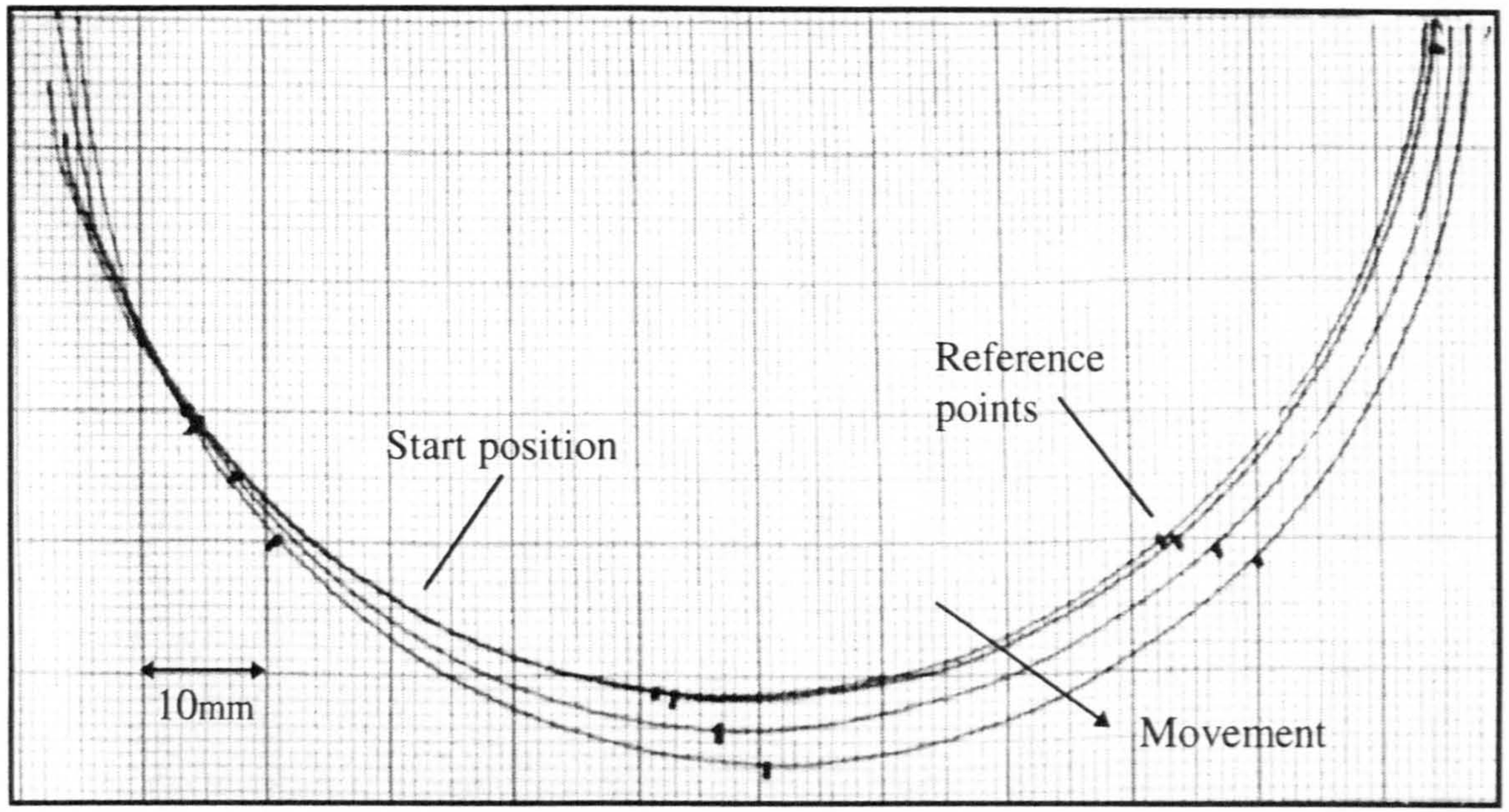

Figure 3.14 Example of movement observed when using Carborundum coated belts. Tested using N.Touts quick method.

3.7 Pinned belts

The investigation into the properties of leather demonstrated the complex nature of the material and highlighted a number of the problems that were later manifested in positional errors occurring during manipulation. If these problems were to be overcome and positional accuracy assured a method of overcoming the material properties, chiefly that of the collagen fibres, is required. The Autoscan had demonstrated at an early stage that manipulation could be achieved using abrasive rollers and later by the use of carborundum belts, which by their very nature bed into the nap of the leather. This proved that the idea for a semi-intrusive drive medium was one that could potentially provide accurate manipulation. What was needed was to take this idea one step further and use a series of short pins which are capable of piercing their way into the nap of the leather as opposed to bedding into the nap surface. The concern is that the grain surface should not be damaged. As a result a quick experiment was conducted to observe the effects of a pin array on leather strips, before continuing.

3.7.1 Effect of a pin array on sample leathers.

In order to test the effects of pins on a number of leathers a sample pin array was constructed by punching a series of staples through a leather substrate. The substrate was then glued to a wooden surface to both secure the pins and to provide a solid surface. Each of the protruding legs of the staples were then cut short at an angle of approximately 45° to leave a short sharp pin about 0.3-0.5mm high. Figure 3.15.

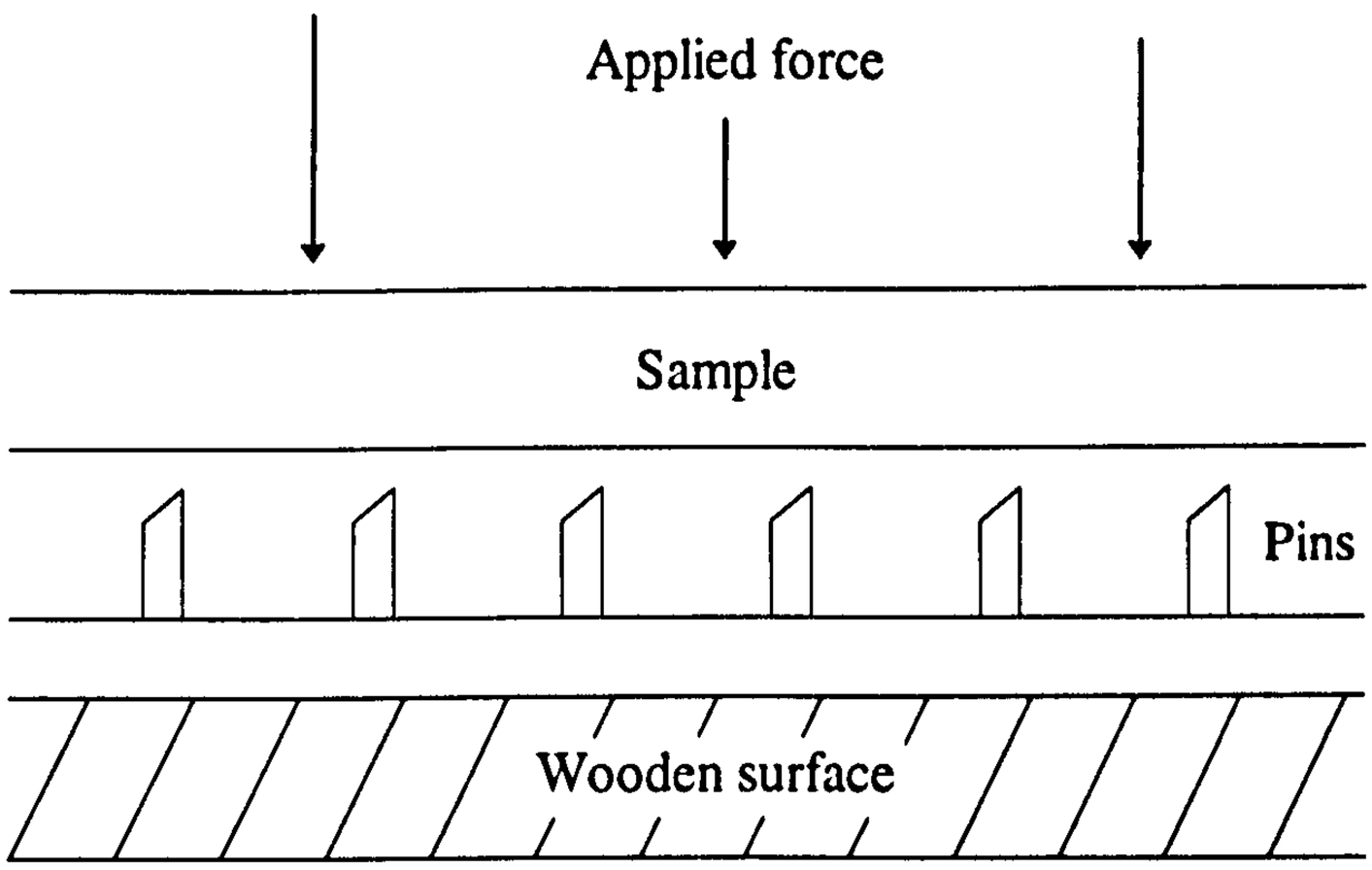

Figure 3.15 Quick test of pins on sample leathers.

The staples were inserted approximately 10mm apart in order to allow the sample leather to dip between pin pairs as opposed to a higher density which would cause the sample to ride on the tops of the pins. This ensured that the pins bedded well in to the samples.

A number of leather samples were cut into strips 150mm x 20mm and in turn placed onto the pin array nap side down. Pressure was applied to the grain surface forcing the sample to bed into the pins which were 'wiggled' to ensure the pins penetrated into the leather sample. A number of samples showed slight marking where the pins entered the nap and one very thin stiff leather displayed evidence of the pins position on the grain surface in the form of small bumps. However in all instances the leather recovered from these effects after brushing or flexing. The force was applied by

hand pressing hard down onto a cardboard medium placed on the sample. These results encouraged further investigations to be made into the holding forces required to prevent slip on a pinned belt.

3.7.2 Determination of required holding force for pinned belts.

It can be hypothesised that the pinned belts will hold the workpieces far more rigidly for a given holding force/pressure than for previous materials such as the carborundum belts. However to prove this a series of measurements were taken using a cross-section of leathers in order to determine the holding properties of the pins when an adverse external force is applied. Appendix C.3, describes the experiment and contains the results obtained. A summary of the results can be seen in Figure 3.16.

Recalling from Section 3.5.1 that a possible pulling force of 5.2N can occur during the operation of the Autoscan, it can be seen from Figure 3.16 that the corresponding minimum holding force is less than 1Kg, or approximately 10N. Consequently a required holding force of 1.5Kg, (15N), will be adopted to allow for a reasonable safety margin. With reference to Appendix C and Figure 3.12 it can be seen that the Nercoprene foam offers excellent compliant properties and that for a holding force in the order of 15N, (applied over an 8mm diameter area), a compression of approximately 2.7mm is obtained.

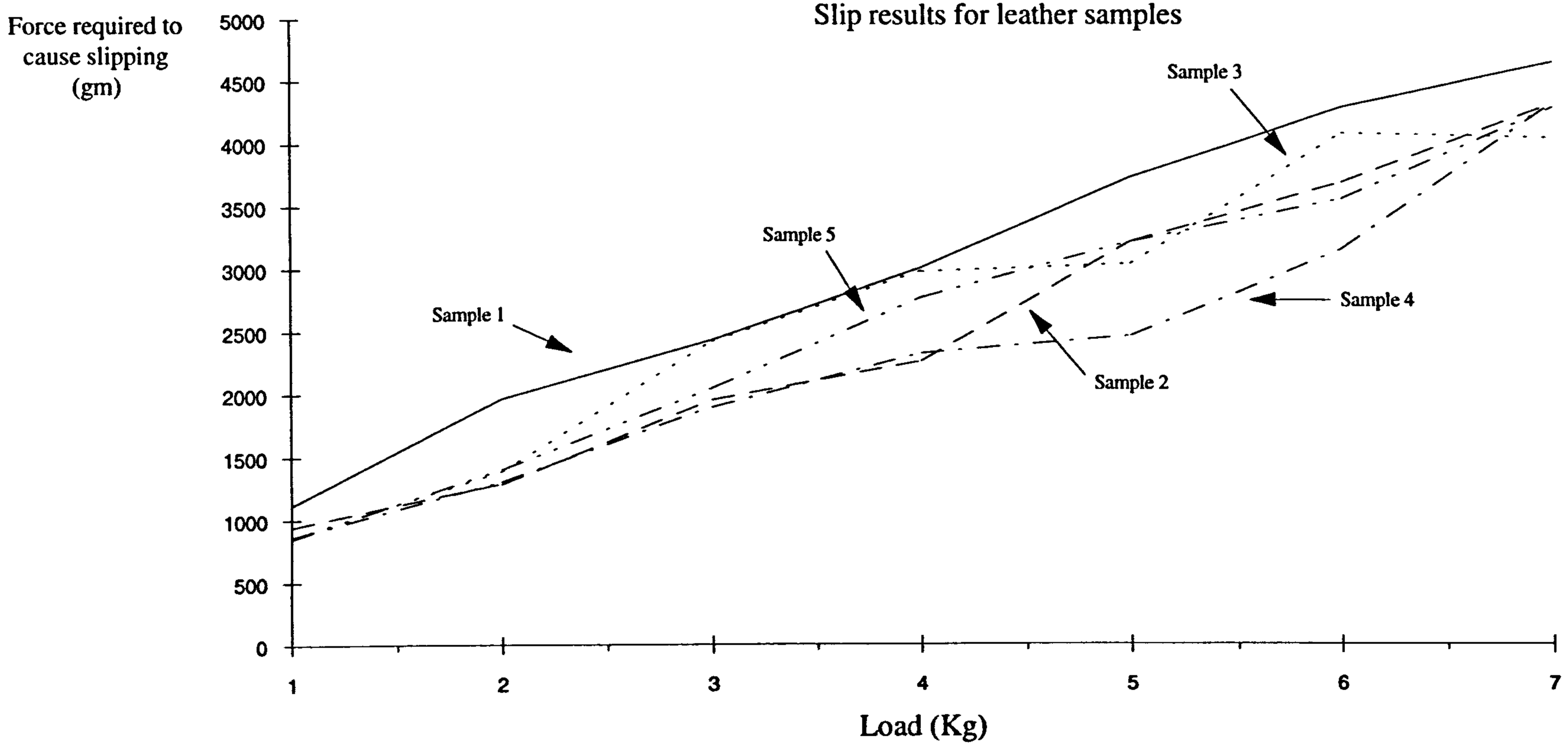

Figure 3.16 Slip vs applied force for leather samples on a pinned belt.

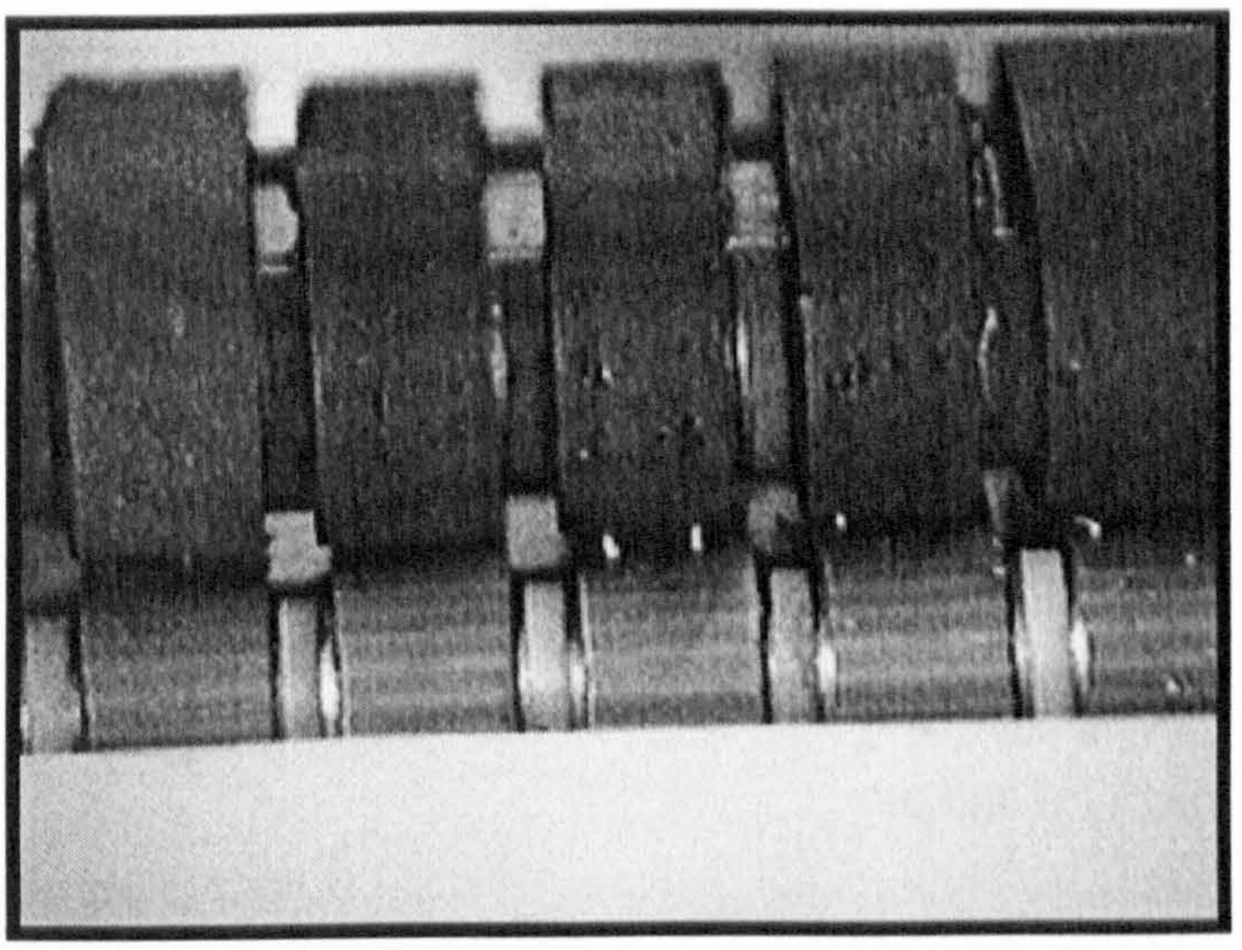

a) The narrow belt arangement and the PTFE spacers

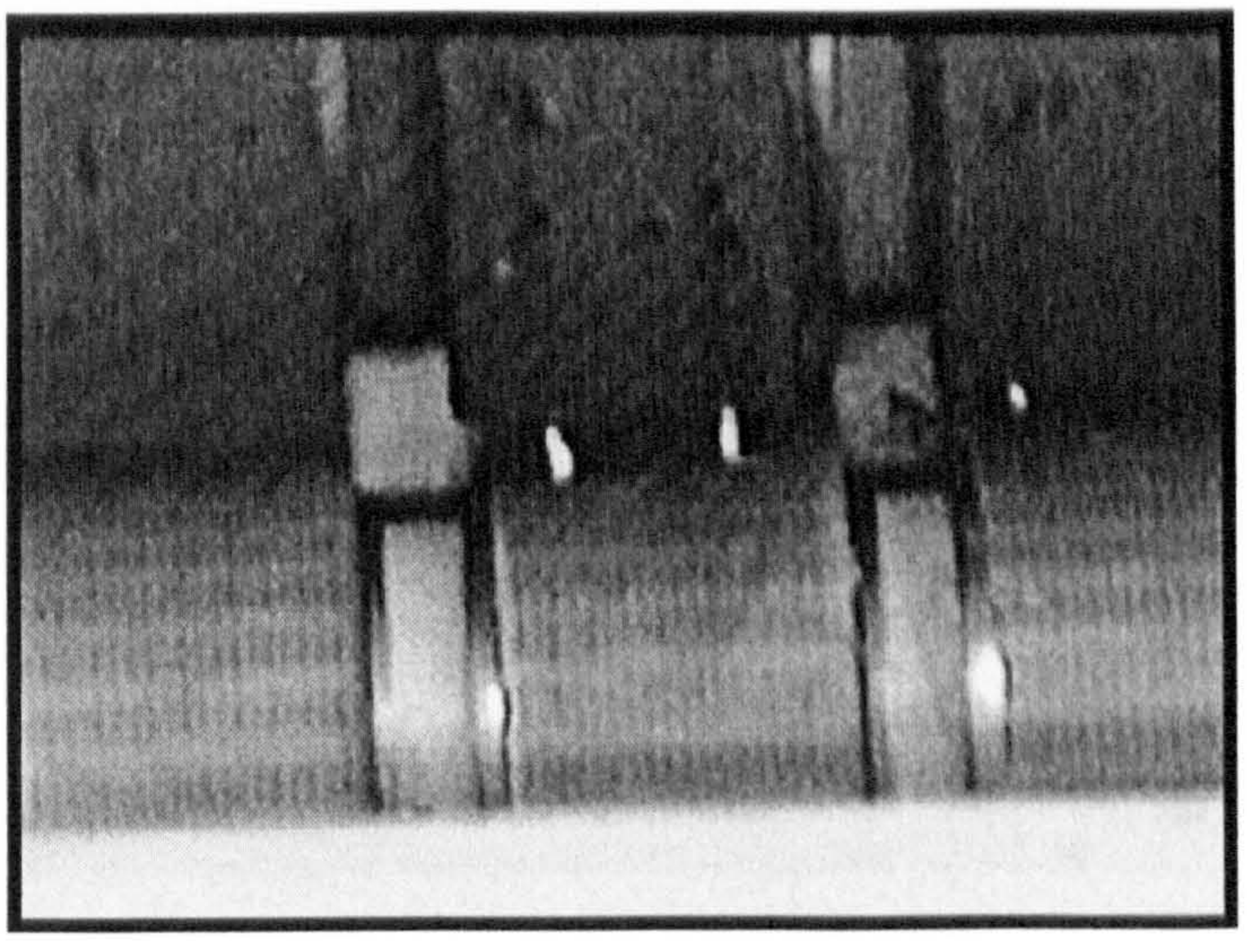

b) Close up showing the pins on the lower belt surface

Plate 6. Thre Autoscan configured for testing the compliant and pinned belt combination.

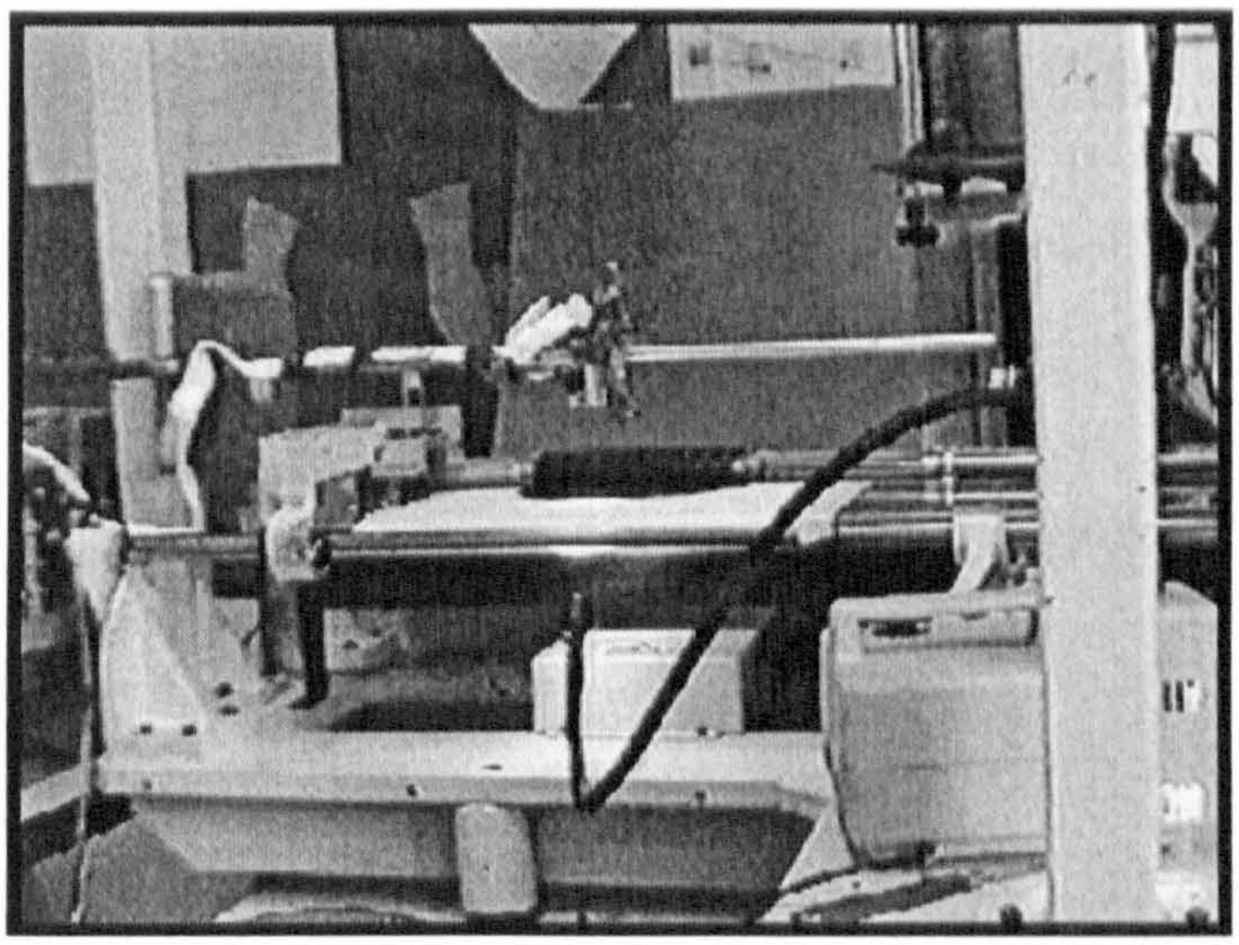

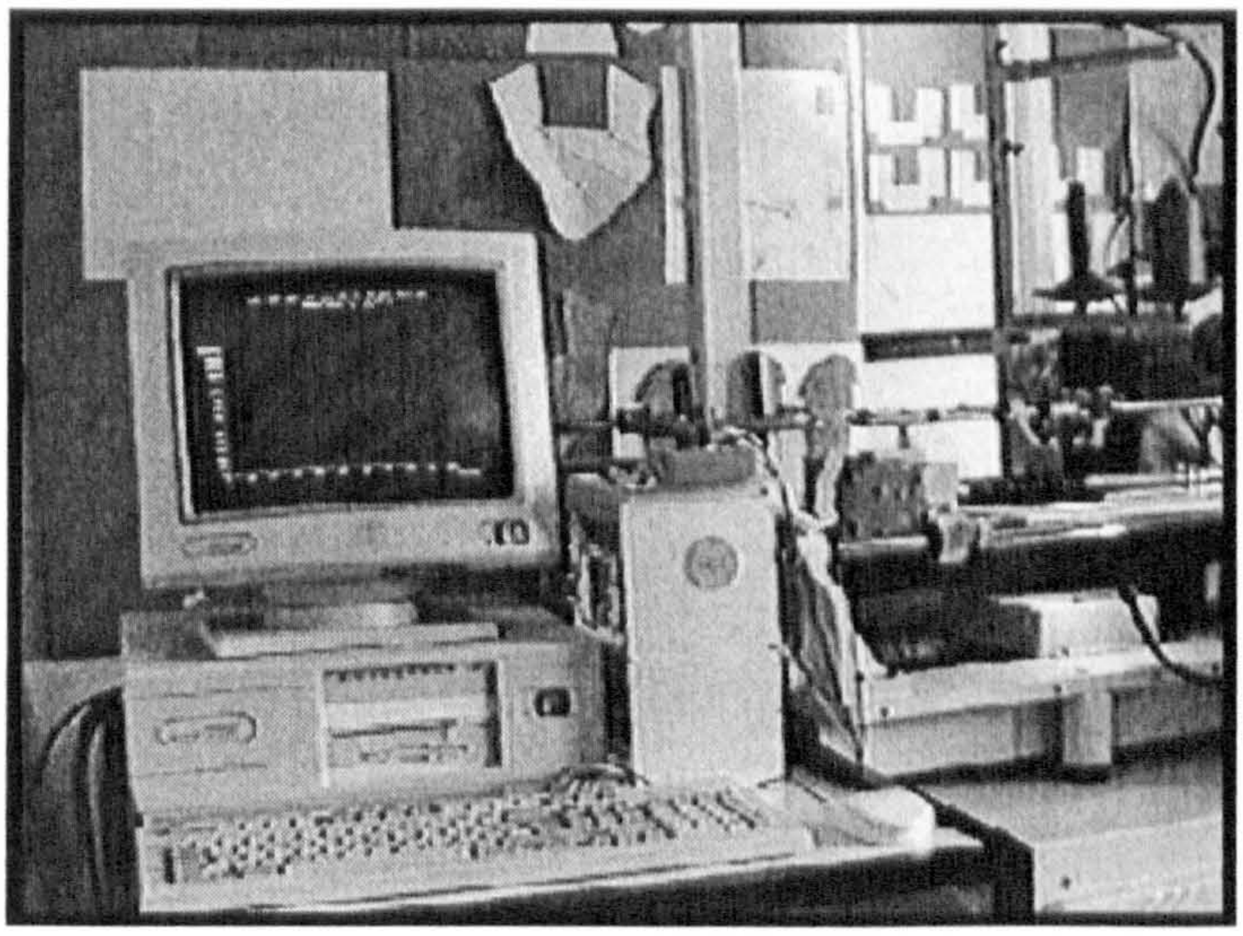

Plate 7. General views of the Autoscan during testing.

The drive belts on the Autoscan were replaced by pinned belts. The pins were made by inserting staples through the belts between the teeth approximately 10mm apart. The pins were then bent as in Figure 3.17 to ensure they were firmly secured into the belt substrate.

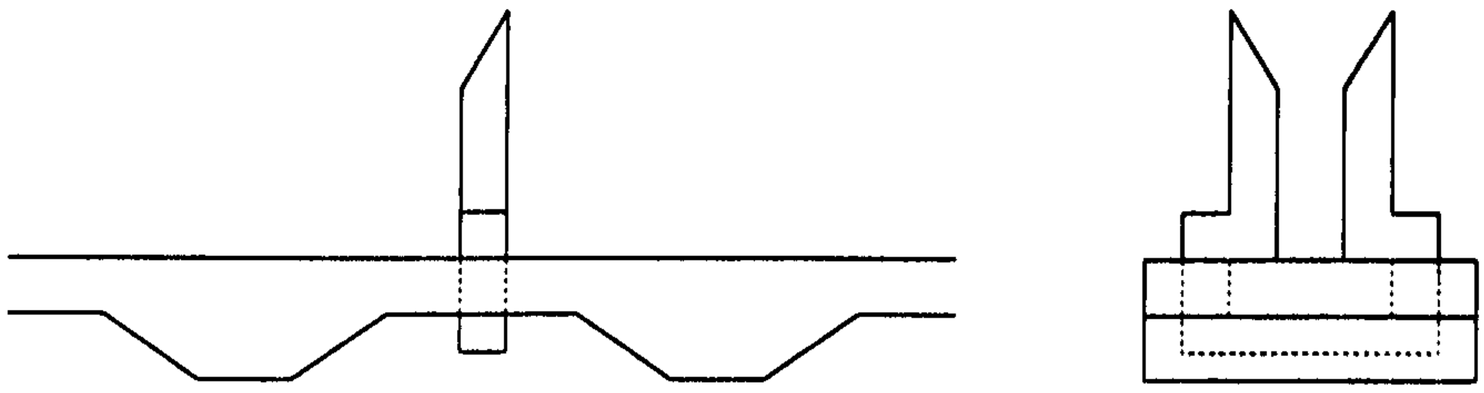

Figure 3.17 Pinned belt construction.

Plate 6. shows a head on view of the assembled configuration of pinned and compliant belts actually used on the Autoscan during evaluation.

Plate 7. contains general views of the Autoscan configured for measuring handling performances using the line-scan camera method.

3.7.3 Measurement of workpiece movement for pinned belts.

Once the new belts were assembled on the Autoscan and performance measurements taken it soon became apparent that no movement could be detected using either the method employed by D.L.Smith[1] or N.Tout[42]. Consequently an alternative mechanism for measuring the movement of a sample workpiece during testing was required. This resulted in the development of a line-scan camera system which provided an excellent method by which to monitor the edge position without having to stop the machine.

The camera, a 128 pixel line-scan type is capable of being focused to give a resolution of 0.078mm per pixel. This allows for highly accurate measurements to be taken rapidly and in a fully automated manner.

In order to evaluate the pin array belts to a high degree of confidence 9, (5 flat and 4 compound), sets of samples were tested. This resulted in a total of 63 different parts, covering a wide range of leathers, suede, synthetics and shoe components being tested. Each sample underwent 100 cycles, each cycle consisting of 2 x 25mm movements. A reversal of direction was made as the end of the first movement so that the second movement should restore the sample to its original position. A measurement was taken by the camera at the end of each cycle so that a record could be made of the sample's behaviour. The full procedure is described in Appendix D. Table 3.1 shows the types of samples used.

Example measurements results, taken using the line-scan camera can be seen in Appendices G-H for flat and compound parts respectively.

Symbol	Type	Samples	Description
DWFL	Flat	17	Leather discs 170mm diameter
DWF	Flat	7	Leather discs 110mm diameter
DWFS	Flat	6	Suede discs 170mm diameter
DWFI	Flat	9	Imitation leather discs 170mm diameter
INSOLE	Flat	8	Suede insole shoe components
DWCR	2.5D	5	Compound part with long straight step
DWCS	2.5D	5	Compound square part with straight step
DWCC	2.5D	5	Compound part complex step profile
Brogue	2.5D	1	Compound actual shoe upper
	Total	63	

Table 3.1 Samples used during the performance analysis of pin array belts using the line-scan camera method.

3.7.4 Movement results for flat samples.

The implementation of the line-scan camera allowed for the degree of slip to be accurately measured for large number of cycles without the need to stop the machine. Figure 3.18a shows a typical result for a flat component, whilst Figure 3.18b shows the slip measured per cycle. It can be seen that there is no net movement over the 100 cycles the sample was tested. When movement does occur, it was observed that the edge of the component was 'flapping' as it changed direction between cycles, Figure 3.19.

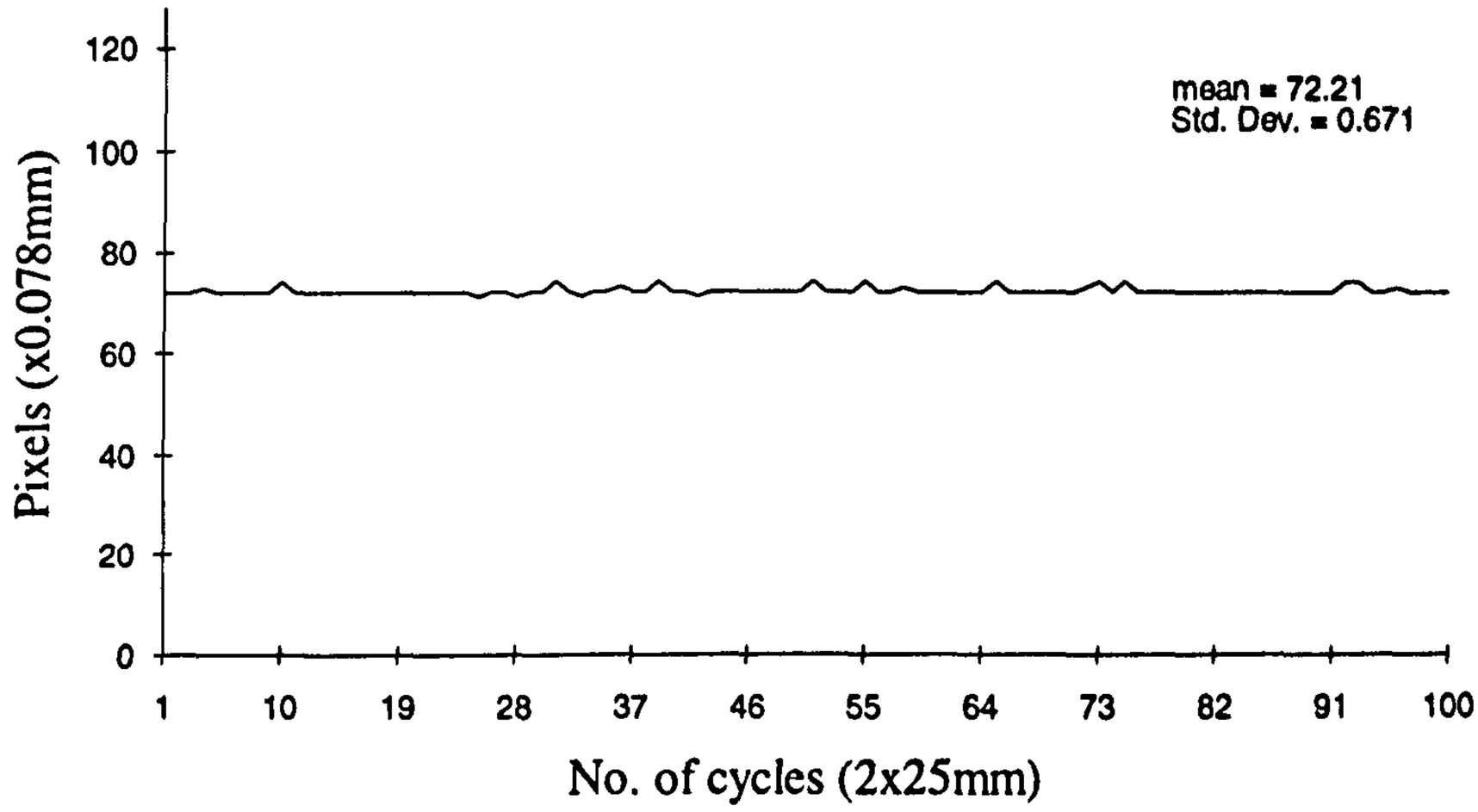

a) A typical example of results obtained for a flat leather disk.

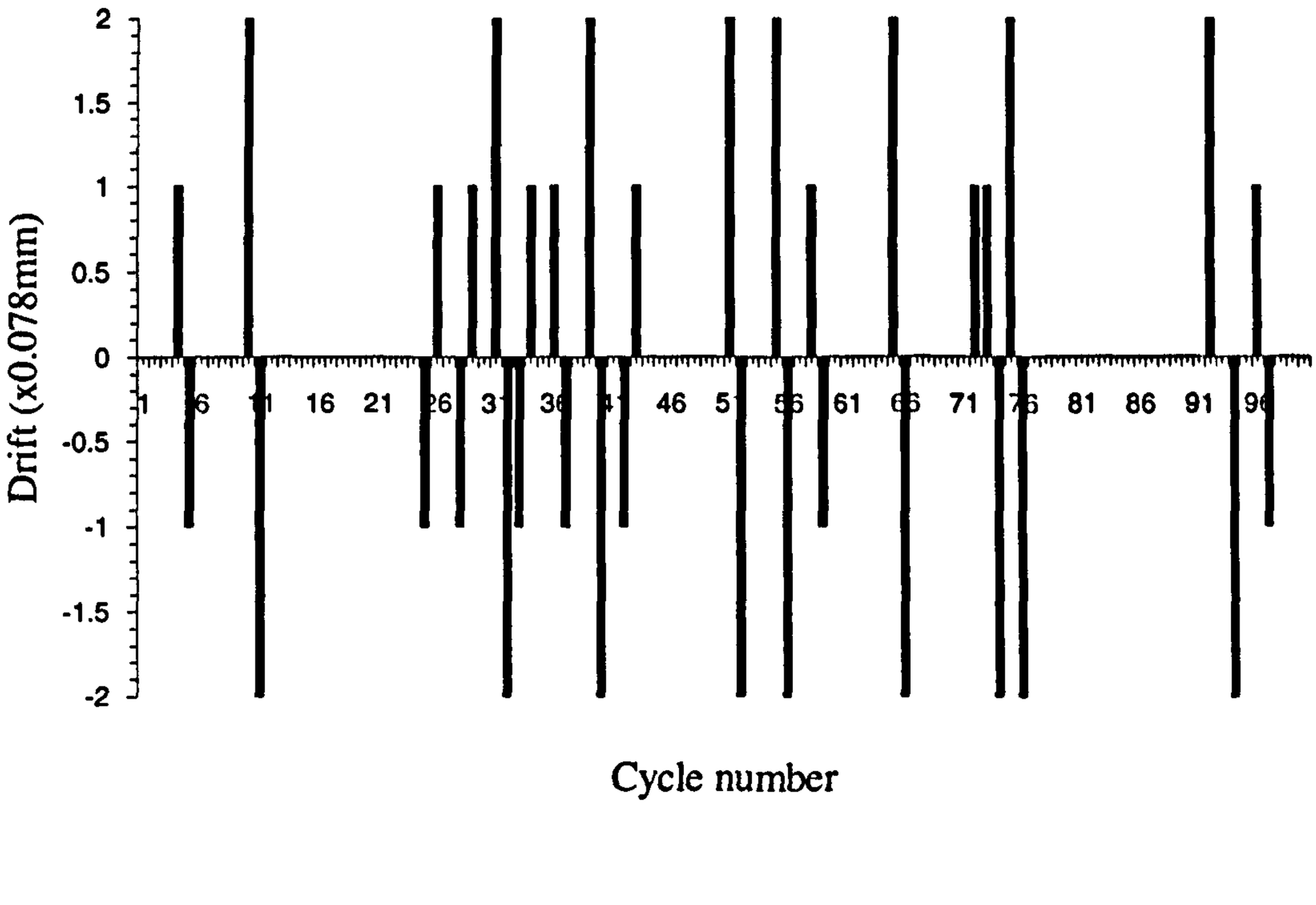

b) Degree of movement measured per cycle

Figure 3.18 Typical movement results measured by the line-scan camera for sample DWFL8.

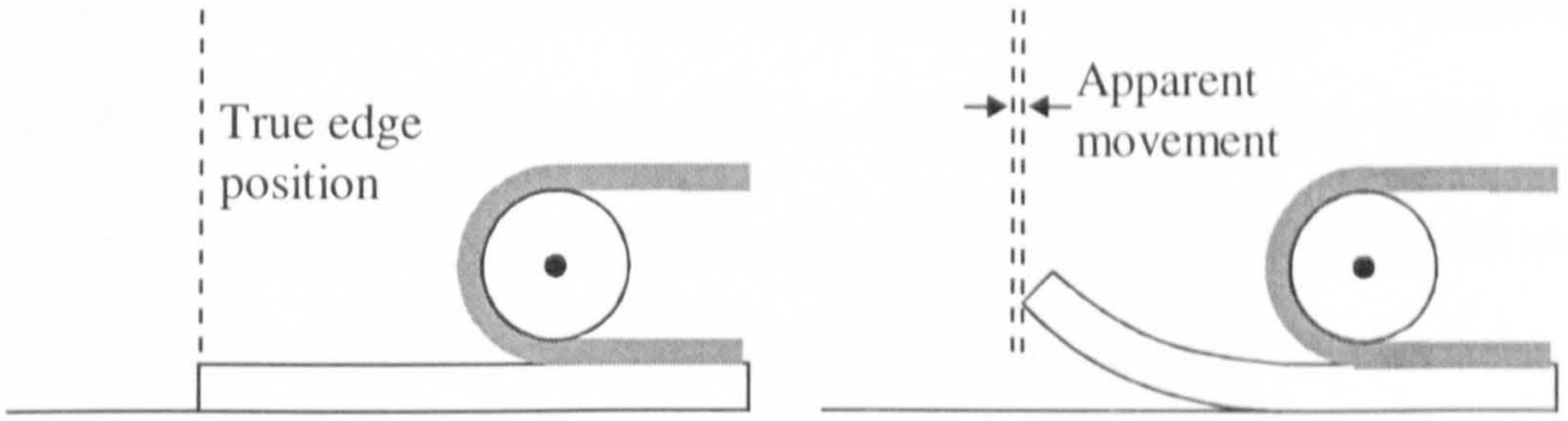

Figure 3.19 Edge flapping causing the appearance of slip.

This results in an apparent movement in the edge of the part being detected by the camera. However on subsequent cycles the edge lies flat producing a true edge reading. Figure 3.18b shows this effect over the test cycles. Appendix G, Figure G.6 shows the symmetrical positional error distribution for flat parts, about zero, demonstrating this effect across all the flat parts tested.

For each of the flat sample types the sample mean, ($\bar{x}_{flat}$), and standard deviation, (σ_{flat}), can be calculated based on the measured movement per cycle. Table 3.2.

	Sample				
	DWFL	DWF	DWFI	DWFS	INSOLE
$\bar{x}_{flat}$	0	0	0	0	0.22
σ_{flat}	0.52	0.30	0.44	0.67	1.78

Table 3.2. Movement figures obtained for Flat samples

These figures demonstrate a high degree of handling ability for pinned belts with positional accuracy being maintained across the range of samples. Indeed approximately 90% of measurements show no movement of the sample at all.

The INSOLE components exhibit a higher degree of positional error than any of the other flat samples. This is largely due to their limp nature being unable to be supported between the front and rear belt systems and not due to workpiece movement within the handling mechanism. Appendix G, describes this in greater detail.

3.7.5 Movement results for compound samples.

The object for the research was to develop a handling mechanism capable of manipulating not only flat parts for decorative stitching but also compound 2.5D parts in order to perform constructional stitching. To test the handling ability of the pin array belts on compound parts a number of test samples, Appendix D, were constructed and manipulated in the same manner as for the flat components.

For each of the sample types, the sample mean, ($\bar{x}_{compound}$), and standard deviation, ($\sigma_{compound}$), can be calculated based on the measured movement per cycle. Table 3.3.

	Sample			
	DWCC	DWCR	DWCS	BROGUE
$\bar{x}_{compound}$	0	0	0	0.10
$\sigma_{compound}$	0.22	0	0.20	1.52

Table 3.3. Slip figures obtained for Compound samples.

These figures are very similar to those obtained for flat parts, indeed they are slightly better. This is most likely due to the nature of the materials from which the

compound parts were made. All the parts were made from high quality leathers and consequently did not cover the range of material properties tested for flat parts.

Once again, approximately 90% of cycles show no movement of the sample demonstrating that the handling mechanism is equally capable of handling compound and flat parts.

The only movement that can be seen in the results, is for the brogue shoe sample. This is believed to be due to its large and complex shape catching on the support table early in the testing cycles, at certain orientations. Once the pins have become bedded into the nap of the sample, after 5 to 10 cycles, this early handling error can be seen to be eliminated, Figure 3.20. Appendix H, contains additional examples for the other compound parts tested as well as further examples of tests performed on the brogue component showing how the apparent handling error can be eliminated at certain orientations.

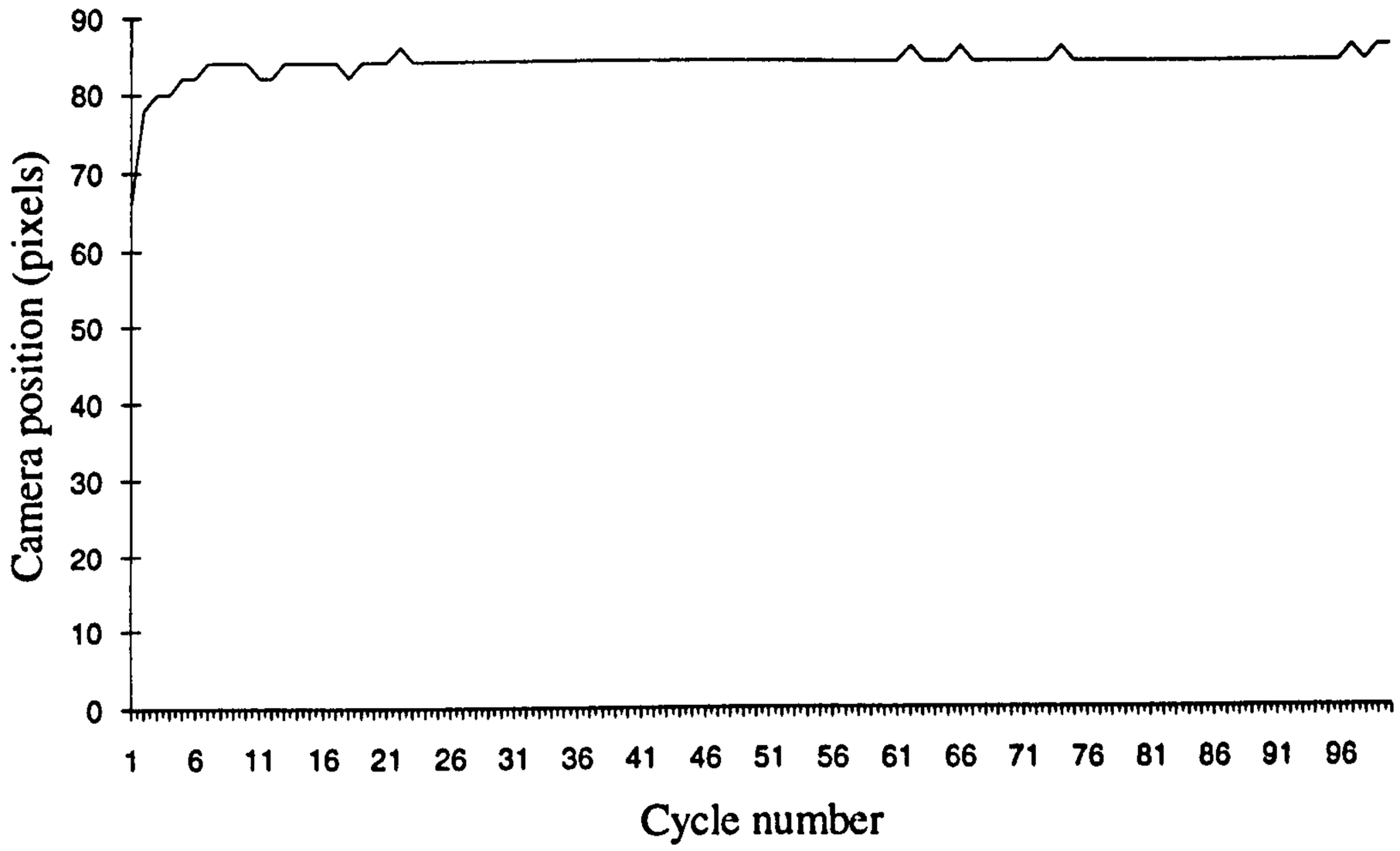

a) A worst case result obtained for a BROGUE shoe component.

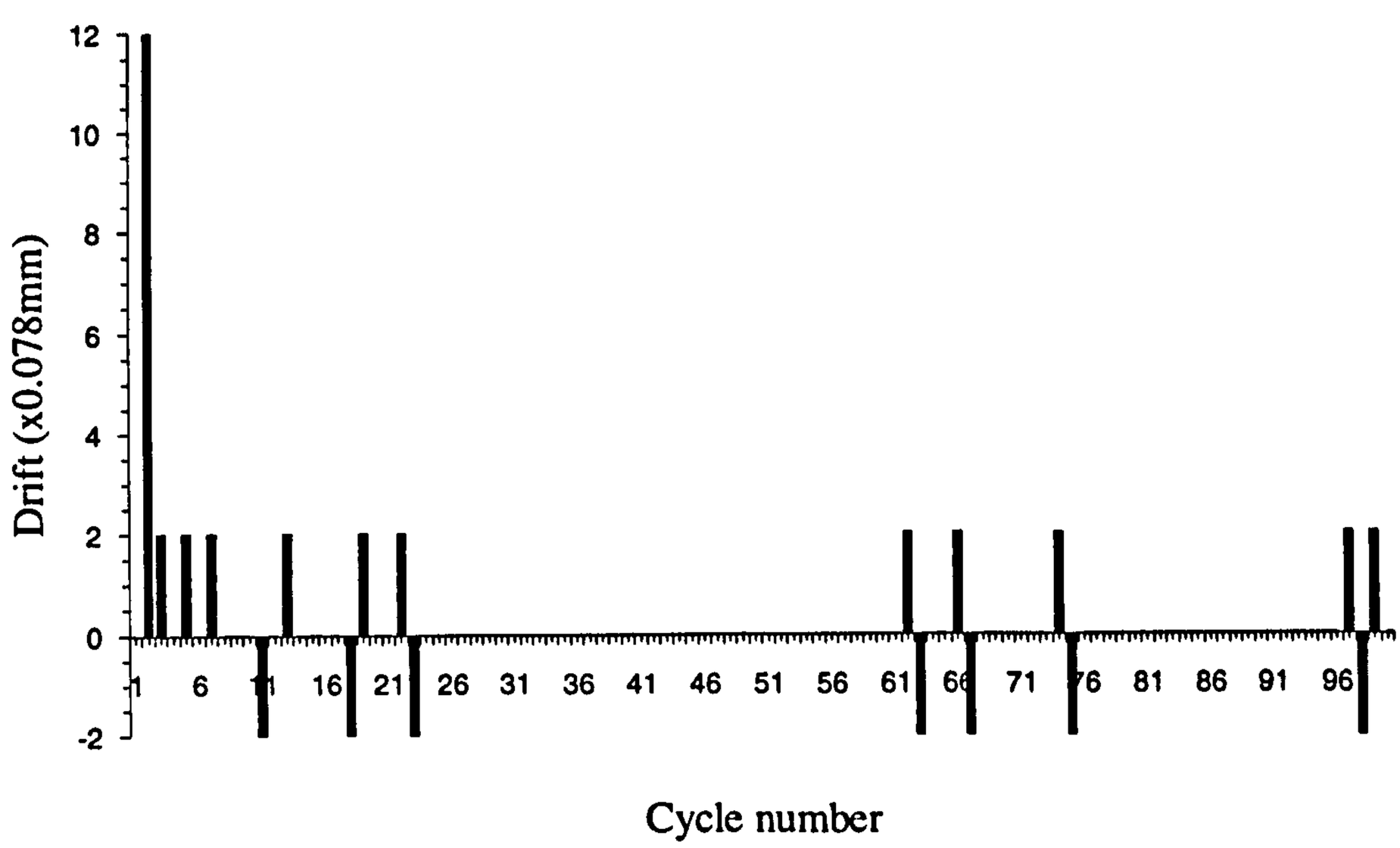

b) Degree of movement measured per cycle

Figure 3.20 Typical movement measurements obtained by the line-scan camera for sample BROGUE shoe component.

3.8 Conclusions on leather handling.

The Carborundum coated belts were able to bed into the nap of the leather but were not capable of penetrating into the Collagen layer, and as such were only partially able to hold the workpieces during manipulation. Results obtained using this type of abrasive material bonded to the belts, although not in themselves providing a solution to the problems of drift and slip did however demonstrate the validity of a semi-intrusive medium. The plurality of pins provided a mechanism by which the driving surface could physically lock itself into the workpiece and as such eliminate the material properties from causing movement during manipulation. The results in Appendices G-H, and described previously show this to be the case across a wide spectrum of leathers and synthetics. However the most encouraging results were gained from the compound parts which had considerable variations in sample thickness as well as presenting significant step functions, (>2mm), to the handling mechanism.

Defining the population of flat parts to be all flat parts tested and similarly, the population of compound parts to be all compound parts tested, it can be seen from Figure 3.21, that the statistical properties of mean movement and standard deviation for the two populations are very similar. Appendix I calculates that in order to be 95% confident that a cycle will not result in a positional error of greater than 0.2mm from the population mean, for both flat and compound parts, only three samples, (cycles), need be performed. The level of 95% confidence was stipulated by D.C.Reedman[17] for industry acceptance. This demonstrates a high degree of positional accuracy by the handling mechanism, regardless of workpiece type. It is however, important to recognise the

limitations of the handling mechanism that were demonstrated by the flat shoe insole components and the complex compound brogue workpieces.

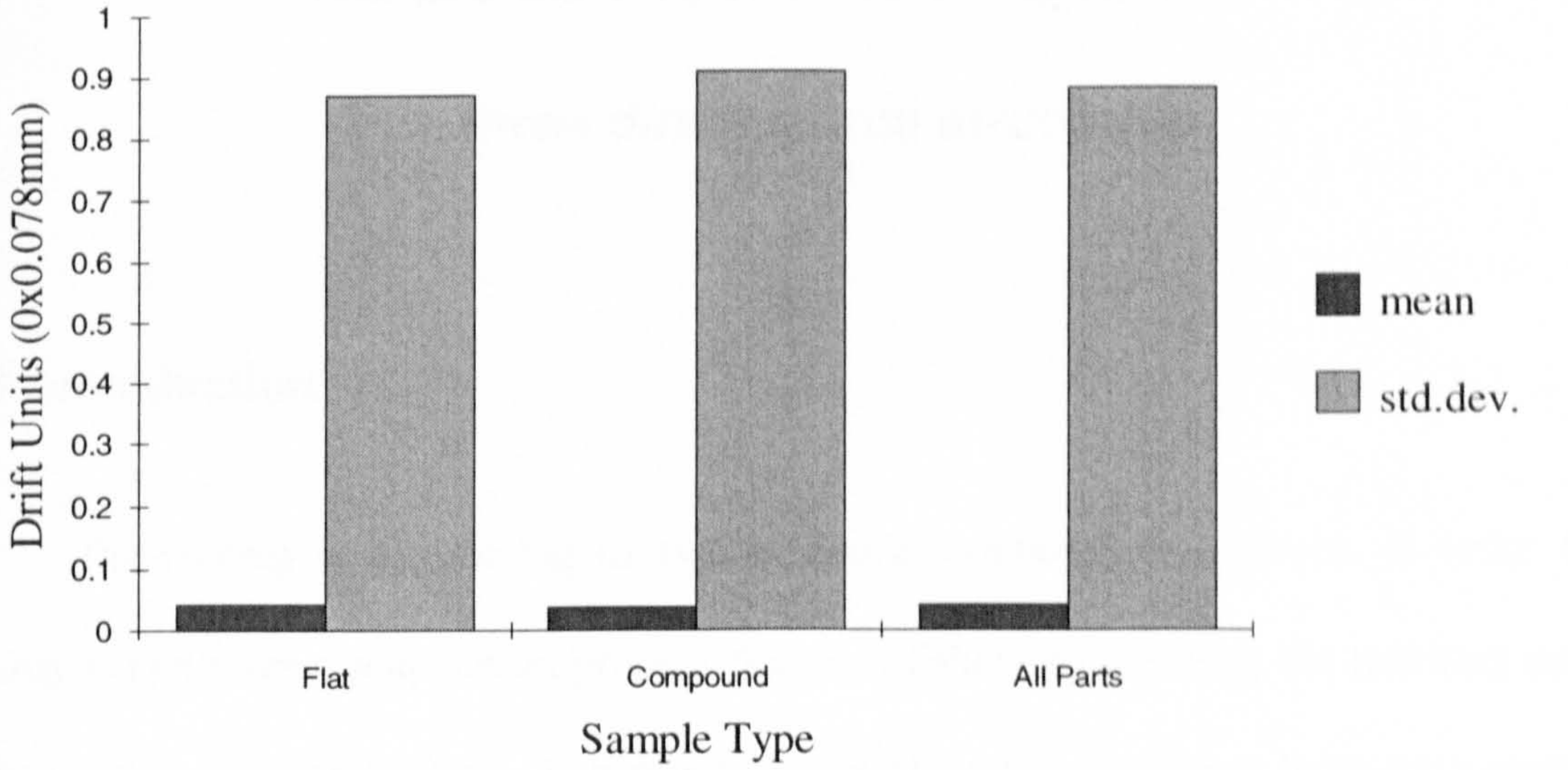

Figure 3.21 Statistical comparison of flat and compound parts tested.

Further developments will need to be made into determining the optimum handling area and support table dimensions in order to overcome these limitations. The technology transfer of the pin array type belts has been made from Hull University to B.U.S.M Leicester by the author. The mechanism is scheduled for evaluation and further development on a fully operational Autoscan at some point in the future, depending on commercial pressures.

The idea of implementing a belt mechanism has already been implemented at B.U.S.M using a single wide belts to replace each original roller set. These were initially subject to local distortions causing "soft spots" on the belt as well as severe problems with the power required to drive them. The belts were coated with small Carborundum particles and produced reasonable results for the majority of workpieces. It is however still very limited with regards to the constructional stitching of compound parts.

Chapter 4

The pre-tacking of shoe components into three dimensional structures

4.0 Introduction.

Pre-tacking is the joining of two or more individual workpieces, in order to greatly simplify the manipulation process that may follow by allowing the resultant part to be treated as a single object. This process generally involves using a temporary means to form a join, although a more permanent mechanism can be used if required. Traditionally pre-tacking has been used in garment manufacture where the limp nature of fabrics makes handling particularly difficult. The join is typically formed by the implementation of loose stitches, these stitches being removed after subsequent operations have formed a permanent bond between the components.

Pre-tacking is generally regarded as a manual operation as it requires great dexterity and adds the overhead of an additional operation to the assembly process. As a consequence modern manufacturing processes have largely eliminated the need for pre-tacking by altering garment design and by the introduction of task specific machinery. This chapter aims to outline the operations and principles behind the pre-tacking of separate leather components for shoe upper assembly. These principles will then be applied in a proposal for pre-tacking a number of 2-D, components in such a manner that the resultant, compound, part is three dimensional.

4.1 Pre-tacking of lamina.

To the best of the author's knowledge automated pre-tacking has not been applied to shoe manufacture in any commercial machine. E. Adams[2] produced a prototype 2-D pre-tacking system at the University of Hull in conjunction with B.U.S.M in 1990. Here the shoe components to be joined had previously had a re-activatable adhesive applied to the contacting surfaces. The components were then selected, correctly orientated and the adhesive re-activated. By pressing the components together they became joined and resulted in a workpiece that could be treated as a single part.

The case for using adhesives for pre-tacking leather components, as opposed to stitches, is a strong one. The application of stitches requires complex handling and could severely damage the cosmetic appearance of the finished Upper. The stitches have the added complication of having to be removed at a later date, thus, introducing a further complex operation. Adhesives in contrast only need be applied to the contacting surfaces and consequently cause no detriment to the cosmetic appearance of the finished part. Certain types of adhesive do, however, set hard and as such can interfere with subsequent stitching operations.

Individual shoe components are generally quite small and flat requiring two points of contact to be maintained for any component part. A number of exceptions to this rule exist, the most obvious being circular parts that are axially aligned, these only require a single point to be placed at the centre. Other exceptions arise when more than two components are to be joined to form the pre-tacked part. As a result it simplifies matters if the pre-tacking of multiple components is considered to be the repeated joining of only two lamina. Where three components constitute the final part, two components

could be joined using two points. The resulting part can then be treated as a single component for the next operation. Consequently quite complex parts can be constructed from a number of basic components in a relatively simple manner.

4.2 Pre-tacking into three dimensions.

The 3-D shape of a shoe upper prior to lasting is constructed out of a 2.5-D part, assembled from a number of parts by the sewing together of disparate curves at the heel, in a process called closing. This still requires complex manual manipulation of the workpieces to be joined as few mechanisms for automating this process exist. The curved edges of the workpiece need to be brought together in a controlled manner, whilst at the same time either stitching along the overlap join, or zigzagging from part to part across the edges to form a 'Butt' join using machines similar to the Pfaff 418-49[13].

If parts could be pre-tacked together prior to the final joining process, the final stitching of such workpieces would be greatly simplified, as the resultant pre-tacked component could be treated as a single workpiece.

4.2.1 Pre-tacking principles.

In general the edge of a part can be described as a series of polynomials and as such can be mathematically complex to define. This mathematical description of the edge profile of the part equally well describes a line which has no physical constraints. However, the components to be joined have physical properties such as area, thickness

and mass. As a result this model can be simplified for real components as a number of restrictions exist on the possible locus of the edge of the part.

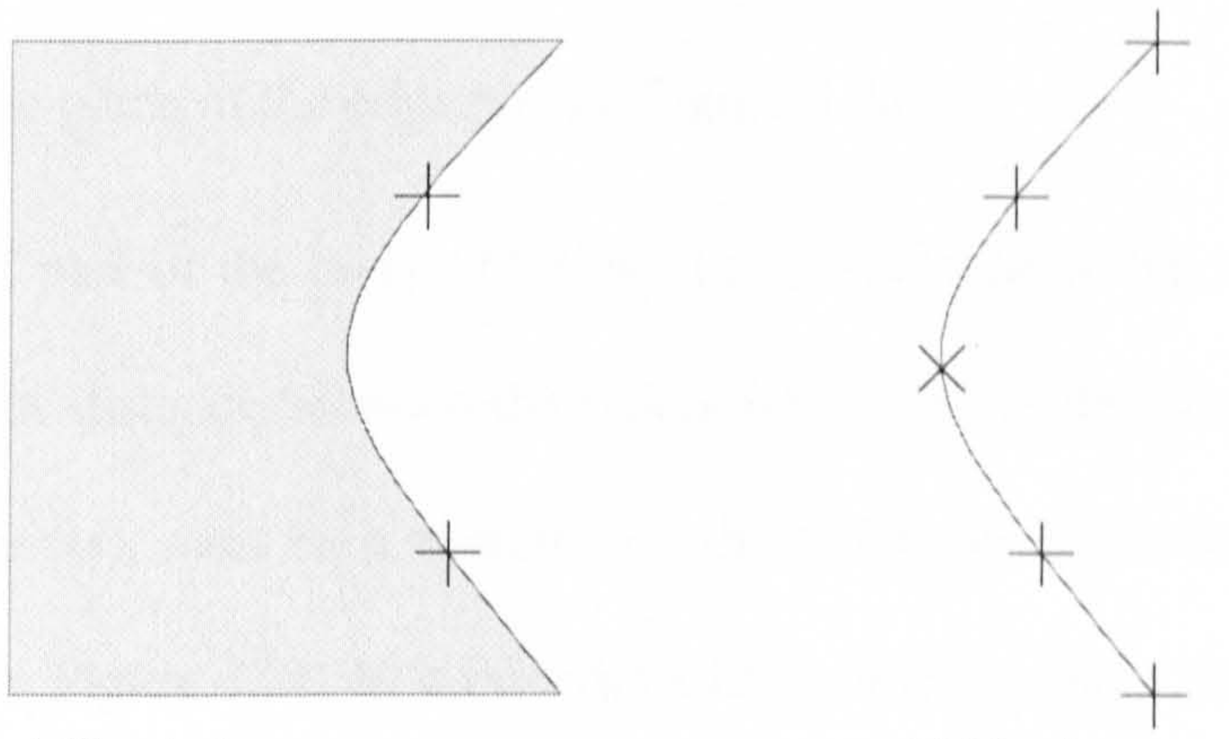

a) Physical component b) Line in space

Figure 4.1 Reduction in required points resolution by considering physical properties.

For example the edge of the part cannot move so that it would lie outside the body of the part when that part is in its 2-D, (flat), state. If it were to do so, the part would either have stretched or, in the limit, torn. If the line of the edge is to remain in plane and only the body of the component is allowed to become deformed from the flat, then the problem of defining the points at which the pre-tacking bond need be made in order to ensure accurate results is further simplified.

By considering such boundary conditions a hypothesis which describes the edge behaviour of a part given a degree of deformation can be proposed.

4.2.2 3-D pre-tacking hypothesis.

Consider a 2-D part which has finite area, such that it can not be approximated to a line and whose edge profile can be described as a series of ellipses. If its edge points

are to be constrained to the same plane, then only three points on the edge of the part for each ellipse need be defined for the edge of the part between these points to be similarly defined. This is providing no singularities are introduced and no part of the body of the workpiece lies in the plane of the edge points; Figure 4.2a.

However, if part of the body of the workpiece is to lie in the same plane as the edge points, then the distance between the points where this body enters and leaves the plane, (the plane points), must be a maximum if the points along the edge are to remain in the defined plane; Figure 4.2b. In a material such as leather, there can then be said to be a line of force between these two points of such magnitude as to hold the points of the body along the line connecting the plane points in plane. As a result if the body that is to lie in the defined plane is known, then the remaining edge points are known if they are also restricted to the said plane. Consequently, if the whole of the body of the part is to remain in a defined plane, then any two points on the body of the part will define the edge points. I.e. the general rule for 2-D pre-tacking.

4.2.3 Limited contact points.

The hypothesis leads to the possibility of using limited contact points to perform an accurate pre-tack and that a continuous join need not be required in order to accurately align the workpieces. Hence, for the accurate alignment of two separate parts only a finite number of points need to be matched if the conditions for the hypothesis are met.

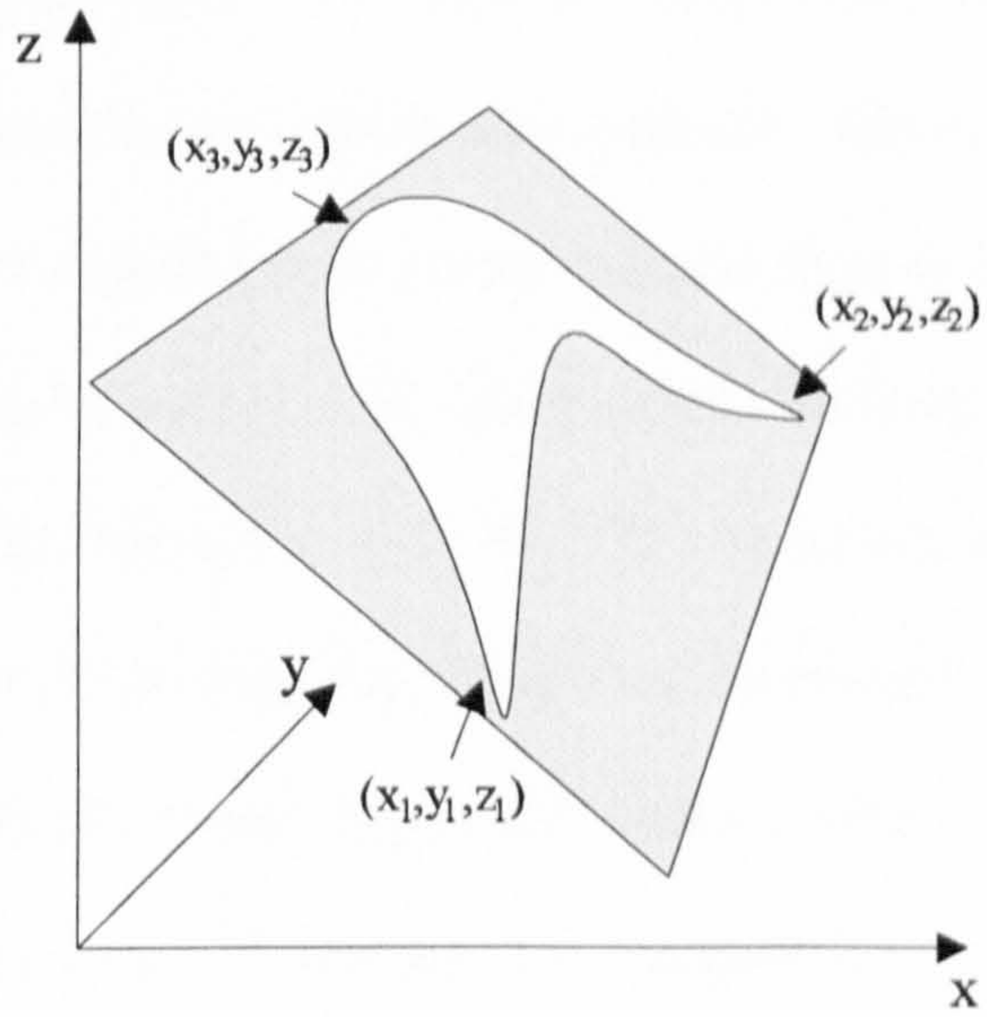

a) 1st condition

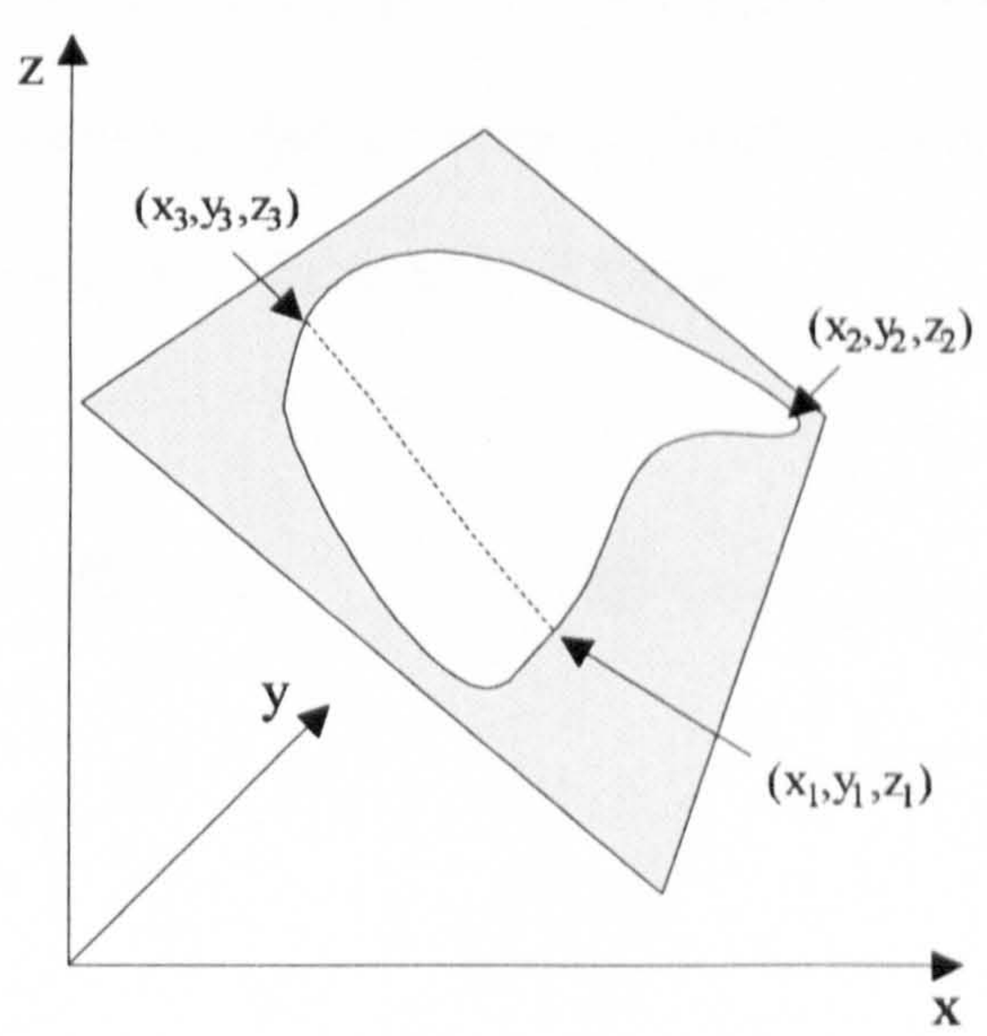

b) 2nd condition

Figure 4.2 Three dimensional pre-tacking.

The minimum number of points required to perform this task is three, as three points are needed to define a plane. This minimum requirement works well for the simple components typically encountered during shoe assembly, however like 2-D pre-tacking additional points may be required if the shapes become large or complex. Some complex curves which would require two ellipses and thus mathematically up to 6 points to define can be created during the manipulation of the 2-D component into the final 3-D shape. This is achieved prior to performing the actual bond, by controlling the orientation of the selected pre-tack, (control), points. Figure 4.3 shows a simple case where a part lying flat has a profile (a). For simplicity one possible manipulation point is fixed and the other is rotated through known angles, (b & c), relative to the reference. In order to achieve these results the body of the part must leave the plane to which the edge has been restricted. Such manipulations as well as being restricted by the properties of the material handled can result in undesirable effects such as creases.

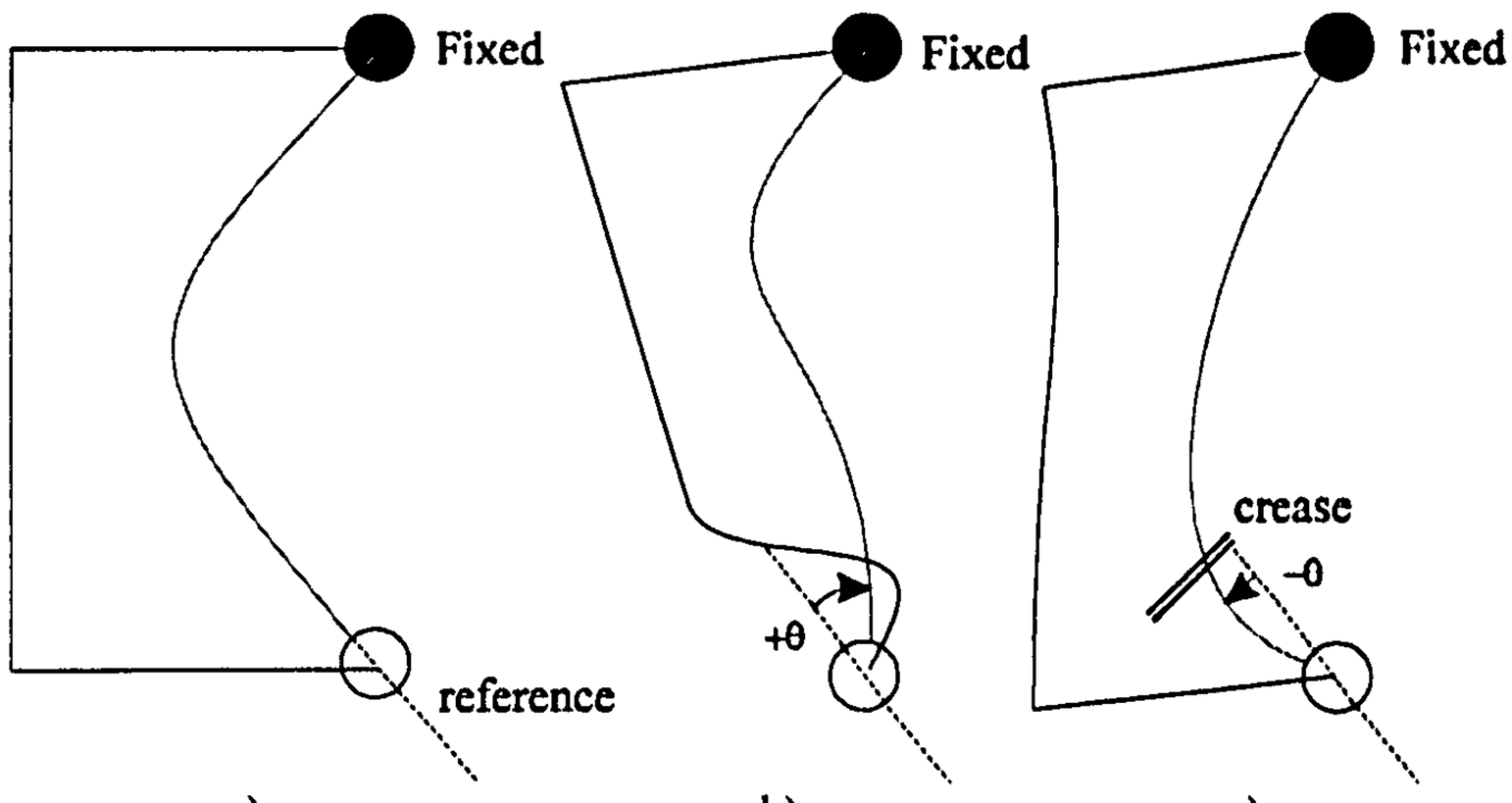

Figure 4.3 The effects created by controlling gripper rotation on the edge of a part during 3-D pre-tacking.

This method of orientation is analogous to Bezier curves which implement control points. These control the height and slope of a curve by their distance and angle relative to the node from which they extend. Here the loacation of the control points is limited by the physical properties as the part and can not be located anywhere in space as with Bezier curves. The distance to the control point is thus determined by the rotation of the manipulated point with respect to the reference angle and must be in such a position that the edge of the part remains in the defined plane. Consequently such curves can be calculated in advance and incorporated into component design. A manipulator can then be programmed to automatically perform the operations required to deform a 2-D lamina into a 3-D component whose edges follow known paths.

4.2.4 The manipulation process.

Where two simple parts such as those in Figure 4.4a, are to be joined, both of which initially lie in the 2-D plane but will result in a 3-D component after joining, only three points need be defined.

The three points are selected on one of the two component parts, e.g. part [a], such that when manipulated they match similar points on the second part [b], the resultant workpiece being of the required 3-D form. As a result if part [a] is gripped at these three points when in its 2-D state and then deformed by moving two of the points relative to the third in the 2-D plane, the body of the part becomes distorted into 3-D. Once the three points are correctly located in X and Y, (Z remaining constant), the points can be rotated to affect the line of the edge. The second part [b], in its 2-D plane can then be lowered to make contact with the now deformed part [a] and a join made at

the three plane points. The edge points of part [a] become restricted to the plane defined by the second part and are therefore defined. This results in a single 3-D part as depicted in Figure 4.4b. Once the bond has taken place the resulting 3-D part can be removed from the pre-tacking manipulator and allowed to relax. This often results in the part that had remained flat during the whole process becoming deformed into the 3-D plane due to the stresses generated in the leather during the pre-tacking operation.

4.3 An experimental pre-tack system.

Figure 4.5, shows a diagram of the simple experimental manipulator constructed to test the hypothesis on simple workpieces. Two of the grippers are able to be moved in the X and Y directions under computer control. The third gripper remains fixed providing a reference point from which the grippers can be positioned relatively within the plane. The plane of the join is defined by the height of the three manipulators.

The mechanism for loading, performing the actual join and unloading the completed, now 3-D workpiece is depicted in Figure 4.6, which shows the implementation of a gantry carrying a vacuum plate as described by E. Adams[2]. This system was originally constructed to perform pre-tacking of 2-D workpieces but is equally suited for the construction 3-D parts. This is due to both of the parts initially being 2-D and even after the joining process has taken place, the second part still remains in its 2-D state with the deformed first part lying below it whilst still being held by the manipulator. As a result the vacuum plate is capable of attaching itself to the completed part using the undeformed part to achieve a hold.

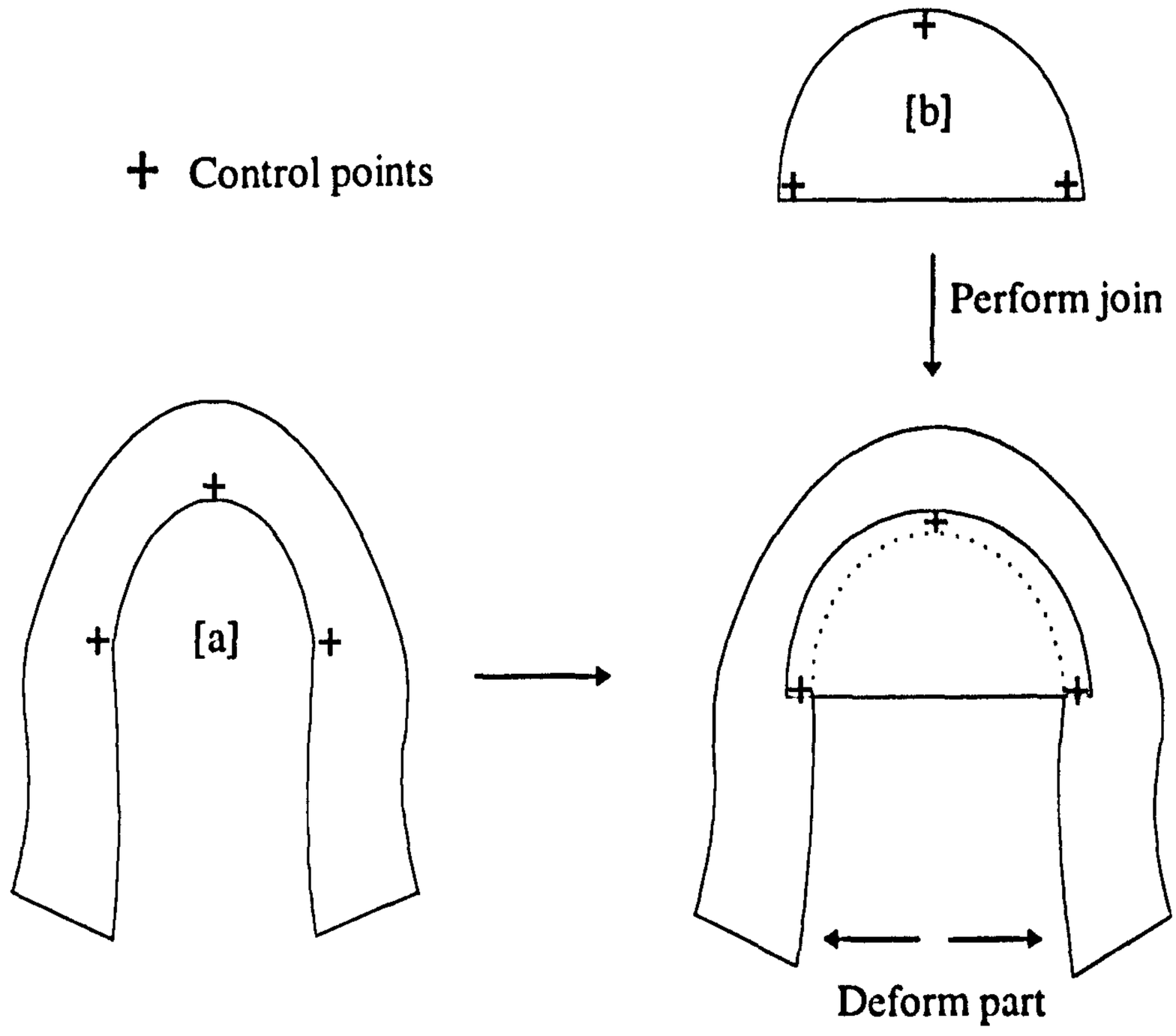

a) Performing the pre-tack

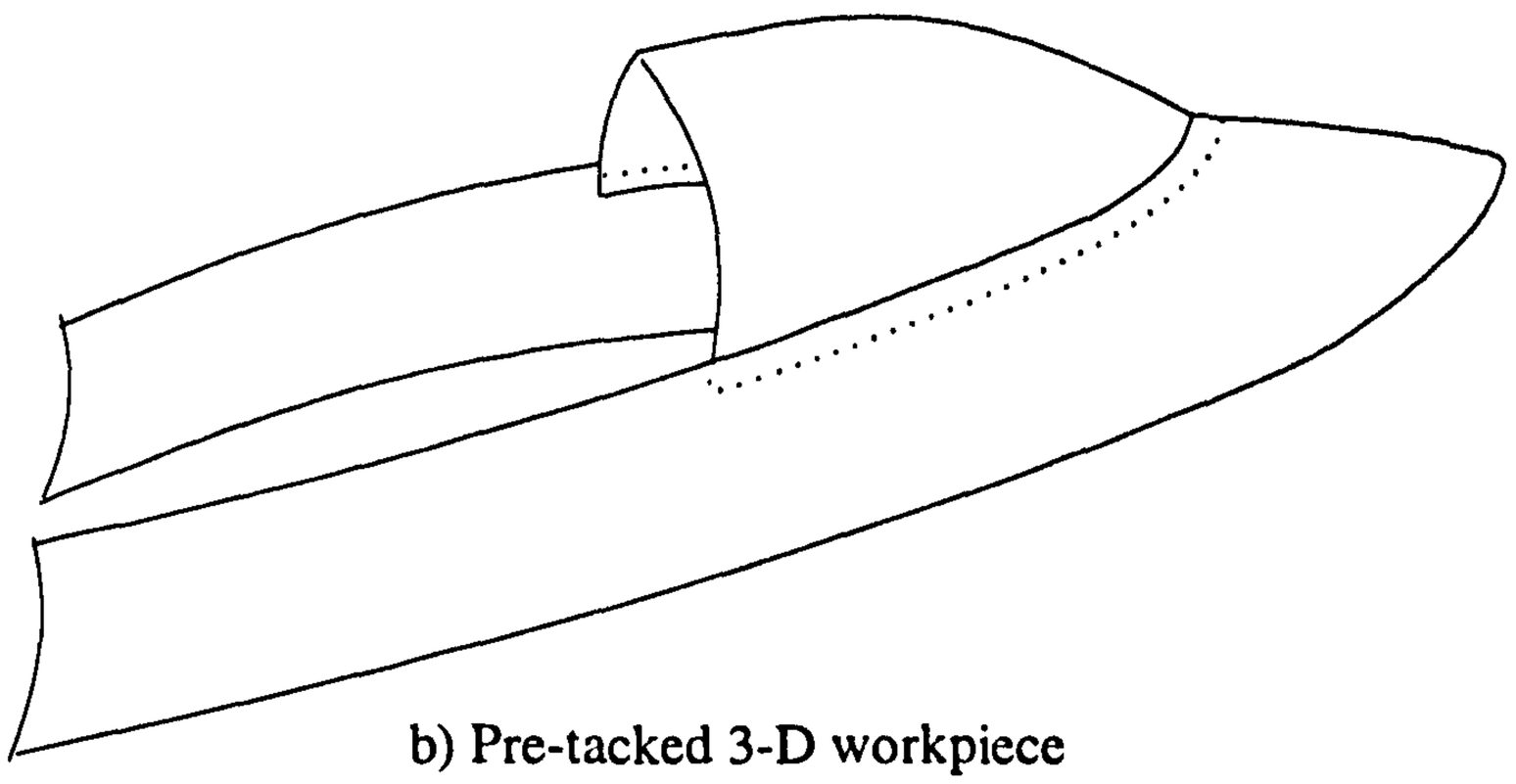

b) Pre-tacked 3-D workpiece

Figure 4.4 Pre-tacking an upper component.

This would then allow for complete automation to be achieved where the component parts could be fed into the system using conveyor belts. The separate component parts being removed from the belt by the vacuum plate and delivered to the work area by the gantry. Once the formation of the 3-D part was complete the gantry would then take the part from the work area and deposit it either into a bin for completed parts or onto another conveyor in order to transport it to another operation.

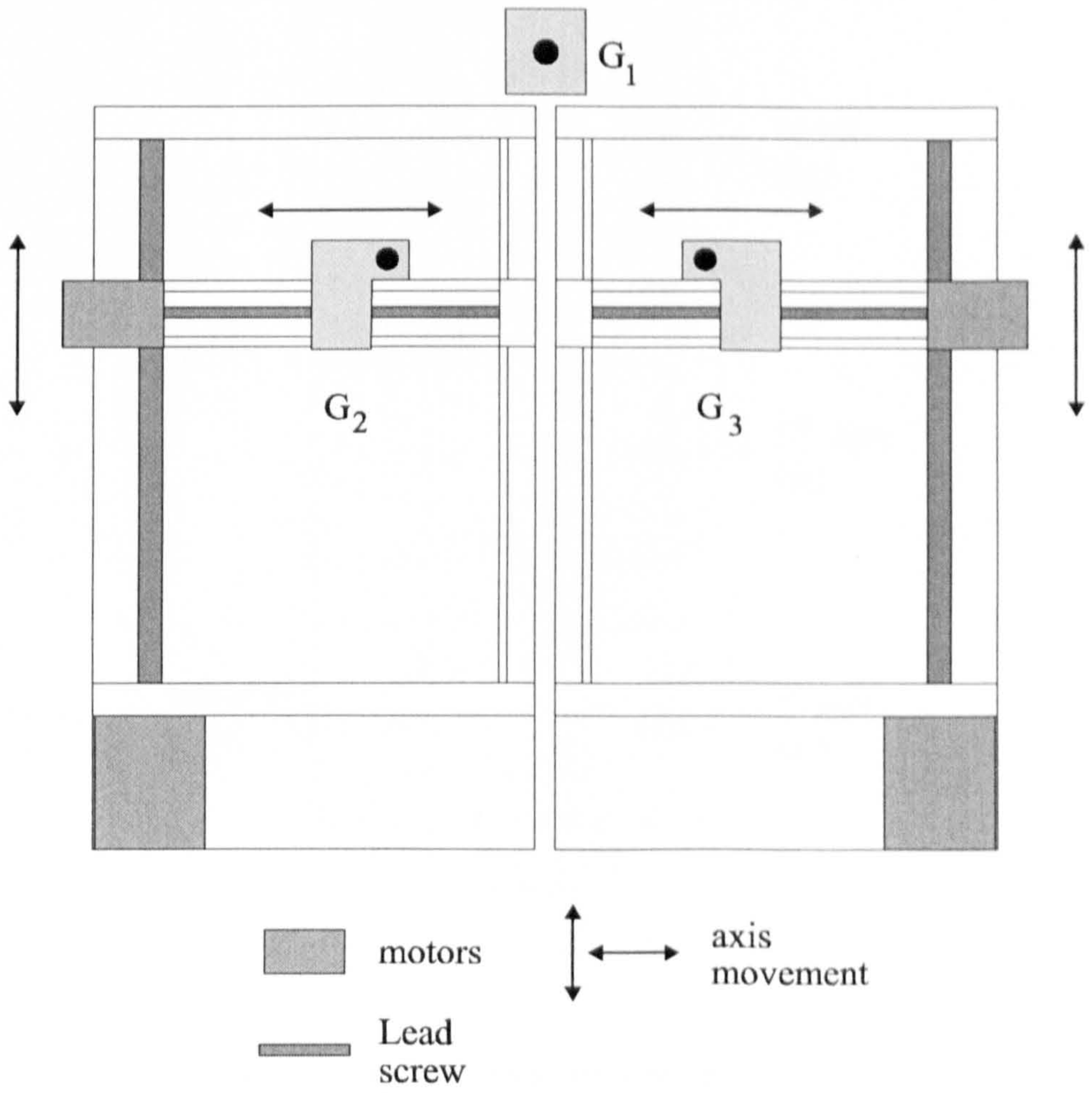

Figure 4.5 Limited contact pre-tacking.

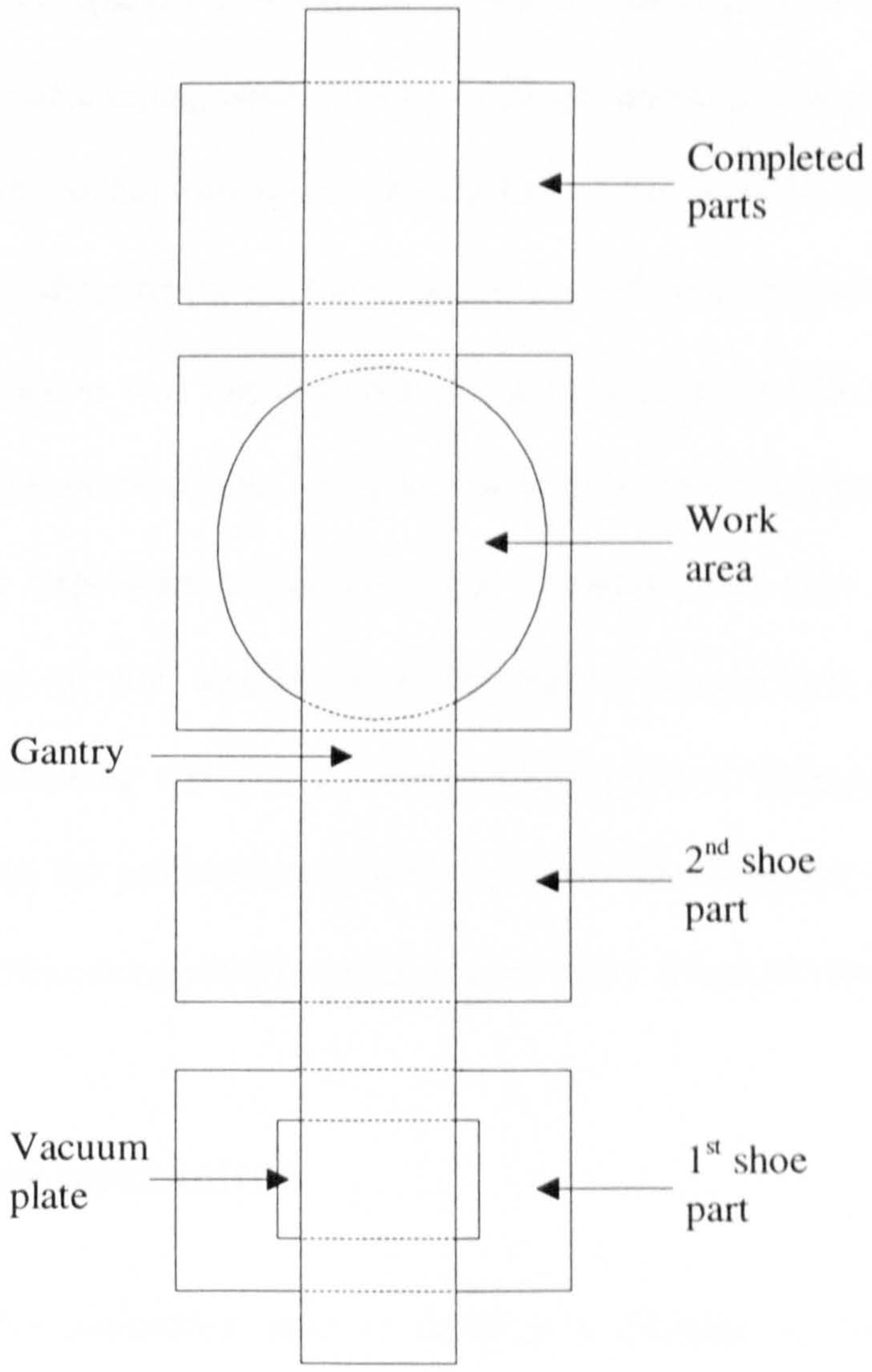

Figure 4.6 Schematic representation of a complete pre-tacking system.

4.4 The pre-tack medium.

Generally in garment manufacture pre-tacking is performed by placing a small stitch to hold the separate parts together, however, for shoe making this is not desirable. This is due to the complexity it would add to the pre-tacking system which would then require some form of stitching head. This could be overcome by using staples to form the join, however both mechanisms pierce the surface of the parts leaving ugly holes after their removal, thus affecting the cosmetic appearance of the finish part. As a result a fast acting contact adhesive was implemented as the pre-tacking medium as this does not effect the final appearance of the workpiece or require removal after final joining. The adhesive used for experimental purposes was a 'super glue' type gel. This had the beneficial property of not soaking into the leather components too quickly after application, thus allowing time for the manipulation process. Although the gel worked well in experiments, for practical reasons it may prove an advantage to implement a re-activatable adhesive to the part(s) some time prior to the actual pre-tack operation.

4.5 The gripping mechanism.

Considerable difficulties exist in devising a gripping mechanism to hold the workpieces during the manipulation process. One proposed solution is to locate the parts onto pins located at the gripper heads. This would ensure that no lateral slippage of the part could occur whilst it was being deformed. This however, is not a feasible solution as it damages the surfaces of the components being handled and does not provide a means

of securely holding the point in a manner so as to allow for it to be rotated.. As a result a number of non-destructive methods for gripping the components have to be considered.

these being :-

- Physical gripping,
- Vacuum suction,
- Magnatak adhesive compound.

Nb. Electrostatic gripping was also briefly investigated. However the surface area required to hold a part securely prohibited its use for this application.

4.5.1 Physical gripping mechanisms.

The physical method can be sub-divided into two categories, the first being a method by which the part is clamped between an upper and lower surface. This was found to have a number of limitations. The predominant problem being that the part could only be gripped near to the edge and access was required to both sides of the part by the gripper. Furthermore, as the pre-tacking medium was a fast acting contact adhesive, the gripper itself often became glued to the part.

The second method involves pinching the part from one side only using three steel points to ensure stability at the gripping position. This eliminated the problem of gluing the gripper to the part as no part of the gripper was exposed on the bonding side. For some workpiece types however, the surface of the part at the points of contact became damaged. No serious damage occurred on very soft leathers or suede's which had the ability to be deflected by the gripping points and then recover after being released. For the majority of cases such damage would not be seen as it would be hidden within the pre-tack join. However if the manipulation were required to take place on the grain, (best), side it would be unacceptable. As a result surface pinching as a gripping

mechanism is far too inflexible to be employed in a general 3-D pre-tacking system. It might however, find a use in a more specific area where only suede is to be handled, or where the slight surface marking will be covered by another part.

Both of these mechanisms require a high degree of actuation, which for a simple system with only a few points to control may well be acceptable. For more complex systems with more points the control workspace could become highly congested. Consequently more compact mechanisms capable of perfoming the manipulation are required.

4.5.2 Vacuum gripping mechanisms.

To overcome the access problem to both sides of the part and remove the need to operate close to its edges, vacuum systems were investigated as they are both clean and simple to control. However, although the vacuum could generally hold a part prior to deformation it was found that for a large number of cases (materials that are not readily pliable or whose surface can be described as 'rough'), the shear forces introduced by the deforming process caused the part either to slip or become completely detached from the vacuum grippers. It should also be noted, that even for the more pliable materials, initial holding often failed due to the porous nature of the material. This was due to the contact area between the gripper and the component having to be kept to a minimum in order not to restrict the movement of the component during the manipulation process.

A method which significantly reduces the slippage due to the lateral motion of the gripping head when manipulating the part is to make the surface of the gripper around the point where the vacuum is applied to have very high friction, with respect to the

surface of the workpiece. One such medium was to found to be 'Blue-Tak' which is partially adhesive in its own right and as such provides an extra gripping force. Indeed it was found that the Blue-Tak on its own could hold well enough to perform operations on paper and some fabrics. In addition to its tacky property it is also compliant allowing it to fill any small gaps between the vacuum gripper and workpiece surface when the component was pressed down onto the manipulating head. This ensured the suction power of the vacuum was directed solely at the surface of the workpiece. A further support mechanism that proved effective was the implementation of a ring of pins fixed around the vacuum gripper. The pins were stood slightly proud ($\approx 1_{mm}$), in order to ensure they did not penetrate so deeply through the component as to cause damage that could be seen, or in the case of dense materials prevent the component from being seated correctly onto the vacuum head. This mechanism eliminated the effects of drift during manipulation but was still unable to maintain grip across a wide range of leathers. In addition the pins had to be constantly adjusted to cater for leather thickness and density.

4.5.3 Magnatak gripping.

The final method considered was Magnatak 7000. Magnatak is a form of adhesive which when set provides a tacky surface which can provide a firm hold whilst at the same time not producing a permanent bond. After manipulation the part can be cleanly separated from the gripper with no Magnatak residue being left on the part.

A problem arises in that unlike the physical and vacuum methods, the tackiness of the Magnatak is exhaustible especially when the nap side of the leather is to be manipulated. This flesh side often contains a large number of loose fibres that are able to

break away from the leathers surface and adhere to the gripper, thus quickly clogging up the Magnatak compound.

It is possible to rejuvenate its properties to a large extent, so long as it has not become completely clogged, by gently wiping its surface with a damp cloth and allowing a small drying time. Initial experiments showed a refresh rate of once every 100 operations to ensure reliability when operating on the grain side, with this rate having to be increased ten fold if the flesh side is to be gripped. Unlike the vacuum and physical methods the gripping mechanism cannot be switched off by the control system in order to release the completed workpiece, as a result the workpiece needs to be peeled from the Magnatak in order for the part to be removed from the grippers. Figure 4.7 shows the gripping heads that were designed to perform this task. The implementation of solenoids allowed the gripping surface to be retracted through a collar which acted to peel the workpiece from the Magnatak compound.

The experimental system implemented the Magnatak compound to provide the gripping mechanism. This was done in order to minimise the complexity of the mechanical and control systems as much as possible as three grippers were required. The object of the exercise being to determine the validity of limited contact points as a method of pre-tacking into 3-D, rather than produce a commercial standard pre-tacking system.

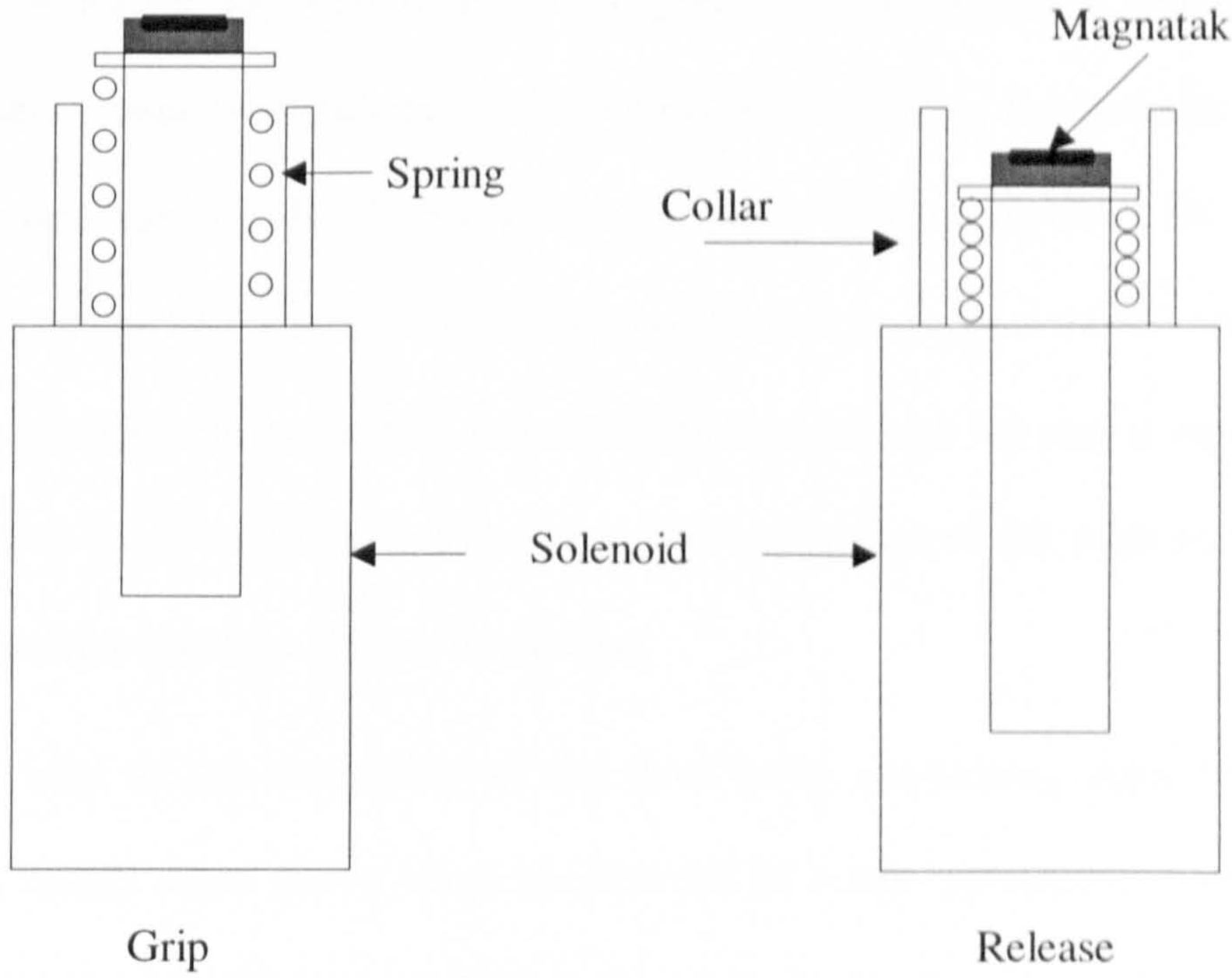

Figure 4.7 Pre-tack gripping mechanism.

4.6 Results.

Once the components have been pre-tacked together they must undergo final stitching to provide a permanent join. The ultimate proof of whether or not pre-tacking of components into 3-D is of value, depends on how greatly it simplifies the operations which are to follow. In order to stitch the parts so that the edges remain correctly aligned, either component that makes up the resultant workpiece, must remain in the 2-D plane so as to ensure stability. This is generally the part that had remained flat during the pre-tack operation. The actual sewing operation can then be performed on a standard flat bed sewing machine, the bed acting as a solid plane upon which the part is supported and kept flat. Care must be taken not to distort the natural line of the edge as this would result in misalignment errors being introduced.

In order to test the ability of the three point pre-tacking proto-type system outlined, a simple shape whose characteristics can be easily represented mathematically was used, Figure 4.8. By implementing such a test sample the desired locations of the edges of both workpieces are well defined both before pre-tacking and after final stitching. Consequently measurements can be taken to record the accuracy of the pre-tacking processes. The parts consist of a circular disc 130mm in diameter, (part [a]), and a larger semi-circular component with a diameter of 148mm, (part [b]). The line of stitching is 6mm from the edge of the pre-tacked part. The location of the control points are also illustrated.

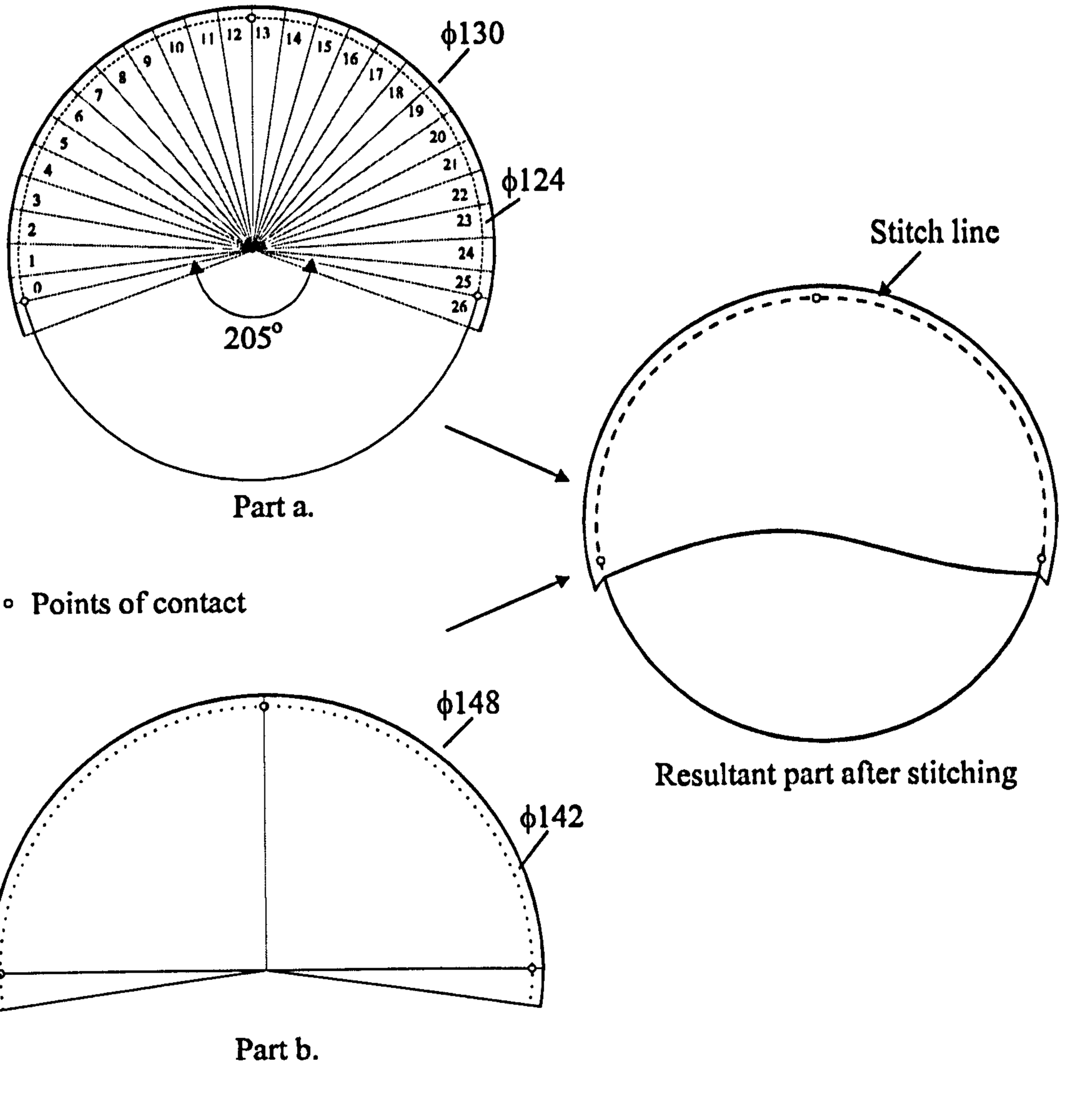

Figure 4.8 Component used to test pre-tack principle.

Part [b] is loaded into the pre-tack system and held at the selected control points. These are then manipulated to align with similar points on part [a]. Adhesive is then applied to part [a] before part [b] is lowered to form the bond. Once the adhesive has set the pre-tacked part is then released resulting in a 3-D compound, pocket shaped, component.

Twenty paper samples were produced so as to measure the effects of pre-tacking. Paper was used for a number of reasons. Firstly it allowed for the exact cutting pattern to be printed directly onto the sample thus resulting in a well defined cutting pattern. Accurate leather samples were difficult to produce and had edges that were subject to fraying, resulting in difficulties in obtaining accurate measurements. Paper samples also have the added property that the edge can only be flexible in one direction at a time, thus removing any benefits that may be gained from the flexibility of leather components.

Measurements were taken of the discrepancy between the edges of the joined parts, after stitching, at the 27 points shown in Figure 4.8 using a travelling microscope.

Figure 4.9 contains a plot of the average misalignment errors for the twenty samples for each measurement position. These results show that at the control points, where manipulation occurs, the alignment errors are very low,. Those that do occur are due either to mechanical limitations of the handling mechanism, or incorrect cutting of the samples. Experiments showed that the cutting of the patterns could produce errors of around 0.5mm in extreme cases. Between control points the degree of misalignment increases to a maximum, with the largest observed error on any sample being 1.2mm. Generally however, the positional errors are very low. In excess of 60% of measurements show no measurable misalignment, Figure 4.10.

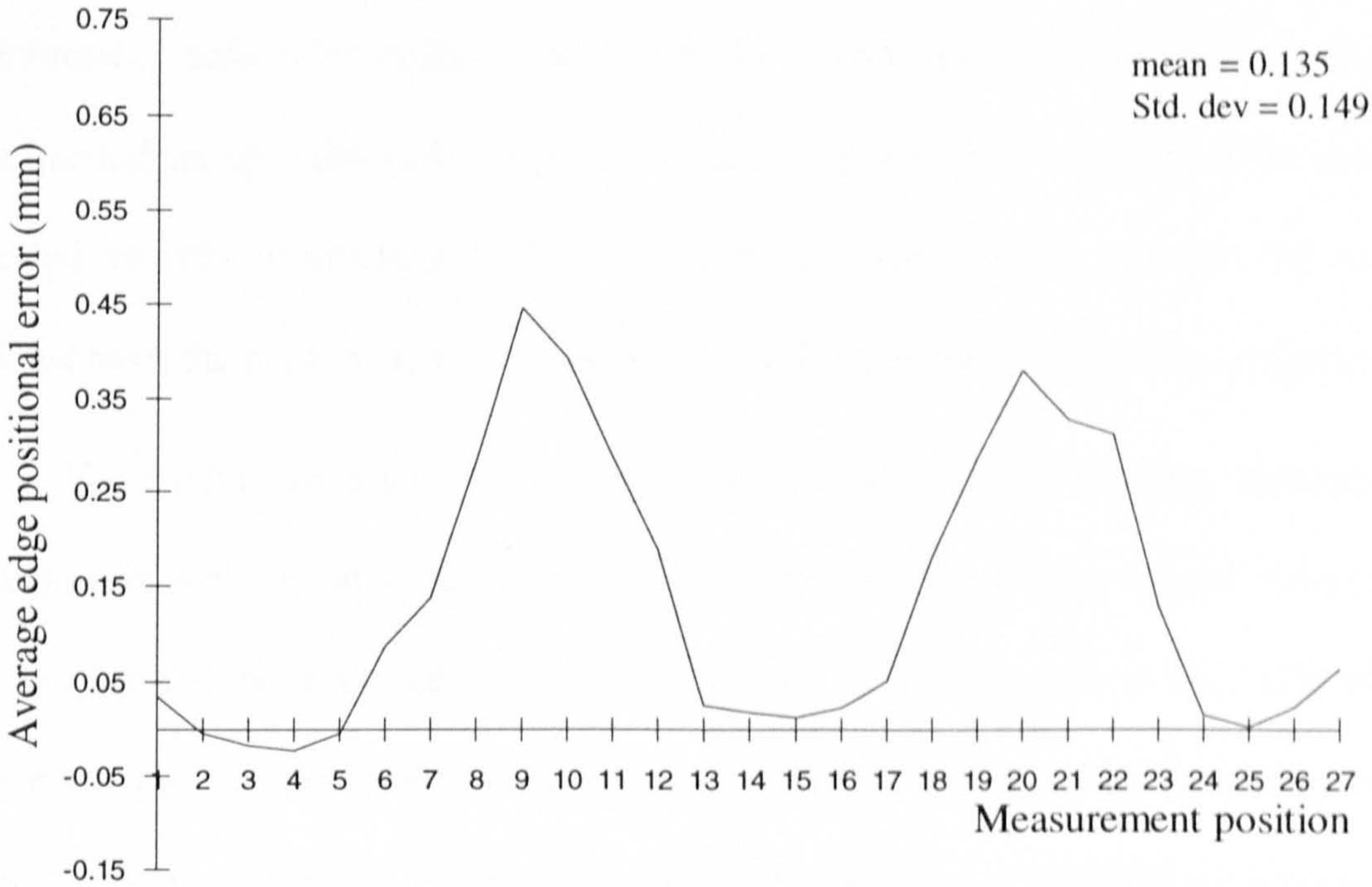

Figure 4.9 Average misalignment error measured after final stitching.

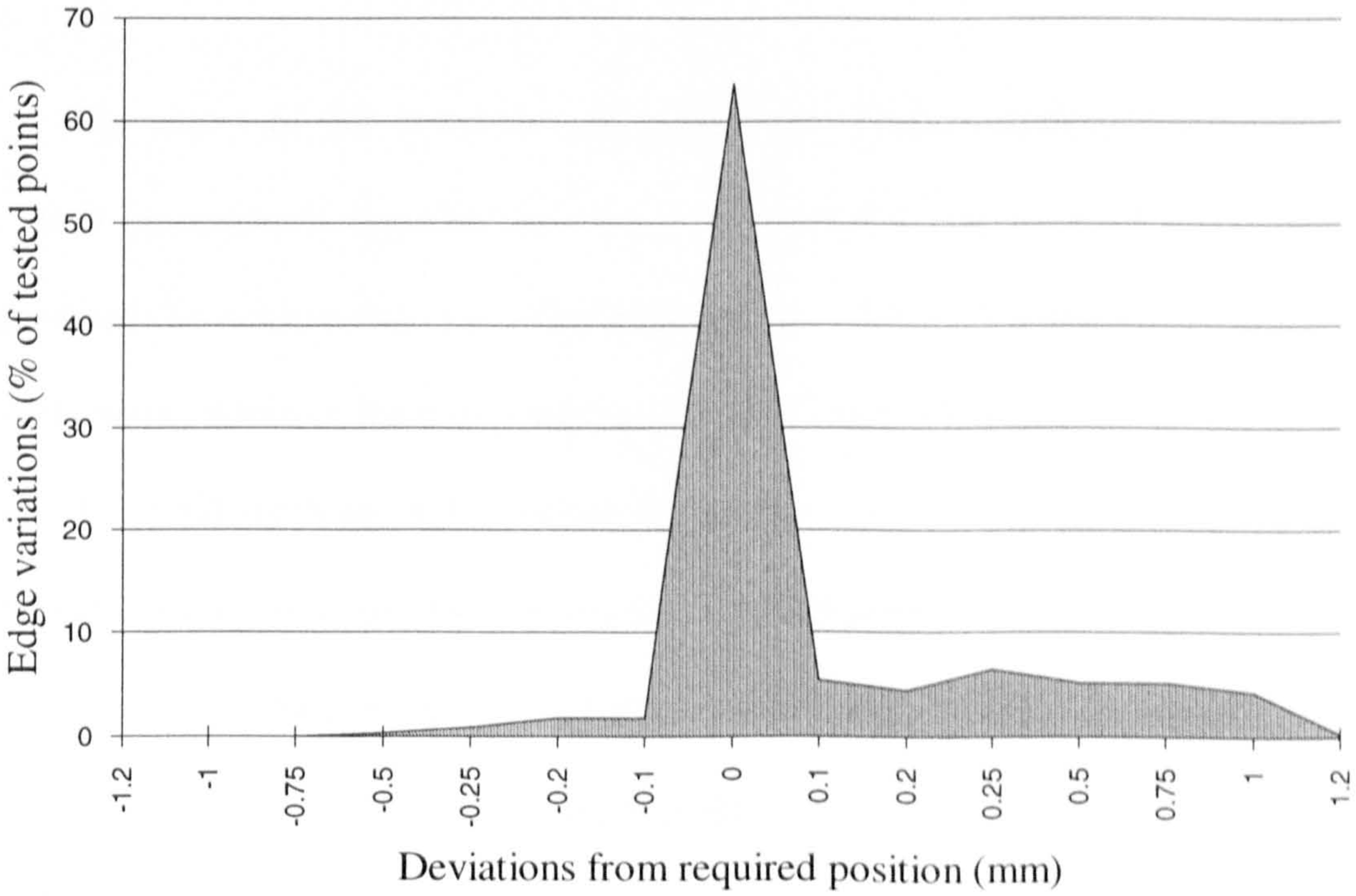

Figure 4.10 Chart showing the error distribution across the test samples.

A number of other component shapes, including representations of shoe components, made from leathers and fabrics have been similarly pre-tacked using the experimental set-up. Although the positional accuracy is hard to quantify all the samples provided visually satisfactory results after stitching. Appendix J, contains the results obtained from the paper samples as well as information on other samples investigated.

The Author has attempted to stitch the same components directly, without pre-tacking, with little or no success. It was found that even with the desired component position marked onto the plane to which it was to be stitched, it was difficult to manipulate the components correctly during stitching. By implementing the pre-tack system, components were successfully assembled quickly, in a highly repeatable and accurate manner across the range of materials tested.

4.7 Discussion.

The object of this research was to produce a basic mechanism for pre-tacking two, 2-D components together in such a manner that the resultant part was three dimensional. To achieve this, it is either required to produce a continuous bond along the lines of contact between the two components, or to select a number of key points to join, which after final stitching, will produce the desired result. The operations required to manipulate a component to produce a continuous join would be very complex and if such an operation could be performed, then it should be implemented to produce a final join and not a pre-tack. This approach was investigated by J. Grantham[15], at Hull University in 1992-3, for the constructional stitching of disparate curves. This machine was both complex in operation and slow due to the component becoming unstable at stitching

speeds in excess of 200 stitches/min. Consequently it was preferred to pursue the mechanisms that are employed for 2-D pre-tacking and determine a set of conditions that could be applied for manipulation into 3-D. This produced the minimum requirement of three points for stability, these capable of being orientated in X, Y and θ. The prototype system proved effective for simple and indeed some quite complex manipulations across a wide range of leathers and additional materials.

Pre-tacking adds an operation to the processing of a component and due to its complexity has rarely, if ever, been implemented in commercial machines. However, by its very nature it assembles the component parts to a reference position and as such may remove the need for the stitch marking operation that would normally have to be performed in order to guide an operator during stitching. Thus rather than being regarded as an additional operation it may in certain cases be regarded as a replacement for stitch marking. The outlined method demonstrates that complex handling mechanisms need not be required for a relatively wide range of parts. pre-tacking into 3-D can be performed simply and quickly with the actual manipulation and bonding process taking under 2 seconds to complete. This provides the possibility to fully automate a pre-tacking system capable of assembling complex parts from their basic components. It is envisaged that such complex parts could form the input to automated handling and stitching machines. These machines currently either incorporate complex manipulators or are very task specific[33-36]. By pre-tacking the components prior to final joining a far greater variety of parts could be assembled in an automated manner.

Chapter 5

Edge Following

5.0 Introduction.

Shoe uppers are constructed from many separate components, a number of which need to be stitched together to form larger, more complex workpieces. This process either being performed manually or by machines similar to the M.P.C.S. introduced in Chapter 1. Here the parts are clamped in to pallets, which are manipulated according to a previously taught stitch pattern under a sewing head. The Autoscan, described in some detail in Chapter 3, was designed to eliminate the need for the pallets, however the stitching process is still performed open-loop based on a template. Consequently there is no ability to counteract for any positional or structural variations in the presented part.

A number of mechanisms which can visually obtain information about an edge during manipulation, in order to allow for closed loop feedback, will be discussed in the following sections.

5.1 The implementation of lasers.

Traditional edge following methods use either back or top-lighting combined with a light detector, generally in the form of a camera. These systems determine the edge position by detecting a change in contrast across the observed image. In the case of backlighting the contrast variation results from the edge to be followed obscuring part of

the light source from the camera. Where top-lighting is implemented the light source is angled across the edge from behind the topography of the edge producing a shadow. The resulting light-dark(shadow)-light pattern is then observed, enabling the edge position to be estimated. Such edge determination methods are cheap, safe and convenient, however they do not provide a great deal of information about the actual topography of the edge. They are also susceptible to ambient and material variations. Modern developments into laser technology offer an alternative to white light methods and provide greater potential to maximise the amount of information that can be extracted from a given component.

5.2 Laser triangulation.

Laser triangulation can performed by projecting a light stripe on to a surface which is being viewed by an area camera offset from the laser axis. The line-stripe, as perceived by the camera, becomes distorted according to the profile of the surface and the camera and laser angles.

For edge following, a typical triangulation configuration can be seen in Figure 5.1. Here the laser is projected at an angle of 90° to the surface of the edge, with the area camera viewing this area at an angle θ. This ensures that the line-stripe represents a cross-section of the edge in the vertical plane only, with the angle of the camera allowing the effect of the edge profile to be viewed.

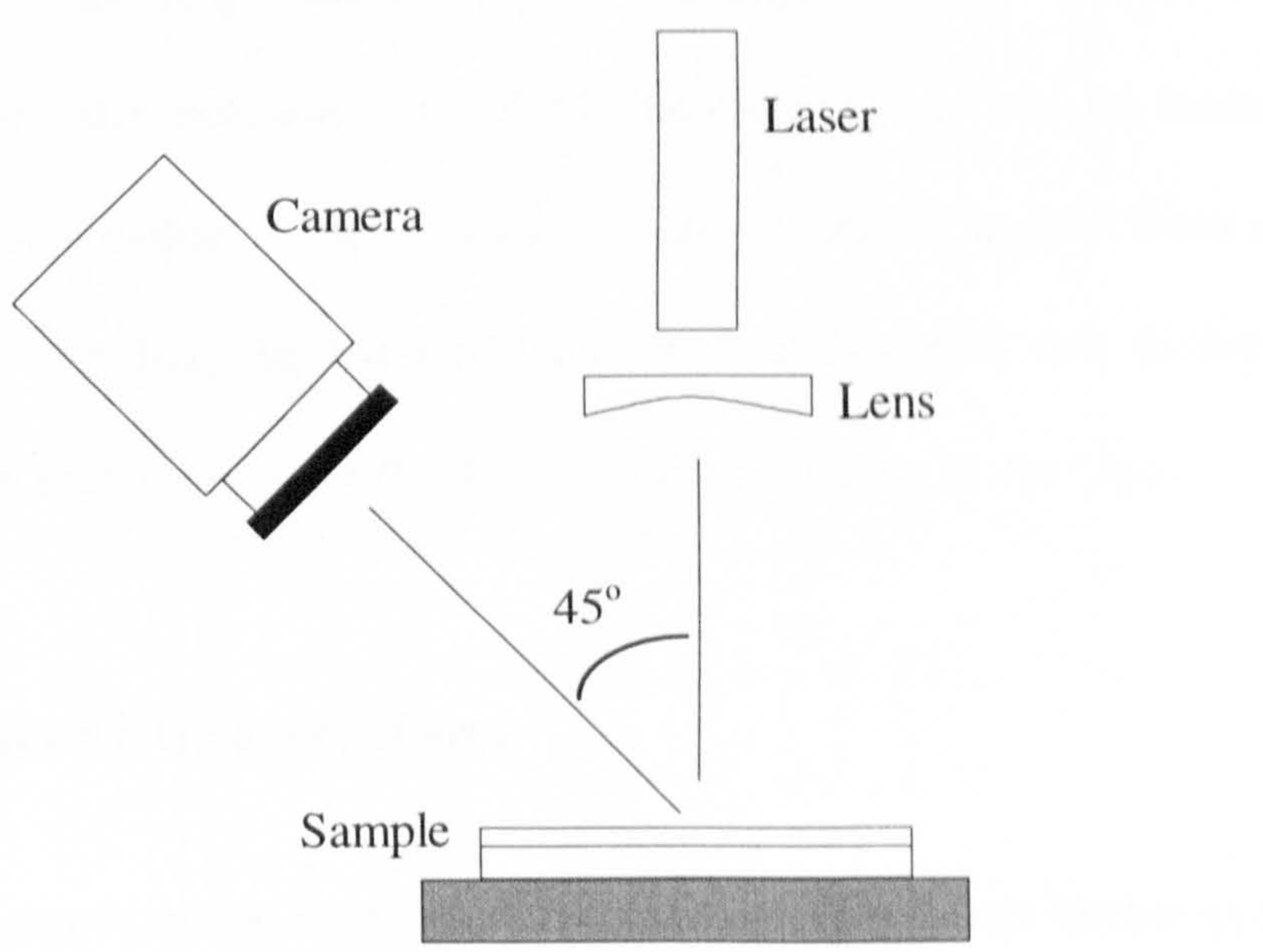

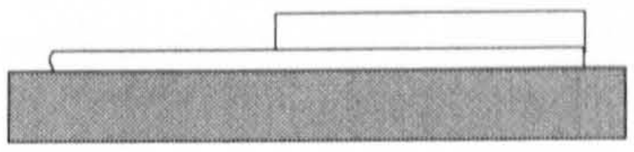

Sample profile

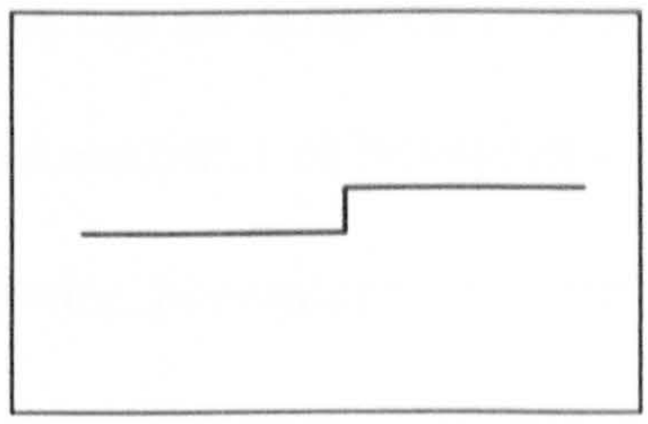

Camera image

Figure 5.1 Simple laser triangulation configuration and camera image for a sample profile.

5.3 Simple edge following using laser triangulation.

When the triangulation arrangement in Figure 5.1 is implemented the image viewed by the camera contains a deformed line, with the main feature being a discontinuity in the line-stripe caused by the change profile. Where a simple approximation to the edge position is required this discontinuity can be located with simple image processing methods. Figure 5.2a contains an image obtained from a square cut edge. It can be seen that the line-stripe has been broken into two distinct parts, vertically offset from each other, with the discontinuity occurring at the edge.

5.3.1 Edge characteristic extraction.

Once an image of the line-stripe has been obtained, it requires further processing in order to extract a value for the edge position. This can be achieved in a number of ways, such as region growing[50]. However the implementation of histograms provides both a simple and informative mechanism. By calculating histograms for average pixel intensity for each line in both the X and Y axis of the image (Figure 5.2b) information as to the thickness of the edge in addition to its position, can be obtained. The histograms are lightly smoothed before processing in order to reduce specular effects. The observed edge thickness being a function of the actual edge thickness and the camera angle, θ. Assuming that the laser and camera are correctly aligned, the Y axis histogram shows two peaks which correspond to the perceived positions of the line-stripe. The X axis histogram shows a drop in intensity at the edge. Appendix K, shows the effects observed due to camera or laser misalignment.

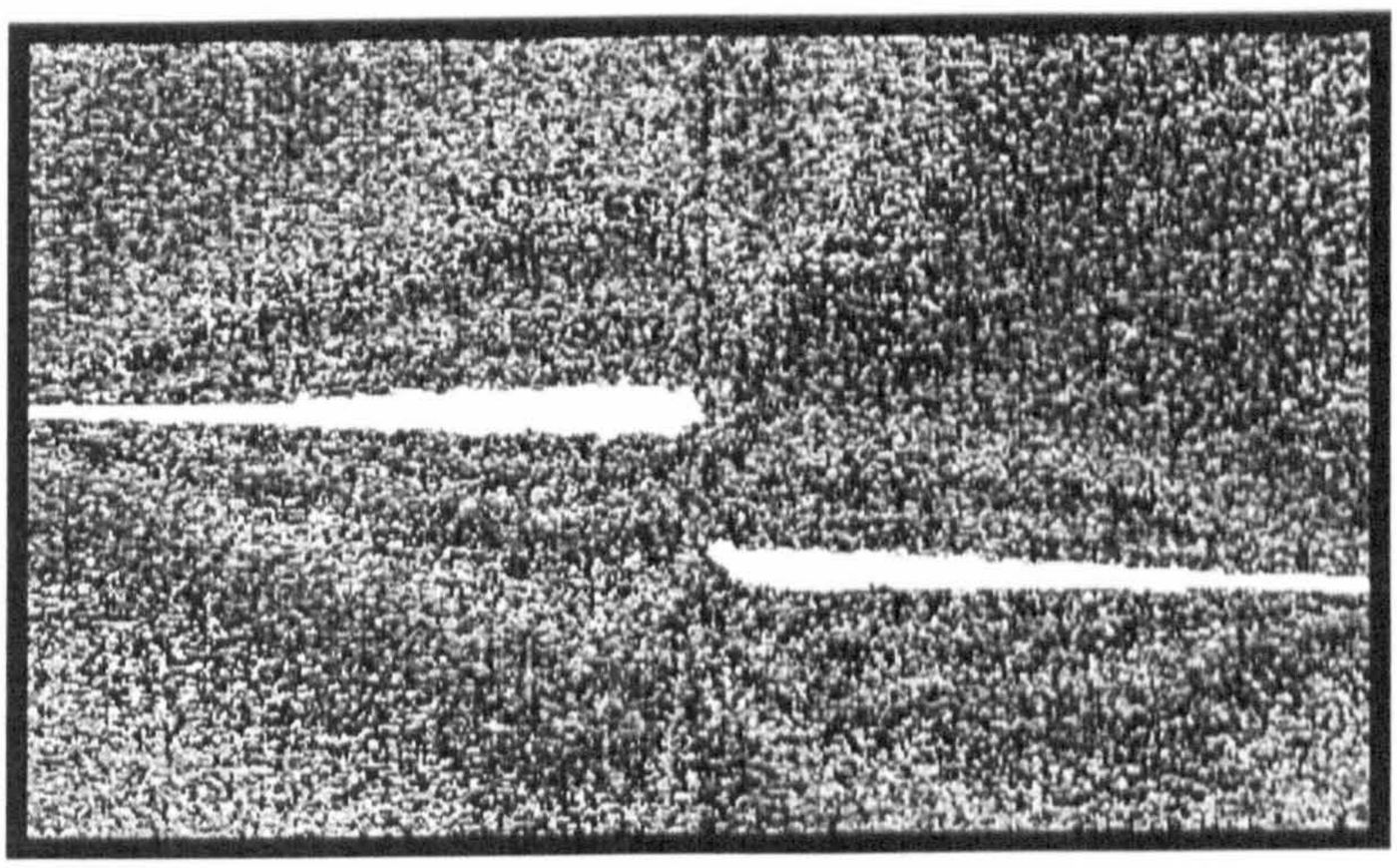

a) Grey scale image obtained by a camera for a square cut edge.

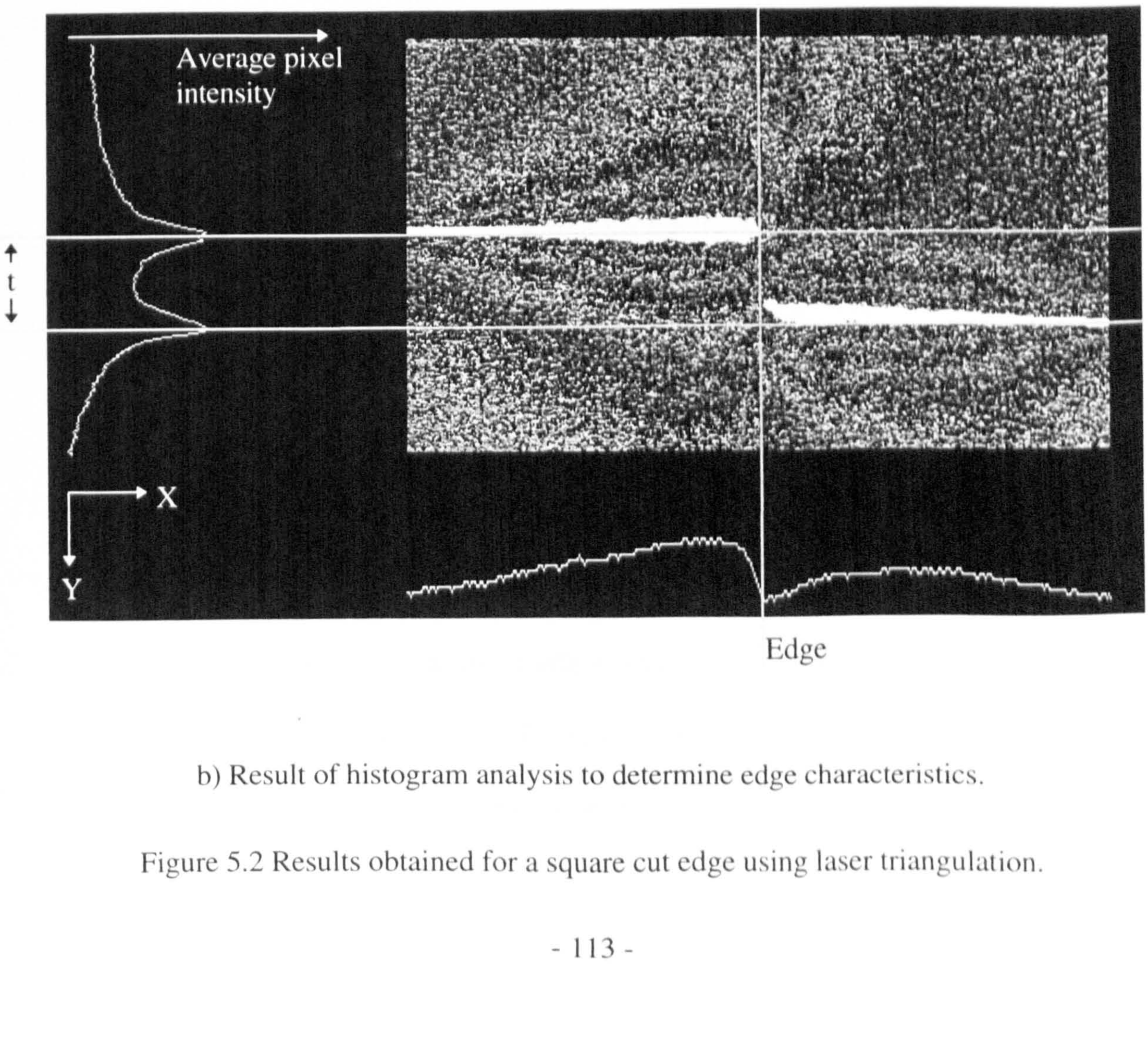

b) Result of histogram analysis to determine edge characteristics.

Figure 5.2 Results obtained for a square cut edge using laser triangulation.

In order to determine both the location of the edge of the part and its thickness, t, a threshold level is required. This level will determine from what point on the histograms measurements will be calculated.

For a square edge, where the parts of the laser line-stripe, as perceived by the camera, remain horizontal, the peak values of the Y axis histogram can be used to determine an approximation to the thickness of the edge. This is due to the gaussian distribution of light intensity over the line-stripe, (Appendix K). The actual edge position being determined by the inflection point in the X axis histogram caused by a drop in intensity at the edge.

5.3.2 Limitations of simple edge following.

The simple method for extracting the edge of a part described above allows for a number of edge characteristics to be determined both quickly and simply, as would be required for closed loop edge following on stitching machines. However, where the edge characteristics are more complex, such as those created by folding, or where some misalignment exists between the camera, laser and the edge, then further processing is required. In addition where the surfaces do not lie flat, or complex edges, such as those found on an Oxford brogue, arise (a zig-zag cut edge with decorative holes punched close to the edge), the histograms are not well behaved.

Figure 5.3 shows a number of effects that can be observed for a brogue vamp component with an edge thickness of 1.6mm. The X axis histogram has been lightly smoothed using pixel averaging in order to remove the effects of the punched holes.

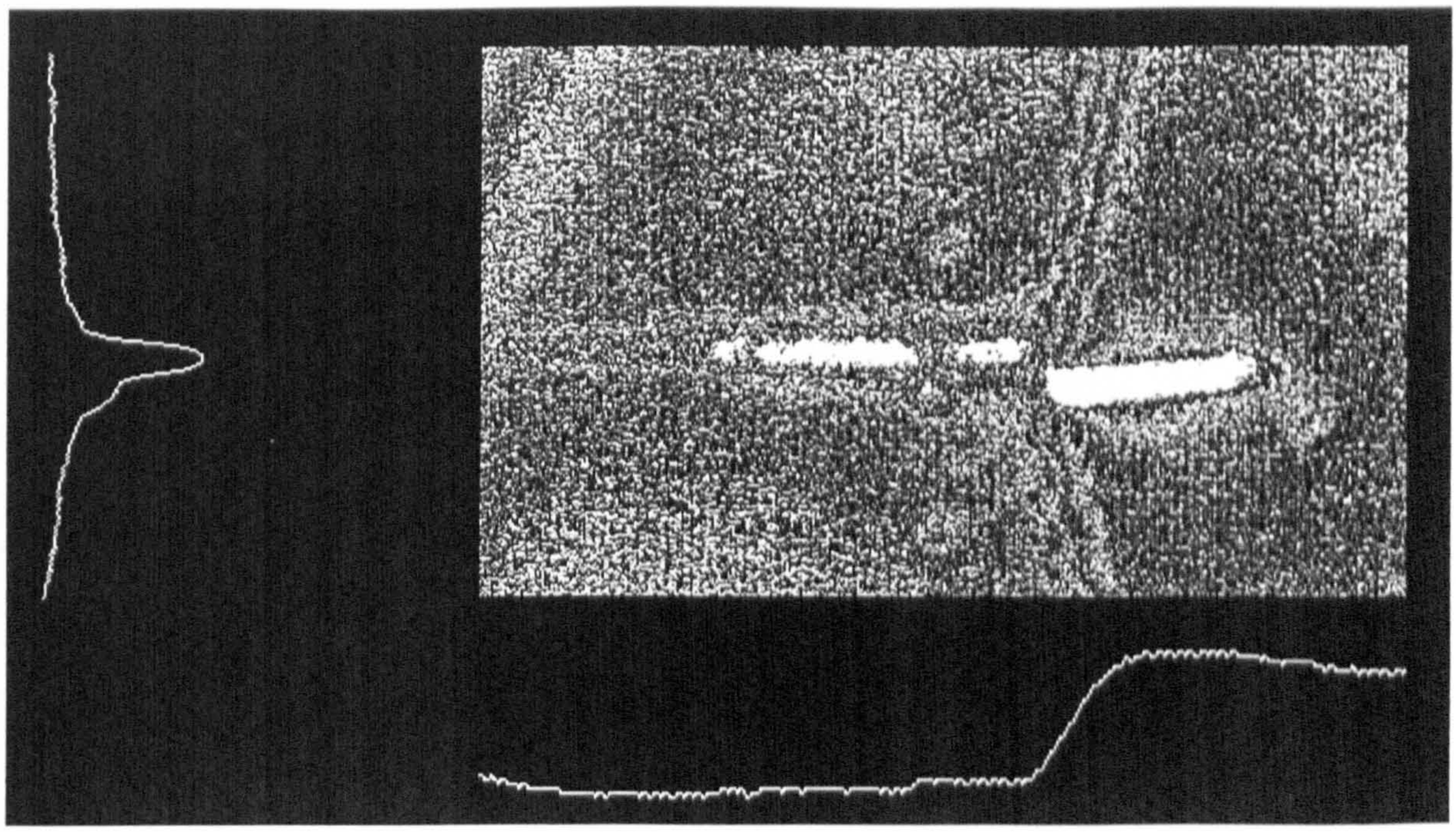

a) Image obtained from a 1.6mm thick brogue component edge.

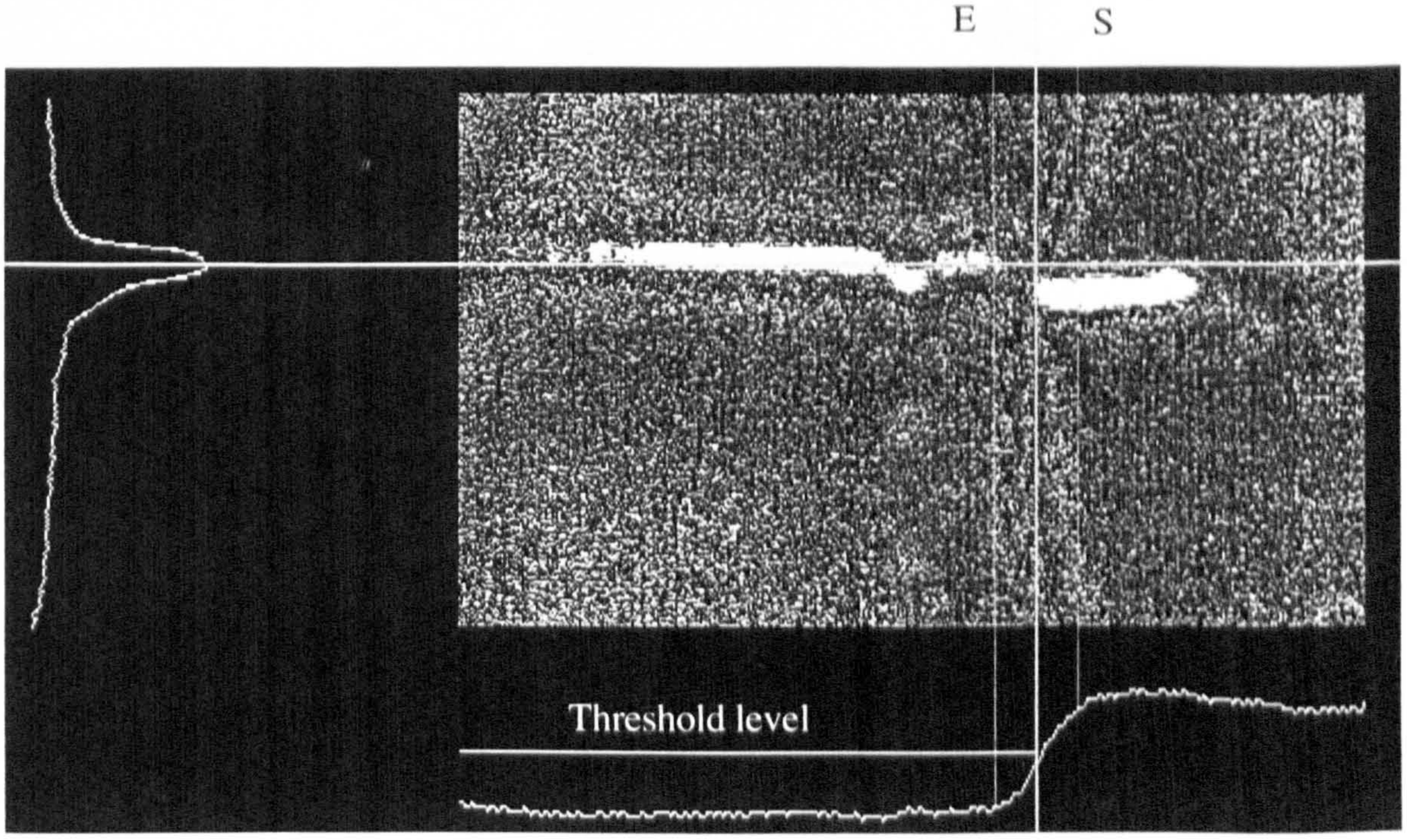

b) The effects of topography on a brogue component edge.

Figure 5.3 Results obtained for a Brogue component edge.

It can be seen from Figure 5.3 that the edge of the part is not lying flat and consequently the Y axis histogram peaks, previously seen for an ideal square cut edge, have merged. This means that the edge thickness of the part cannot be determined for this type of image using this simple approach.

Figure 5.3b demonstrates how the topography of the edge can cause uncertainty to arise as to the position of the edge. This effect is a result of the camera being orientated at an angle to the workpiece. If an obstruction exists between the camera and the point at which the laser crosses the workpiece then the line-stripe cannot be observed. Figure 5.4.

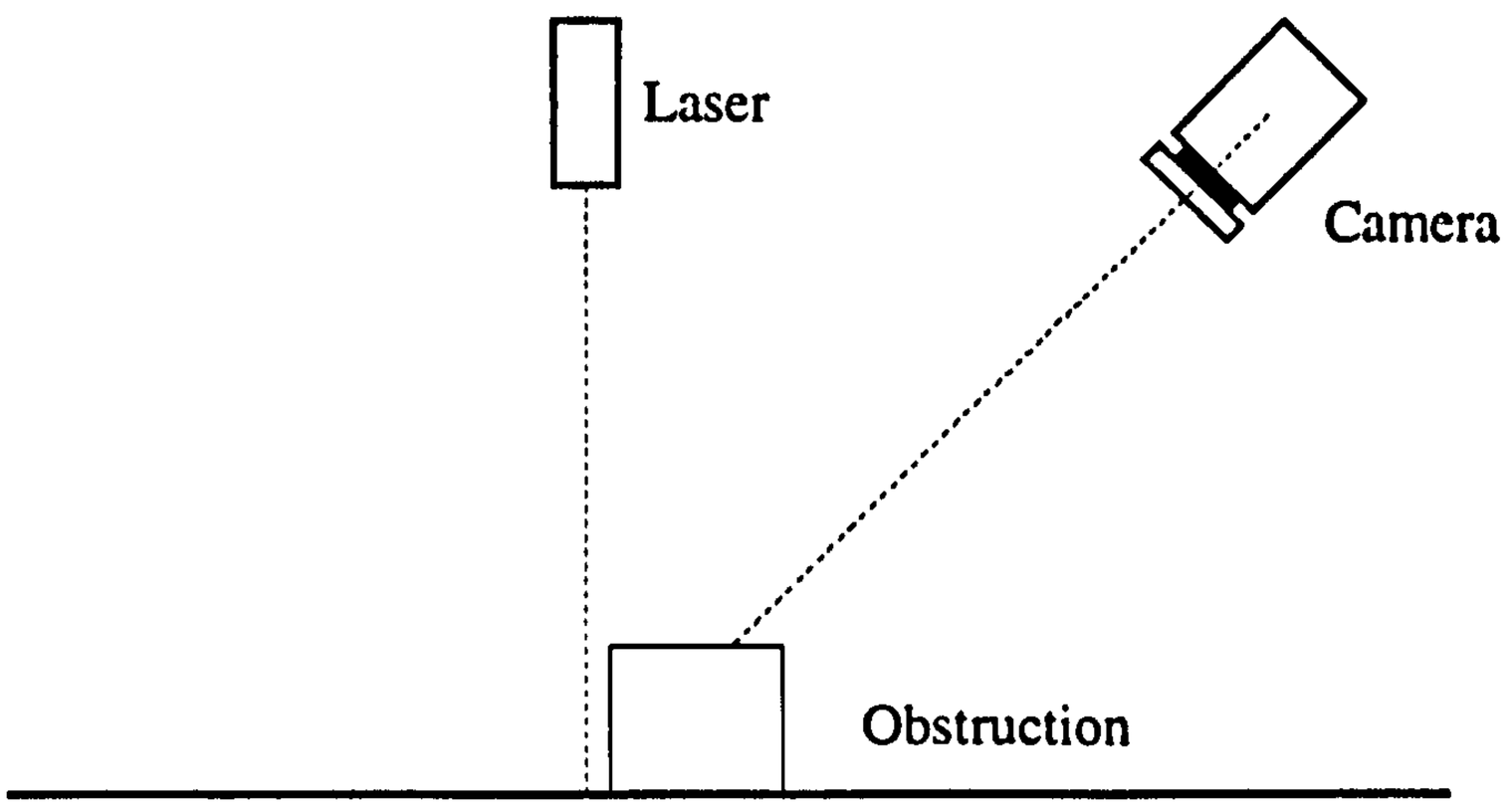

Figure 5.4 Information loss due to obstructions.

The actual edge for the image in Figure 5.3b, could lie anywhere between the histogram limits, E and S. Furthermore the smoothing operation performed on the X axis histogram results in the position of point S occurring well within the observed second part of the line-stripe. In cases such as these, a representation of the edge position can be obtained by selecting a threshold level which is mid-way between the upper and lower

histogram limits resulting in a maximum error, for this type of edge, in the order of 0.6mm.

In order to overcome some of these limitations and regain the lost information as to workpiece thickness, additional processing can be performed.

5.4 Edge position determination for complex edges.

Where an edge is well defined, square cut, but complex due to the nature of the workpiece (e.g. irregular or non-flat) information can still be obtained in addition to the component's edge position. The implementation of histograms is still used in the early stages of processing to determine the location of the line-stripe within the image as well as determining a threshold level that will be used to perform line thinning.

5.4.1 Accurate edge extraction of square cut edges.

The region of interest is determined firstly by calculating a Y axis histogram as before. This allows for the background intensity threshold level, T_b, to be calculated. By reapplying this to the histogram the location of the line-stripe within the image in the Y axis can be found (Figure 5.5). An X axis histogram could similarly be calculated. However as the line-stripe generally covers the majority of the camera's X axis field of view this is regarded by the author as an unnecessary computational overhead.

The located line-stripe is then thresholded and thinned into a single pixel line. This is achieved by selecting a second threshold level, T_l, which corresponds to the laser intensity on the workpiece. T_l is selected so that pixels whose intensity lies within the top third of the Y axis histogram will be regarded as on, (1), with all others being

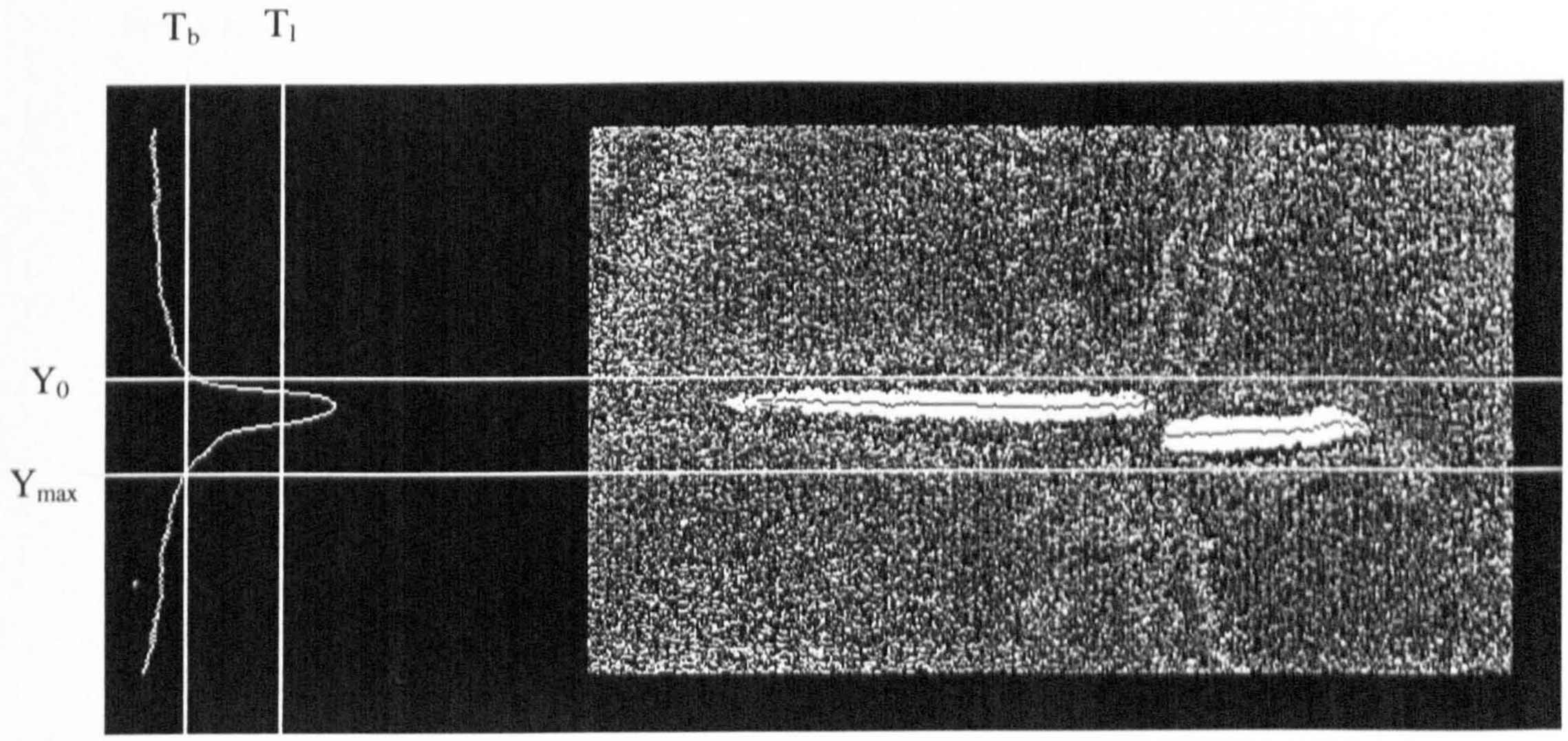

a) Line profile extraction.

b) magnified image of the processed line-stripe.

Figure 5.5 Image processing techniques for edge characteristic extraction.

off (0). This level could be determined by calculating a histogram of number of pixels against intensity, this would however not provide information as to the location of the line-stripe.

The thresholding and line-thinning is performed in one pass starting at the top left-hand corner, (0,0), of the determined area of interest and scanning down the image to Y_{max} before incrementing in X. When a pixel is encountered whose intensity exceeds T_1 a count is started. The count continues for each consecutive pixel whose intensity is also above the threshold level. If a pixel is detected to have a value below T_1 then the count is terminated. The location of the pixel in the centre of the 'on' region is then recorded, the Y search reset to zero and X increased, this process being repeated across the width of the image. However, in order to eliminate specular effects, if the count is less than T_3 (the number of pixels required to define an edge), these pixels are ignored and the scanning process is allowed to continue. T_3 can vary from material to material depending on its surface characteristics, however the author found experimentally that a value of four was adequate for the samples investigated.

This results in an series of rectangular co-ordinates representing the thinned line-stripe. This is processed to locate the discontinuity and the ends, E & S, of the line-stripe sections, thus defining the region in which the edge must lie. In addition, the vertical distance between the line-stripe sections at E and S, allows for the edge thickness to be determined.

This mechanism is more robust than using histograms alone, as it is not affected by small misalignment errors. It also provides the ability to determine the edge thickness with little additional overhead regardless of the histogram shape.

5.5 Edge determination for folded parts.

Where components are to be joined to form a single workpiece the individual part's edges are either square cut, or folded. The case for square cut edges has already been considered, however where the edges are formed by folding additional factors have to be considered. A folded edge is formed by skiving, (ref. Chapter 1, Section 1.2), a percentage of the material from around the edge. Adhesive is applied and the edge folded over to produce a clean 'rounded' edge.

Using the approach discussed in section 5.4, further information relating to the cross-sectional profile of the edge can be obtained. Hence, a square cut edge and its thickness could be differentiated from a folded edge, which in turn could have its degree of pear-shaping, (the blooming effect caused by folding), defined. In addition the information gained could be used for corrective edge following or position identification. This would be achieved by detecting certain characteristics along the edge, such as a joins or seams.

5.5.1 Characteristic extraction.

Once an image has been obtained and processed, as before, to a series of rectangular co-ordinates, representing the thinned laser line-stripe image this information can be processed to obtain a number of key points and distances, Figure 5.6. These can be used in order to enable an approximation of the edge profile to be made.

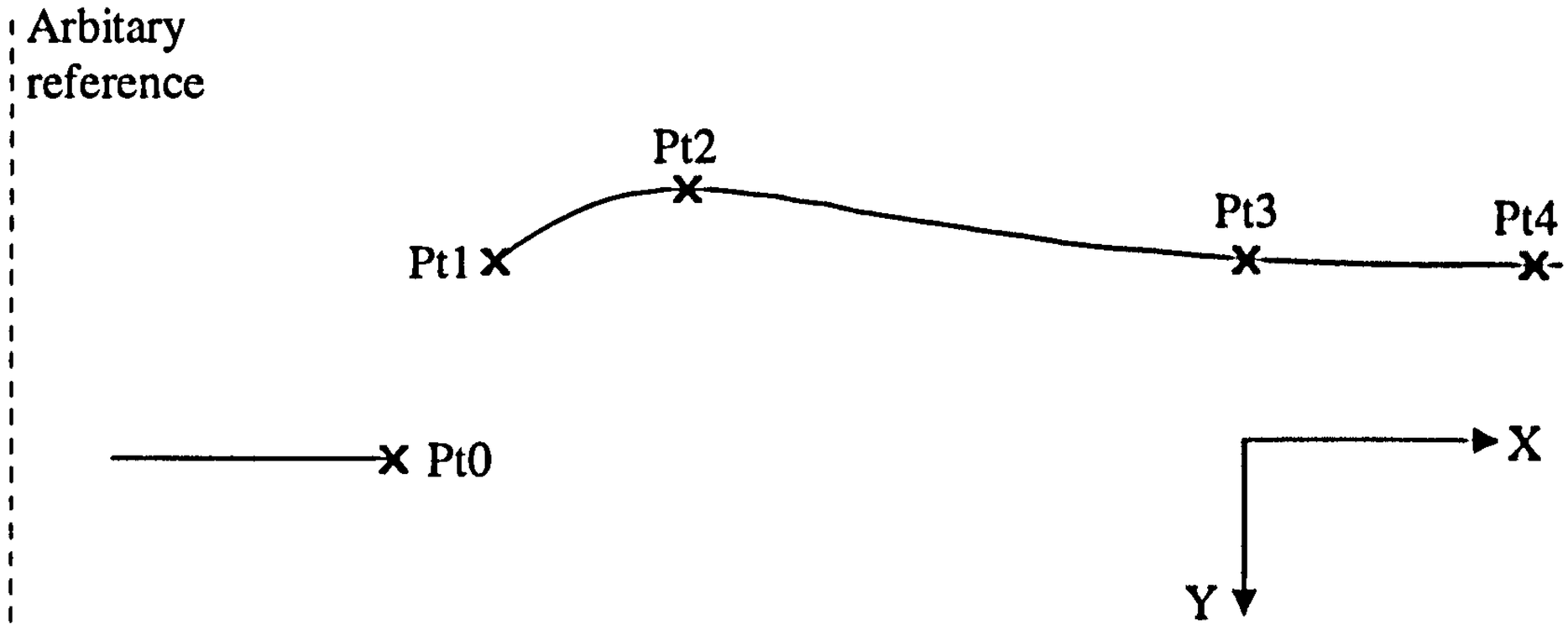

a) Key points extracted

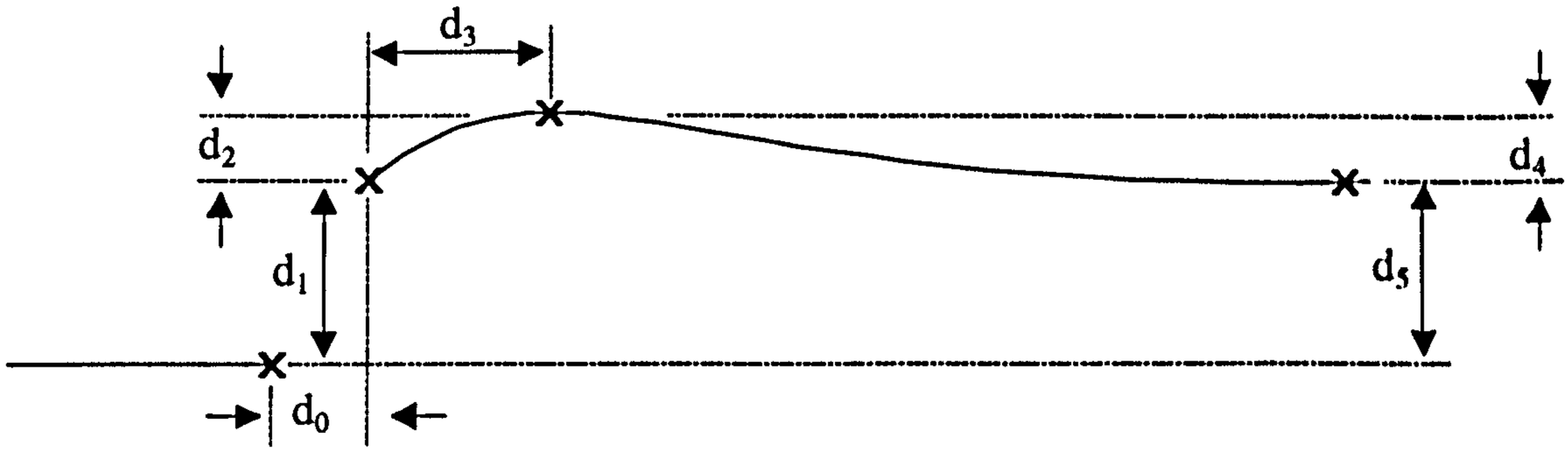

b) Key distances determined

Figure 5.6 Characteristic points and distances used to determine the edge profile of a folded part.

With reference to Figure 5.6 the distance d_5 enables a measurement to be made as to the material's thickness, if it is assumed that at this point the thickness observed is twice that of a single skived thickness. The degree of the fold (amount of pear shaping) is given by the distance d_4 which is quoted as a percentage of the material thickness.

The edge of the workpiece can be said to lie between $pt0._x$ and $pt1._x$ with the gap, ($pt1._x$ - $pt0._x$) resulting from misalignment errors and/or the effect of light roll-off over the curved edge. The true edge is defined as the position of the edge within this gap.

In the following sections a mechanism will be discussed to allow for the true edge position and profile to be determined regardless of the degree of pear-shaping or the roll-off characteristics. In order to achieve this two assumptions have to be made.

Assumptions :-

1. The material thickness is given by $\frac{d_5}{2}$.

2. The profile at the fold, once pear-shaping is removed, is semi-circular with the radius of curvature being that of the material thickness.

5.5.2 Tightly folded edges.

Where tightly folded edges are to be followed the true edge position can be approximated by fitting an ellipse to the extracted edge profile in order to eliminate the effects of roll-off, Figure 5.7.

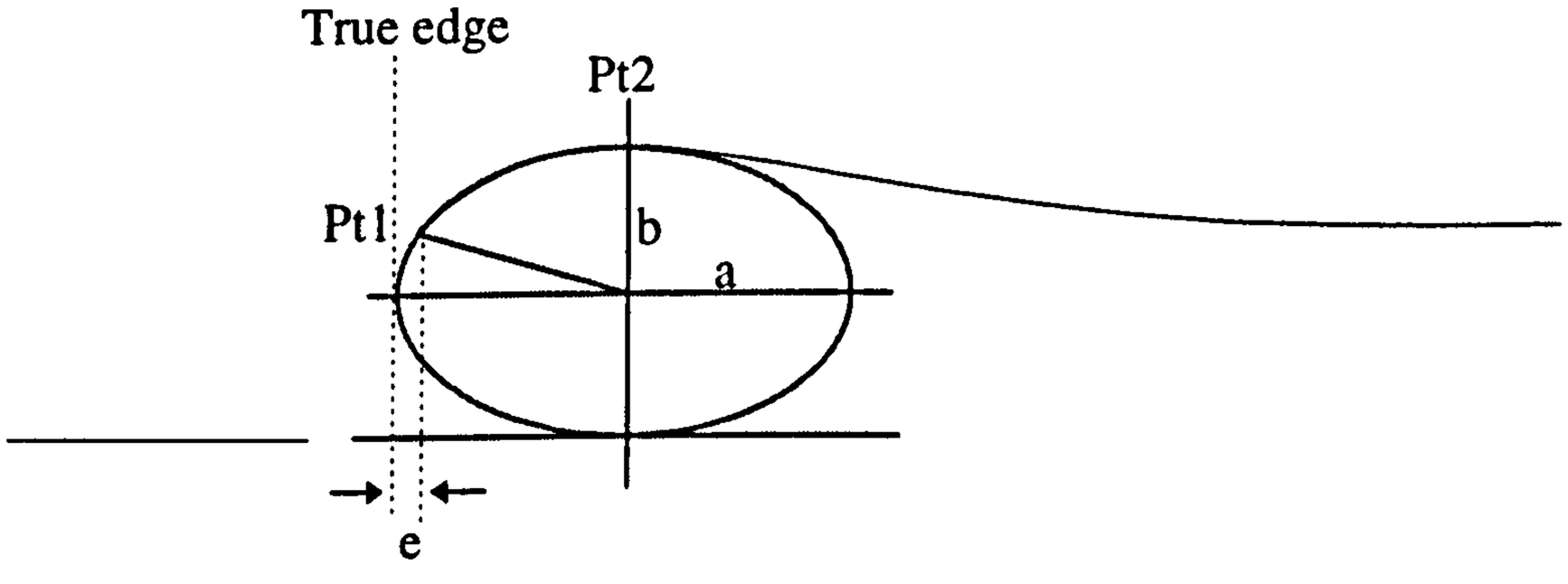

Figure 5.7 Roll-off compensation for a folded edge.

where,

b is given by $(d_5+d_4)/2$
e is the error from the true edge
a is calculated by substitution using the co-ordinates from Pt.1.

The equation of an ellipse is given by,

$$\frac{x^2}{a^2}+\frac{y^2}{b^2}=1 \quad \text{.....Equ.1}$$

rearranging gives,

$$a=\sqrt{\frac{b^2x^2}{b^2-y^2}} \quad \text{.....Equ.2}$$

Therefore, the length 'a' for the major axis of the ellipse can be calculated using Equ.2, by translating the co-ordinate origin to lie at the centre of the ellipse, and by substituting the values for Pt1.

Hence,

$$x = Pt2._x - Pt1._x \text{ , } y = Pt2._y - Pt1._y + b \text{..... Equ.3}$$

The error distance 'e' is then given by,

$$e = a - x \quad \text{..... Equ.4}$$

By adjusting the perceived edge by the calculated roll-off error the true edge position can be identified, thus allowing for fluctuations in the accuracy of the fold to be automatically compensated for. The accuracy of ellipse fit to the profile of the edge can be seen in Figure 5.8(a).

5.5.3 Edge profile representation.

From the extracted information the surface profile of the edge can approximated. In order to complete the cross-sectional representation of the fold and high-light the pear-shaping effect the inner profile has to be determined. This is achieved by selecting a number of points that are the thickness of the part inside the known outer edges. A series of cubic splines are then fitted through these points.

Points used for inner profile determination:-

1. $Pt3_{.x}, Pt3_{.y} + \frac{d_5}{2}$
2. $Pt2_{.x}, Pt2_{.y} + \frac{d_5}{2}$
3. $Pt1_{.x} - e, Pt2_{.y} + \frac{d_5 + d_4}{2}$
4. $Pt0_{.x}, Pt0_{.y} - \frac{d_5}{2}$

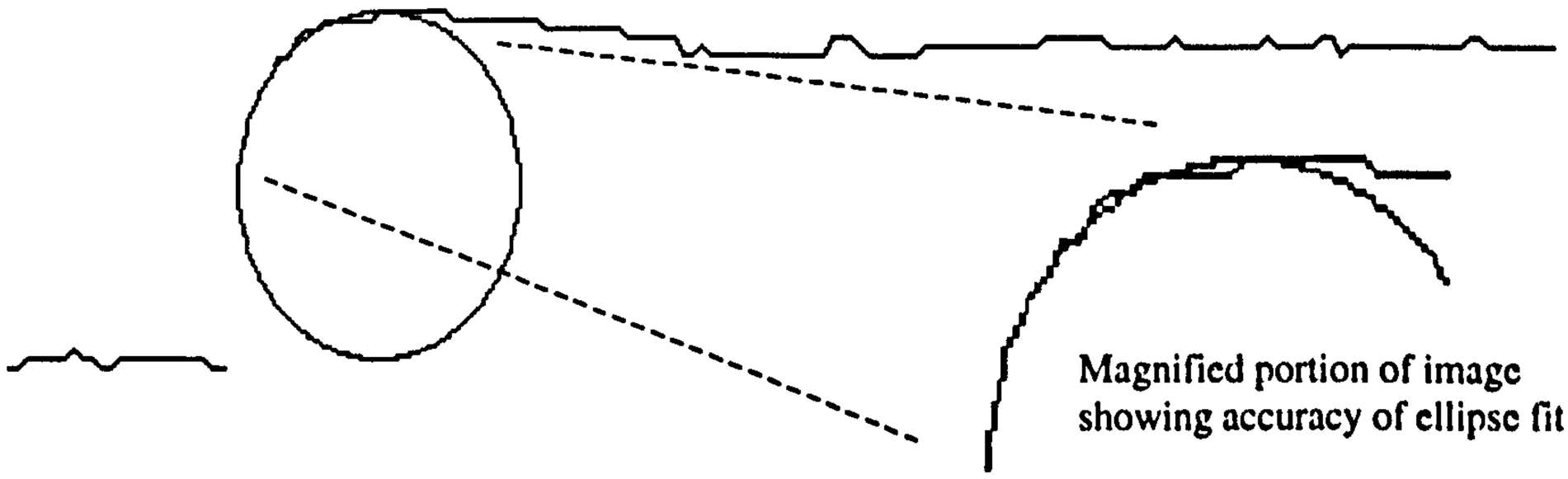

a) Result of fitting an ellipse to extracted line-stripe information

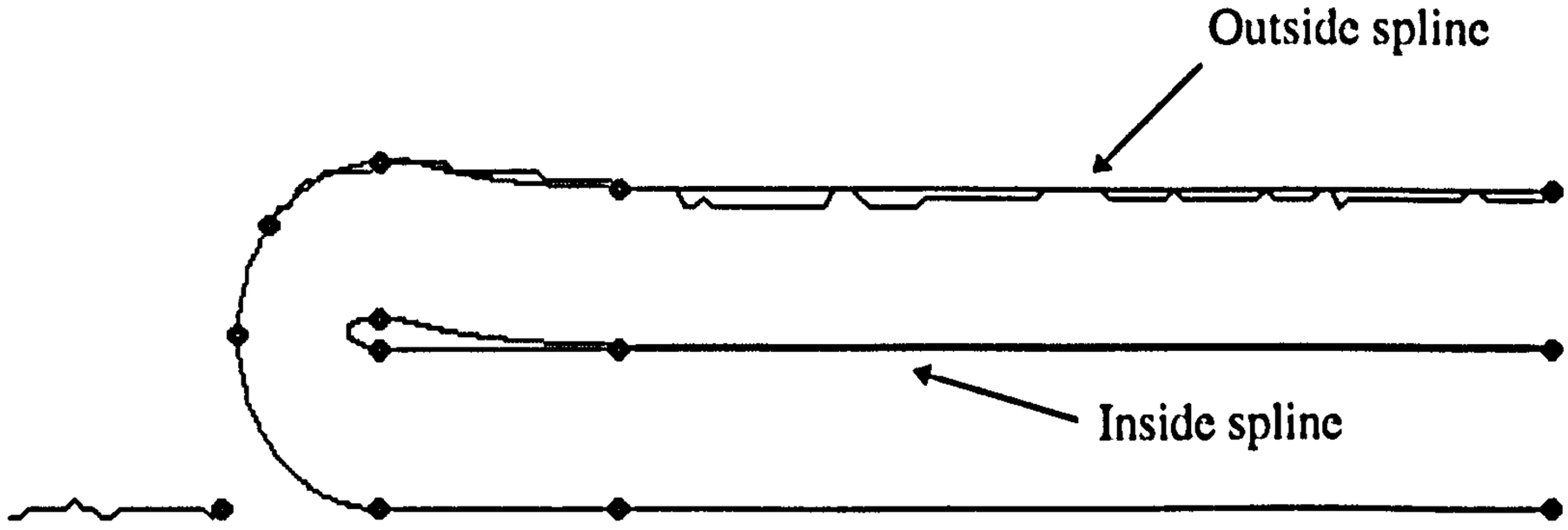

b) Result of combining the inside and outside spline methods
to represent the cross-section of a folded edge

Figure 5.8 The results of processing for a folded edge.
Pear-shaping = 9.0% of component edge thickness.

Figure 5.8(b), shows how, combining the inside spline representation and surface profile, a graphical representation of the fold cross-section can be made.

Where corrective stitching is to be performed, or where the true edge position, after the pear-shaping effect has been removed, is required, some additional processing is needed.

5.5.4 Closed fold edge determination.

The position of the closed folded edge can be similarly plotted in order to achieve a full understanding of the edge profile. This is achieved using assumption 2 (page 122). (I.e. the fold once pear-shaping has been removed is semi-circular with a radius of $\frac{ds}{2}$). However in order to determine where the closed edge is positioned the length of the path between points A to D has to be calculated. Figure 5.9.

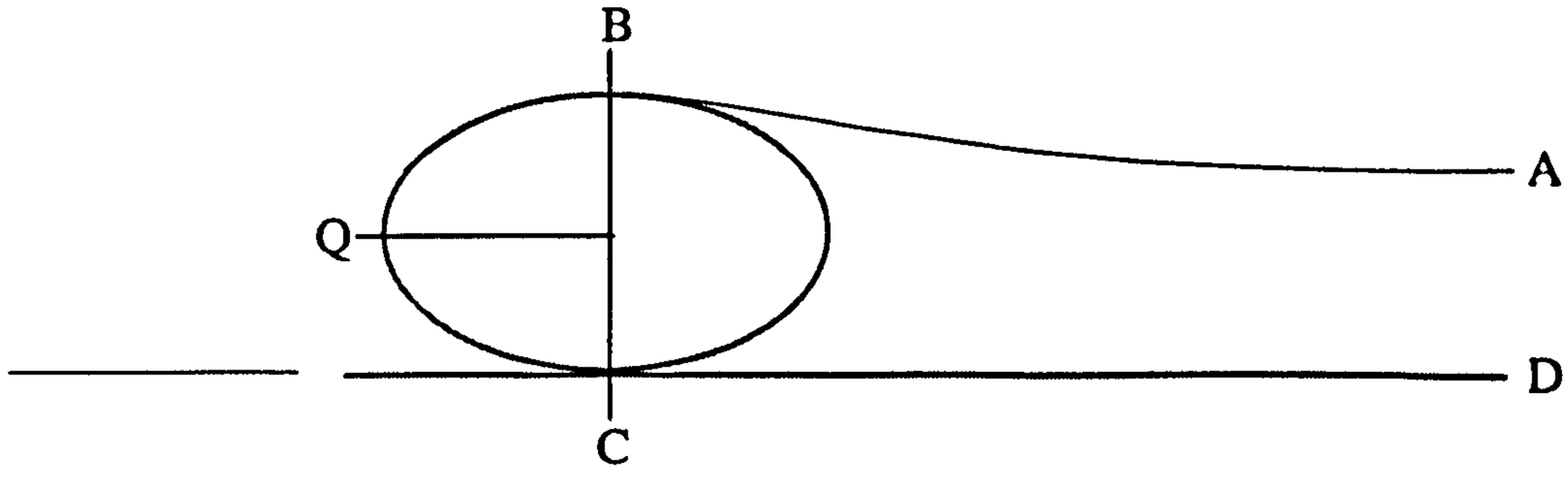

Figure 5.9 Determination of closed edge position for a folded part.

The distance C-D is a straight line whose length is determined from the previously extracted points. The length of the arc B-C is determined by the ellipse used to approximate the edge profile in its natural, pear-shaped, state. The remaining distance A-B can be approximated by cubic splines through calculated points between Q and A, thus ensuring a close fit to the original data. Cubic splines have the effect of smoothing out the extracted profile, thus eliminating any noise that may be present due to surface characteristics or image processing.

As the total profile length A-D remains constant even when the profile is 'flattened, by subtracting the length of the arc for a tight fold, $\frac{\pi d_5}{2}$, the start of curvature can be defined, with respect to the arbitrary reference as,

$$Pt4_{.x} - \frac{AD - \pi d_5}{2}$$

Thus the position of the closed edge is given by,

$$Pt4_{.x} - \frac{AD - d_5(\pi - 1)}{2}$$

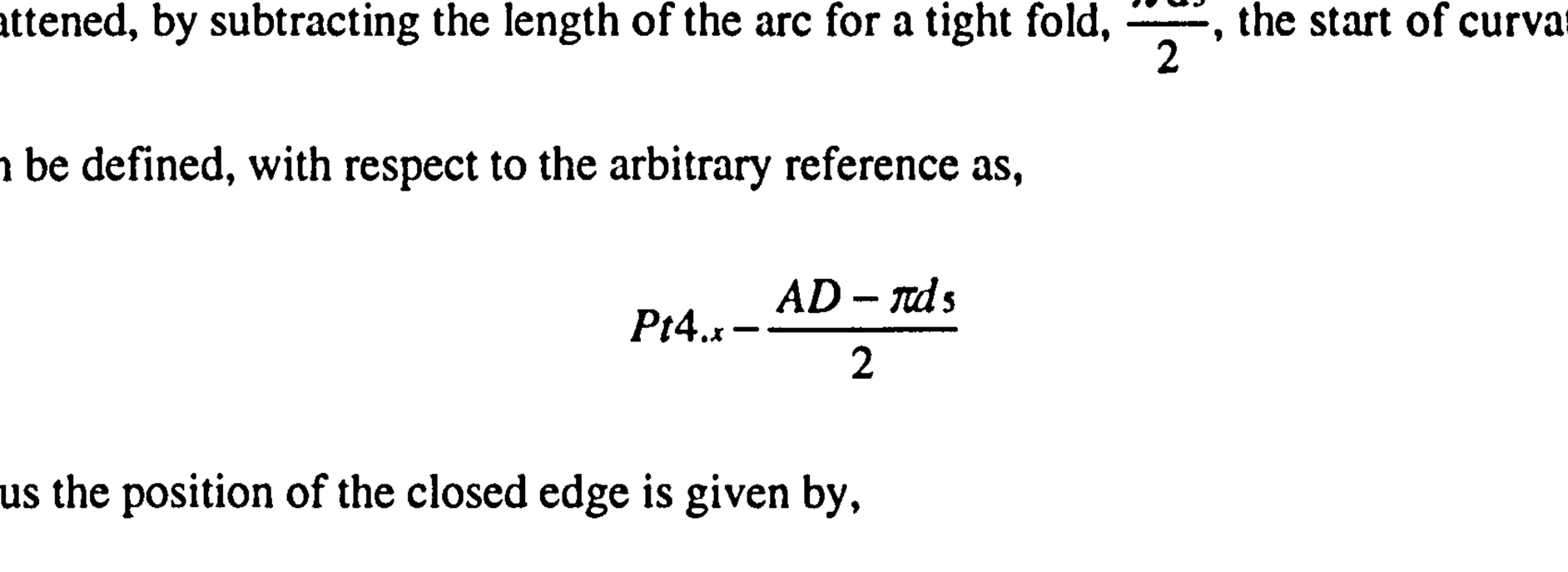

Figure 5.10 Graphical representation of edge profile characteristics.
Pear-shaping = 9.0% of component edge thickness.

5.5.5 Results on edge profile extraction.

In order to evaluate the effects of folded edges on edge following, 5 samples were processed to extract the perceived, true and closed edge positions. Table 5.1, shows the results obtained from these samples.

Sample	Perceived edge (Pixels)	True edge (Pixels)	Closed edge (Pixels)	Pear shaping (%d_s/2)
1	153	143	138	9
2	150	140	133	15
3	116	107	95	72
4	156	140	138	15
5	114	109	95	72

Table 5.1 Edge position results for test samples 1-5.

The experimental configuration was calibrated such that a single pixel represented approximately 25μm. Consequently the variation of 16 pixels from perceived to closed edge position for sample 3 equates to a displacement in the edge of the part of 0.525mm. This may in certain circumstances result in visible variations in stitching accuracy.

It can be seen from these results that the error in edge position from the perceived to the true edge fluctuates and does not directly relate to the degree of pear-shaping. This is most likely due to component-camera misalignment and variations in light roll-off angle, both of which can be estimated.

The edge-camera misalignment, M is,

$$M = Pt.0_x - Edge_{true} \quad \text{Equ.5}$$

The roll off angle, α, (Figure 5.11) can be calculated from the equation of the ellipse used to approximate the edge profile. This is achieved by differentiating the ellipse equation with respect to 'x'.

Equation for an ellipse

$$\frac{x^2}{a^2}+\frac{y^2}{b^2}=1 \quad \text{Equ.6}$$

Solving for y,

$$y=\sqrt{\left[1-\frac{x^2}{a^2}\right].b^2} \quad \text{Equ.7}$$

Differentiating w.r.t. x,

$$\frac{d}{dx}\sqrt{\left[1-\frac{x^2}{a^2}\right].b^2} = \frac{-b}{\sqrt{1-\frac{x^2}{a^2}}}.\frac{x}{a^2} \quad \text{Equ.8}$$

Thus the roll-off angle is defined by the arctangent of Equ.8.

$$\arctan\left[\frac{-b}{\sqrt{1-\frac{x^2}{a^2}}}.\frac{x}{a^2}\right]=\alpha \quad \text{Equ.9}$$

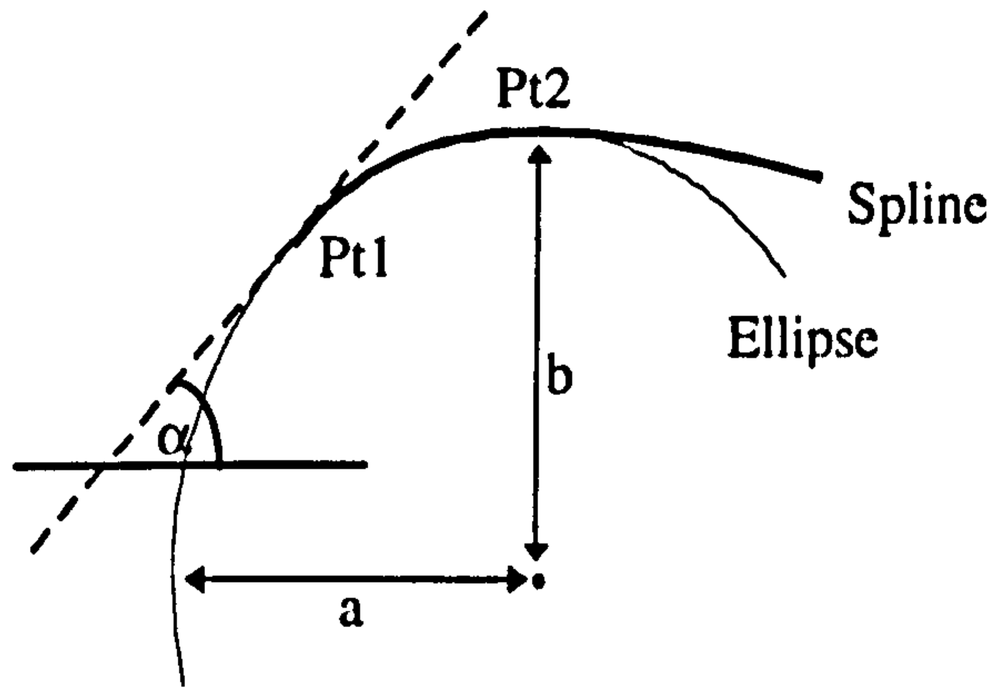

Figure 5.11Determination of roll-off angle for incident laser light.

Consequently by substituting the co-ordinate value for the furthest well defined spline point, Pt1, into Equ. 9, a value for the light roll-off angle can be ascertained. Table 5.2 contains results obtained from samples 1-5 for roll-off angle and edge misalignment.

Sample	a (Pixels)	b (Pixels)	α (degrees)	M (Pixels)	Pear shaping (%d‹/2)
1	46	57	57.3	-5	9
2	46	58	57.8	-2	15
3	51	57	58.4	6	72
4	49	58	47.2	-2	15
5	41	55	67.9	2	72

Table 5.2 Roll-off and alignment errors for test samples 1-5.

The results show that there is no correlation between the degree of the fold (pear-shaping) and the roll-off angle. This is to be expected as the samples had varying surface properties with respect to reflectance of the laser light. Appendix L contains the processed images for these samples.

5.6 Conclusions on edge following.

A number of mechanisms for edge following have been investigated from simple square cut to complex folded edges with each mechanism having its own merits. Consequently the selection of which mechanism should be used for any one application would have to be evaluated against the system performance requirements.

For the purpose of following simple edges, where the need for characterisation of the edge profile is not required and where components have no lining, the traditional back lighting mechanisms still have their place. However, if additional detailed information is required about the profile of the edge then the laser line-stripe methods offer greater rewards. Unfortunately the major disadvantage of laser triangulation methods is that they require a considerable amount of processing to be performed. In addition such systems are costly as they require both a laser and a high definition area camera, together with a powerful processing environment.

Applications for profile extraction of folded edges are mainly limited to corrective edge following, where the edge position after stitching is determined in advance, so as to ensure a smooth stitch line, Figure 5.12(c). If the edge were to be followed without this correction, the resultant stitch line quality may be poor for high degrees of pear shaping and effects similar to those in Figure 5.12(d) may occur.

Figure 5.12(e) shows a possible application where it may be wished to maintain the pear shaping effect. Here the stitch position is selected so as to maintain a consistent fold in order for a lace or top-line tape to be sewn in.

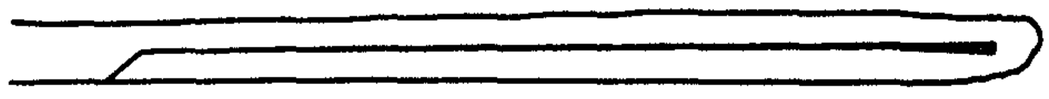

a) Ideal tight fold

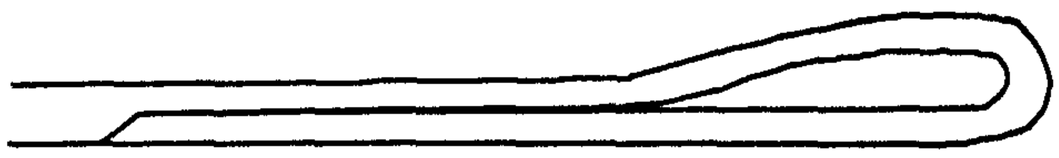

b) A badly pear-shaped fold

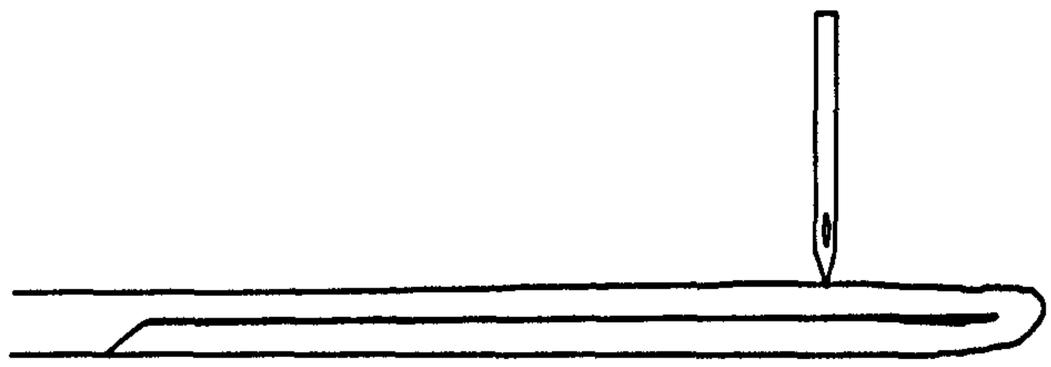

c) Stitching to close the fold

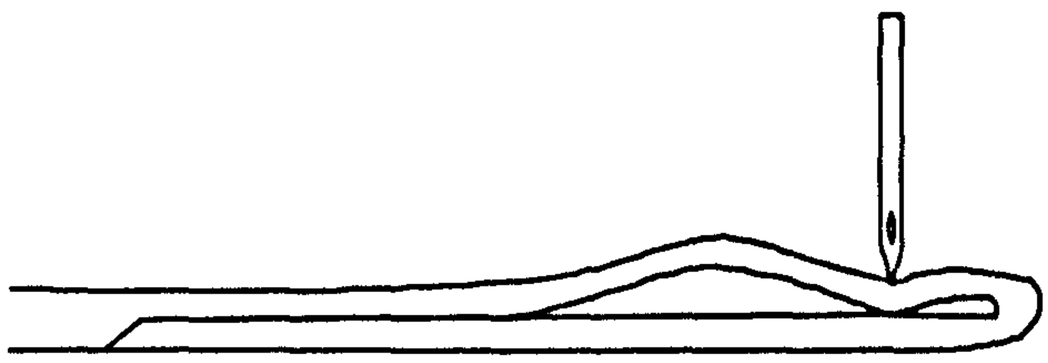

d) Incorrect choice of stitching position

e) Stitching to maintain a consistent pear-shaped fold

Figure 5.12 Possible stitching effects observable for folded edges.

When an edge is placed in the field of view the laser line-stripe appears to be discontinuous with the shape of the line being dependent on the topology of the edge. However even if an edge is not present the same arrangement can provide some very useful information, namely that of the workpiece thickness. If an image of the stripe is taken with no part present, i.e. the line-stripe is incident on the base table (reference plane), its position in the vertical plane of the camera can be recorded. When a part is placed in the field of view the line-stripe will remain continuous, but will be displaced from the reference position due to the part's thickness. Such a system could be used to monitor the consistency of a part's thickness after a thinning process such as skiving.

In contrast the application of lasers for topographic applications can be taken even further with regards to 3-D applications within the shoe making industry. The final operations of roughing, lasting, and soling to be performed in the construction of a shoe, require a high degree of three dimensional information. The following chapter contains an investigation into laser triangulation techniques that could be used to automate these operations.

Chapter 6

3D profile extraction for making processes

6.0 Introduction.

Once the upper has been assembled in the closing room only the 'making' processes remain. These give the shoe its final three dimensional shape. The research into topography for 'making' is a natural progression from the laser line-stripe work on edge following. Here operations which are still manually dependent, (lasting, roughing, cementing and soling) will be discussed with a view to automation.

The object is scanned in a raster manner allowing for a surface map to be constructed. Features are then extracted according to the operation to be performed.

6.1 Lasting.

Lasting, as described in Chapter 1, is the complex task of deforming an upper on a last so as to take a sole and define the final shape of the shoe. Here operator skill is required to ensure correct component alignment before the leather is finally cemented, and / or nailed to an insole 'rib'. The rib acts as the base of the shoe until it is soled, as well as providing support to the wearer when the shoe is complete. The edges of the upper are gripped by a series of pincers which can be manipulated to pull parts of the

upper so that it becomes orientated on the last to the operator's satisfaction. This is a highly skilled task as the result determines the symmetry of a pair of shoes. Consequently lasting operators are amongst the most respected and highly paid shoe makers.

In order to automate the lasting process the vision system has to be capable of detecting small fluctuations in pattern. To achieve this an accurate representation of the upper, when on the last, is required. It should be noted that it is beyond the scope of this thesis to develop mechanisms capable of performing adjustments to the orientation of the presented objects.

6.1.1 Upper topography.

In order to view the whole width of a presented shoe, the laser line-stripe has to have a length in the order of 120mm, with the camera configured to observe this area. Consequently to be able to detect features on the upper the camera has to have sufficient resolution. The camera implemented consisted of a 512 x 512 pixel array, giving approximately 4 pixels per millimetre.

In order to scan the surface of the upper on the last, whilst it is held in the pincers of the lasting machine, the laser has to be moved relative to the shoe as the orientation of the last is fixed. Figure 6.1 shows how this is achieved by stepping the laser through small angles. For a very large shoe the required scanning distance could be in the order of 200mm. Hence, with the laser located some 500mm above the shoe, this results in a total angular movement of approximately 11.3° either side of the vertical. To achieve a

high scanning resolution the laser was coupled through a 100-1 gearbox to a 1.8° stepper motor. This resulted in a single step of the motor producing a scanning movement of 0.16mm on the reference plane.

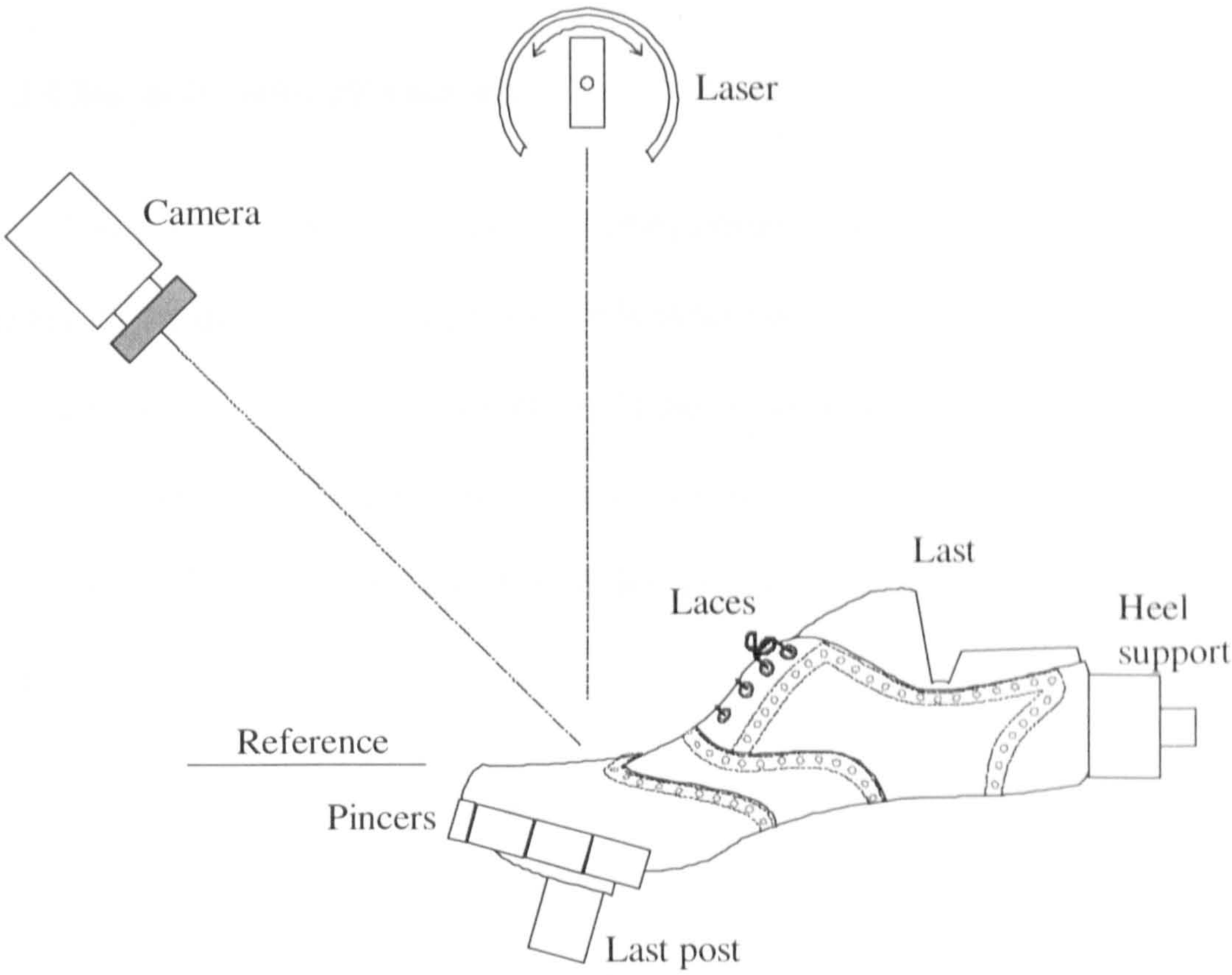

Figure 6.1 Scanning configuration for Lasting applications.

This resolution is far in excess of any practical value, as processing time has to be kept to a minimum. In a shoe factory the turn round time between shoes is typically six seconds, with three seconds being 'bedding time', (i.e. the time taken to ensure the adhesive forms a strong, permanent bond). However, to be able to cover a size range, the scanning resolution has to be graded in accordance to the shoe size. Thus a model

size 8 may have a scanning resolution of 5mm, however, if a size 5 was loaded the laser movement would have to be graded to give a resolution of approximately 4.5mm in order for the same features to be extracted.

6.1.2 Characteristic extraction.

Every style of shoe has its own characteristics some of which can be very complex. If the shoe is to be lasted correctly these characteristics have to be extracted and their position relative to the orientation of the last determined. These parameters can then be compared to a template to enable the required manipulations to be performed. The template is derived using the same techniques as those described in the following sections.

The first feature to be extracted is the orientation of the last. This is required to determine if the last has been presented correctly to the machine. It also forms a reference to allow comparisons to be made with the template. This is determined by considering each line-stripe in turn. The depth of the image, d, is divided into three and the width, w, of the image across the top third measured. The mid point of this value is then said to be the centre of the last. Figure 6.2 shows how this performed. This method cuts off the ends of the line-stripe thus removing any edge effects that may be present due to misalignment.

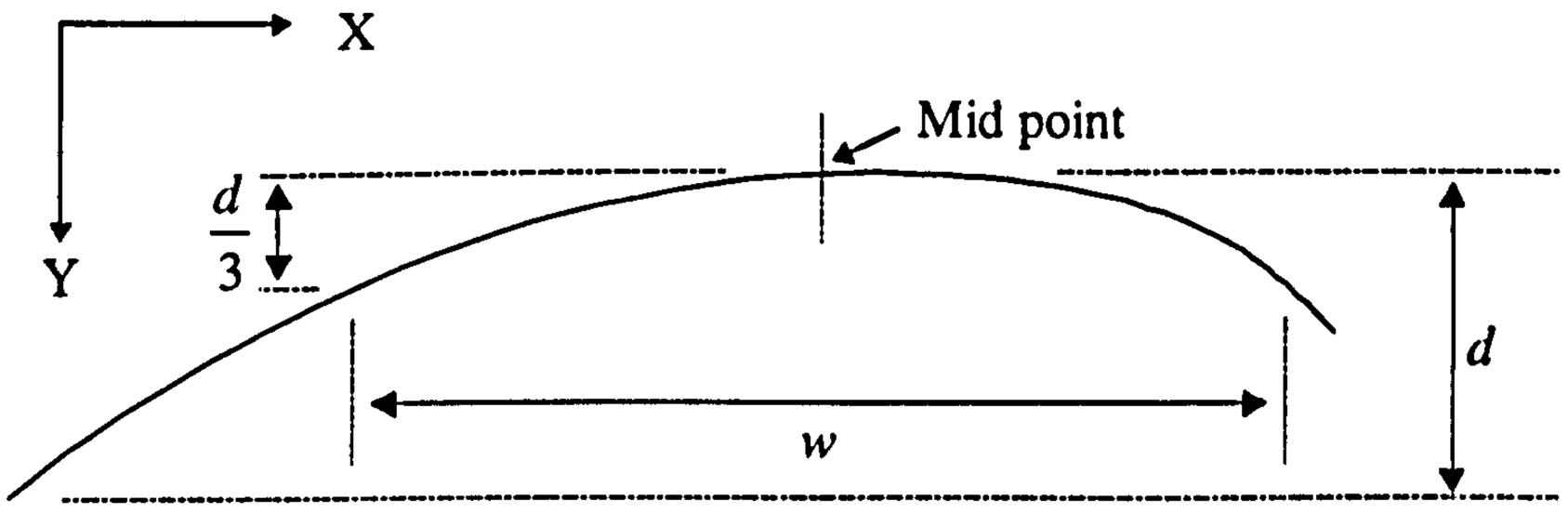

Figure 6.2 Determination of Last alignment.

By repeating this procedure for the line-stripes over the forepart of the last a series of co-ordinates can be determined. A line of best fit is then made through these points in order to compensate for fluctuations in the images. The angle this line makes with the reference defines the angle of the last. Figure 6.3a-b shows an image of a brogue upper with the reference and calculated centre lines. The reference is perpendicular with respect to the camera and starts at the mid point of the toe. The toe position being well defined by the mechanics of the lasting machine.

The value for last angle can be interrogated to decide if it has been presented to the machine within an acceptable tolerance. This value was selected to be 3° as this corresponds to a maximum vertical, Y, displacement of approximately 0.25mm or 1 pixel. If the last alignment is outside this value it is rejected and must be re-loaded. Even within this tolerance this can produce horizontal, X, positional errors with respect to the template, in the order of 8mm. Consequently the data points need to be adjusted such that the angles for the template and the current last match. This is achieved by adjusting the template data such that the perceived last angle is zero before saving. By similarly adjusting the image under investigation a match can be made. The data can only be

moved in the X direction as a true rotation would result in the line-stripes becoming skewed. Figure 6.3c shows the effect of compensating for last misalignment.

This method of last angle determination, although it does not identify the true centre of the last, it is highly consistent from style to style. As the template is derived in exactly the same manner there is a constant reference within any given style. Appendix M.1, contains examples of last alignment determination and correction for a variety of shoe styles. The results show that the points extracted in order to calculate the centre line of the last, have very little deviation about this line. This is especially true over the forepart of the last where there are no significant topographic changes. For this reason the points used to calculate the centre line are restricted to those located within the first third of the shoe length. The remaining points are displayed for reference only.

Once the line-stripe data has been corrected, it has to be compared to the template data in an attempt to determine the manipulations required to align the features. Two possible methods of comparing the extracted data against that of the template will be considered. Those of 'feature extraction', and 'positional comparison'. The first method requires that there are a number of identifiable features present on the upper. It then uses the location of these features to determine the degree of manipulation required to locate them correctly with respect to the orientation of the last. The positional comparison method considers the general form of the line-stripe without regard to particular upper characteristics.

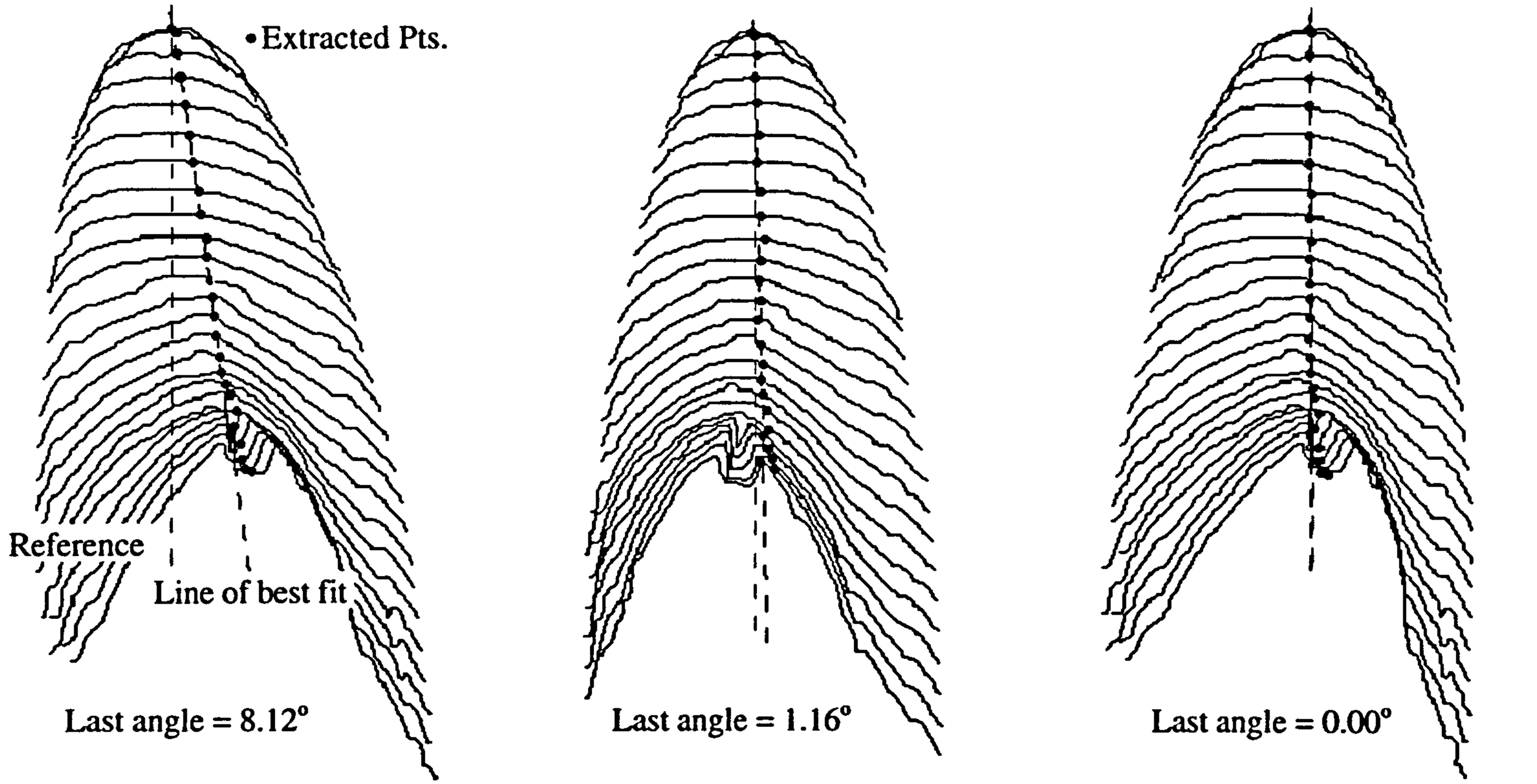

a) Unacceptable last angle b) Last loaded within tolerance of 3° c) Image a) after angular correction

Figure 6.3 Examples of Last alignment errors for a Brogue style upper. (Sample 1).

The features to be identified have to posses characteristics capable of being detected above those of background noise. The 'noise' is a result of the material finish, which may contain decorative stitching, punched holes or decorative coatings. Thus to achieve satisfactory results, this method is restricted to styles where the upper has significant changes in contour. These are located by interrogating the line-stripes for certain gradient characteristics. The most effective of which is a positive-negative-positive gradient which locates ridges within the image. Figure 6.4 contains the image of a moccasin type shoe after processing. The figure shows the image as perceived by the camera and with the data rotated to represent a view from above, (visual aid only), highlighting the profile defined by the extracted points. In this instance only the forepart, (approximately 40% of the shoe length), is processed as this is the critical region for this type of shoe. It is often the case that only the forepart can be processed as the uppers are generally laced during lasting to prevent undue movement of the upper on the last.

Figure 6.5 shows the same image after full processing. Here the whole image has been searched with both positive and negative gradient features displayed. In addition the highest point for each stripe has been recorded. A quick measure of comparison between the observed image and that of the template can be made by scoring. This procedure counts the number of features on each line-stripe. If there is a high degree of variation between the scores of the image and the template, the wrong style may have been loaded and should be rejected.

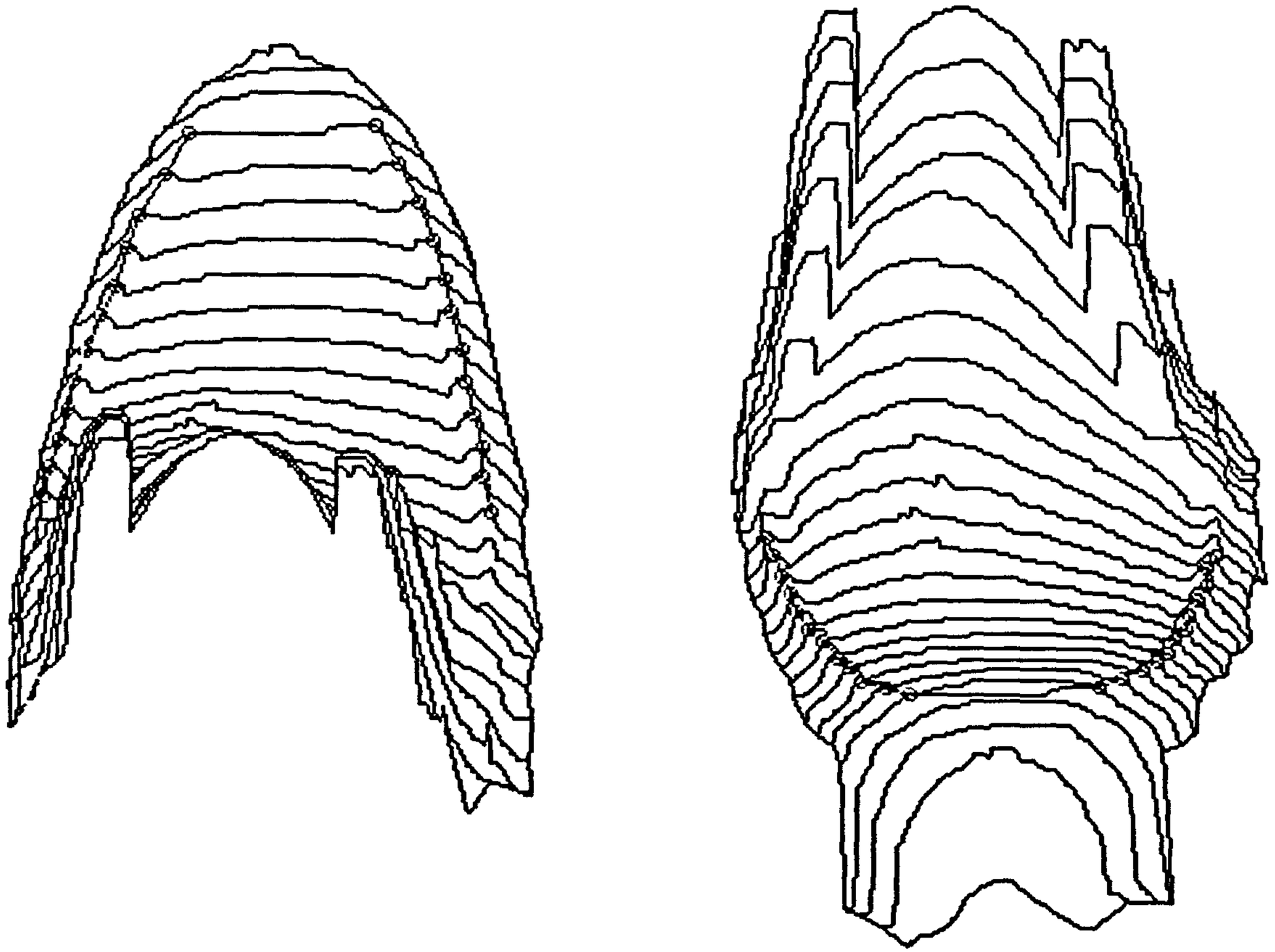

a) View from above b) Camera view

Figure 6.4 Moccasin type shoe with extracted forepart characteristics. (Sample 3).

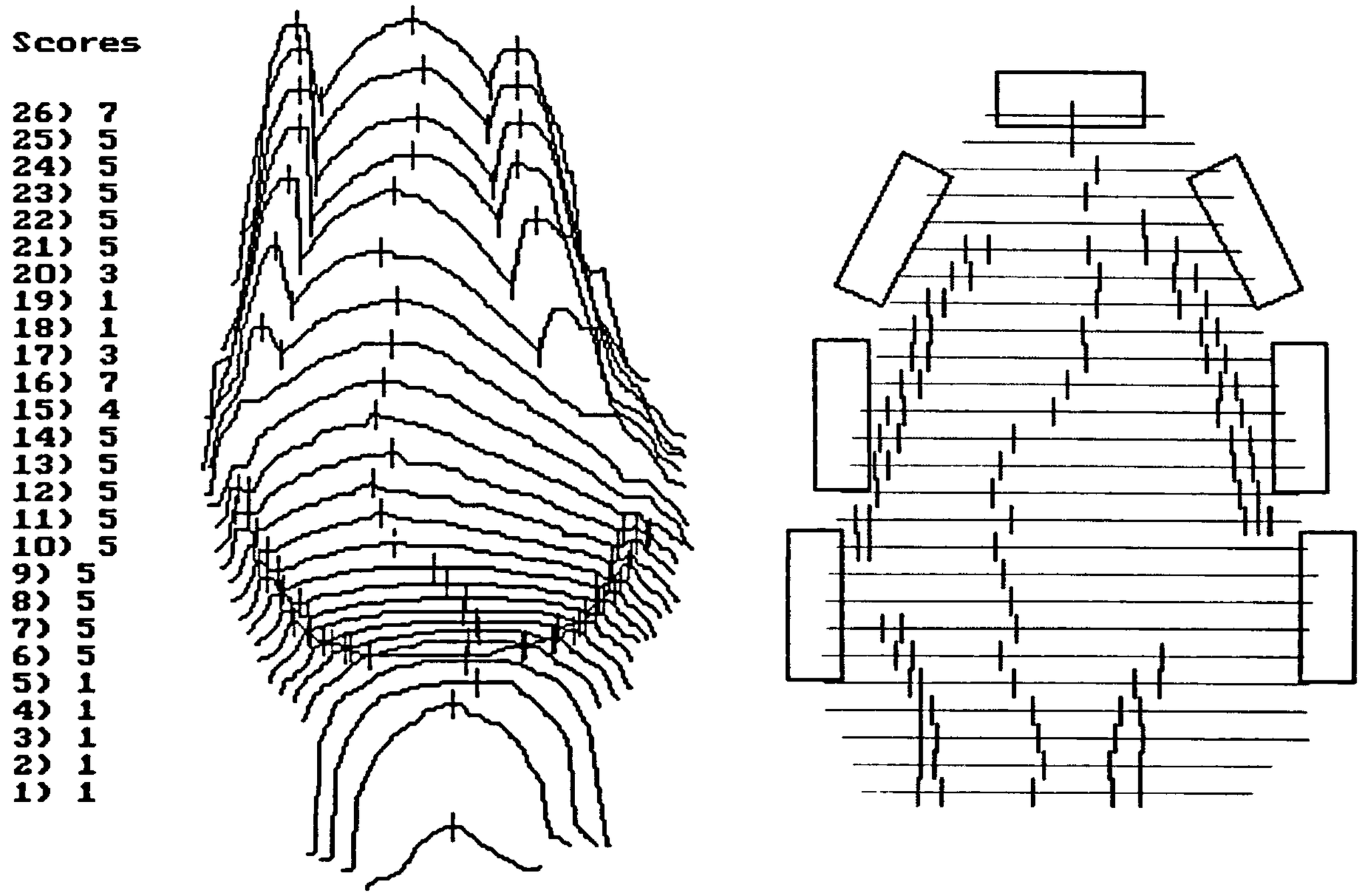

a) 3-D view of upper

b) Lasting plan view

Figure 6.5 Moccasin style shoe with full characteristic extracted. (Sample 3).

Figure 6.5b has the extracted points plotted with respect to the pincers used to perform the alignment manipulation. By comparing the relative positions of these points to those of the template the degree of required manipulation can be obtained. Appendix M.2-3, contains further examples of feature extraction for a number of shoe styles.

6.1.3 Profile matching.

This method performs a comparison between the extracted line-stripe and the template. As the upper can be manipulated by the pincers from both sides each line-stripe is divided into two about the extracted centre line. Before the comparison can be performed the object line-stripe has to be adjusted vertically, to correspond to that of the template, to ensure the best possible match. If this stage is omitted then the subsequent comparison can be highly inaccurate. The extracted line-stripe section is then passed across the respective template section and the degree to which the stripes match measured. The comparison histogram can then be examined in order to define a value for the positional accuracy of the line-stripe. From these values the required degree of manipulation can be determined for each pincer. The histogram is a measure of the number of matching points between the template and the specimen line stripes.

It can be seen from Figure 6.6, that the results obtained, for the brogue sample demonstrate a high degree of alignment. (Figure 6.6a shows the results of correlating the template data with itself). In this particular case the upper is well aligned to the template, however, should there be a poor match then the shoe could be rejected.

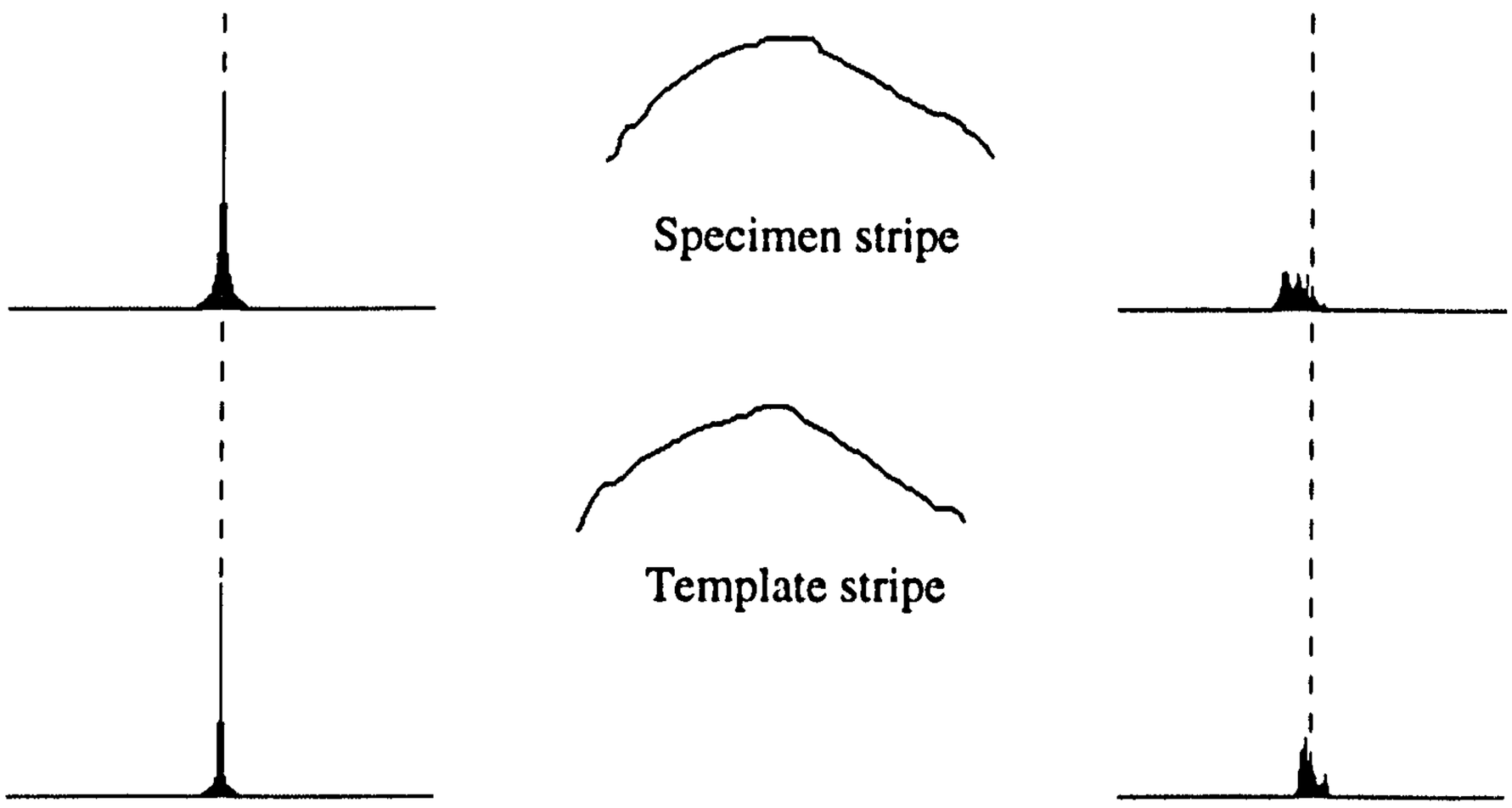

Figure 6.6 Results of line-stripe comparison.

Appendix M.4, contains further examples of line-stripe comparison measurements, including comparisons made between different shoe styles.

This method is subject to errors as the location of any single pixel is not well defined. The same shoe can be scanned several times, each producing slightly different results. This could to some extent be overcome by 'smudging' the template image. Here, the single pixel line would be increased by two or three pixels, thus increasing the band where a match occurs.

6.1.4 Discussion on lasting.

Feature extraction methods require a significant topographical characteristic such as moccasins, as previously illustrated. In this case the information required for manipulation can be readily extracted. This method also offers the benefit of requiring little data to be stored in the form of the template. Only the type of feature, the region to scan and the co-ordinates of the extracted features need be recorded.

The implementation of the positional comparison method is dependant on the accurate loading of the shoe into the machine and scanning of the object, although some degree of misalignment can be compensated for by additional processing. It is also liable to give false information due to the features of the upper generally covering only a small percentage of the line-stripe. Consequently the comparison histograms tend to be strongest when the edges of the shoe align, and not the upper features. Appendix M, Section 3, contains examples of the problems encountered using this method.

The aim of the research in this chapter was to investigate the difficulties involved in implementing vision techniques to enable automation of the lasting process. This proves to be an area where automation will be difficult to implement for general purpose work. However by increasing the resolution of the image system it may be possible to implement feature extraction for a sub-set of shoe styles. Of the methods investigated it is not believed that the positional comparison measurement, discussed in section 6.1.3, although simpler to implement could produce results accurate enough to be viable. However an understanding of the problems involved in performing automated lasting based around a vision guided system has been achieved.

6.2 Bottoming applications.

Once the shoe has been lasted, defining its three dimensional shape, it passes on to the bottoming section, for the remaining operations to be performed. Bottoming encompasses a number of operations, the chief ones being roughing, cementing and soling. The requirements of a vision system for these operations are essentially the same. Currently these operations are semi-automated, with the machines performing open loop based on a manually taught template. Here methods for removing the need for a template will be discussed.

6.2.1 Path determination.

The same principles to extract the raw line-stripe data are applied for bottoming applications as those described for lasting in the previous section. However in this case the laser is held stationary and the shoe is passed beneath it. Figure 6.7, shows the experimental set-up used for the purpose.

By moving the shoe through known movements under the laser, a raster style image can be built up of the shoe topography. This method of scanning the shoe is particularly suited for bottoming machines where the shoe is currently loaded in a similar fashion. Once the base of the shoe has been scanned the image line-stripes can be processed to extract the information required for automation.

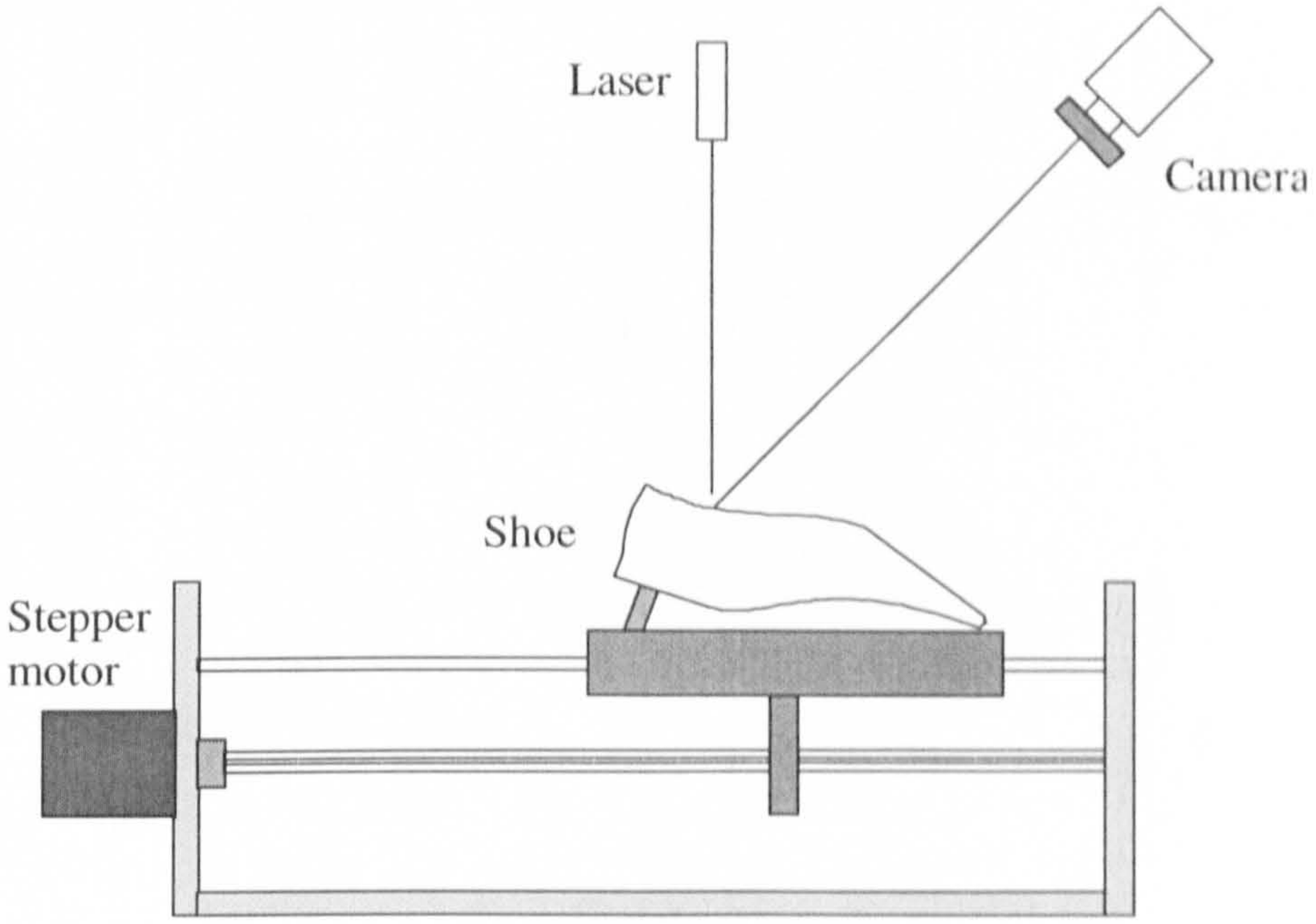

Figure 6.7 Scanning configuration for bottoming operations.

6.2.2 Edge extraction.

From the line-stripe data the points defining the sole line have to be determined. This can be very subjective for certain types of shoe, (e.g. lady's courts), as no clear edges exist across the instep. This prohibits determination of the edge by looking for a specific change in gradient. However, in all cases the edges are still generally well defined around the regions of the heel and toe. As a result a method capable of detecting the instep is required. This can then act as an input into a formula for extracting the sole line edge co-ordinates.

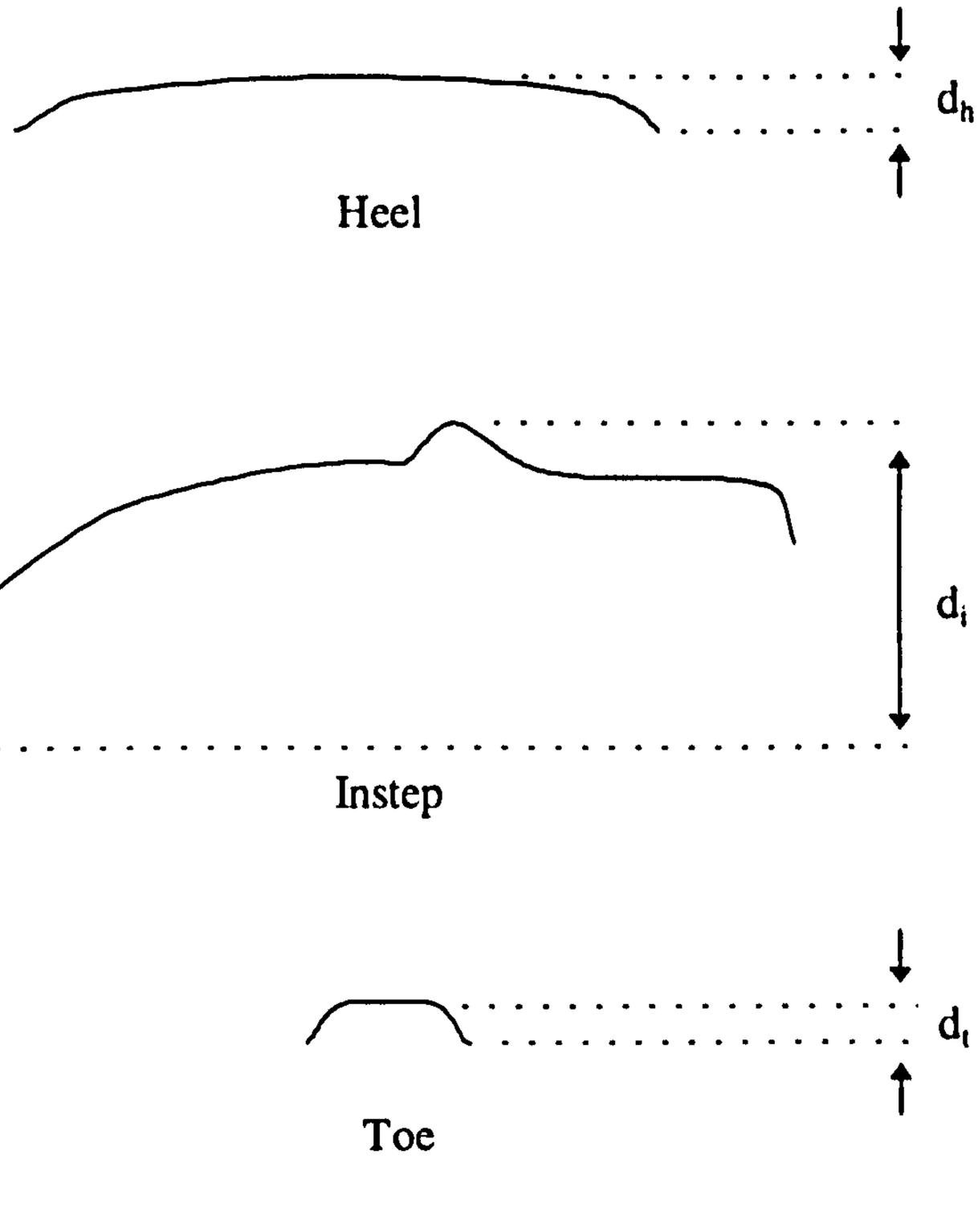

Figure 6.8 Insole position determination.

Figure 6.8 shows extracted line-stripes and shows how the depth of the image varies along the length of the shoe. Where the edges are well defined at the heel and toe, the roll-off at the edge is quite steep resulting in a shallow image, (d_h and d_t). However at the instep, the roll-off is very gentle resulting in a much deeper image, (d_i). Consequently,

$$d_i >> d_h \text{ or } d_t$$

Thus by measuring the depth of the image the location of the instep can be determined. Figure 6.9 shows a graph of extracted roll-off angle against image depth for a lady's court shoe. The values were extracted by manually selecting the sole line edge on each line-stripe and the software reporting the angle at that point.

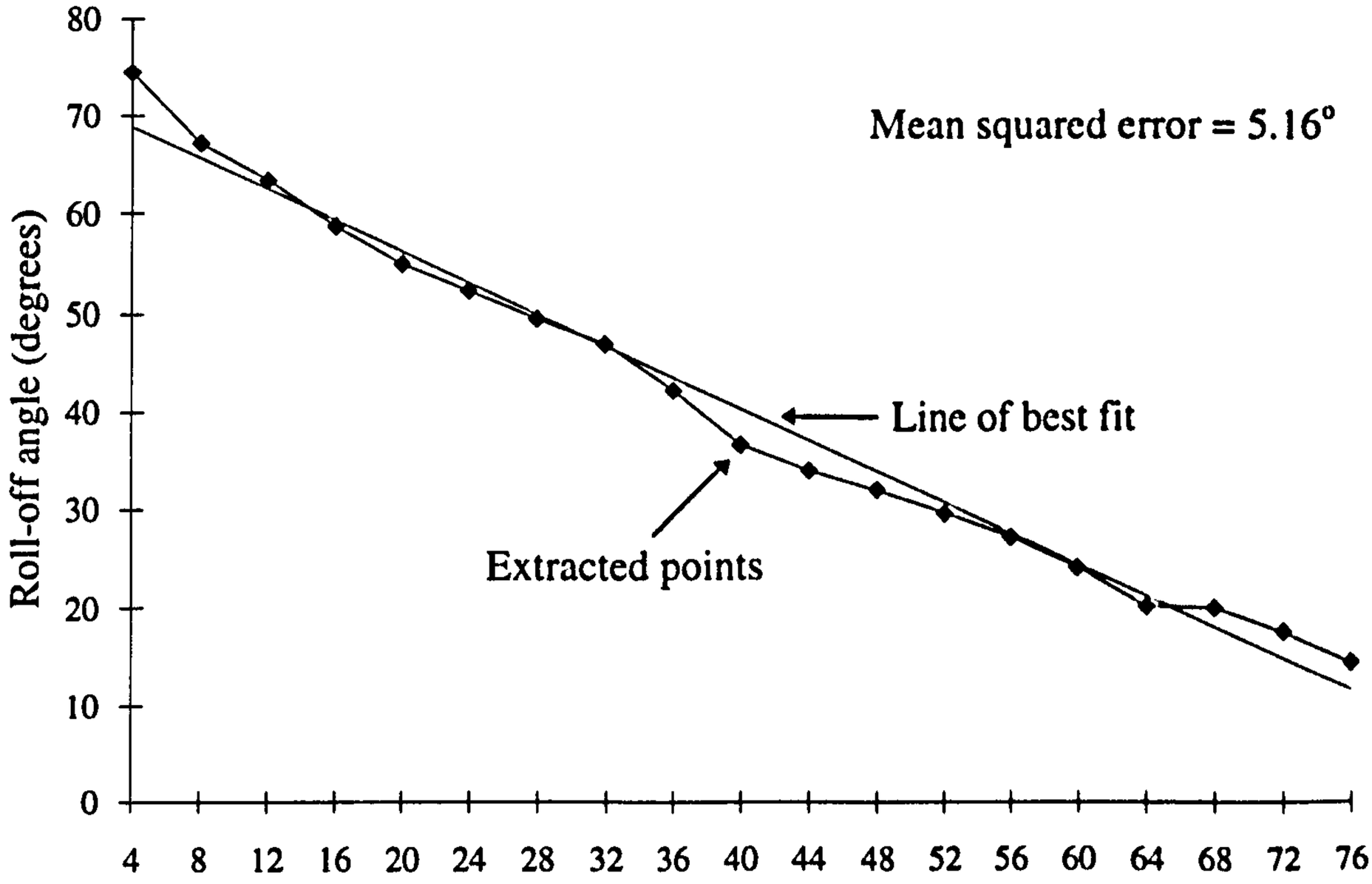

Figure 6.9 Ideal angles for edge co-ordinates extracted from a lady's court shoe.

It can be seen that the angle for roll-off against image depth can be approximated to a straight line. For the above example, the equation for this line is given by,

$$\text{Roll off angle} = -0.802 \times \text{Image depth} + 72.256 \text{ degrees}$$

Thus, by applying this formula an approximation can be made as to the location of the points which will be used to define the sole line. Figure 6.10 shows a plan view of the extracted sole line points taken from a lady's court shoe.

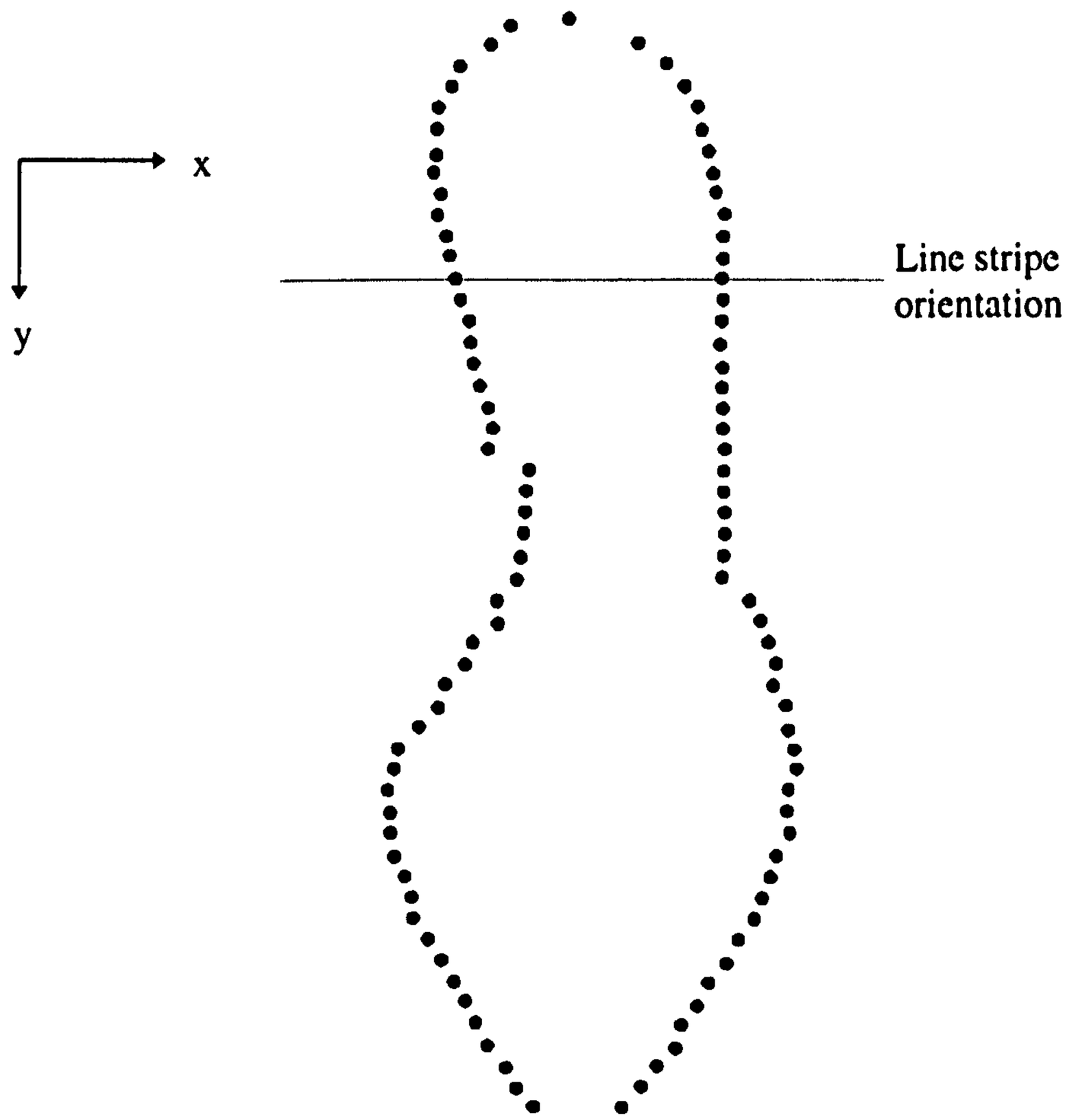

Figure 6.10 Sole line points extracted from a lady's court shoe.

It can be seen from Figure 6.10, that the majority of extracted points follow quite closely the shape of a shoe bottom. However, due to the uneven nature of the material and a join in the upper material at the instep, a number of points appear miss-placed. In order to overcome these effects, a method of effectively smoothing the line through these points is required.

6.2.3 Sole line determination and correction.

Even after taking precautions to determine as accurately as possible the edge position, errors can still occur. Once the whole part has been scanned the data can then be analysed in an attempt to reduce these errors by the use of point interpolation. Here a number of points are considered to determine the line of the edge. To achieve this it must be assumed that the majority of the extracted edge points are correct. This will allow for erroneous points to be adjusted so as to fall into line.

The method employs cubic splines to trace around the points, starting at the well defined region around the heel. The splines are calculated across four points, two points either side of the point under investigation. The distance between this point and the calculated point, as defined by the cubic spline equation, is calculated, d. (Figure 6.11 shows the region of the instep in Figure 6.10). This result can then be compared with a defined tolerance level. Should the point be within this tolerance it can be passed over, if it is outside the tolerance level it must be corrected. This can be achieved by moving directly to the calculated position, or by moving a percentage of the distance, d. The latter allows for some fluctuations in the surrounding points. It should be noted that the current point's adjusted co-ordinates will be used as an input for the next iteration of the of the spline process.

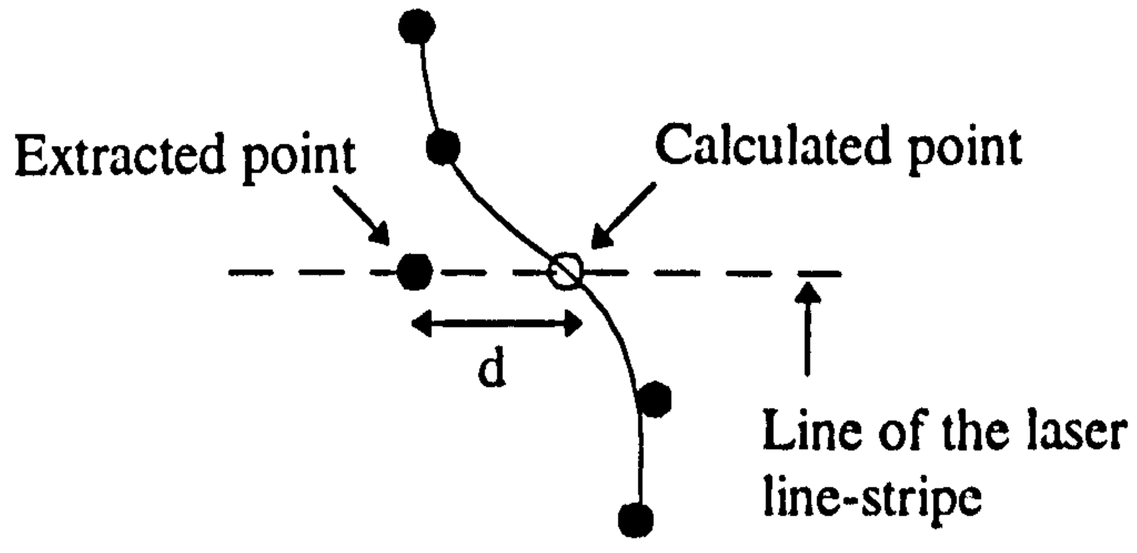

Figure 6.11 Point error correction using cubic spline interpolation.

Sole line determination is achieved by moving the spline iteratively around the extracted points until all points the are within an experimentally determined tolerance. This has the effect of smoothing any large irregularities. In an effort to achieve maximum accuracy a mechanism to 'lock' points whose positional error was less than the selected tolerance was investigated. Once locked a point cannot be moved by a future iterations.

6.2.4 Results of sole line determination.

Figures 6.12 shows the results of processing on a court shoe in plan view, whilst Figure 6.13 plots the sole line onto the 3-D line stripe data. (The acceptance tolerance level for point accuracy was set to 2 pixels, (≈1mm)). In order to test the effects of point locking and determine the degree by which points should be adjusted, a series of images were processed with varying parameters. The results of this can be seen in Appendix N.1. When the points were locked, it was observed that the irregularities that existed in the original data were largely removed irrespective of the degree of correction, (how far a given point was moved towards its calculated position on a single iteration). In addition

the overall shape of the profile remained true. However, when the points were unlocked poor quality results were obtained. This was particularly true for points adjusted by 50%, or more, of the calculated error distance. In these examples the sole profile became narrowed around at the region around the 'ball' of the foot due to excessive smoothing.

The experimental results lead to the conclusion that the procedure of locking points within the given tolerance increases the accuracy of the processing. This can be further enhanced by adjusting erroneous points by 25% of the calculated error. The tolerance level of 2 pixels was determined experimentally also. Values of higher tolerance resulted in high numbers of iterations having to be performed for no perceivable gain. If the value was too low then little correction occurred.

The information calculated so far for the line of the sole is only two dimensional. Consequently there is a need to extract further information, with respect to the vertical variations of the shoe bottom, in order for automated operations to be performed. This information can be simply extracted from the line-stripes during processing.

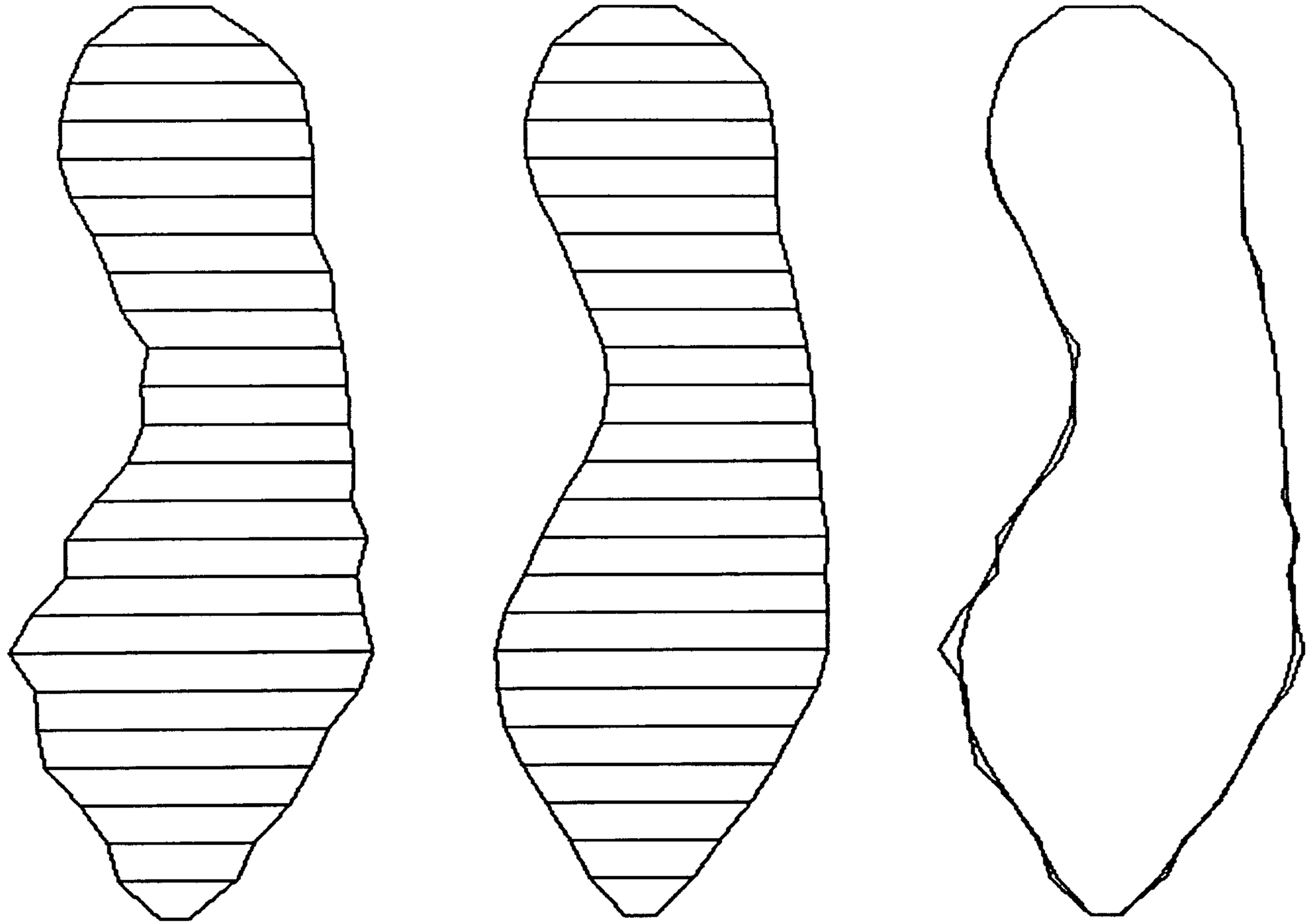

Figure 6.12 Plan view of sole line extraction for a court style shoe

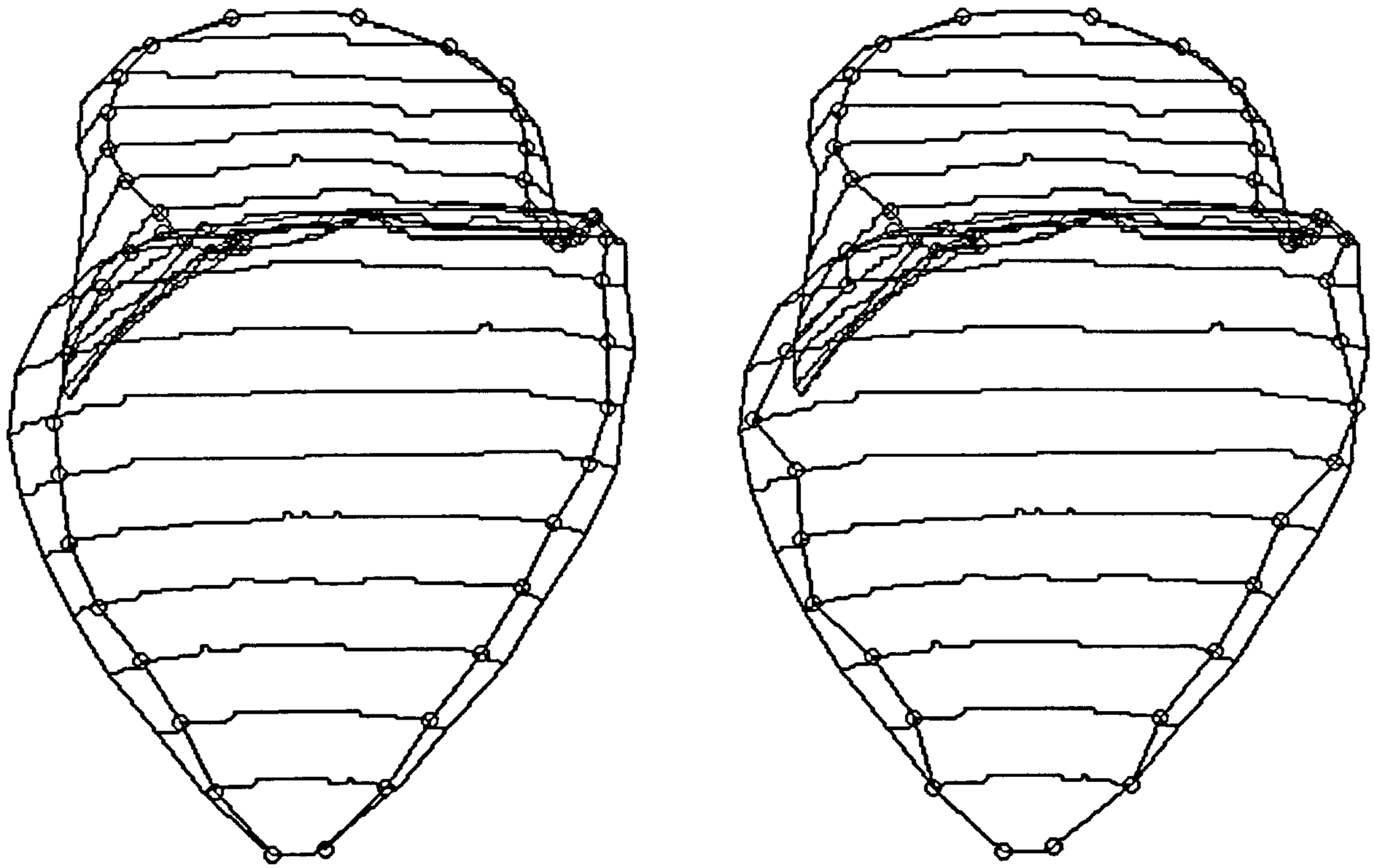

After processing

Before processing

Figure 6.13 3D plot of extracted sole line before and after processing.

6.2.5 Z-axis profile for depth control.

The profile of shoes can vary considerably from style to style. Men's shoes are generally flat prior to soling which may add a small heel. However, lady's shoes can vary from the flat into extreme contours in order to have a high heel attached. This information can be extracted from the line-stripes as they are processed.

Due to the camera being at an angle to the laser, (typically 45°) the laser line-stripe over the base of the shoe, as perceived by the camera, represents a cross section of the shoe. In addition the location of the perceived stripe, P moves up and down the cameras field of view depending on the height of the object, D, (Figure 6.14).

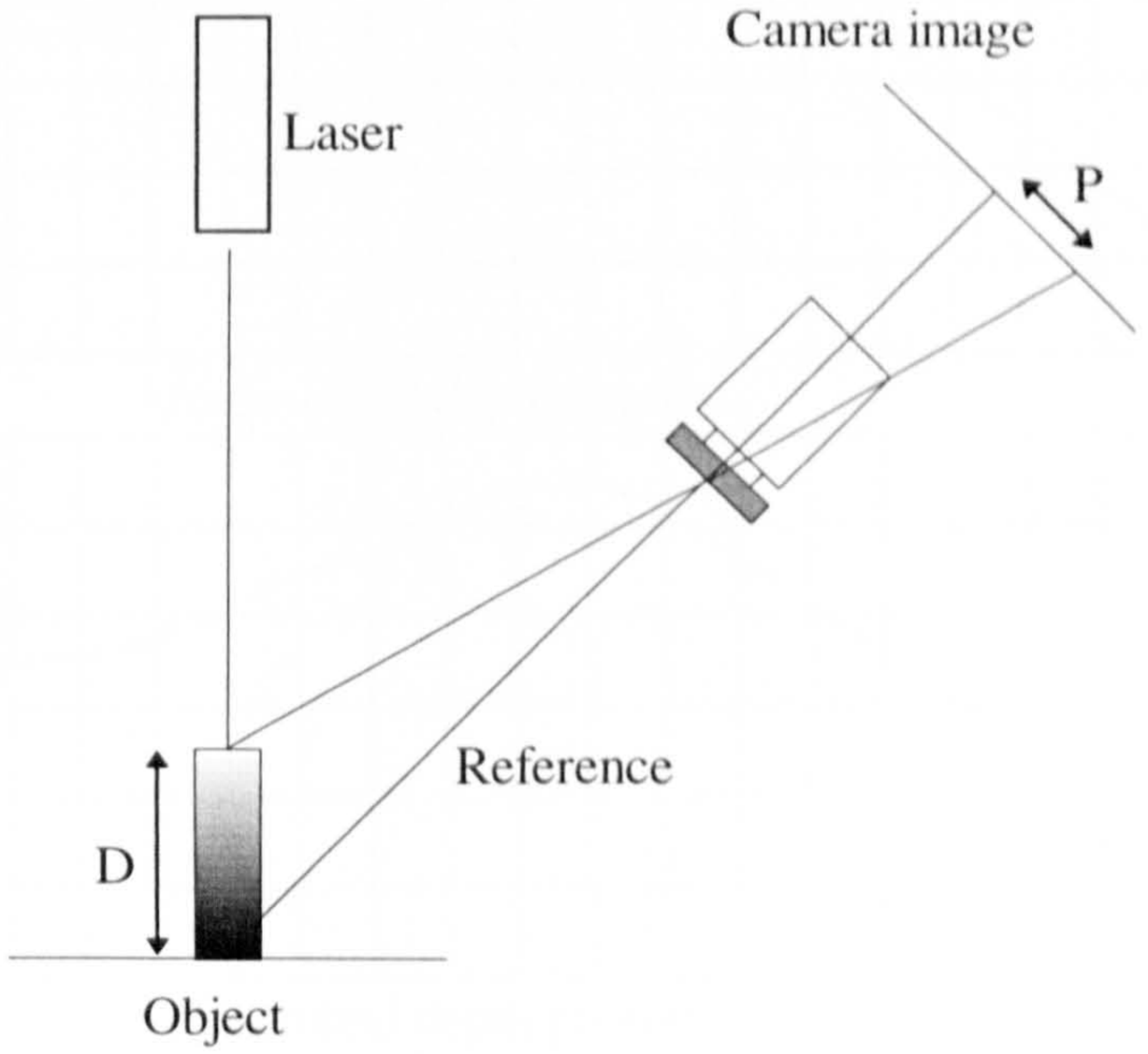

Figure 6.14 The effect of varying object height on the camera image.

Thus by calibrating the perceived height, using known object dimensions, a value corresponding to the Z-axis profile can be obtained. However, the point on the stripe selected to measure against must be selected carefully. There are two chief candidates for this task. The first being the point defined by the sole line calculated previously. Unfortunately, due to the pleats introduced by the lasting process the contour can vary significantly from point to point. Due to the base of the shoe being approximately flat across its width, a more accurate position on which to base a depth profile is along the centre line of the last. Figure 6.15 shows a depth image extracted from the lady's court shoe processed in Figure 6.13. The images were taken using screen capture techniques direct from the processing software.

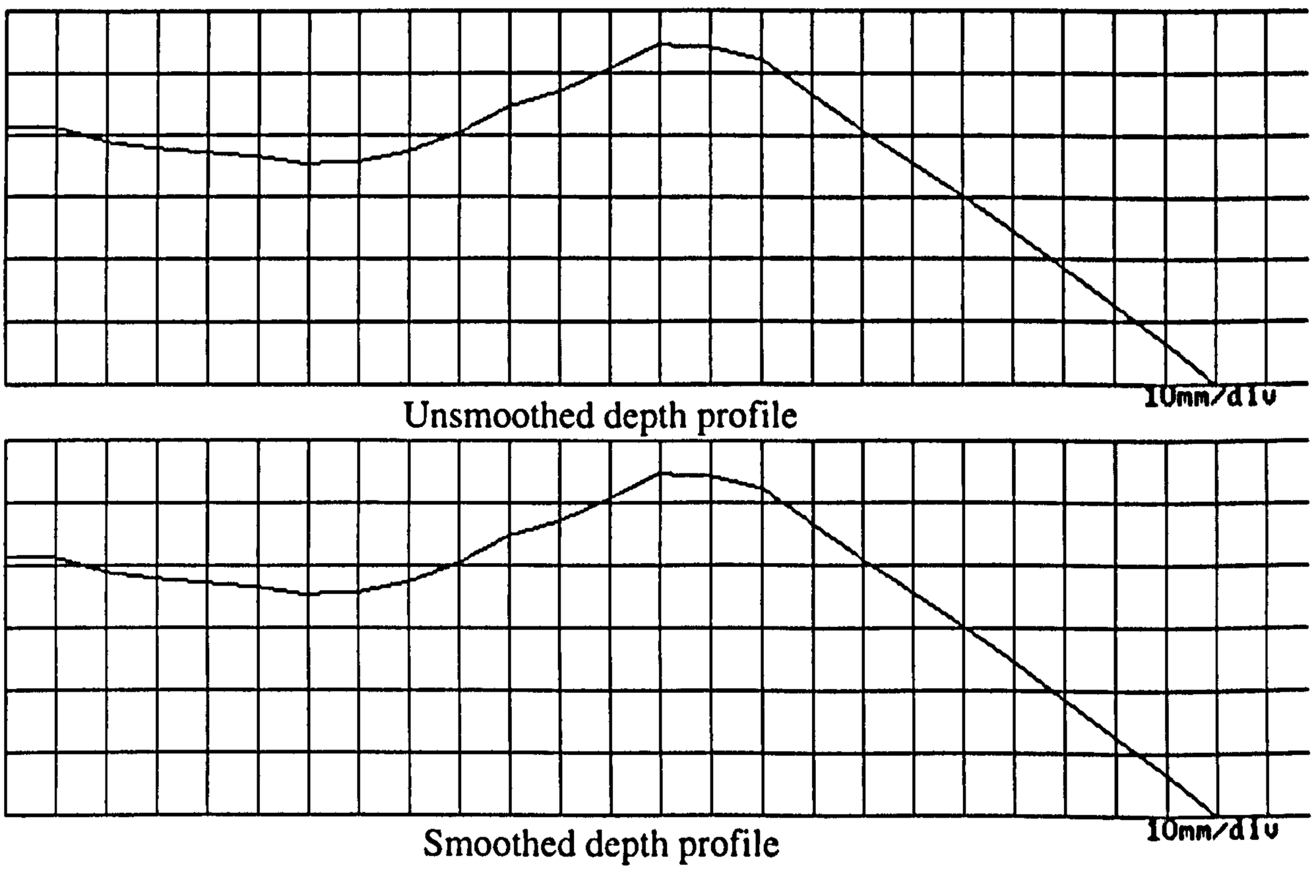

Unsmoothed depth profile

Smoothed depth profile

Figure 6.15 Depth profiles extracted from a lady's court shoe.

Figure 6.15, shows both the raw depth data and the same data after smoothing. The smoothing is performed in the same manner as that previously described for extracting the sole line. Additional images are contained in Appendix N.2.

The methods discussed in Section 6.2 allow for the determination of control parameters in three dimensions suitable for the majority of bottoming operations. The following sections outline how this information could be used for a number of specific areas of potential automation within the field of bottoming.

6.3 Roughing and cementing.

The process known as 'roughing' follows immediately after the lasting process and is concerned with removing the pleats formed in the upper material. This is performed by a machine that automatically follows a manually taught path and uses a rotating wire brush to scour off excess material, each style having its own manually taught parameters. By implementing a vision system significant advancements in automation could be made. There are two possibilities as to how this may be achieved.

The first method requires mounting the vision system onto the head of the rougher, thus effectively edge following. The same principles as those described could be implemented to extract information for brush manipulation, however it would not be possible to interpolate to reduce errors. This could be overcome in one of two ways. Either by navigating the edge twice, once to build up an image of the shoe bottom and once to perform the operation. Or by having a teach cycle to allow the machine to learn

the shape of the shoe and save it as a template. This would effectively replace the current manual method. A mechanism capable of performing such an operation would be complex and bulky and either time consuming or still open loop in operation.

A second preferable alternative has already been mentioned in Section 6.2.1. Here the shoe is scanned as it is loaded into the machine. This then allows for the orientation of the laser and the camera to remain fixed. In addition every shoe would be scanned and processed on an individual basis, removing the requirement for templates and teaching.

Cementing is the application of adhesive to the roughed base of the shoe to enable bonding to the sole. Consequently the line of the cement can match that of the rougher, the only addition being a line of cement down the centre of the last. Indeed, a new generation of B.U.S.M machines combining roughing and cementing are already under development. In this event only a single vision system is required to cover both roughing and cementing so long as information is retained between the processes.

6.4 Shoe soling applications.

Currently the majority of shoe soling is performed manually using a technique know as 'spotting'. Here the operator ensures that the location of the toe is correct before locating the heel. The shoe is then placed in to a press to perform the final bonding. By employing vision technology to this area both components could be scanned and the process of spotting automated. The mechanisms outlined for lasting and

bottoming operations to be performed on the last are equally valid for soles. Figure 6.16 contains the processed image of a gentleman's sole, before and after edge smoothing. Figure 6.17 shows a three dimensional view of the same sole. It would be expected that the inside surface of the sole should be scanned as it is required to mate with the shoe bottom. However, the inside surfaces of soles can be very complex so as to provide cushioning for the user. On a sports boot there can also be high walls which are difficult for vision systems to perceive. Consequently it was found that scanning the outside of the sole gave better results as the edges, particularly at the toe and heel are well defined. Appendix N.3 contains examples of processed sole images.

6.5 Discussion on Automation in shoe bottoming.

The investigations into vision applications for shoe bottoming have determined areas where such systems could be of practical value. In addition methods for extracting information to enable the automation of these operations has been determined. The areas of roughing and cementing would be best addressed in a single machine capable of scanning each shoe as it is presented. This would in turn result in a fully automated machine, requiring little additional taught data.

The application of vision technology to soling would provide the largest step forward in this field since the sole press. Unfortunately, due to the need for a vision system and a mechanism capable of performing the required manipulations the complexity of the machine would vastly increase.

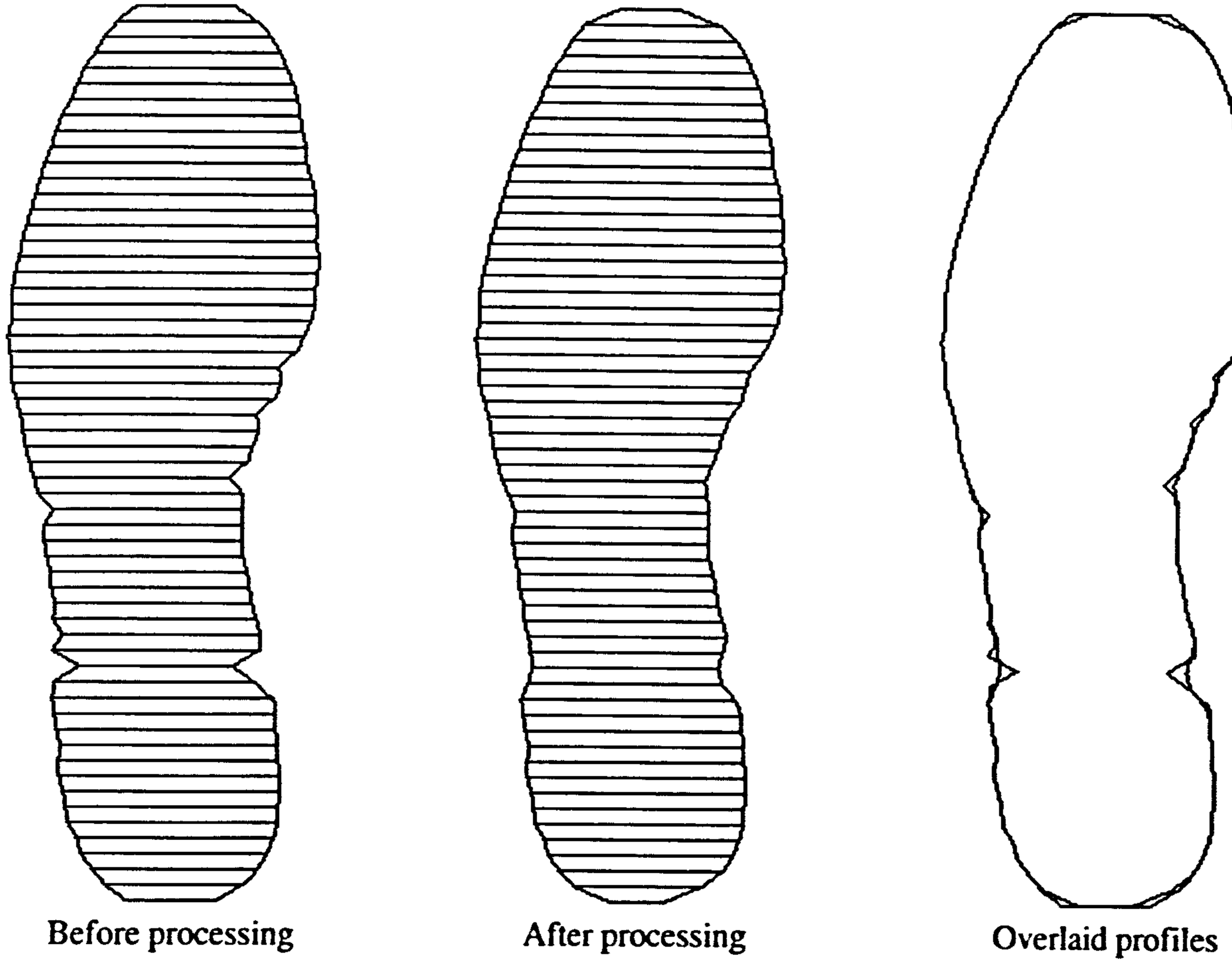

Figure 6.16 Plan view of sole line extraction for a gentleman's sole

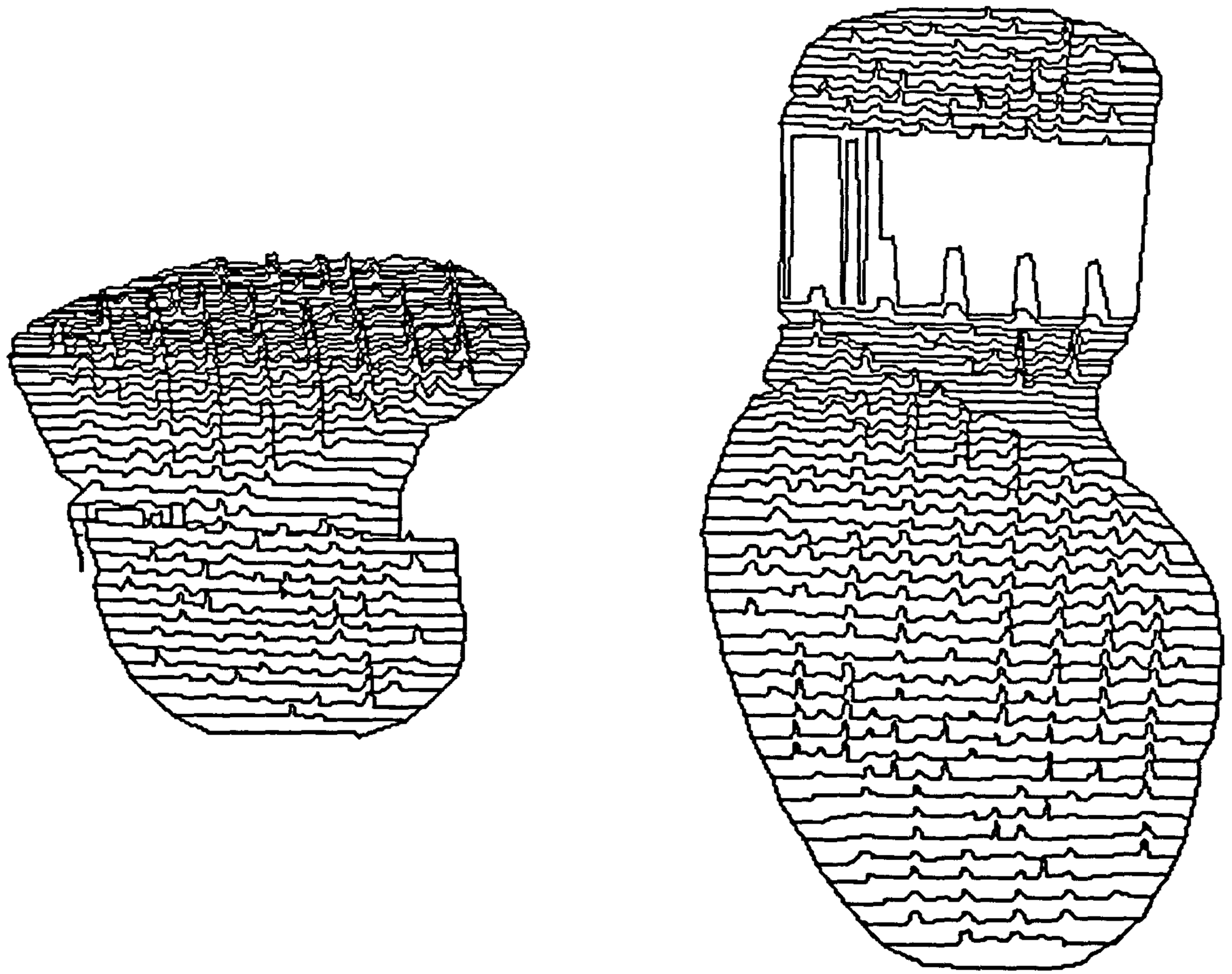

Figure 6.17 Gentleman's shoe sole image .

Chapter 7

Discussion and conclusions

7.0 Discussion and conclusions.

This thesis describes the processes that may be performed in the construction of a typical shoe. It covers operations on flat and three dimensional workpieces which require a great deal of manual input. In order to approach these operations with a view to automation, it is required that there is an understanding of the characteristics of the materials to be handled. Chapter 2 contains the results of an investigation into the morphology of leather. This showed the complex and variable structure of leather as a natural material. It also demonstrated how the properties of an individual leather component, and hence how it would handle, vary according to the location on the hide from which it was taken. The information derived in this chapter proved of great value in Chapters 3 and 4 where the effects observed during manipulation could be directly related to the material structure. This allowed for mechanisms to overcome or utilise these properties to be determined.

Chapter 3, forms the main part of the thesis and was concerned with the handling of flat leather workpieces pre-dominantly for decorative and constructional stitching. The object of the study was to determine an accurate mechanism for manipulating the workpieces under the stitching head and eliminate the existing high degree of 'drift' previously observed. The research developed a series of belts capable of covering a wide

range of material types and properties by implementing a combination of a compliant upper belt substrate and an intrusive lower belt surface. The very nature of the lower surface gave a novel approach to material handling. The studies showed how such a surface made from a series of short sharp pins could penetrate the surface of the workpiece, without permanent damage, and at the same time overcome the materials variable properties, (Chapter 2). The initial goal of the research was to perform accurate decorative stitching. However, the mechanism developed proved not only capable of this task, but also of performing constructional stitching to the same high degree of accuracy, thus allowing pre-tacked compound parts to be joined in a fully automated manner. This operation is currently only possible on machines such as the M.P.C.S. made by B.U.S.M. which require a large amount of bespoke tooling and labour. Thus, by automating the process, significant savings can be made within this area in both time and cost. To this end a technology transfer has been made to B.U.S.M who are now investigating the results with a view to commercial adoption on their Auto-scan stitching machines. This work also resulted in a patent application[26] being filed by B.U.S.M and an invention disclosure[27] for a novel tensioning mechanism.

The proposed mechanism orientates the workpiece beneath a stitching head open loop, positioning being based on an original scan of the part. In order to improve the accuracy of stitching still further in the case of constructional stitching a means of detecting the edge would be required. This would then effectively close the loop and allow for fluctuations in the edge path to be compensated for. This requirement resulted in Chapter 5 on vision mechanisms for edge following.

In Chapter 4 the process known as pre-tacking was investigated. This work resulted in an invention disclosure[24] being filed at B.U.S.M. The results show that a number of components which are initially flat can be joined so as to result in a three dimensional compound part. This part can then be stitched to form a permanent join using conventional mechanisms in a greatly simplified manner. The study also demonstrated the limitations of such a system especially when performed in an automated fashion. However, the principle of limited contact points is still of value and for certain components types such mechanisms may be valid.

Chapter 5 investigated mechanisms using laser triangulation for the determination of edge position and form, for the purpose of stitching. The use of lasers enables a significant amount of information to be derived using relatively simple techniques. Methods for following both square cut and folded edges have been addressed and the limitations of these methods discussed. The research demonstrated that for folded edges care is required where the fold is not well defined as this uncertainty is echoed in the perceived position of the edge. The research demonstrates how the characteristics of the fold can be determined and consequently how the position of the true and closed, (tightly folded), edge can be defined. This work has resulted in a patent application[25] into the use of laser triangulation in shoe machinery. In addition the work resulted in a contract being instigated at Leeds Metropolitan University into a vision based constructional stitching machine based on an M.P.C.S. The use of laser scanning for topography determination is not limited to applications such as edge following, but can be expanded to encompass complex three-dimensional objects. This, therefore, means there is a niche for vision systems in the final operations of shoe manufacture.

Chapter 6 used the knowledge and experience gained and reported in Chapter 5 in order to develop techniques to extract the surface topography of the finished upper on the last for the operations of lasting, roughing, cementing and soling. These are all areas where early automated equipment was subject to errors and as such subsequently found it hard to become established within the industry. By implementing vision technology the possibility of damaging a workpiece or not performing the task to a suitable standard could be vastly reduced. The results contained within this chapter show how the lasting operation, which requires knowledge of the topography of the upper, once on the last, is exceedingly complex due to the lack of identifiable features in many cases. It is believed that further, extensive, research will be required if vision lasting is to become a reality. Consequently it is expected that this will be the last area in which automation will occur within the shoe making industry. In contrast, where the bottom of the shoe requires interrogation for roughing, cementing and soling it is possible to extract the desired information. This has resulted in new research contracts being placed both at Bradford University and Hull University in order to look at roughing and soling respectively.

The objective of the thesis, (to investigate methods of automating processes within the shoe industry), has, the author believes, been achieved. This is born out by the patent applications and new contracts that have arisen directly as a result of this research. With further research ongoing, chiefly in bottoming and stitching applications, it will not be long before a new generation of automated machinery becomes available to the shoe making industry. B.U.S.M are in addition are to start development on a combined roughing and cementing machine which will have an inspection vision system capable of determining the quality of the roughing process prior to cementing.

References.

[1] Smith, D.L. 'The Manipulation of Leather Workpieces for the Assembly of Shoe Uppers', Ph.D. Thesis, University of Hull, August,1991.

[2] Adams, E.W.J. 'The Joining of Leather Pieces for Shoe Upper Assembly', MSc. Thesis, University of Hull, April 1992.

[3] Inui, S. Shibuya, A. 'Objective Evaluation of Seam Pucker Using Automated Contactless Measurement Technology', International Journal of Clothing Science and Technology, Vol 4, No 5, 1992, pp 24-33.

[4] McCartney, J. Hinds, B.K. 'Computer Aided Design of Garments using Digitized Three-dimensional Surfaces', Proc. Instn. Mech. Engrs, Vol 206, Part B, Journal of Engineering Manufacture, August 1992, pp 199-206.

[5] Wust, C. Capson, D.W. 'Surface Profile Measurement Using Color Fringe projection', Machine Vision and Applications, Vol 4, 1991, pp 193-203.

[6] Porat, I. Alagha, M.J. 'An Optical Technique to Detect Miss Stitch in Real Time', International Journal of Clothing Science and Technology, Vol. 4, No 4, 1992, pp 23-27.

[7] Gersak, J. Knez, B. 'Reduction in Thread Strength as a Cause of Loading in the Sewing Process', International Journal of Clothing Science and Technology, Vol. 3, No 4, 1991, pp 6-12.

[8] He, G.P. Kraus, K. 'A Method to Design Filters for Image Smoothing', Pattern Recognition Letters, Vol 13, No 7, July 1991, pp 509-515.

[9] Ray, B. Kr. Ray , K.S.'Detection of Significant Points and Polygonal Approximation of Digitized Curves', Pattern Recognition Letters, Vol 13, No 6, June 1992, pp 443-452.

[10] Akarum, L. Haddad, R.A. 'Adaptive Decimated Median Filtering', Pattern Recognition Letters, Vol 13, No 1, January 1992, pp 57-62.

[11] Kumar, P. Batnagar, D. Umapathi Rao, P. S. 'Pseudo One Pass Thinning Algorithm', Pattern Recognition Letters, Vol 12, No 9, September 1991, pp 543-555.

[12] Chetverikov, D. 'Generating Contrast Curves for Texture Regularity Analysis', Pattern Recognition Letters, Vol 12, No 7, July 1991, pp 437-444.

[13] Pfaff, Technical information and advertising literature.

[14] B.U.S.M, Technical information and advertising literature.

[15] Grantham, J. Personal correspondence, University of Hull.

[16] Beeby, R. 'Shoe Technology Advances Across a Broad Front', World Footwear, Vol 7, No 1, January/Febuary, 1993, pp 14-16.

[17] Reedman, D. Personal correspondence, B.U.S.M. Leicester.

[18] Transmission Developments Co. (GB) Ltd., Dawkins Road, Hamworthy, Poole Dorset, BH15 4HF, Tel 0202-675555.

[19] Fenners, Technical information and advertising literature.

[20] 3M (UK) plc, 3M House, PO Box 1, Bracknell, Berks, RG12 1JU, Tel 0344 858000.

[21] Norton-Wayne, L. Reedman, D.C. Personal correspondence.

[22] Tout N.R, 'Investigation of the Processes Required for the Automation of Stitchmarking in Shoe Manufacture', Ph.D Thesis, University of Durham, 1989.

[23] Topis, S.K. 'Investigation of Electrical and mechanical requirements for Automation of a Process in Flexible Material Manufacture', Ph.D Thesis, University of Durham, 1993.

[24] Hudman, F.M. Taylor, G.E. Taylor, P.M. 'Pre-tacking fexible components in 3D configuration', B.U.S.M case No. 0410.

[25] Hudman, F.M. Reedman, D.C. 'Digitising a three-dimensional surface using a camera having a two dimensional array', European Patent application No. EP0572123.

[26] Hudman, F.M. Tout, N.R. Reedman, D.C. Wildbore, D. 'Autoscan - belt surfaces coated with grit or other projections', Great Britain Patent application No. GB9407960.5.

[27] Hudman, F.M. 'Feed belt tensioning mechanism - compliant surface of pulley applies tension to belt', B.U.S.M case No. 0549.

[28] CY LAN 3D, Technical information and advertising literature,personnal communication, INTECU, Gesellschaft für Innovation, Technologie und Umwelt mbH i.G.Gewerbepark Kelplerstraβe 48, 07549 Gera.

[29] Romans CAD Software, Technical information and advertising literature, STRATEGIES, 41-43 rue de Villeneuve, SILIC 429 - 94583 Cedex France, SRDI, Société de Développment Informatique, 6 rue St Antoine, BP 131-26104 ROMANS.

[30] Torielli, International Patent application number PCT/EP91/00857, International publication number WO 91/17021, International publication date 14 November 1991.

[31] Dunning, D. Preece, C. et al.'Progress in NC Stitching Machines: Improving Shoe Seam Appearance', International journal of Clothing Science and Technology, Vol 5, Number 2, 1993.

[32] Orisol, European Patent application number 88301795.6, Eurpoean publication number EP 0 309 069 B1, European publication date 17 June 1992.

[33] Schaefer, Jr. et al. USM Corporation, United States Patent application number 94,772, Filed 3 December 1970.

[34] Karcher, Jr. et al. USM Corporation, United States Patent application number 299,944, Filed 24 October 1972.

[35] Babson, et al. USM Corporation, United States Patent application number 760,138, Filed 17 January 1977.

[36] Willenbacher, et al. Pfaff Industriemaschinen GmbH, United States Patent application number 328,504, Filed 8 December 1981.

[37] Browne, Norton-Wayne, L. 'Vision and Information Processing for Automation', 1986 Plenum Publishing, ISBN 0-306-42245-X

[38] Banks, S. 'Signal Processing, Image Processing and Pattern Recognition', 1990 Prentice Hall, ISBN 0-13-812579-1.

[39] Spearman, 'The Integument', 1973 Syndics of Cambridge University Press, ISBN 0-521-20048-2.

[40] Wilson, J.A. 'The Chemistry of Leather Manufacture', Second Edition, Volumes 1 & 2, Printed by J.J. Little and Ives Company, New York 1928.

[41] Harrison, Korn, 'Boots and Shoes Their Making Manufacture and Selling', Vol 2, The New Era Publishing Co., Ltd, 12 & 14 Newton Street, Holborn London.

[42] Tout N. R. Personal correspondence, B.U.S.M. Leicester.

[43] Stanley, A. 'Application of Modern Microscopic Techniques to Leather Manufacturing', January 1992, Microscopy and Analysis, pp25-27.

[44] Colls, M. 'The Design and Implementation of a Digital Servo Controller for an Industrial Stitching Machine', Msc. Thesis, University of Hull, September 1990.

[45] Halder, J, Personal correspondence, Department of Applied Biology, Scanning Electron Microscopy suit, University of Hull, Cottingham Rd, Hull.

[46] Bordoli, E, General Editor, 'The Boot and Shoe Maker', Volumes iii and iv, Published by The Gresham Publishing Company Ltd, 66 Chandos Street, Covent Garden, London.

[47] Stanier, Ingraham, Wheelis, Painter, 'General Microbiology', Fifth edition, Macmillan Education Ltd, 1987, ISBN 0-333-41768-2, pp41-42.

[48] Bhattacharyya, G.K. Johnson, R.A. 'Statistical Concepts and Methods', John Wiley & sons Inc, 1977, ISBN 0-471-03532-7, pp272-273.

[49] Roberts, Worcester, Cuttiford, 'Boots and Shoes Their Making Manufacture and Selling', Vol 3, The New Era Publishing Co., Ltd, 12 & 14 Newton Street, Holborn London.

[50] Rosenfeld, A. Kak, A.C. 'Digital Picture Processing', Academic Press Inc, 1976, ISBN 0-12-597360-8, pp322-324.

Appendix A

Results obtained from Scanning Electron Microscope observations of a vegetable tanned, buffalo calf hide

A1. The Scanning Electron microscope

Traditional light and transmission electron microscopes use a broad beam of either photons or electrons which pass through the specimen. A magnified image is then produced by passing the emergent beam through a series of lenses, either glass or electromagnetic. The SEM however uses a totally different approach to produce highly magnified images[47], that of electronic amplification. The surface of the specimen is coated with atoms of a metal, such as gold, before being irradiated by a very narrow beam of electrons resulting in low energy, (secondary) electrons being released. These are then collected by an anode, (positively charged plate), producing an electronic signal proportional to the number of electrons collected. This number is determined by the angle of the surface below the electron beam and the amount of ejected electrons absorbed by the surrounding protuberances on the surface of the specimen. The signal generated by the secondary electrons is then amplified and used to modulate the intensity of a spot on a cathode ray tube. Thus by scanning the tight electron beam and the spot on the cathode tube synchronously in a raster manner a magnified image of the specimen surface can be generated by the cathode ray tube.

The depth of focus of a scanning electron microscope is several millimetres, with an effective magnification range from approximately x20 to greater than x20,000.

A2. Experimental procedure.

In order to determine the orientation, density and collagen bundle size variations across a hide a vegetable tanned, buffalo calf half hide was provided by B.U.S.M.

This was subdivided in to 25 regions, Figure A.1. Preparations were then cut from the centre of each of these regions, by removing a section approximately 10mm x 4mm, such that they followed the line of the backbone. The samples were then mounted and coated in atoms of gold to allow for SEM micrographs, (pictures), to be taken of the dermal layer. All observations were made in the same direction relative to the backbone. This process was conducted by J. Halder[45] of the scanning electron microscopy suite at the University of Hull.

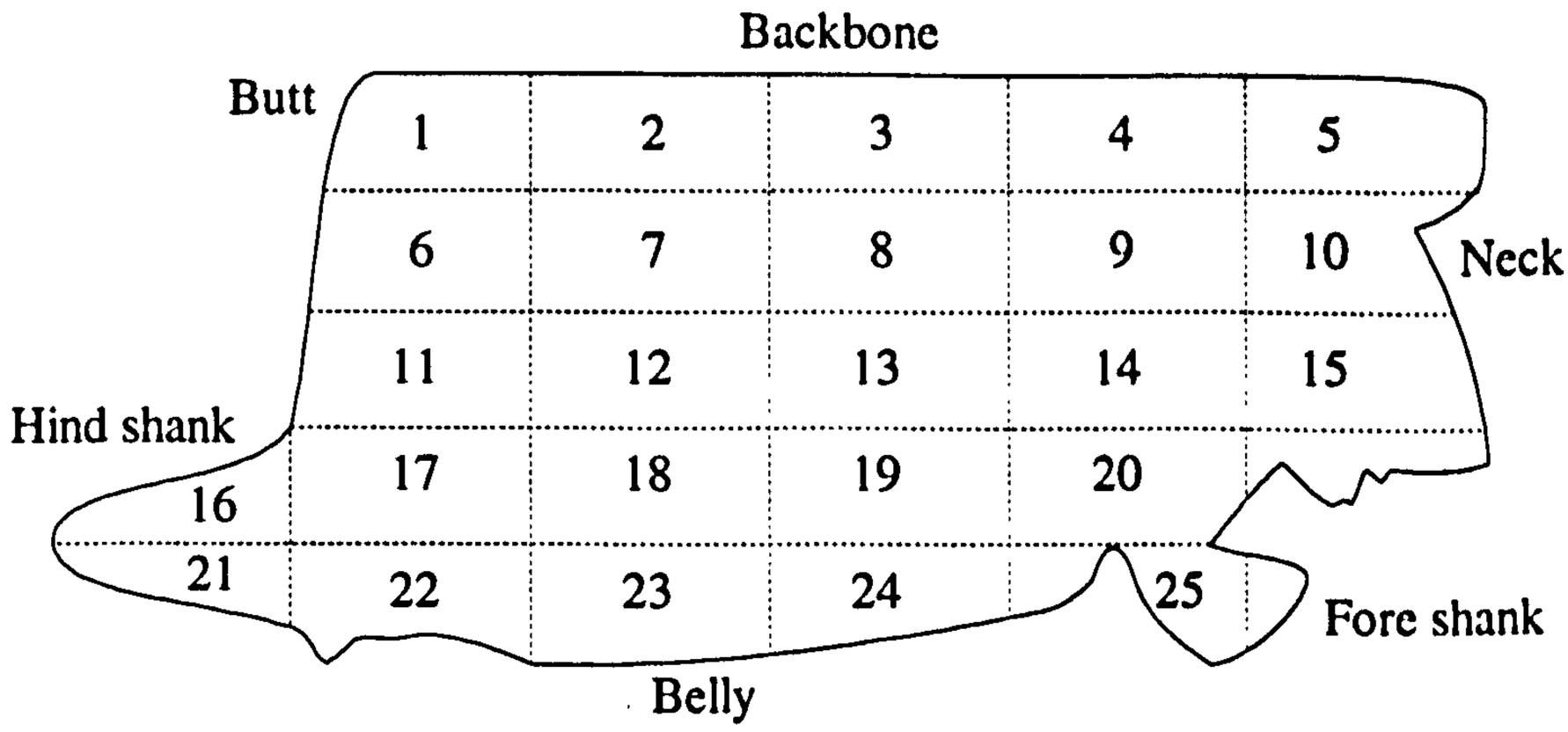

Figure A.1 Location of samples taken for SEM observation

A3. Example SEM micrographs

This section contains plates depicting the observed variations in collagen bundle orientaion, size and density discussed in Chapter 2.

Plates A.1-3, show how the average collagen bundle size varies depending on the location on the hide from where the specimen was taken. Plate A.1, depicts an average collagen bundle size of less than 6.6μm taken from the neck region, (sample 5). Plate A.2, shows a micrograph taken from the belly region, (sample 19) where the average bundle size has increased to between 10-13.2μm. Sample 16, taken from the hind shank is shown in Plate A.3. Here the collagen fibre bundle size has increased to greater than 20μm, but contains only a few large individual fibres.

Plates A.4-6, are examples of how the orientation of the collagen bundles vary according to the flexibility requirements demanded of the hide. Plate A.4 is taken from the area at the butt, (sample 1) where little flexibility is required. Consequently there is a mix of transverse and longitudinal collagen bundles seemingly randomly inter mixed. Where greater flexibility is demanded the percentage of transverse bundles increases as in Plate A.5, (sample 11). Regions requiring a high degree of flexibility, predominantly around the neck and shoulders, require an even greater percentage, (>80%), of transverse collagen bundles, Plate A.6, (sample 8).

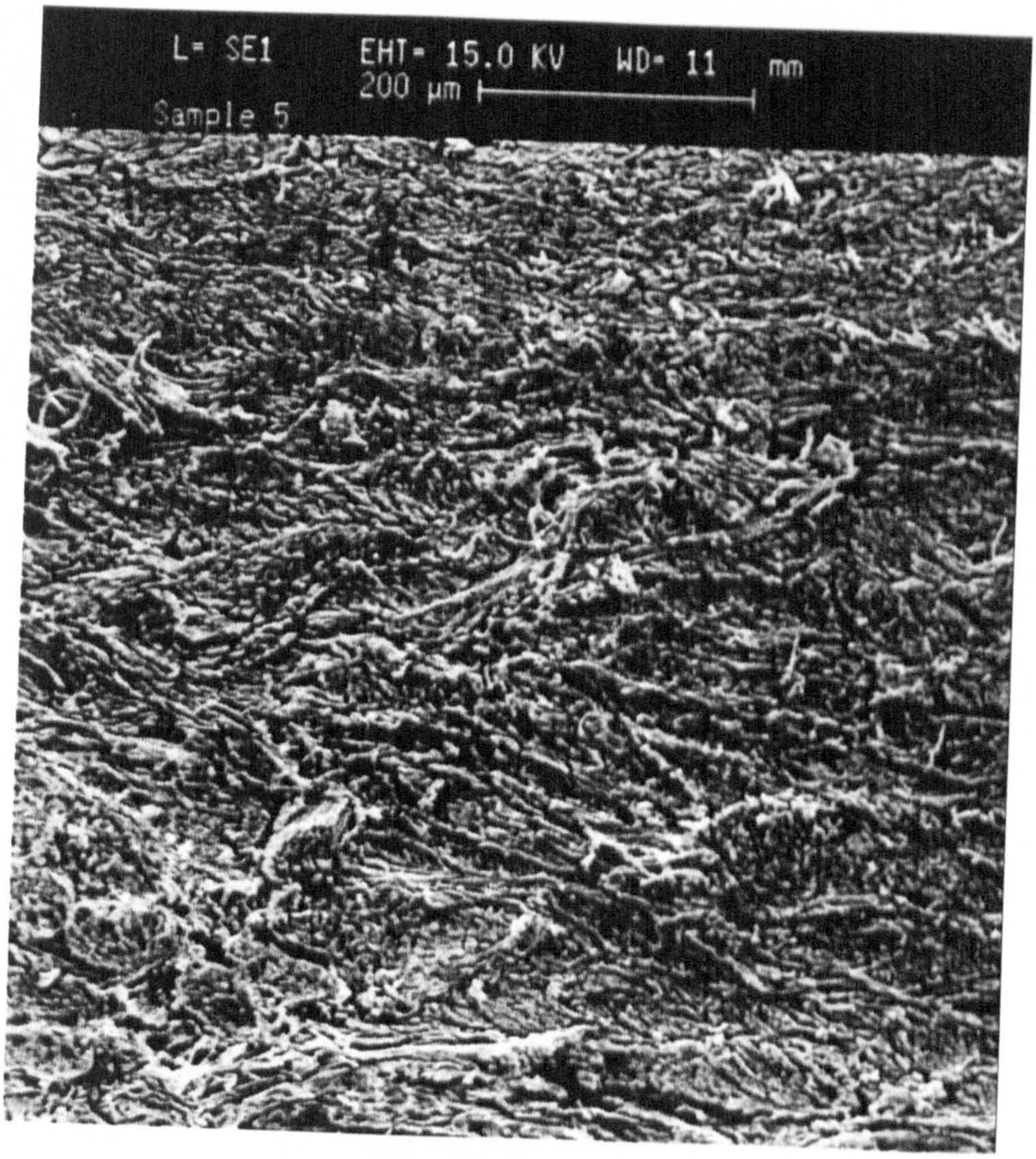

Plate A.1 Sample 5, Showing an average collagen bundle size of less than 6.6µm

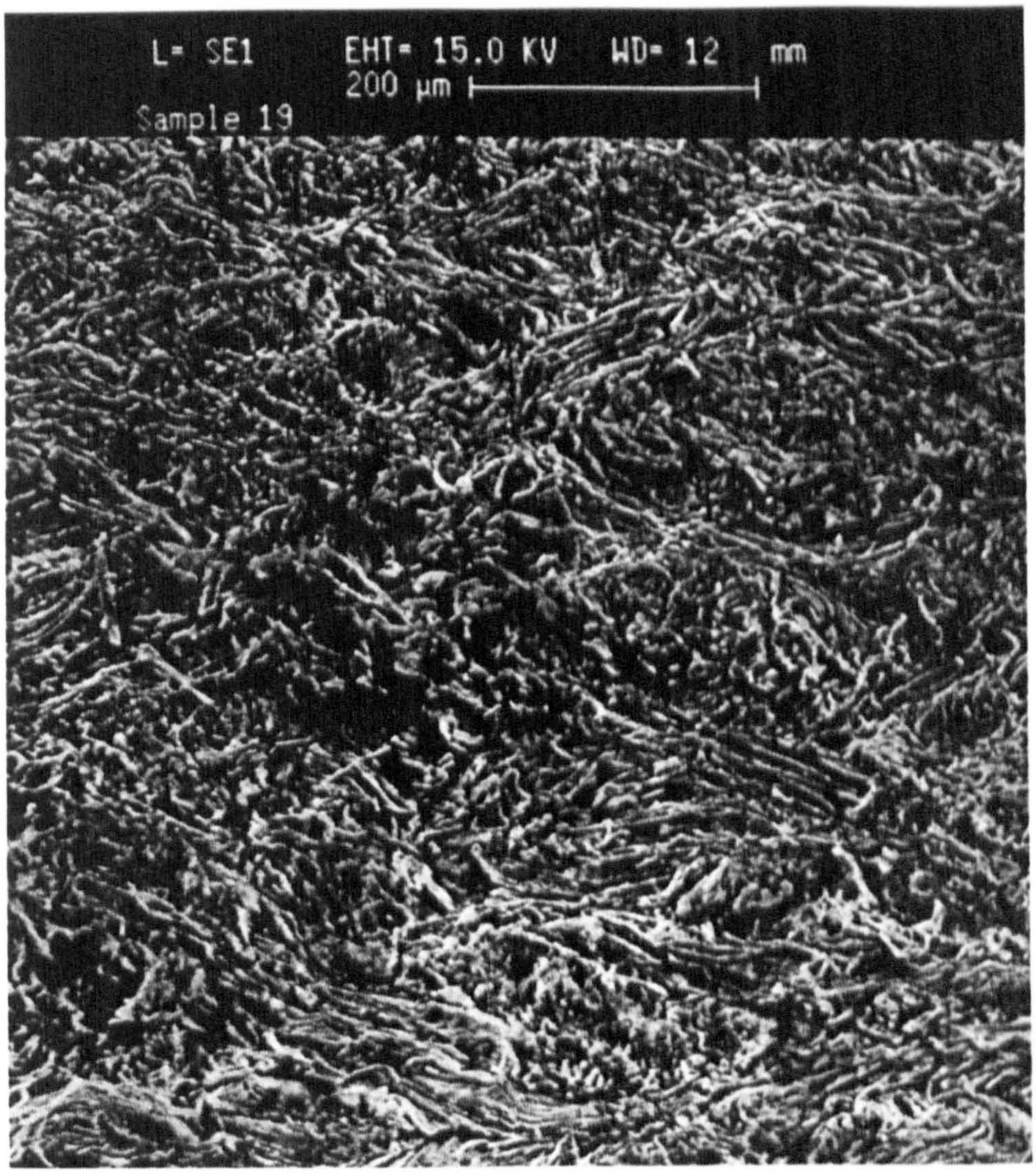

Plate A.2 Sample 19, Showing an average collagen bundle sizes between 10-13.2µm

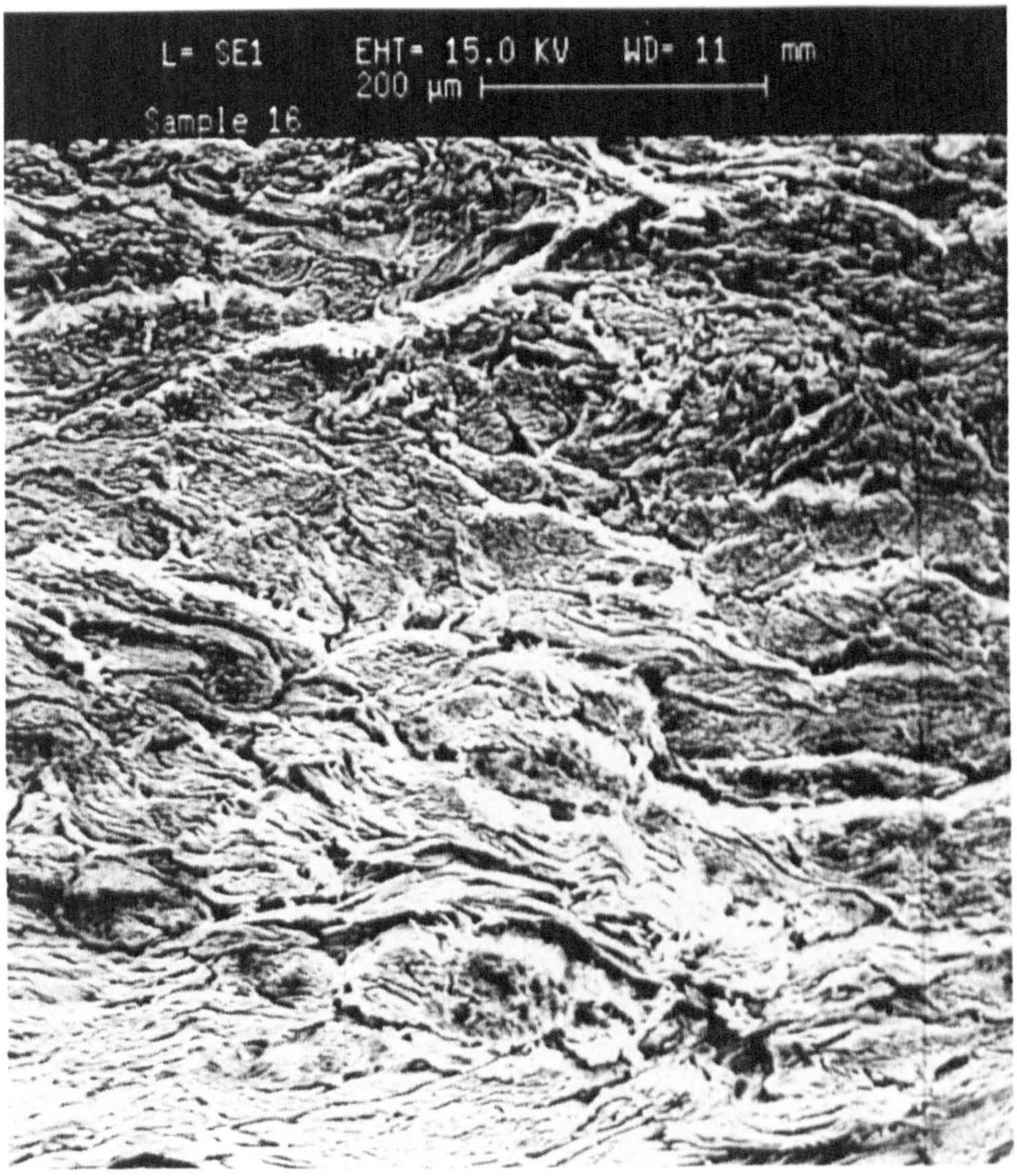

Plate A.3 Sample 16, Showing an average collagen bundle sizes in excess of 20µm

Plate A.4 Sample 1, Showing an approximate 50-50 mix of transverse and longitudinal collagen fibres.

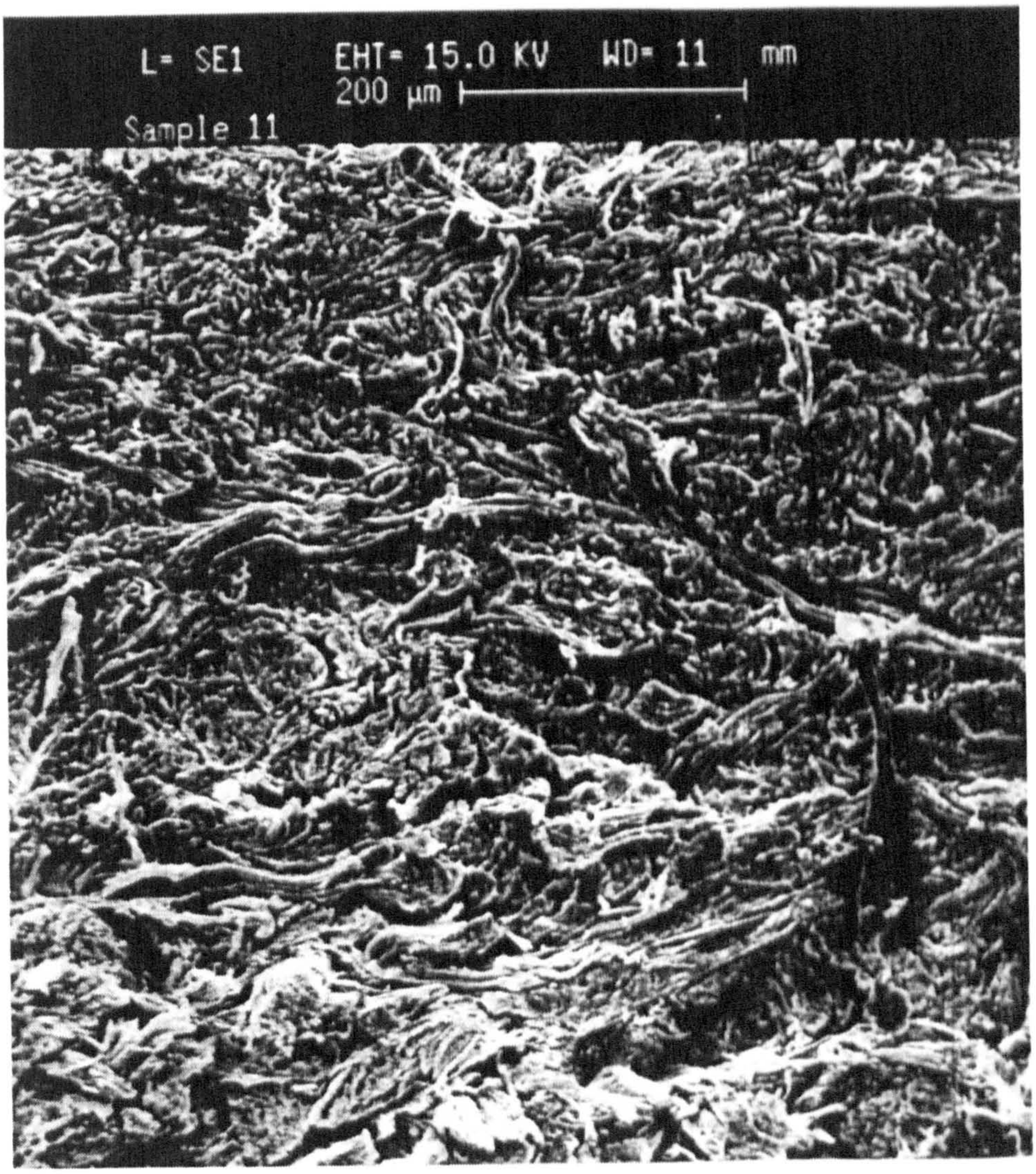

Plate A.5 Sample 11, Showing containing predominantly transverse collagen fibres but with a high degree longitudinal fibres also.

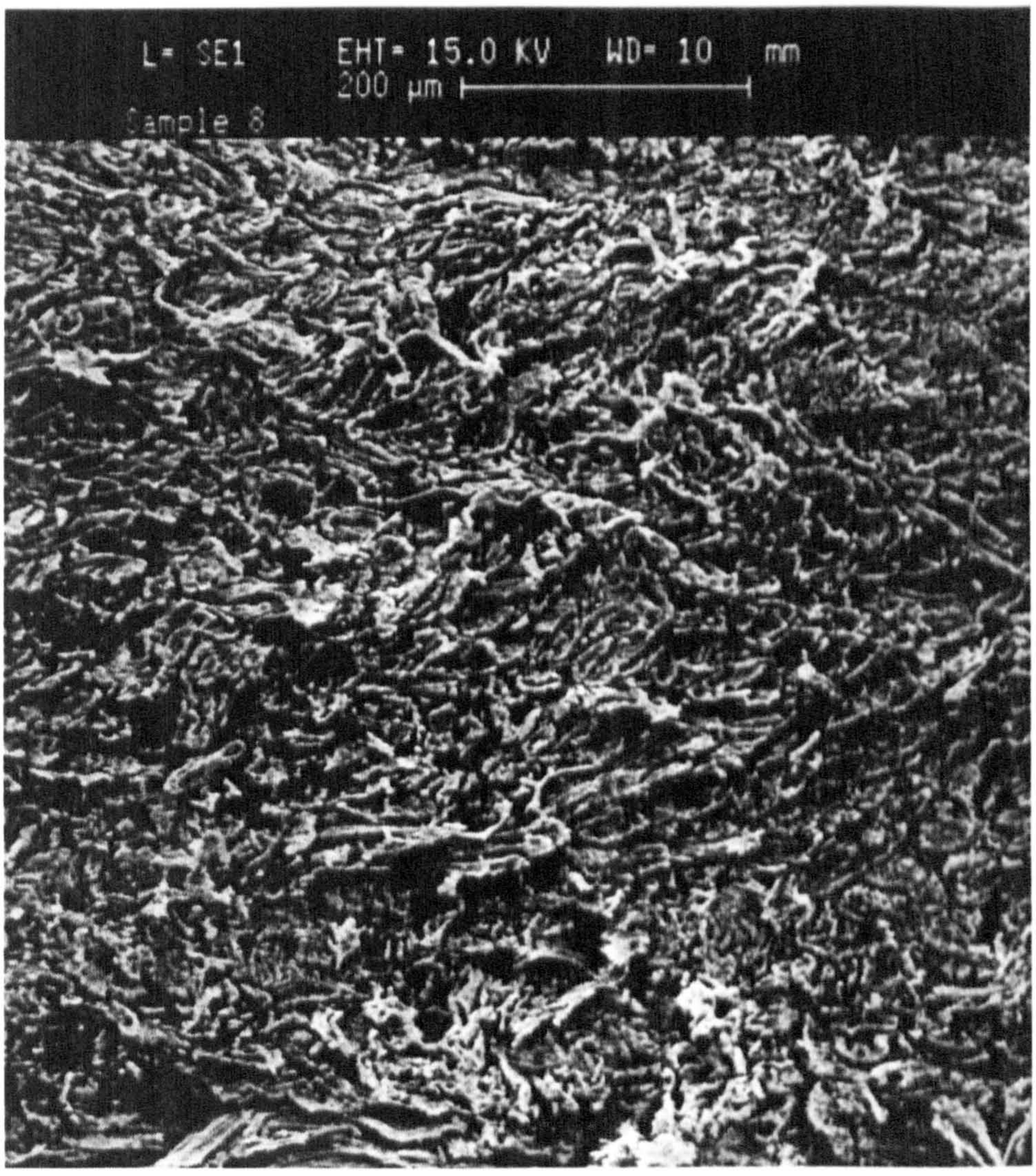

Plate A.6 Sample 8, Showing a complete dominance of transverse collagen fibres, (>80%).

Appendix B

Four-bar-link simulation results.

B.1 Four-bar-link simulation results

This appendix contains examples of the results obtained from the simulation of a four-bar-link in an attempt to identify the causes of thread drag discussed in Chapter 3.

The four-bar-link configuration shown in Chapter 3, as Figure 3.6, has been duplicated here as Figure B.1 for ease of reference. Figure B.2, shows the resultant movements associated with the default settings. The horizontal dashed line represents the plane of the workpiece, assuming that it lies half way through the needle's cycle and is included for reference purposes.

The vertical dashed line pin-points the tensioner position at the point where the needle leaves the workpiece. Ideally, for reduced thread drag, the tensioner should be relaxing at this point. It can be seen in Figures B.2-5 that this is not the case. However, at 90°, (Figure B.6), the tensioner has passed its peak and is starting to relax. Figures B.7-8, show the effect of too great an eccentric length, with the resultant needle motion being drastically reduced. This identifies 90° as the optimum eccentric angle (γ). Figure B.8 shows the standard eccentric length (L_7) at this optimum angle of 90°. It can be seen that the tensioner cycle is still active at the time the needle leaves the workpiece surface. As a result the length of the eccentric must then play an important part in adjusting the needle to tensioner relationship. By increasing this length, (Figures B.6, B.10-11), the needle cycle can be displaced with respect to the tensioner cycle to produce the desired effects. However, by increasing the eccentric length the vertical distance the needle has to travel also increases. This results in higher needle velocities and accelerations, the effect of which has to be determined experimentally.

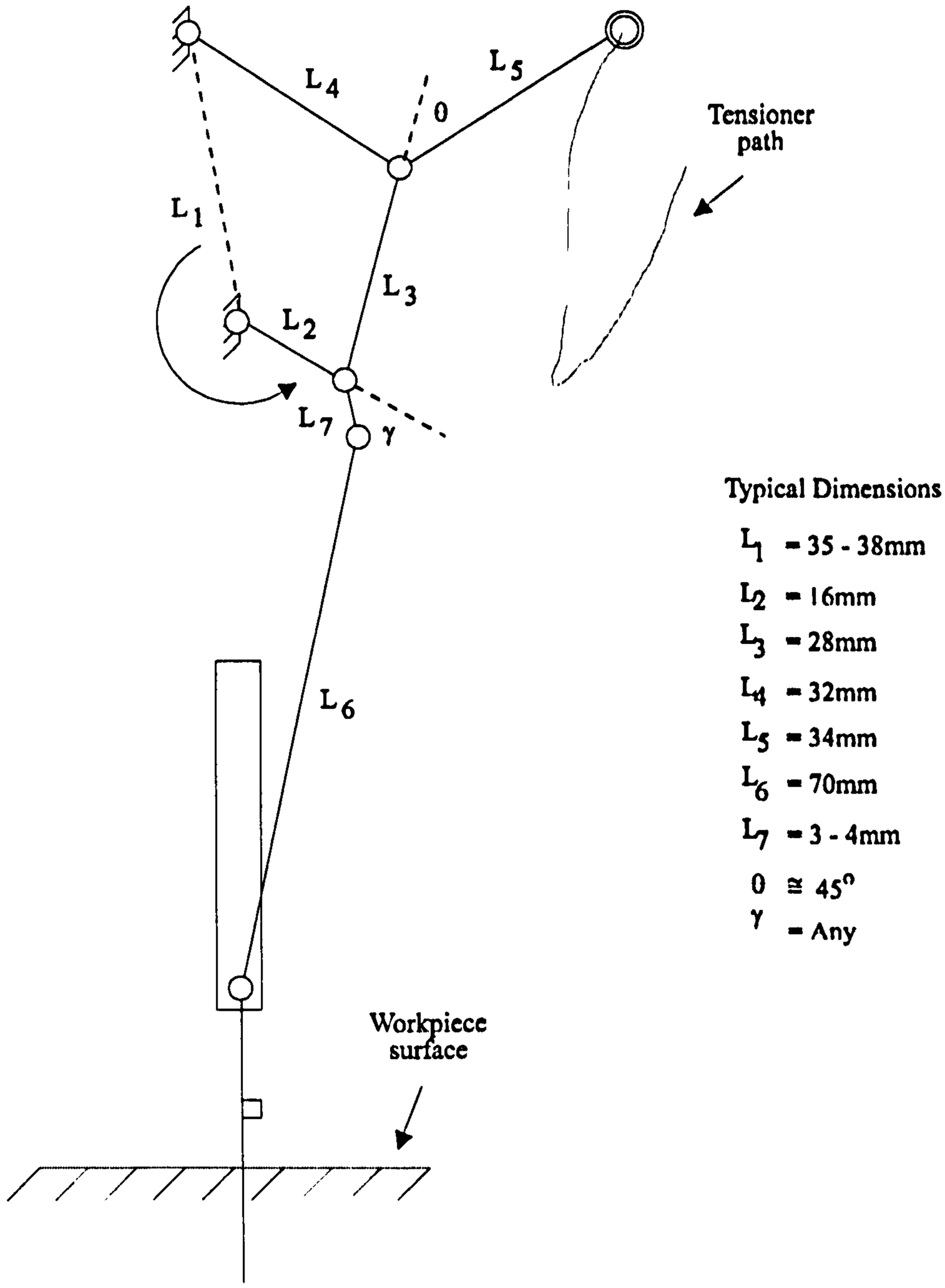

Figure B.1 Typical Pfaff 4-bar-link configuration

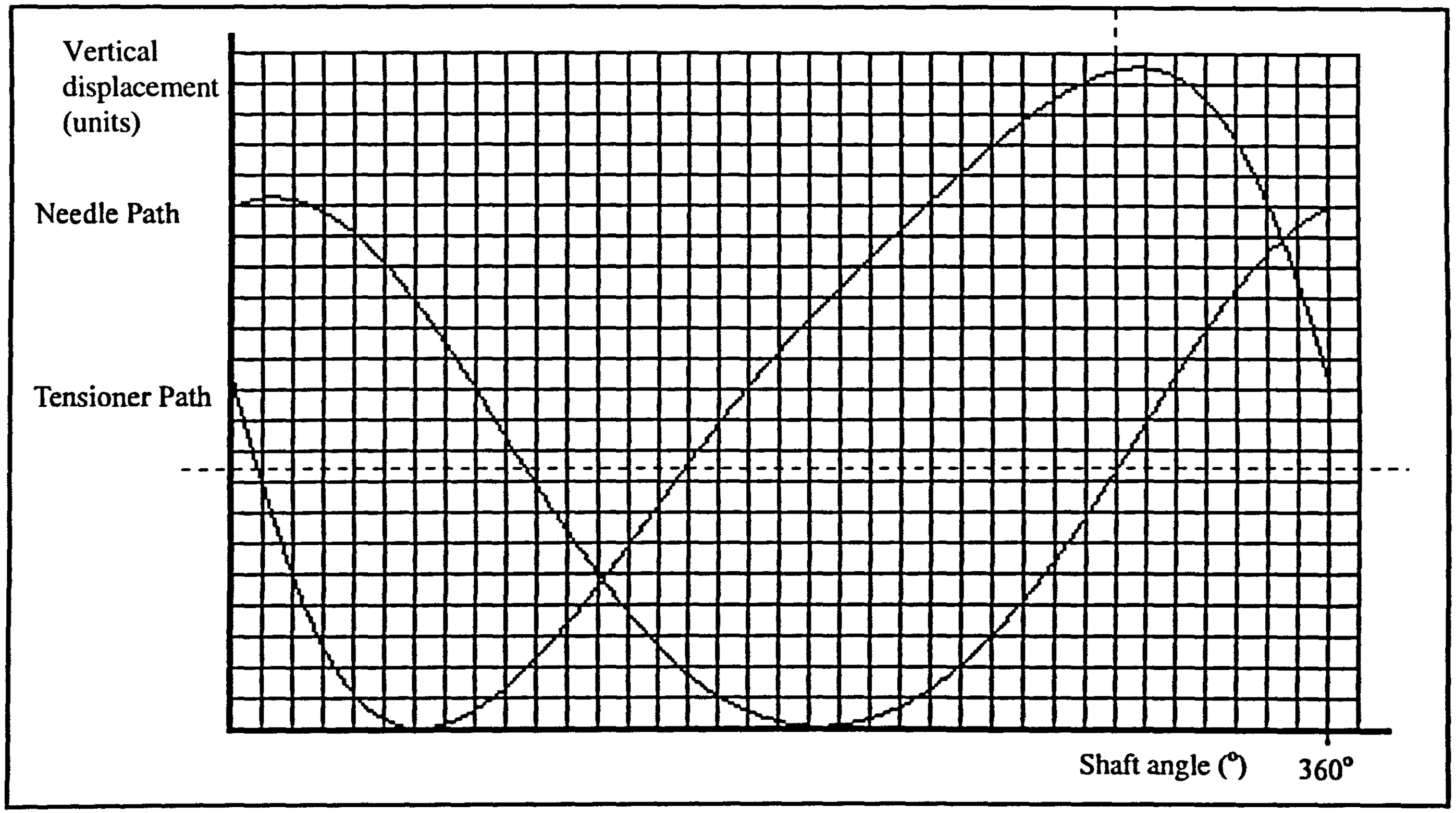

Figure B.2 Default settings (Figure B.1)

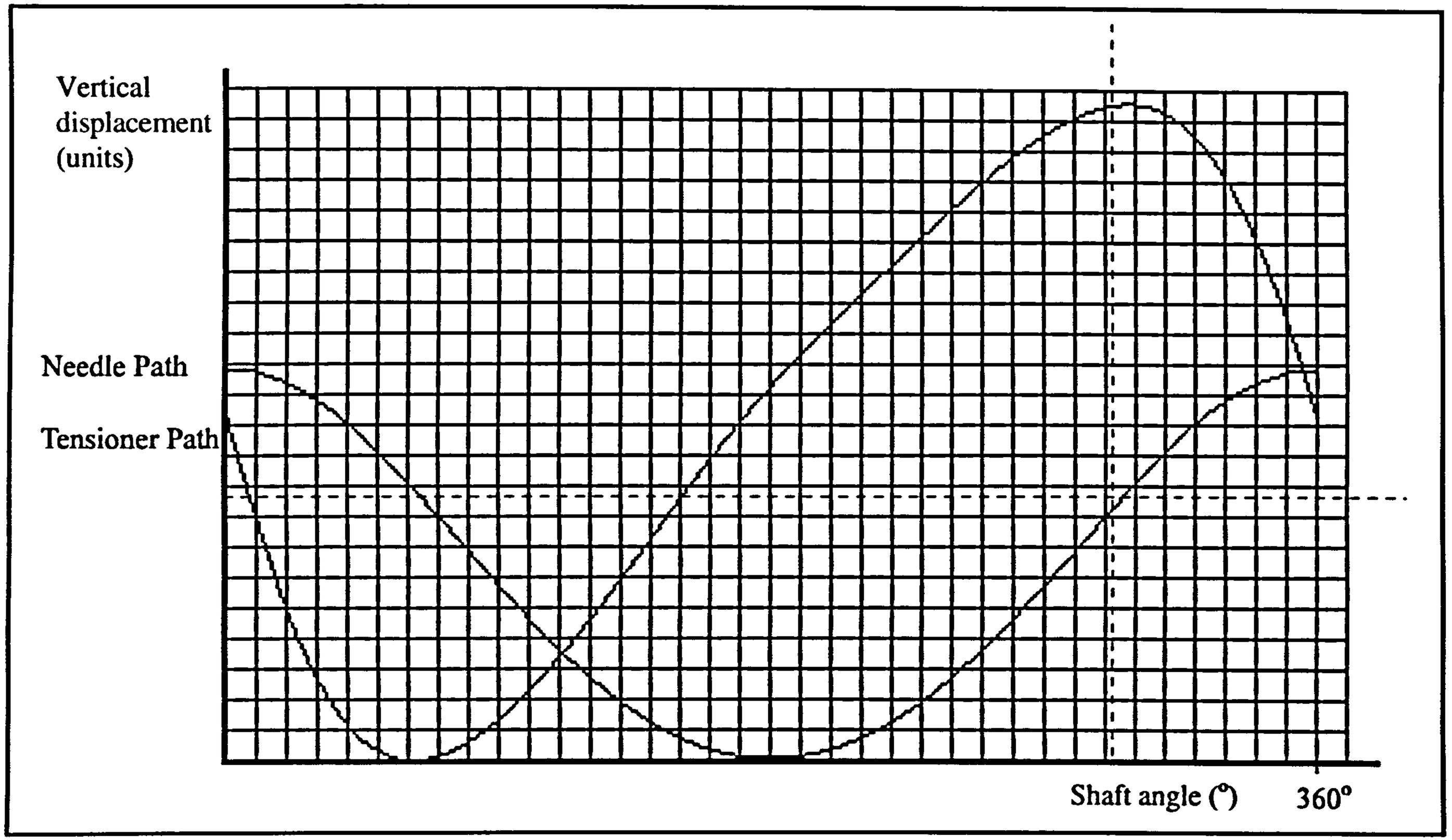

Figure B.3 L7=0 : g=0

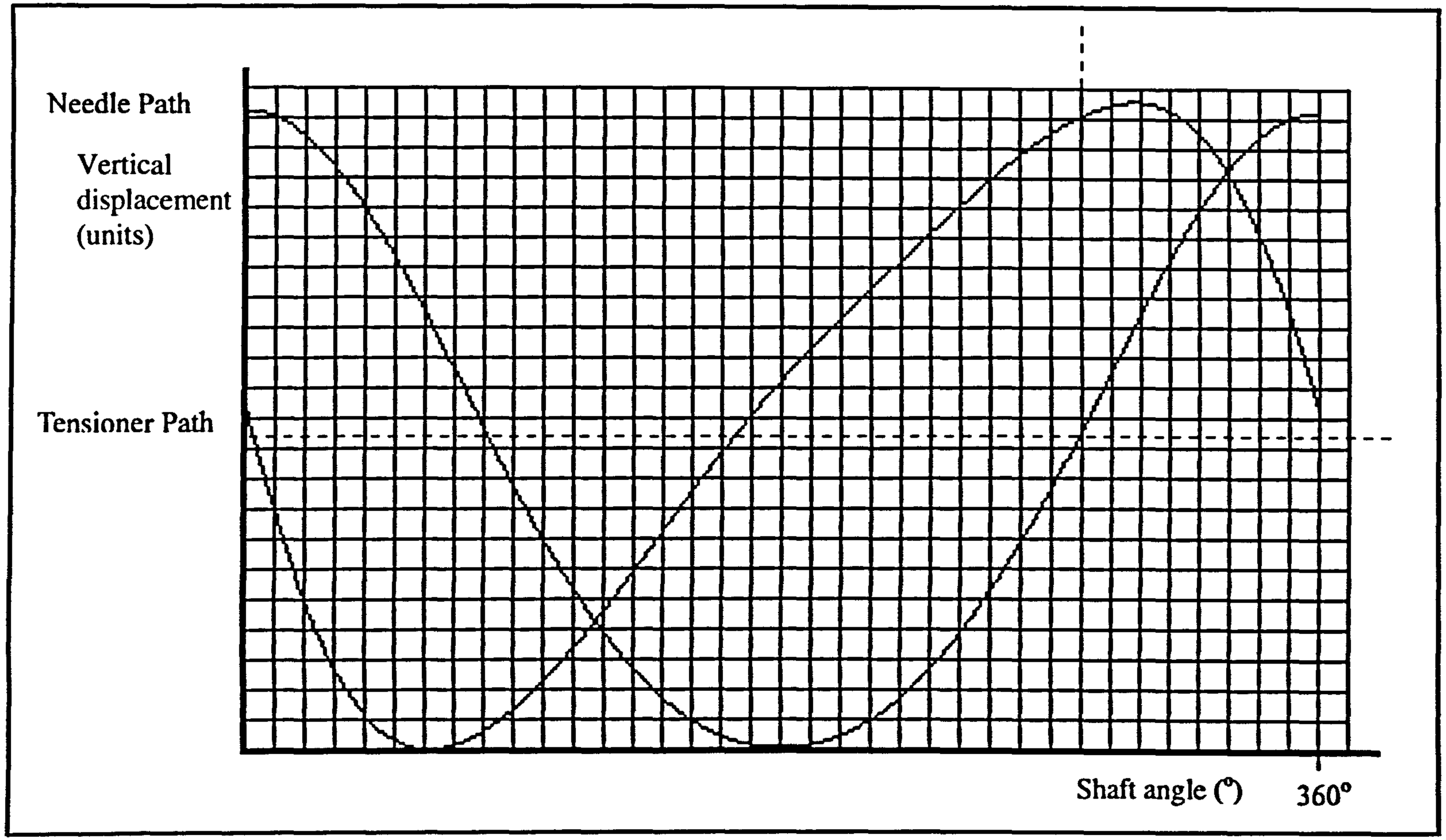

Figure B.4 L_7=7 : γ=0

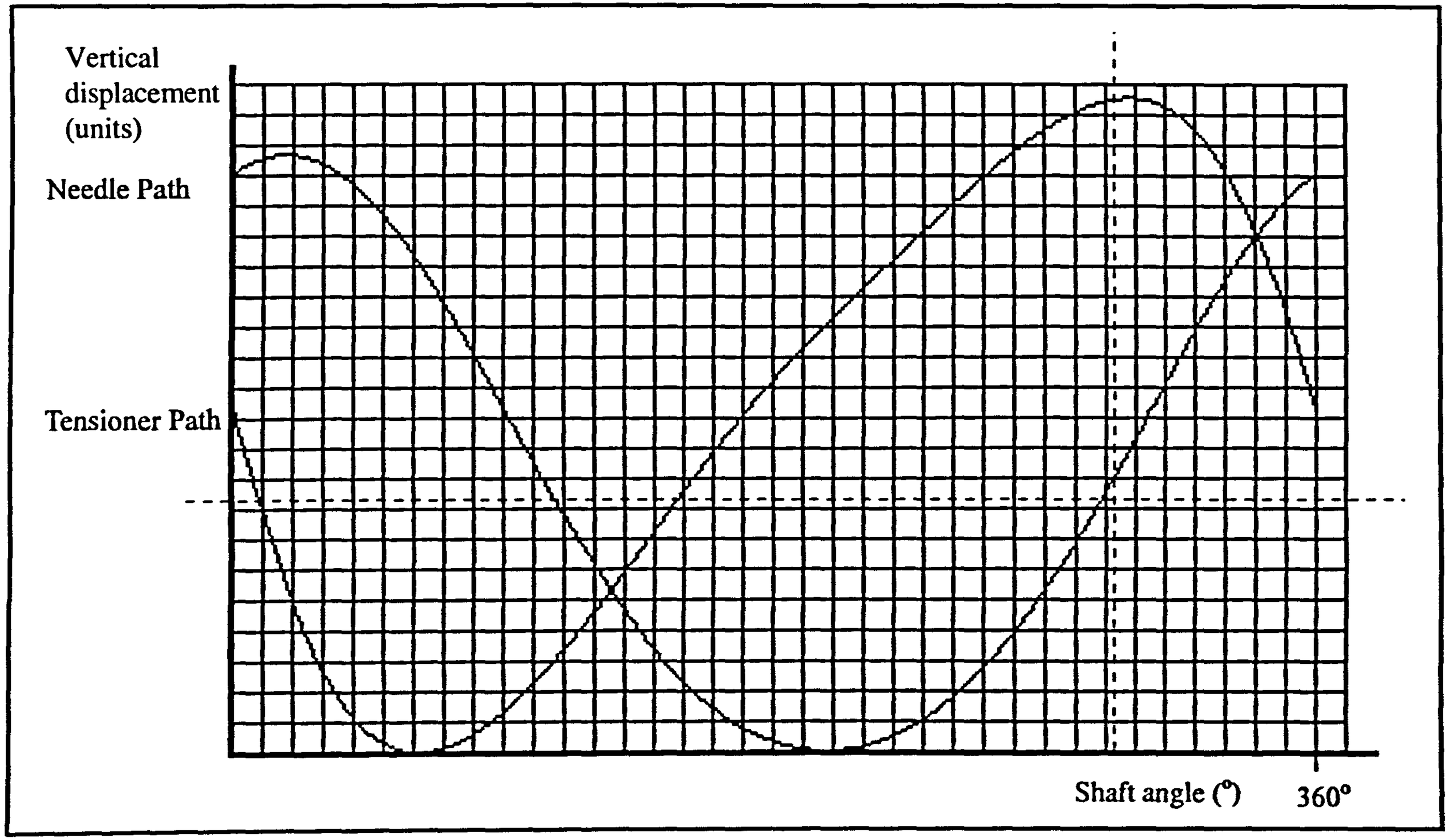

Figure B.5 L_7=21 : γ=45

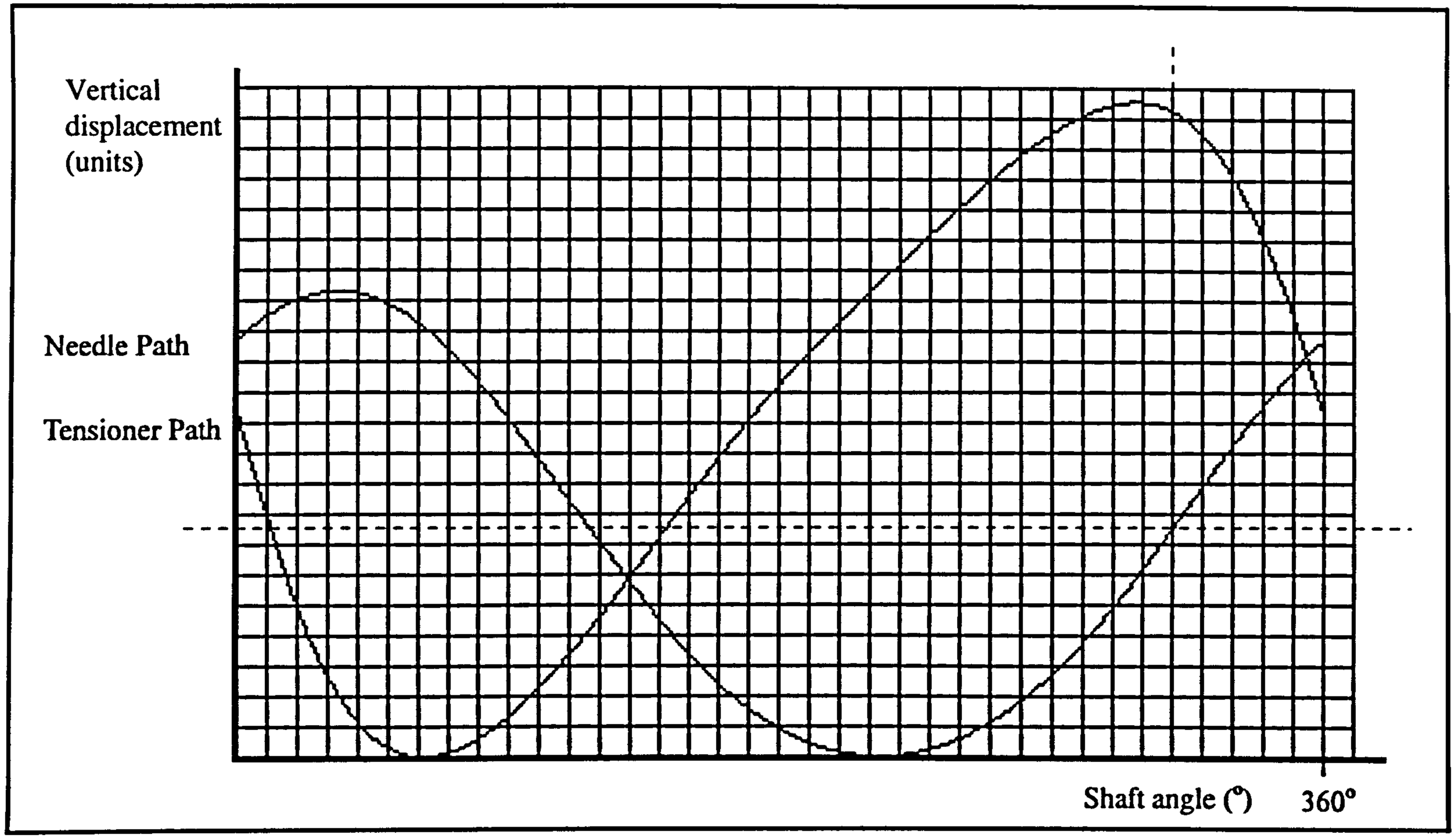

Figure B.6 L_7=21 : γ=90

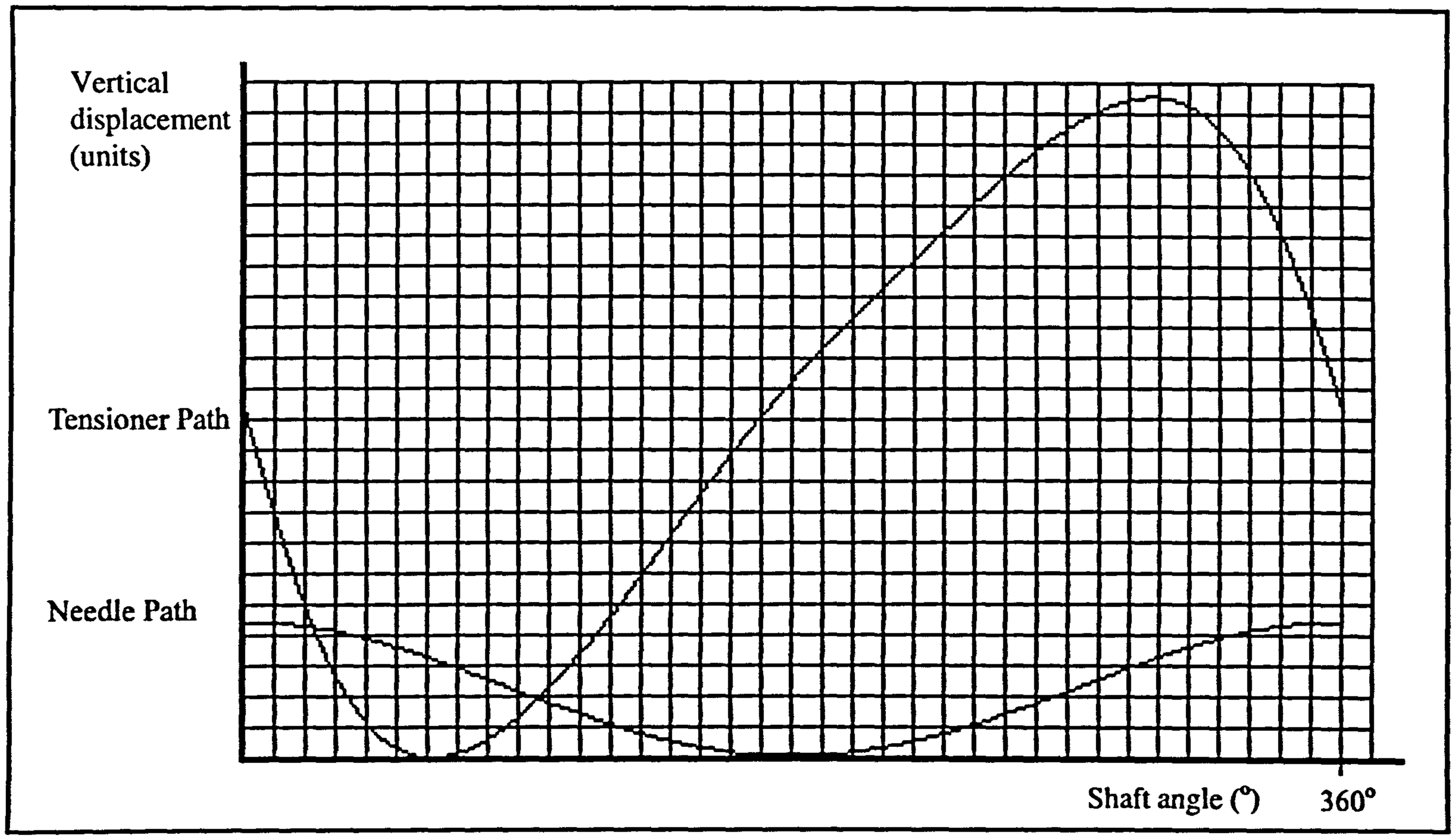

Figure B.7 L_7=21 : γ=135

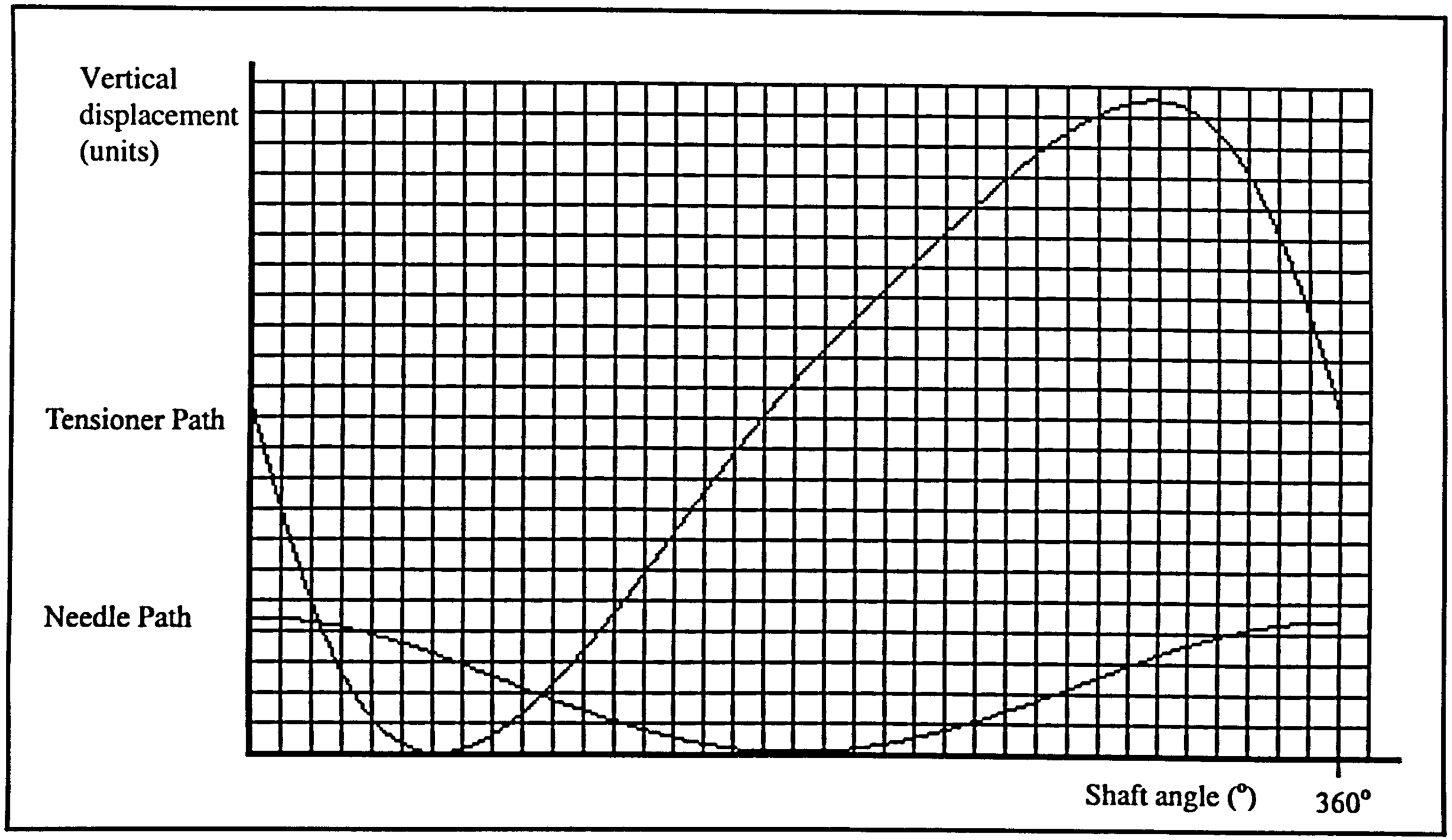

Figure B.8 L_7=21 : γ=180

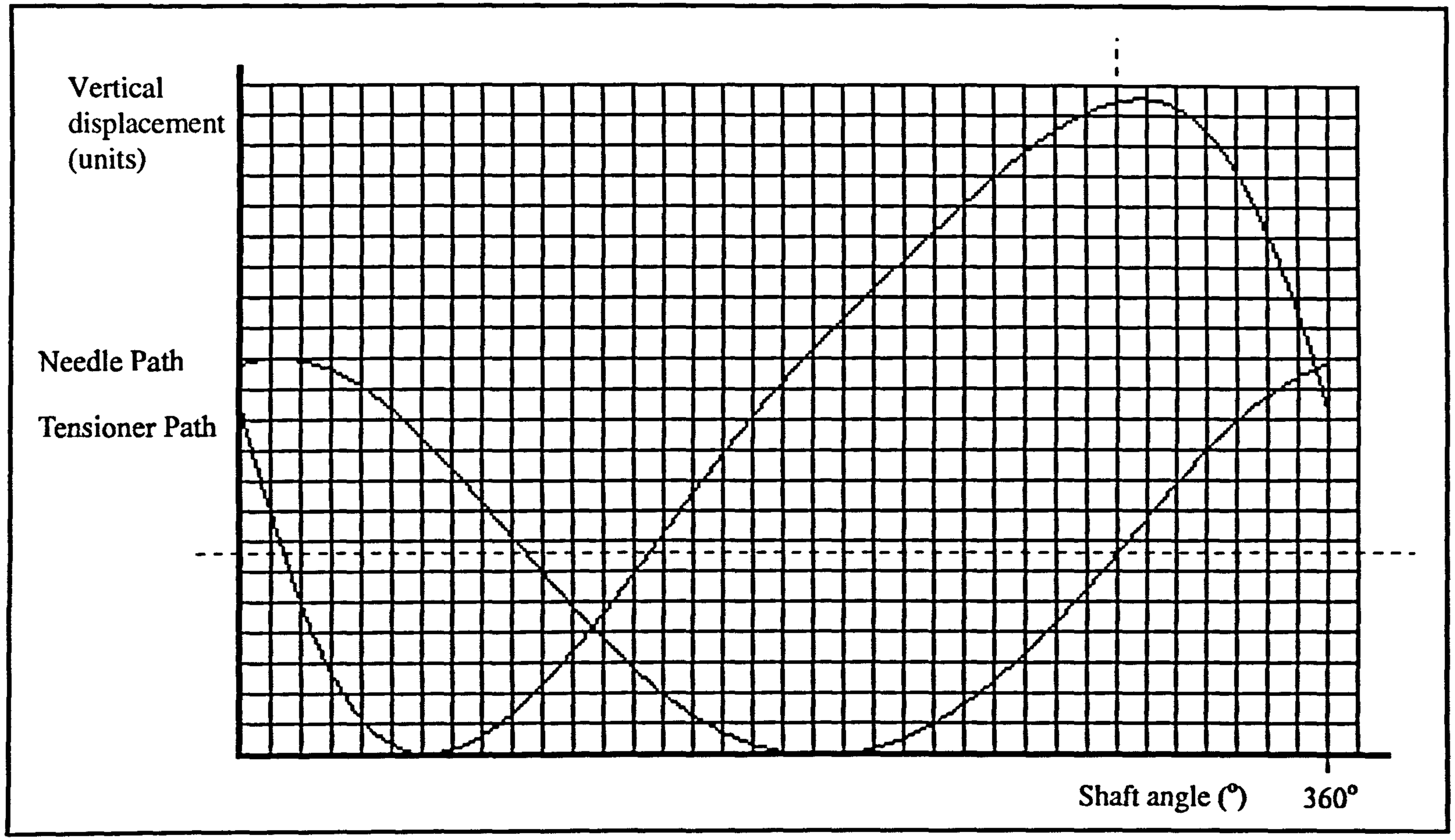

Figure B.9 L_7=7 : γ=90

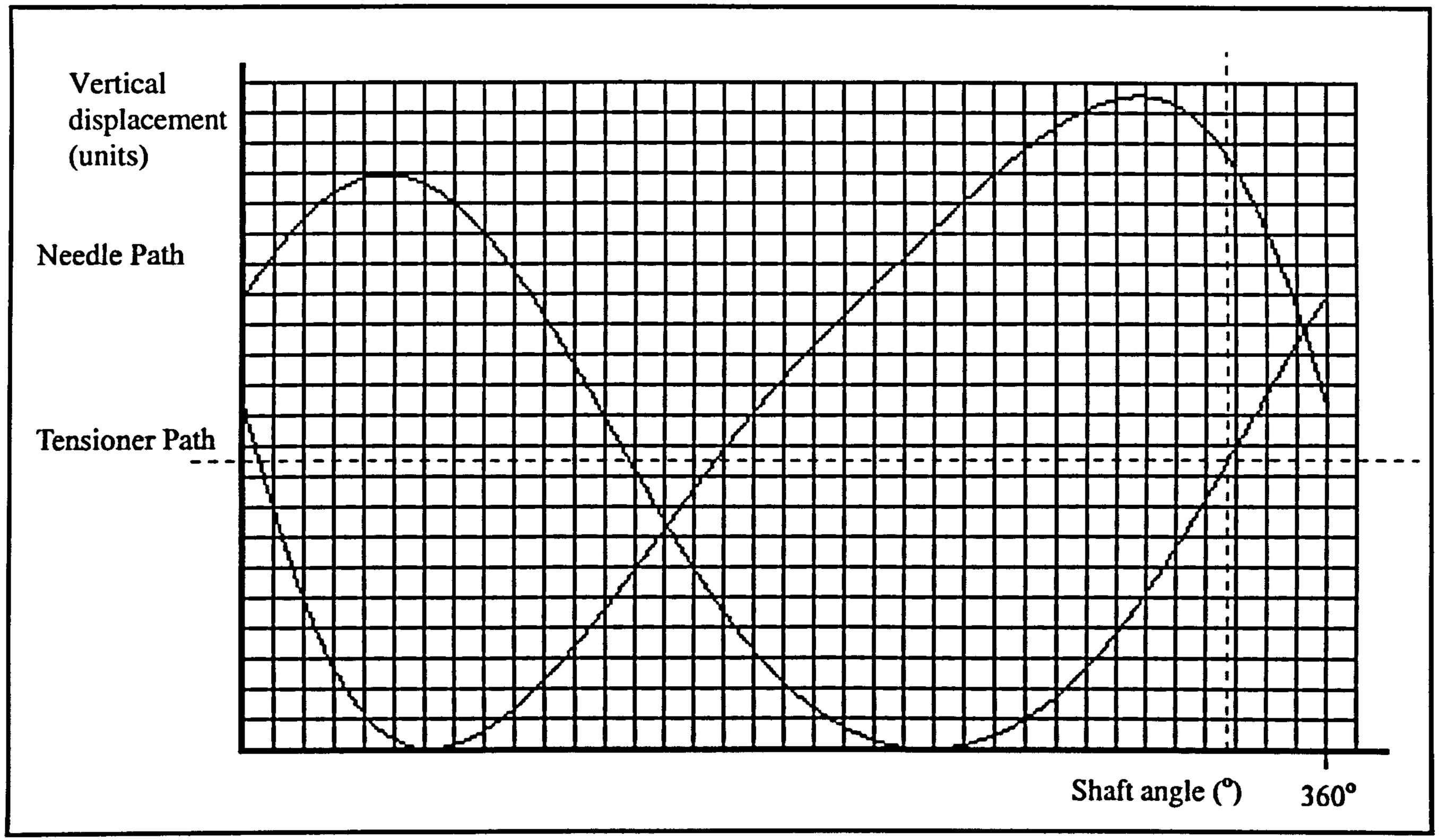

Figure B.10 L_7=35 : γ=90

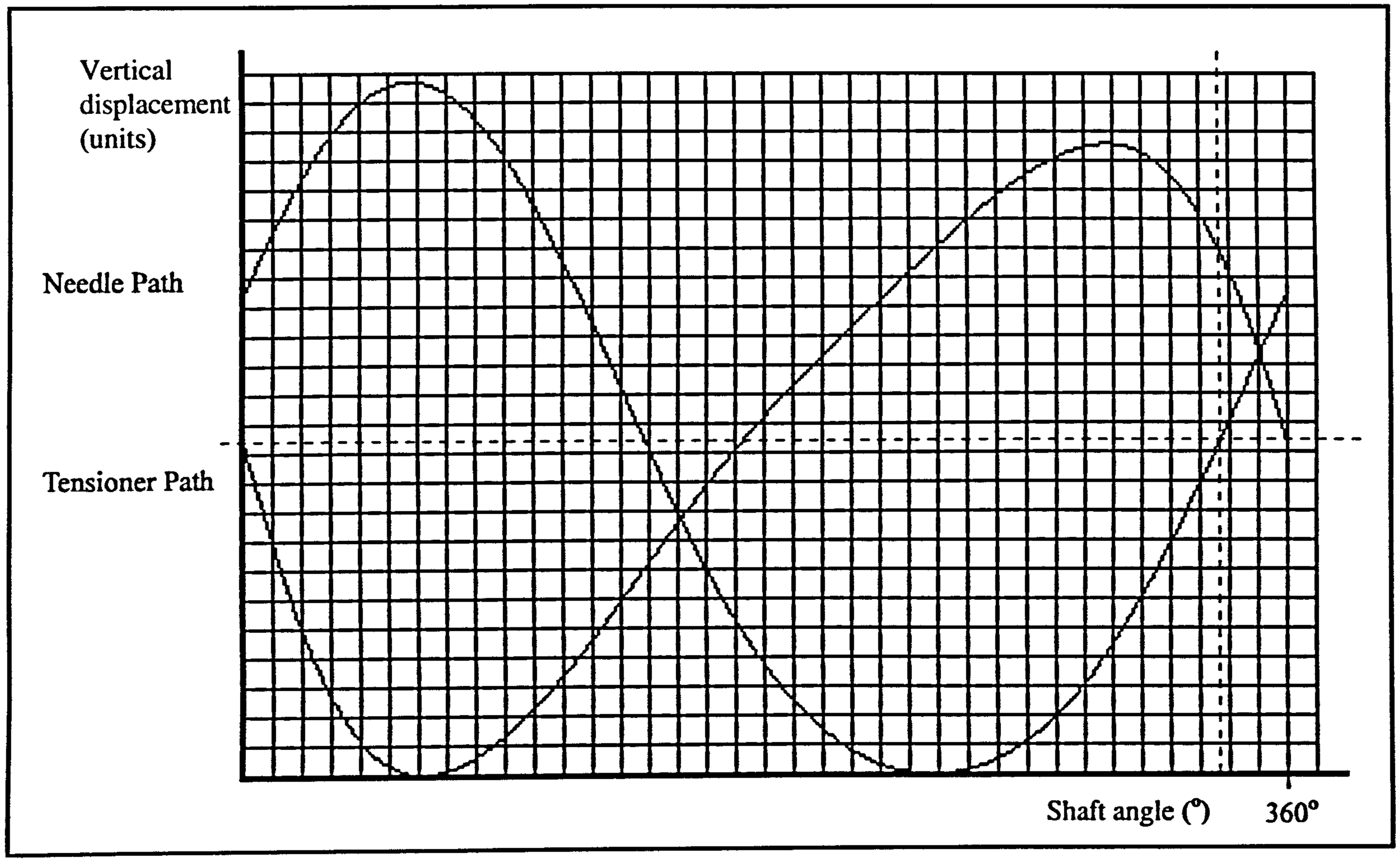

Figure B.11 L_7=50 : γ=90

Appendix C

Foam compression test results
Holding properties of pinned belts

C.1 Introduction.

This appendix is divided into two sections. The first contains results of experiments made to determine the effects of compression on a number of foam type materials believed to be suitable as a compliant medium for the Autoscan. The second section contains the results obtained during the investigation into the holding properties of the pinned belts, a summary of which can be seen in Figure 3.14, Chapter 3.

C.2 Compression characteristics for selected foams.

Samples investigated.

1. EPDM
2. Nercoprene
3. Neoprene

The results were obtained by cutting 10mm square samples from each of the three foams selected. Five sets of readings were made for each sample to alleviate the possible effects of local properties within the foam. The following charts use the mean values obtained. A force sensor with a 8mm diameter probe was advanced towards the sample in 0.1mm steps. This was performed by mounting the force sensor on a linear track driven by a stepper motor. This allows for the compressive force to be plotted against surface deflection.

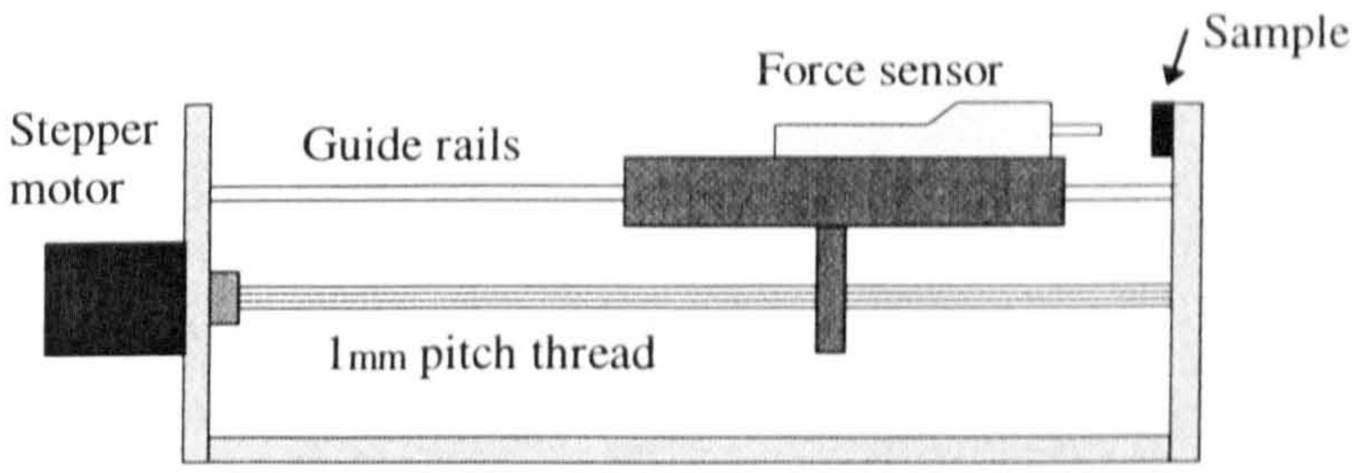

Figure C.1 Experimental set-up for the determination of foam characteristics

C.2.1 Results of compression experiments

Figures C.2 - C.4 show measurements of instantaneous force readings, measured for each deflection. These were obtained by utilising an option provided by the force sensor to record the maximum exerted force. The experiments were performed five times, on fresh samples, and the average values plotted.

EPDM Foam (3.5mm thickness)

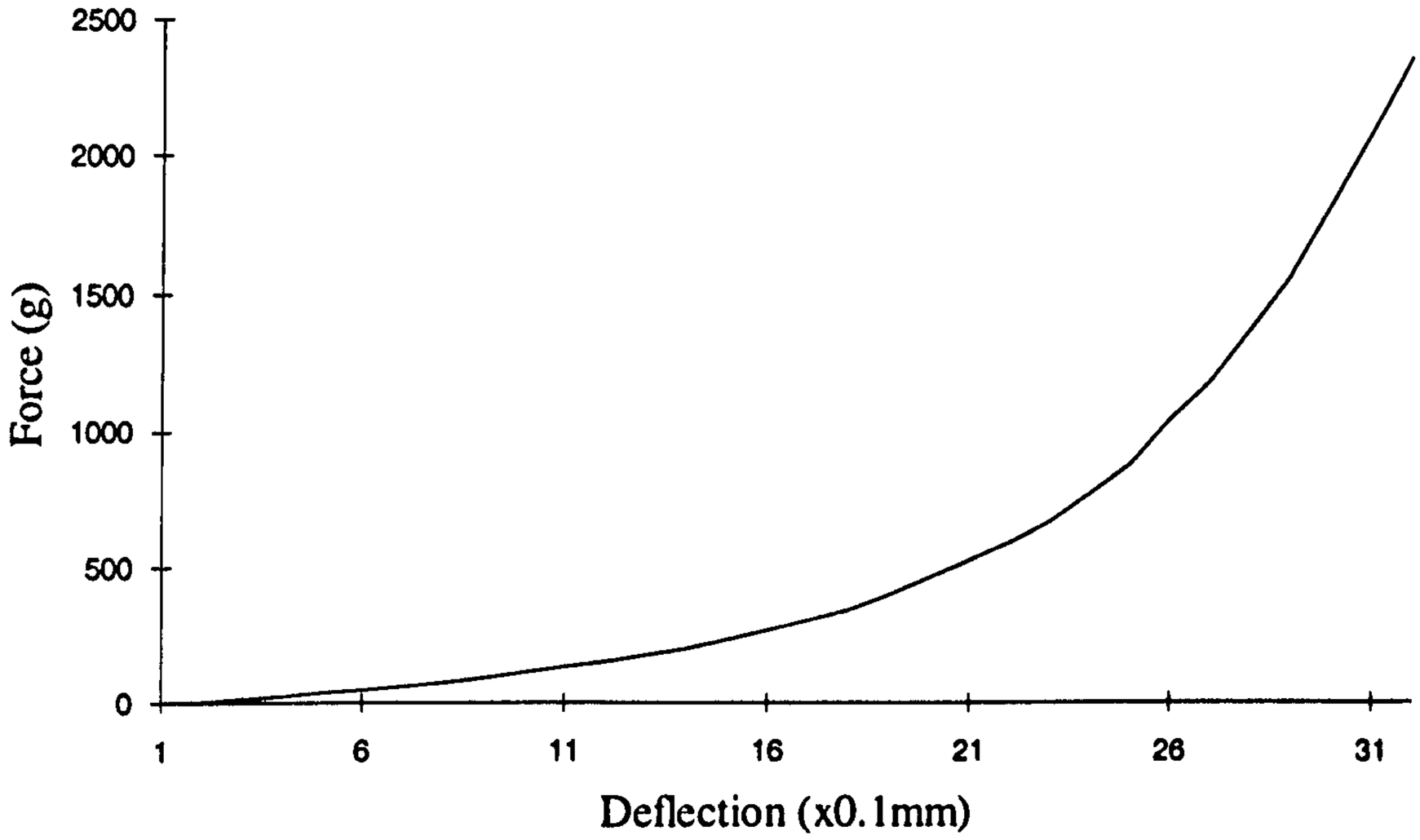

Figure C.2 Compression characteristics for EPDM

Neoprene Foam (3mm thickness)

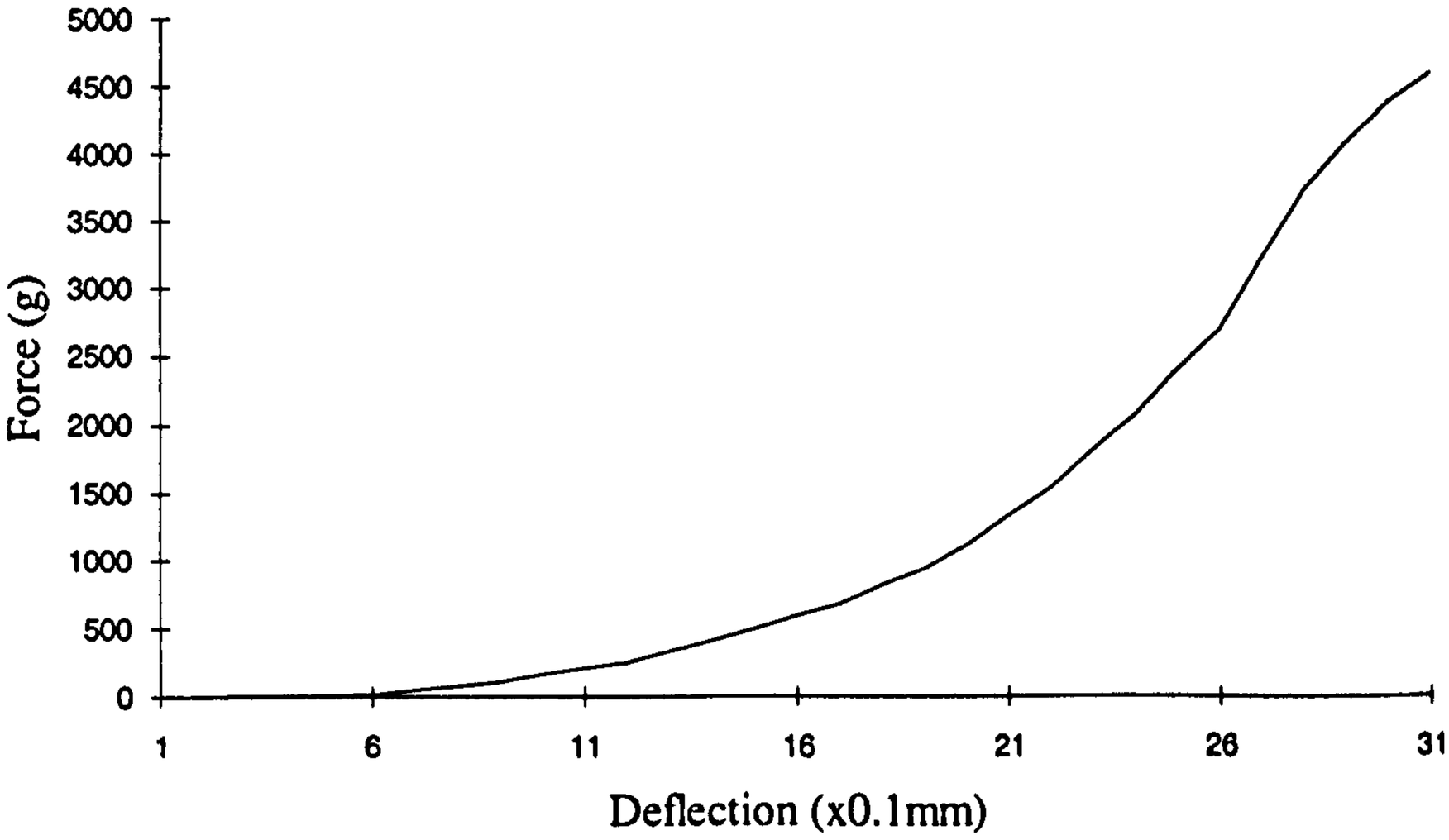

Figure C.3 Compression characteristics for Neoprene

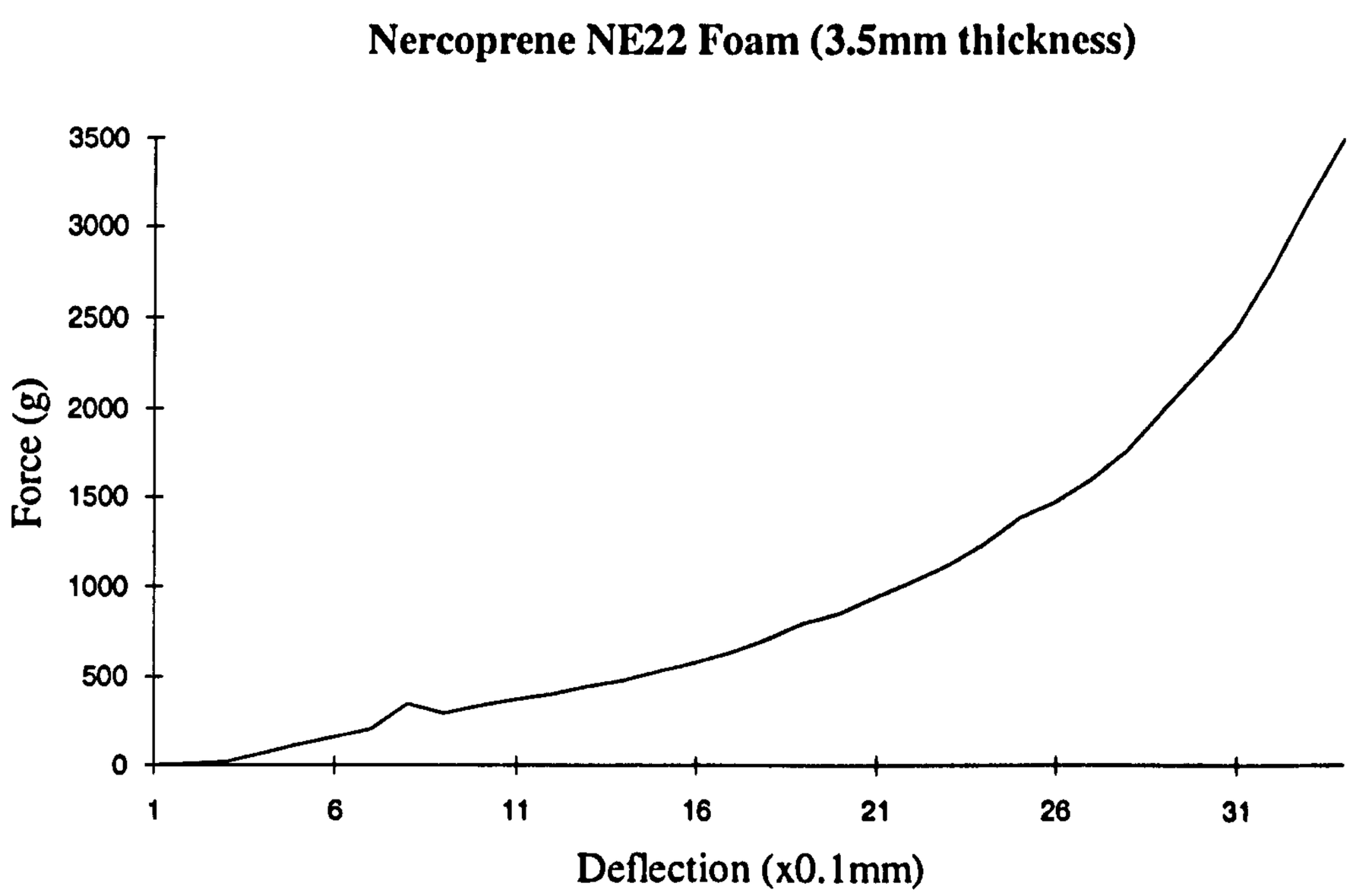

Figure C.4 Compression characteristics for Nercoprene

C.3 Investigation into the holding properties of pinned belts

The forces generated on a typical workpiece during manipulation are discussed in Chapter 3. In order to determine the required holding force needed to overcome these forces the properties of the pinned belts need to be investigated. This section contains the results obtained during this investigation.

C.3.1 Experimental procedure

In order to reproduce the dimensions that would be needed to put such a belt on the Autoscan a length of polyurethane belt 51.5 x 12mm with 5 pairs of pins was constructed and glued again to a wooden base. Five strips of leather were cut 190 x 12mm from a selection of leathers supplied by B.U.S.M representing a cross-section of leathers used within the shoe making industry. A hole punched into one end of the strip allowed for the attaching of a force sensor. The force sensor was configured to display the peak force measured during each test, this ensured that the force being applied at the point of slip was being measured. Measurements of the required pulling force to cause slip were then taken for normal holding forces of 10 - 80N, (1 - 8Kg).

C.3.2 Holding properties of pinned belts

The following are the results of the force experiments described above. They are expressed graphically in order to highlight a number of effects that occurred in addition to slippage. Notably, sample 2 started to stretch under a 5Kg holding force when a pulling force of approximately 3.2Kg was applied before tearing completely. Sample 3 also tore before the maximum measurable pulling force of 5Kg could be applied. In contrast samples 1 and 5 showed no sign of slippage at the maximum conditions. These results show that the pins provide a very secure method for holding leather parts even under high adverse forces.

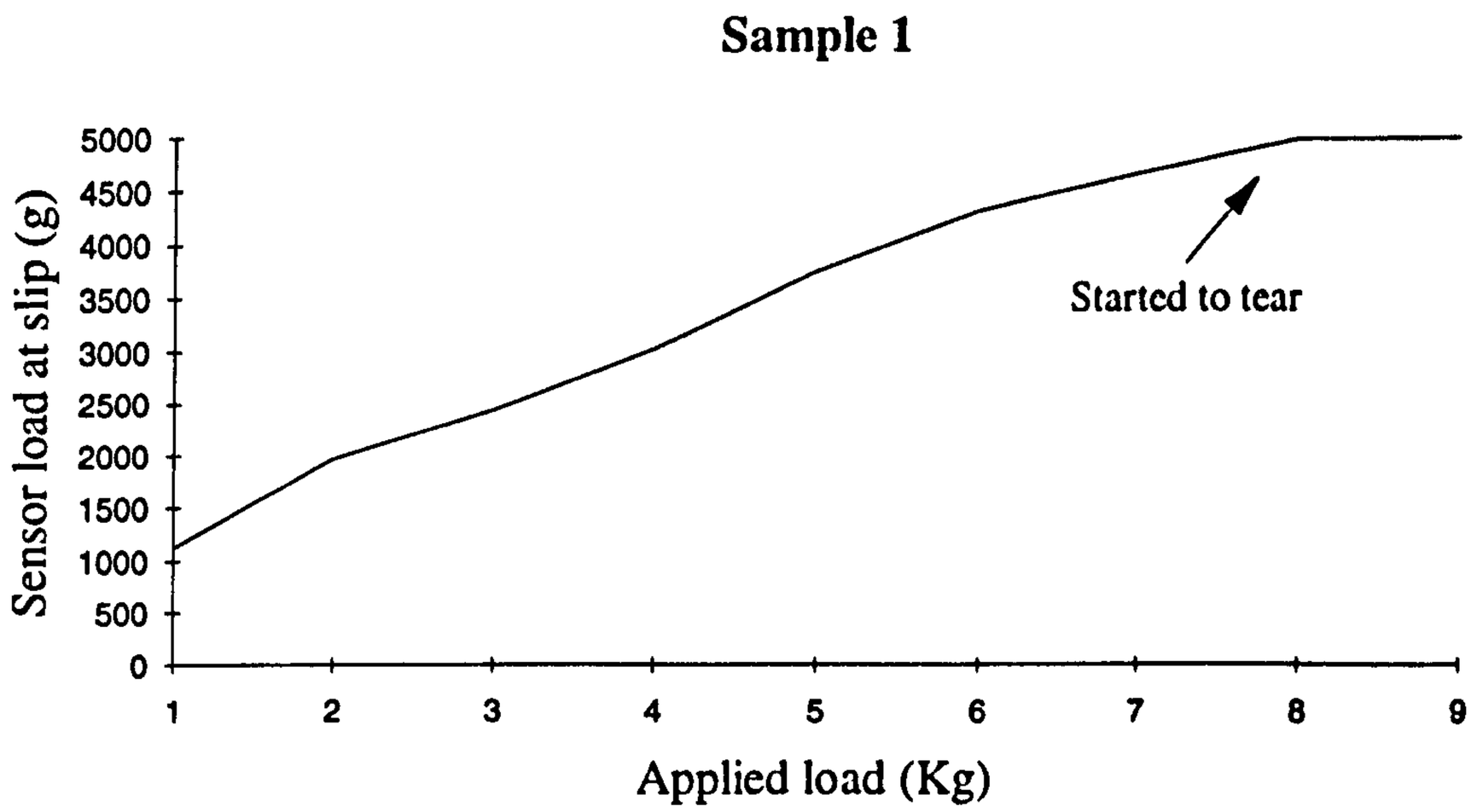

Figure C.5 Slipping force V Load for Sample 1

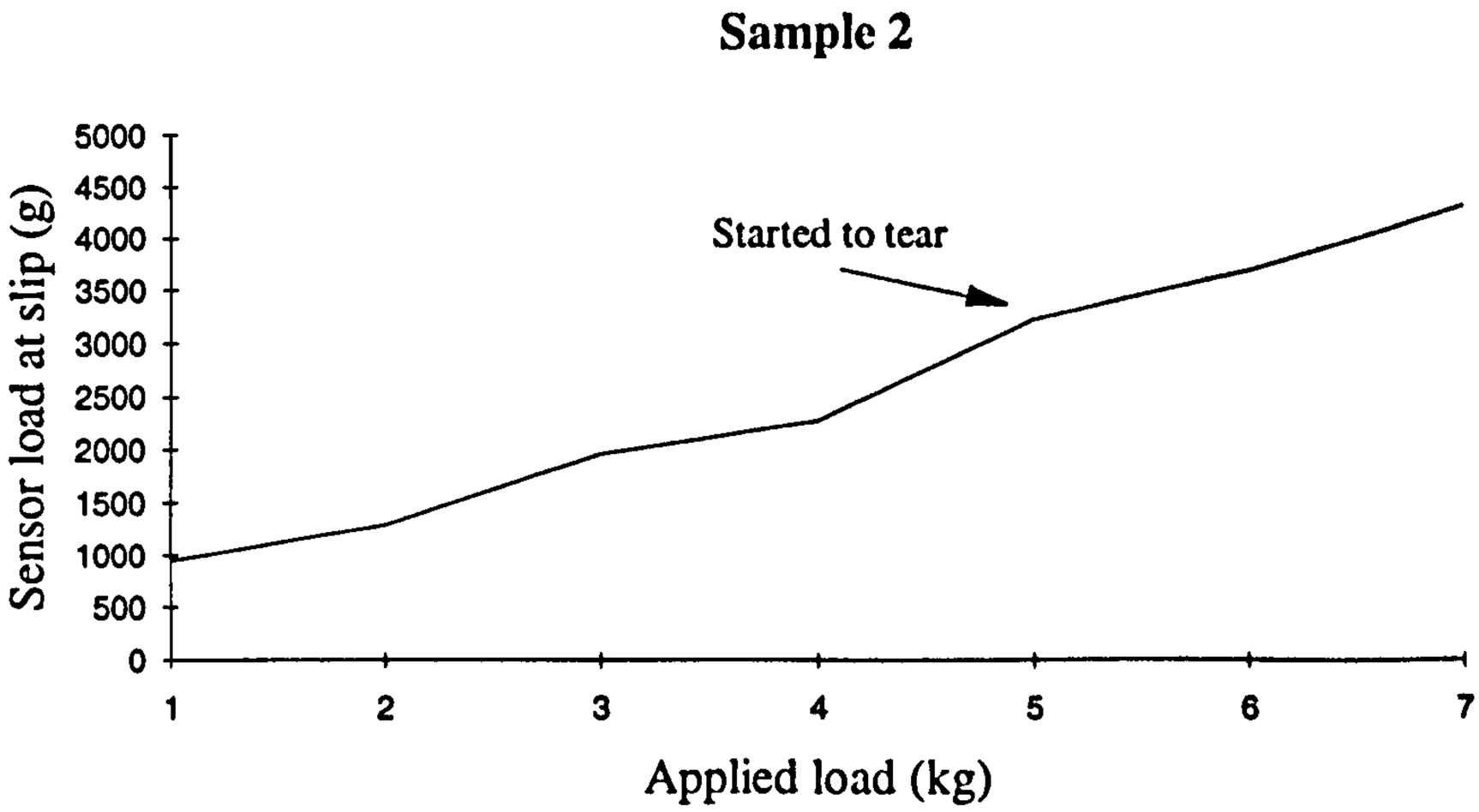

Figure C.6 Slipping force V Load for Sample 2

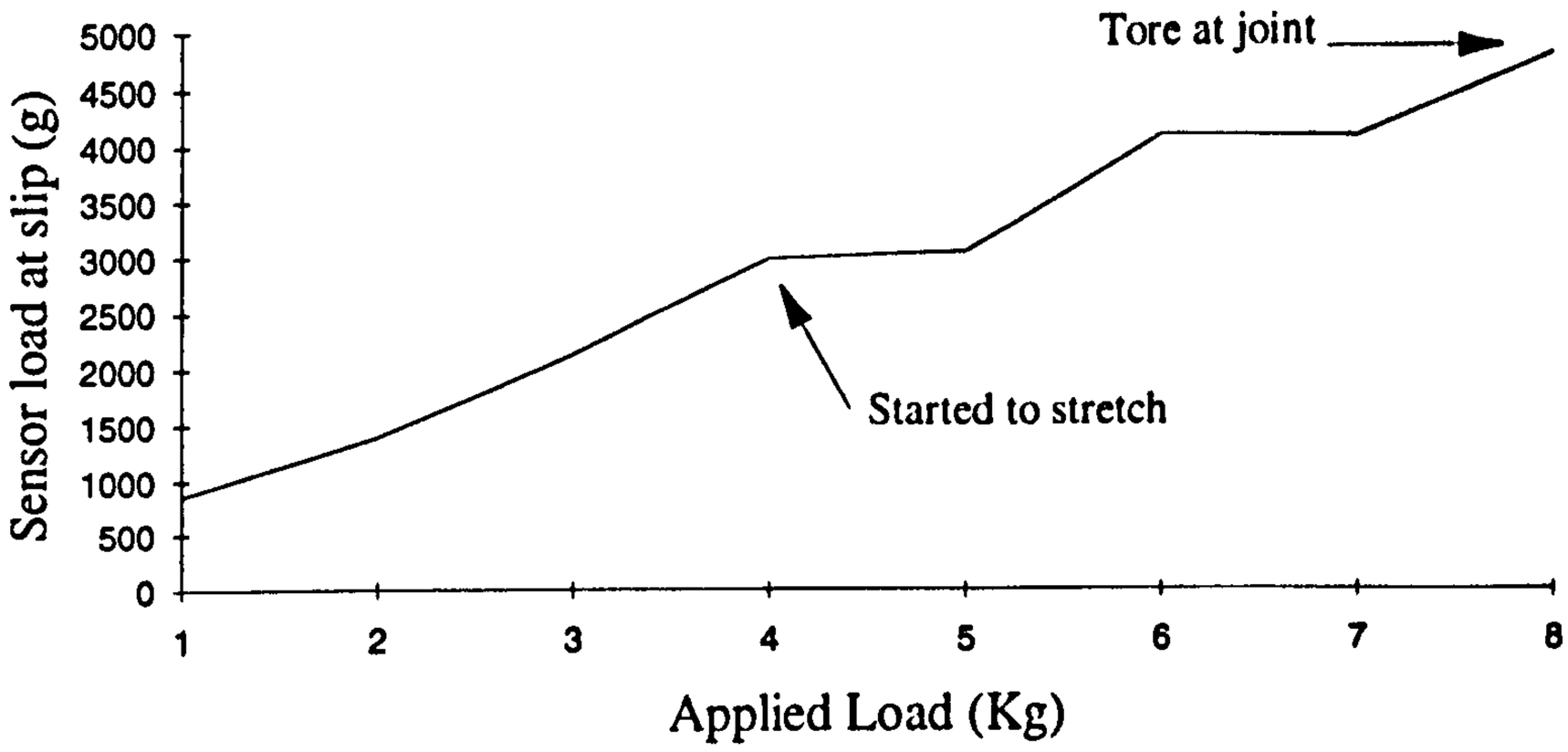

Figure C.7 Slipping force V Load for Sample 3

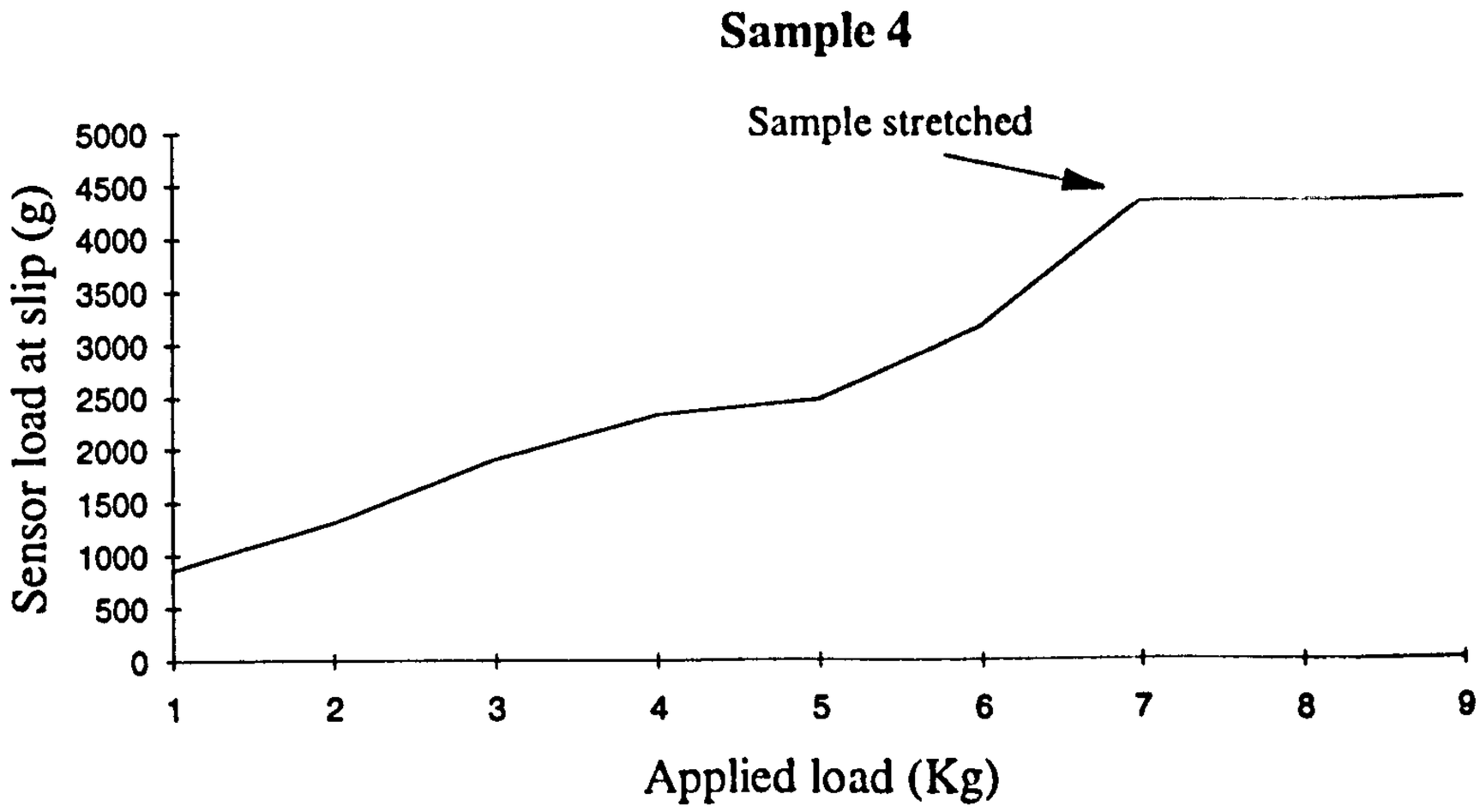

Figure C.8 Slipping force V Load for Sample 4

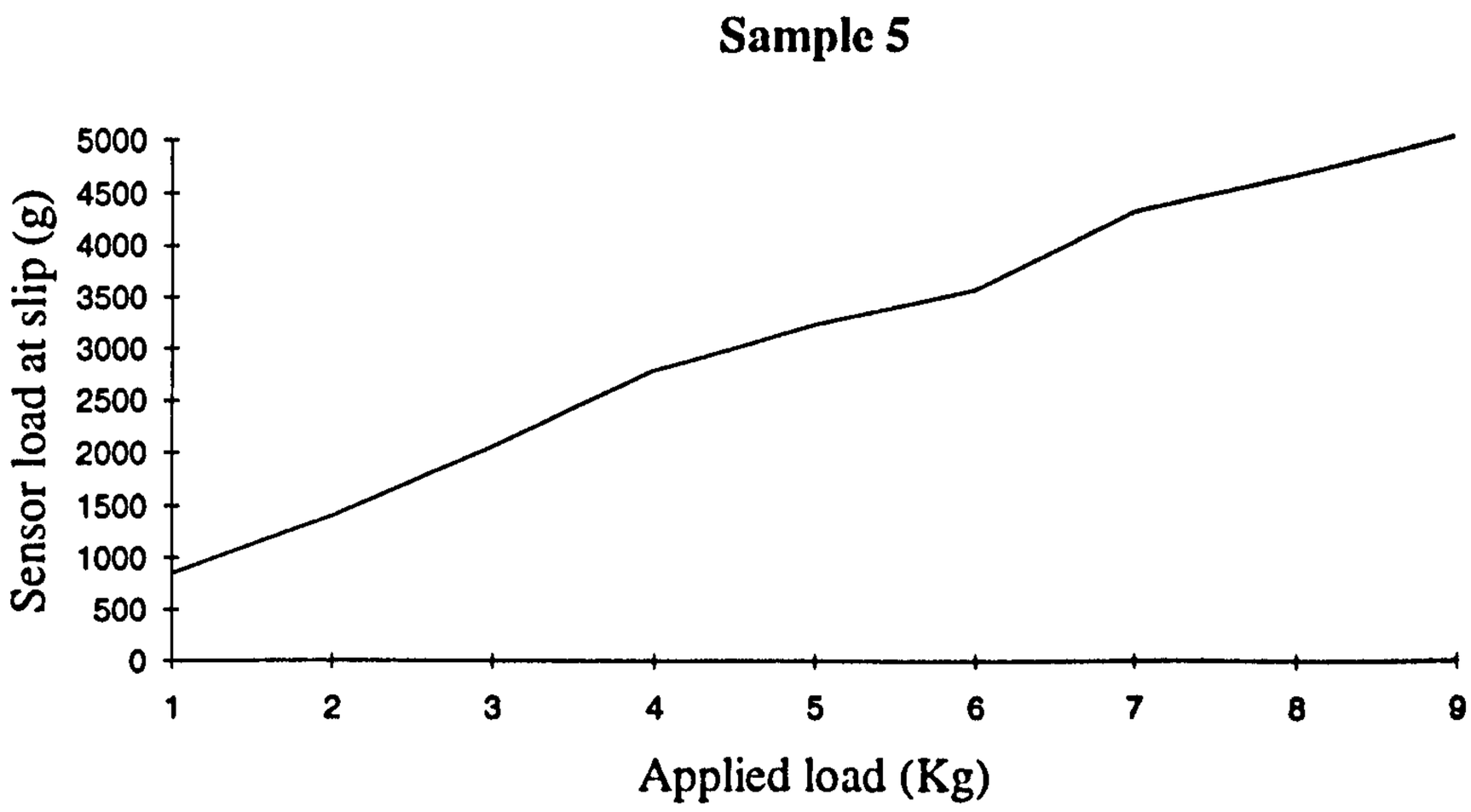

Figure C.9 Slipping force V Load for Sample 5

Appendix D

A summary of experimental procedures implemented for analysing workpiece movement.

D.1 Introduction

The Autoscan was originally designed with a view to handling compound workpieces, as well a single flat components. However it was soon discovered that the roller mechanism employed in controlling the workpiece during stitching was unable to cope with varying thickness across a single part.

In an effort to eliminate the effects of drift on single workpieces as well as handling more complex compound parts, the rollers were replaced with a series of narrow belts. To evaluate this approach and determine its performance compared to that of the original roller mechanism a series of drift experiments need to be performed.

D.2 Description of samples used during drift tests.

A number of differing sample types were used during the drift experiments, however they all fall into two categories, single flat components or 2.5-D compound parts.

D.2.1 Flat (2-D) parts.

The majority of flat parts used were the original 170mm discs used by D.L. Smith[1]. These cover the spectrum of leathers, suedes and synthetic materials expected to be handled by the Autoscan. In addition to the disc samples a shoe insole component

was also tested as it had previously been shown to be difficult to handle. The insole component is made from a suede material and backed with a cotton fabric in order to reduce its elastic properties, however it is still limp and compliant.

D.2.2 Compound (2.5D) parts.

The compound parts, (2.5-D), are made by overlapping and bonding together two flat parts in order to form a single component for the purposes of handling. The term could also be expanded to workpieces consisting of a single part but with significant surface contour fluctuations, such as highly embossed cowboy boot components. For the experiments all the compound parts were formed using the overlapping method and corresponded to one of three shapes shown in Figure D.1. The parts can be differentiated from each other by the reference letters associated to them as follows.

1. CR = Compound ridged
2. CS = Compound squares
3. CC = compound complex

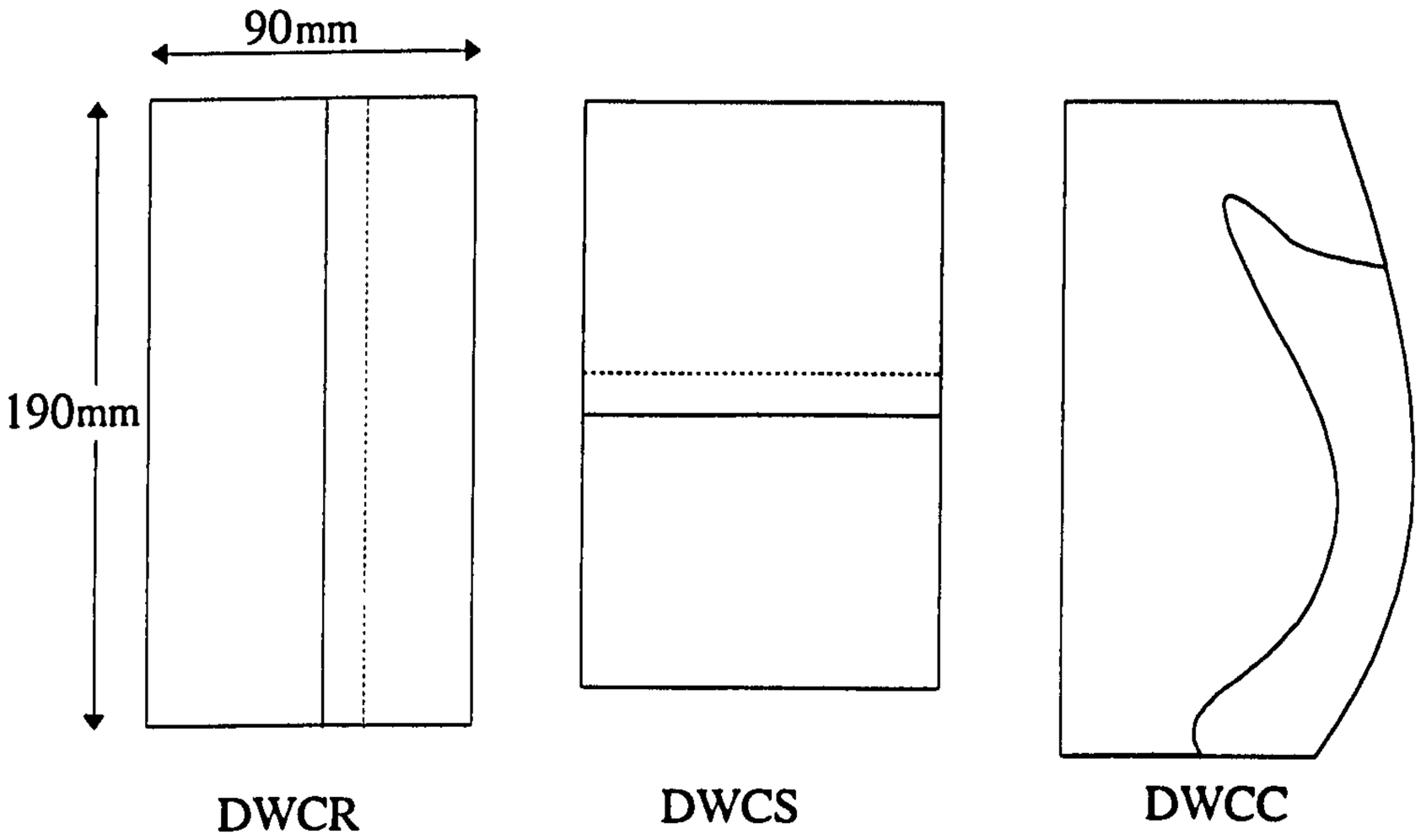

Figure D.1 Compound samples used during the drift experiments.

D.3 Mechanisms for measuring drift.

A method for evaluating the lateral component drift of a workpiece was first devised by D.L. Smith[1]. This method used circular discs cut from a wide selection of leathers, synthetic leathers and some additional complex materials. Discs were used so as to remove the effects of workpiece orientation on the manipulation and reduce edge effects. Additional methods implementing real-world shoe components were devised by Dr. N. Tout[42] of B.U.S.M. Both methods of evaluating drift for flat parts were implemented so as to allow the belt handling mechanism to be compared to the Autoscan's original configuration.

D.3.1 D.L. Smith's drift measurement method.

The circular discs were divided into eight equal sections, Figure D.2, with one dividing line being selected as the reference (0°). The discs were then placed in the handling mechanism for each 45° angle. The disc was then moved forwards 25mm and then back 25mm, forming a cycle containing a total manipulation distance of 50mm. A number of bedding in cycles were employed (approximately 20-25), in order for a steady drift condition to be achieved. The reference position was then recorded before additional cycles were performed. The degree of drift was then measured with a travelling microscope. Measurements were taken at each dividing angle, including both 0° and 360° to give an indication of repeatability.

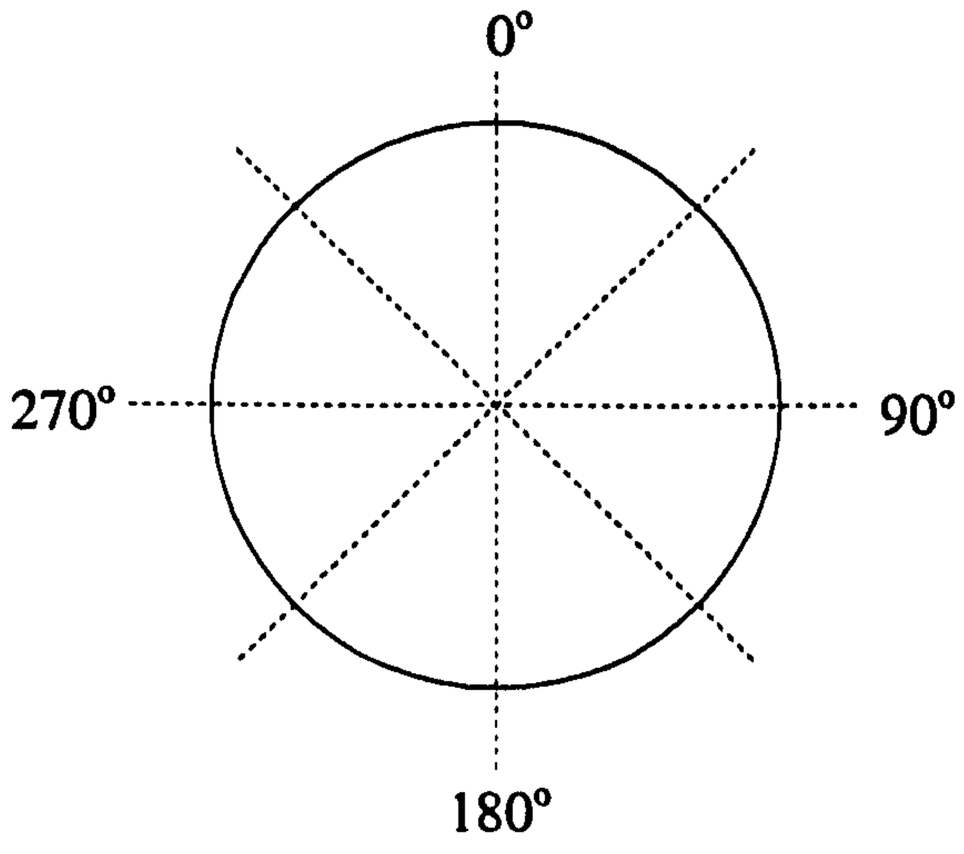

Figure D.2 Segmented disc with reference.

D.3.2 N. Tout's drift measurement method.

This method was originally developed in order to give a quick comparison between differing shoe insole components and roller types, it is however equally valid for other forms of sample. Two points, A and B, are taught onto the sample to be tested. Points A and B are selected so that when the needle is positioned above point A, the heel section of the workpiece protrudes out of the handling mechanism. Similarly when the needle is positioned at point B, the toe section protrudes. Two pieces of graph paper are fixed to the base table and the toe and heel traced onto it when at points A and B respectively, Figure D.3. The workpiece is then cycled between points A and B 20 times, before the new positions of the toe and heel are traced onto the same graph paper.

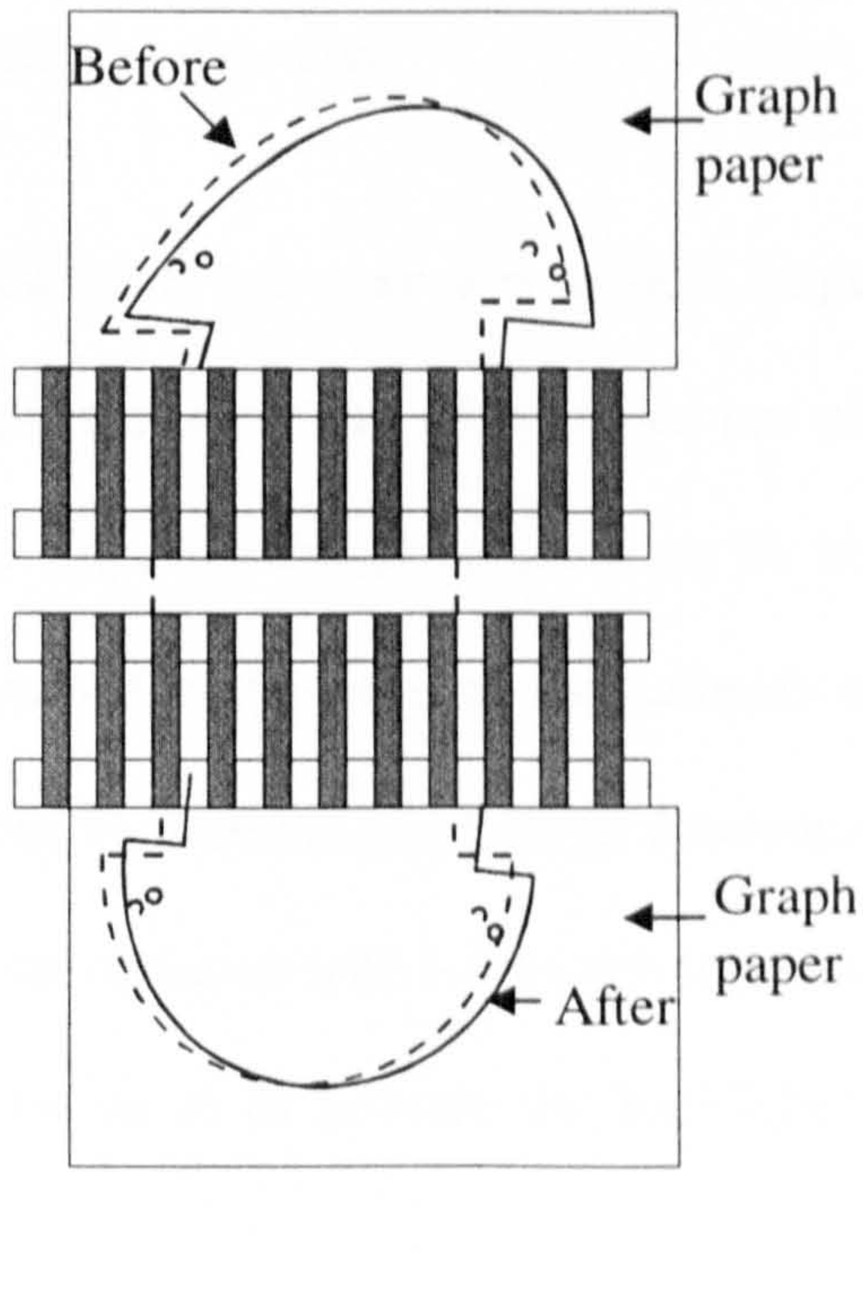

Figure D.3 Tracing drift effects onto graph paper.

This method is cruder than the previous method, but produces a quick and easily visible display of the drift effects, clearly showing both lateral drift and rotation. If perfect handling were to be achieved, the resultant outlines would be superimposed directly onto the originals.

D.3.3 Drift measurement using a vision system.

Once the Autoscan was configured with the pinned belts and the Nercoprene compliant upper substrate it quickly became evident that the degree of drift, (if any), was very small. Consequently it proved impossible to obtain measurements for drift using either of the previously outlined methods. In order to obtain a quantitative drift measurement a line-scan camera was used.

The camera, a 128 pixel line-scan had a focal length of 70mm resulting in a window of 10mm. This gives a resolution of 0.078mm per pixel, consequently allowing for a measurement of the edge positional accuracy to be made to within 0.1mm. The camera was positioned such that the edge of the samples entered the window at the turning point of each cycle. In addition the normal Aluminium support table located in front of the belts had to be replaced with a perspex sheet in order for a Halogen light source to be located below so as to provide the backlighting required to provide the contrast for the camera.

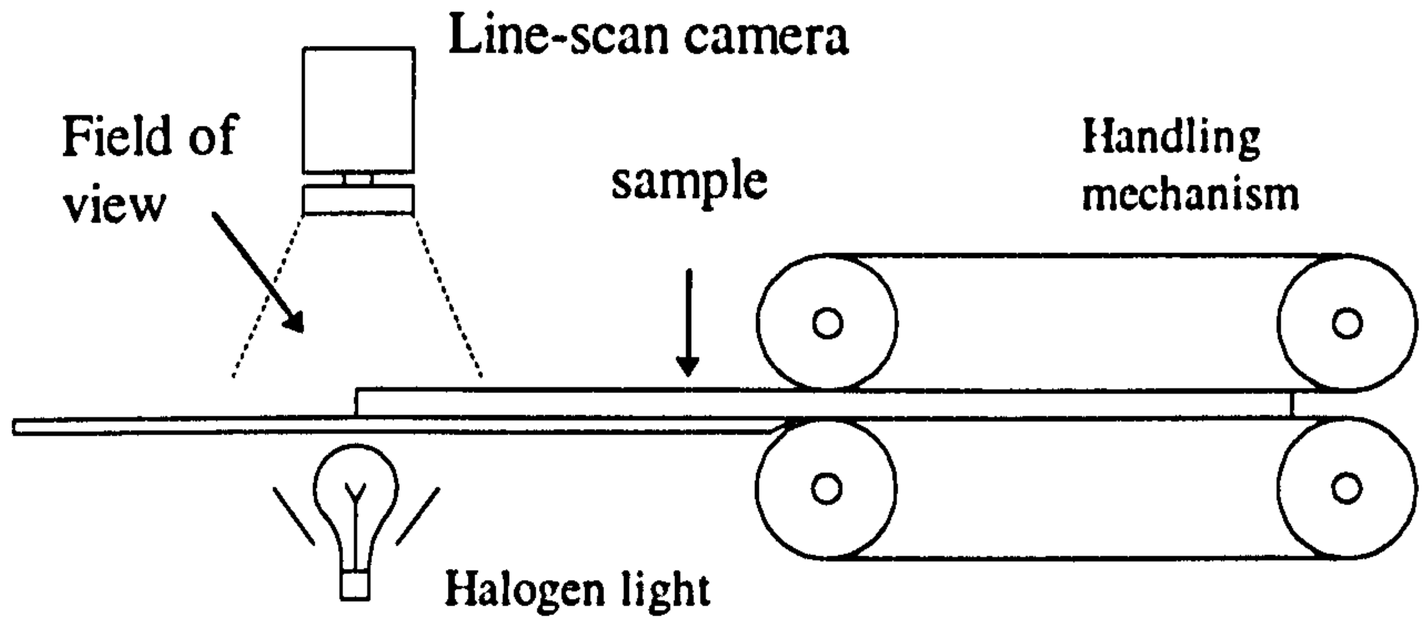

Figure D.4 Line-scan camera configuration for the measurement of drift

This method also gives the added benefit that the machine does not need to be stopped for measurements to be taken, but allows for the edge position to be recorded dynamically.

Appendix E

Drift / Slip results for the Autoscan
Original roller configuration

E.1 Original Autoscan configuration.

The original Autoscan setup comprised 4 banks of 4 rollers, each coated by wrapping an 'Emery' type paper around them in a spiral. This coating was intended to provide significant holding properties during the manipulation of a workpiece during stitching. This section contains examples of typical drift measurements obtained with this mechanism and clearly shows how the degree of workpiece movement is dependent on the orientation of the workpiece when presented to the handling mechanism. When a workpiece is loaded such that the mean nap direction is parallel to the axis of the rollers very little movement occurs. However if the mean nap direction is normal to the rollers maximum movement occurs. This then supports the evidence of a sinusoidal drift profile proposed by D.L. Smith[1] and is a consequence of the material's structure as discussed in Chapter 2. Consequently any pair of movement measurements taken 180° apart should demonstrate similar properties. It should also be noted that the majority of imitation leathers and suedes have a synthetic nap inorder to create the right 'feel'. This has a natural bias due to its method of manufacture and is far more even across a sample that can be found naturally in leathers.

In addition to the profile of each of the drift results, the degree of movement should also be noted. These results were obtained using D.L.Smith's method described in Appendix D. Consequently they only provide a measure of movement for a single 2x25mm cycle after a degree of bedding in, (previous cycles) has been performed. It is therefore reasonable to assume that the workpiece would continue to move during subsequent cycles.

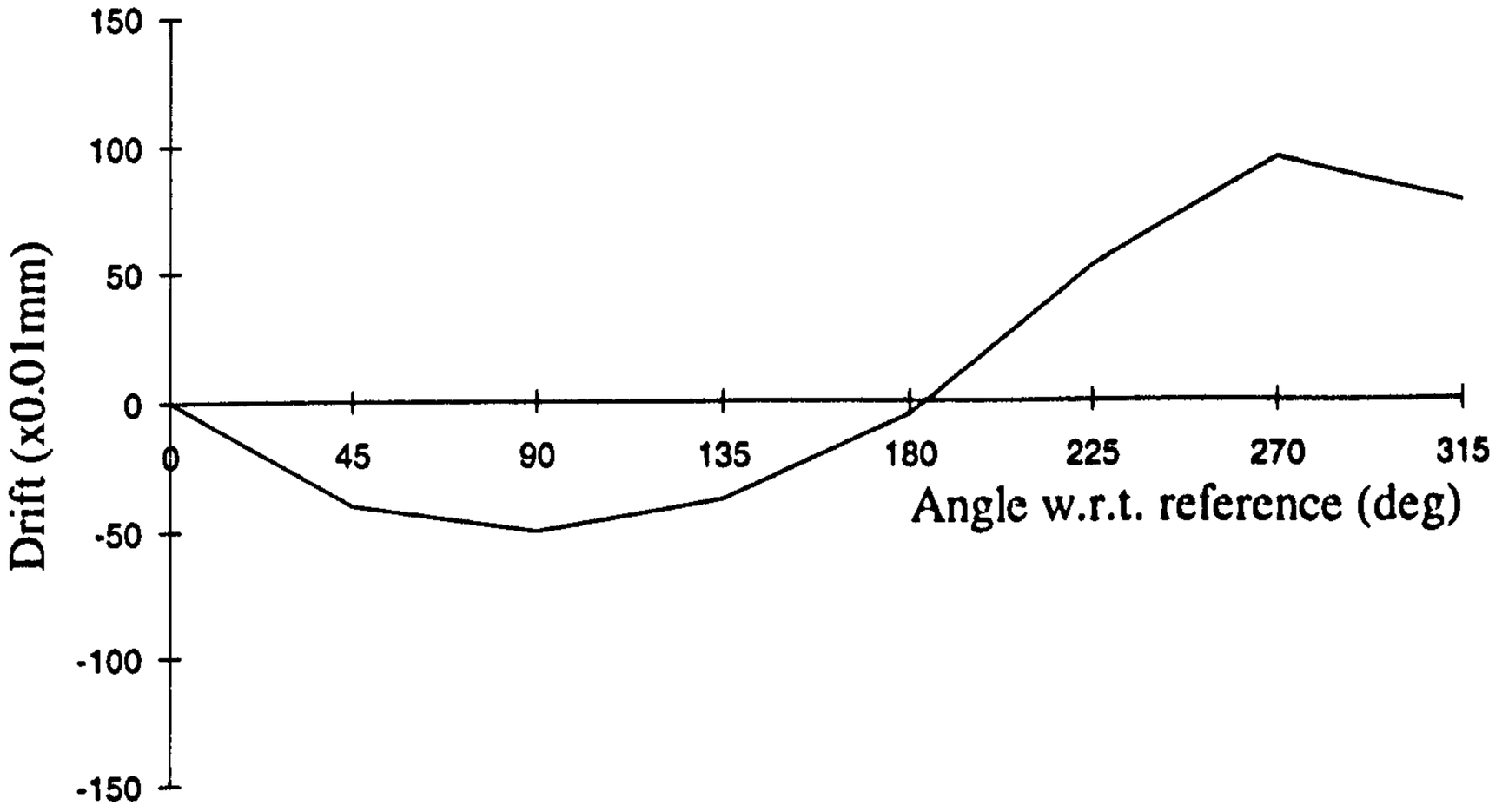

Figure E.1 Drift against load angle for an imitation suede sample

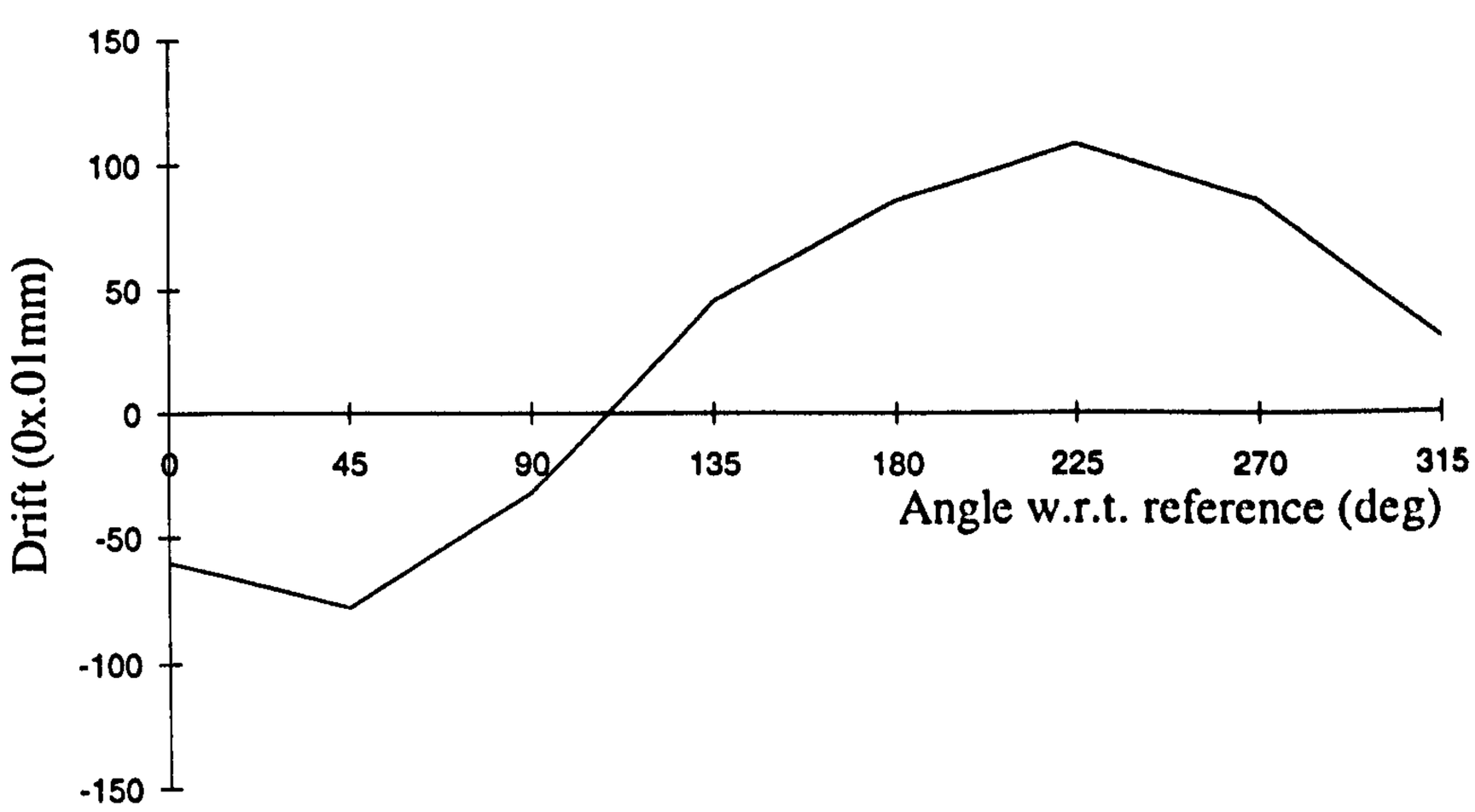

Figure E.2 Drift against load angle for a moss backed suede sample

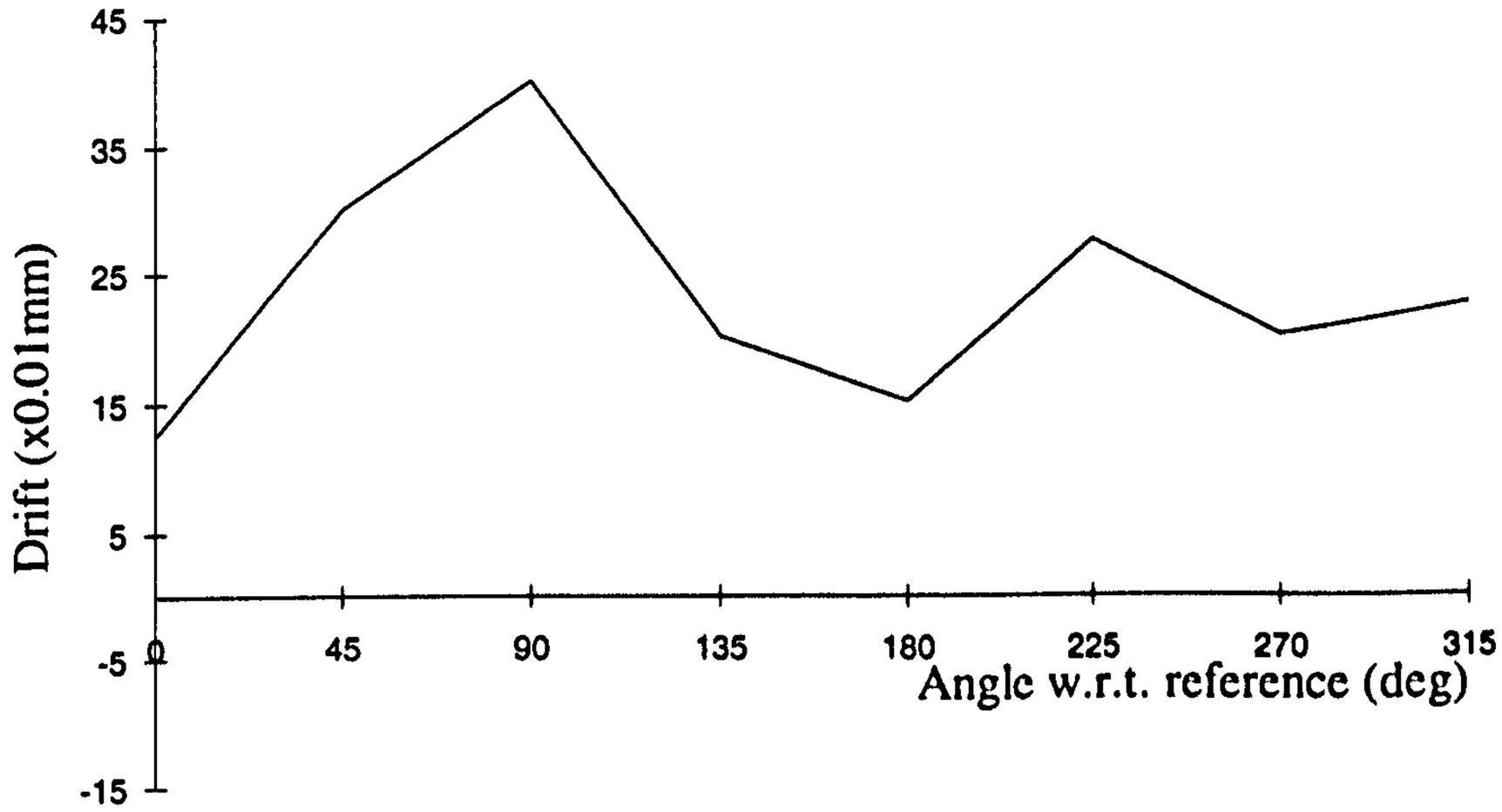

Figure E.3 Drift against load angle for a leather sample

Appendix F

Drift / Slip results for the Autoscan Carborundum belts

F.1 Carborundum belts.

The results included in this section are derived from measurements taken using the quick drift test method outlined in Appendix D. In order to highlight the movement that occured due to the handling mechanism, 5 cycles were performed between each recorded measurement.

Figures F.1-F.8 show results recorded for a typical leather disc (110mm dia.). It can be seen from the results that a fairly high degree of drift still occuring, which increases as the test cycles progess. The direction of workpiece movement is reasonably constant over all the measured angles and does not follow the sinusoidal pattern exibited for rollers. The holding pressure applied during this test could be described as firm, as any increase in holding pressure would result in bending of the belt's support plate, highlighting a limitation in the mechanics of the handling mechanism. Lower holding pressures, however, resulted in considerable workpiece slipping.

Figure F.9 shows an example of a drift recording made using a shoe insole component. This part was identified by B.U.S.M as a particularly dificult workpiece to handle. The result shows approximately 30mm of movement after only 10 cycles, far greater than could be tolerated in commercial machine.

For the purpose of inclusion in this thesis the results were scanned into a computer before being enhanced. A scale is included on each plot so as to negate any scaling effects that may have occured during this process.

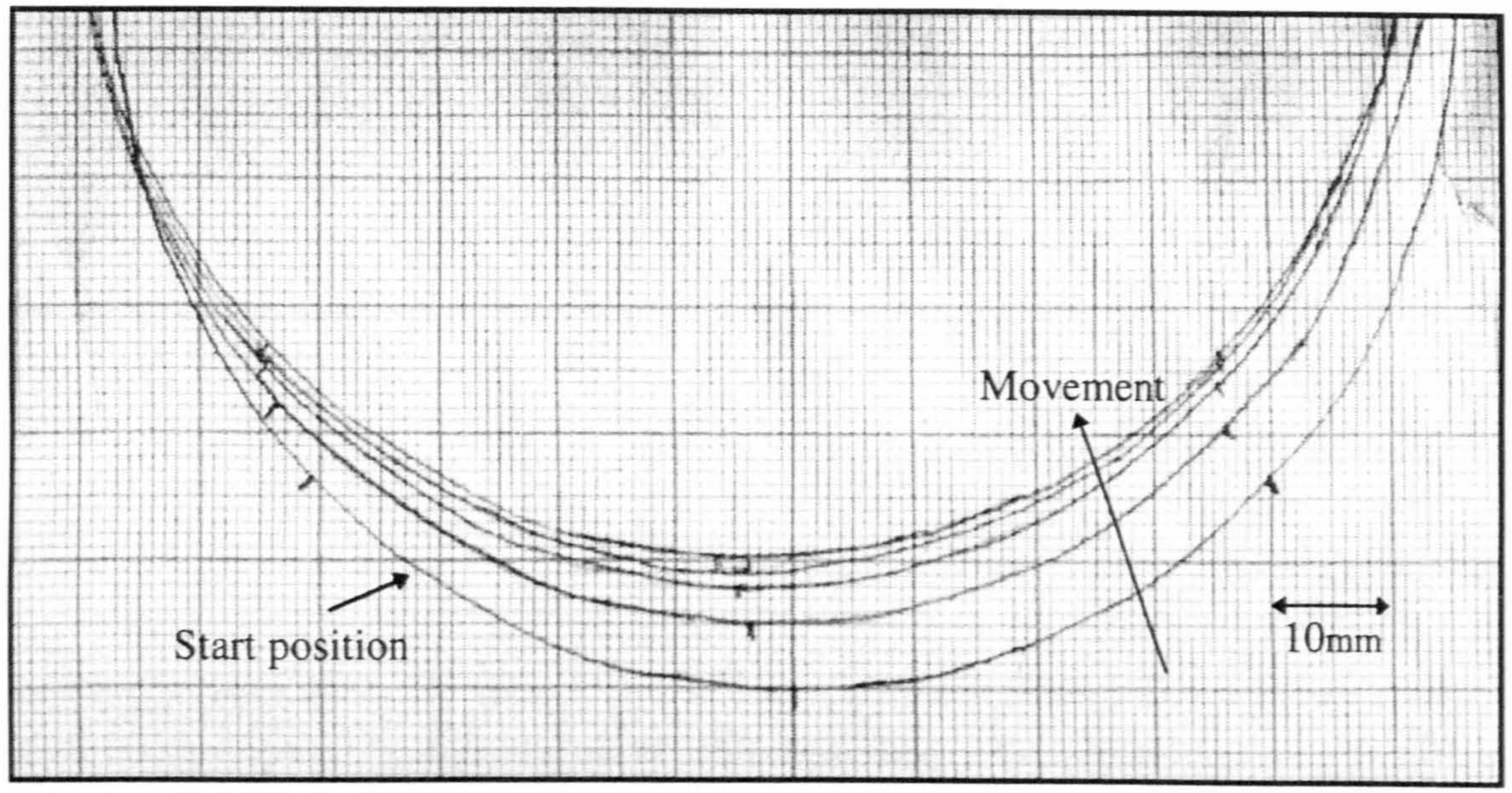

Figure F.1 Observed movement at reference (0^{o})

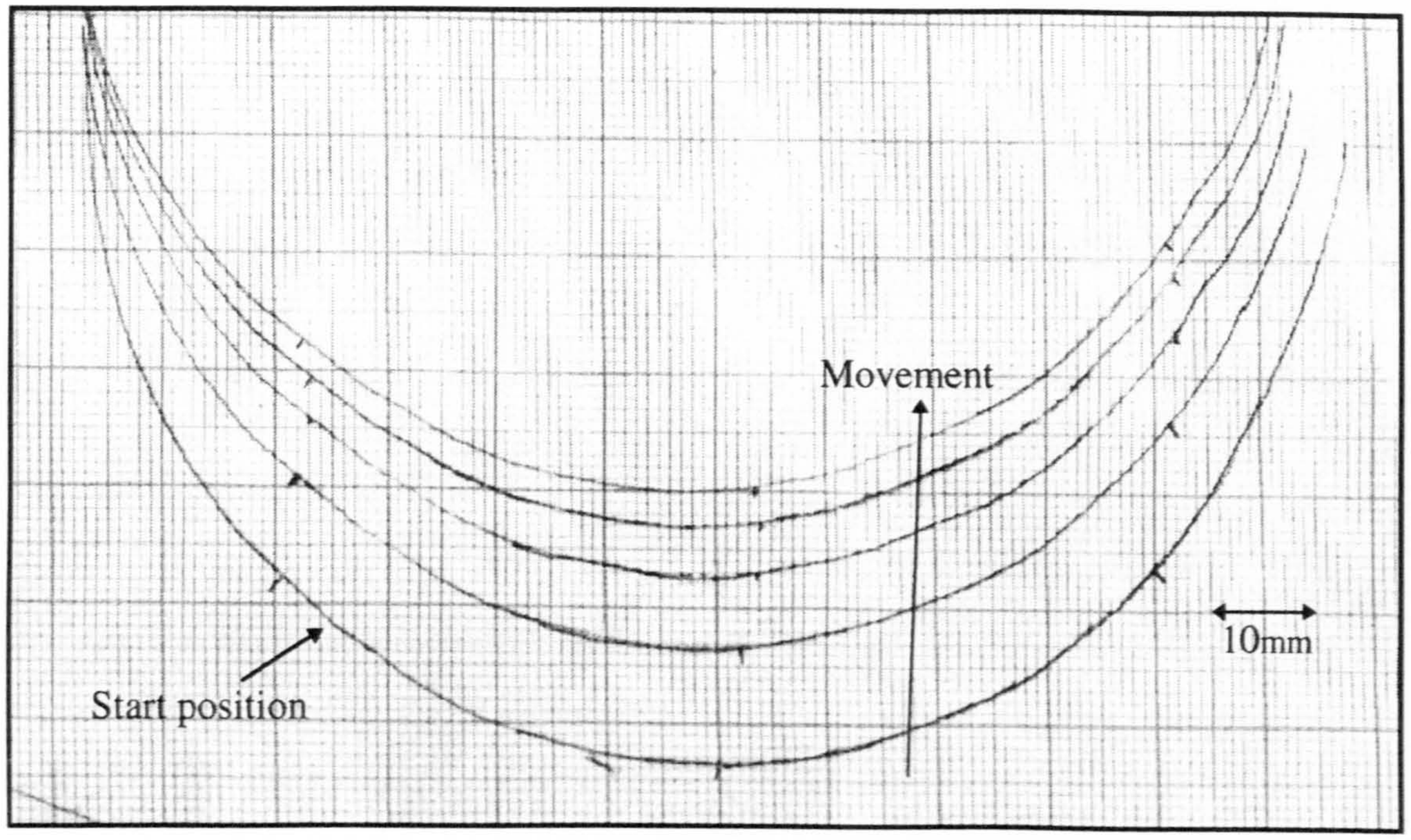

Figure F.2 Observed movement at 45°

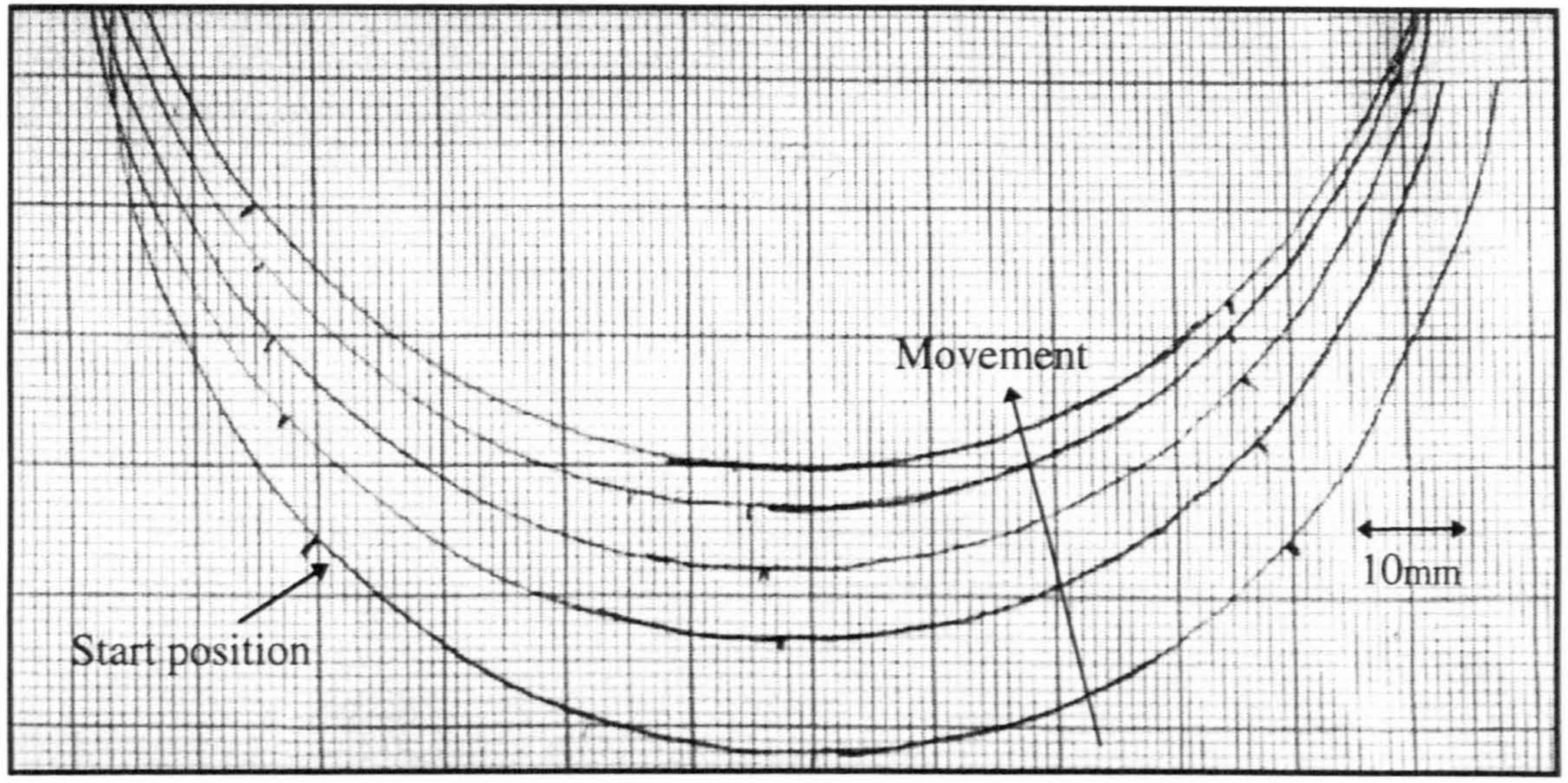

Figure F.3 Observed movement at 90°

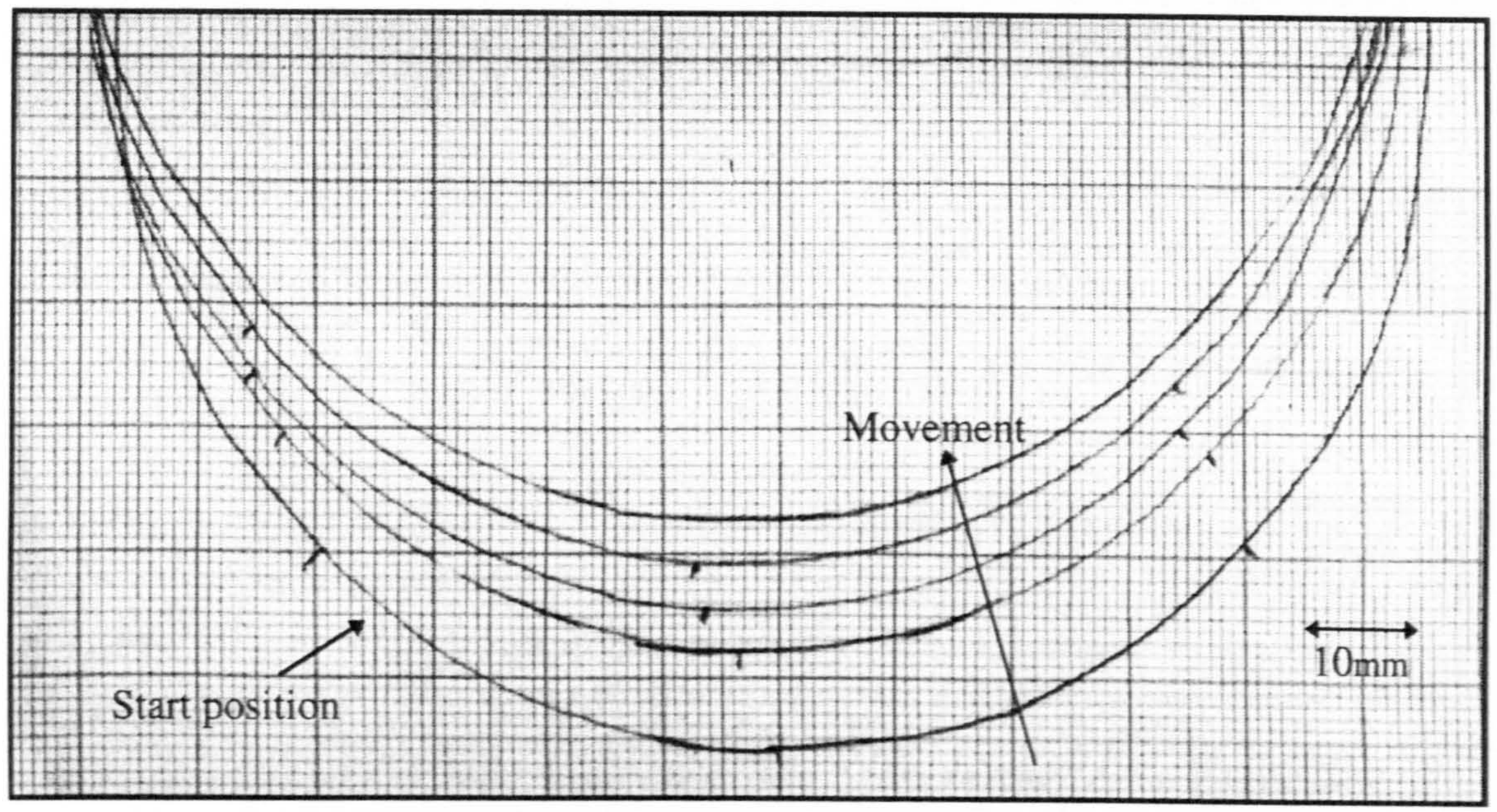

Figure F.4 Observed movement at 135°

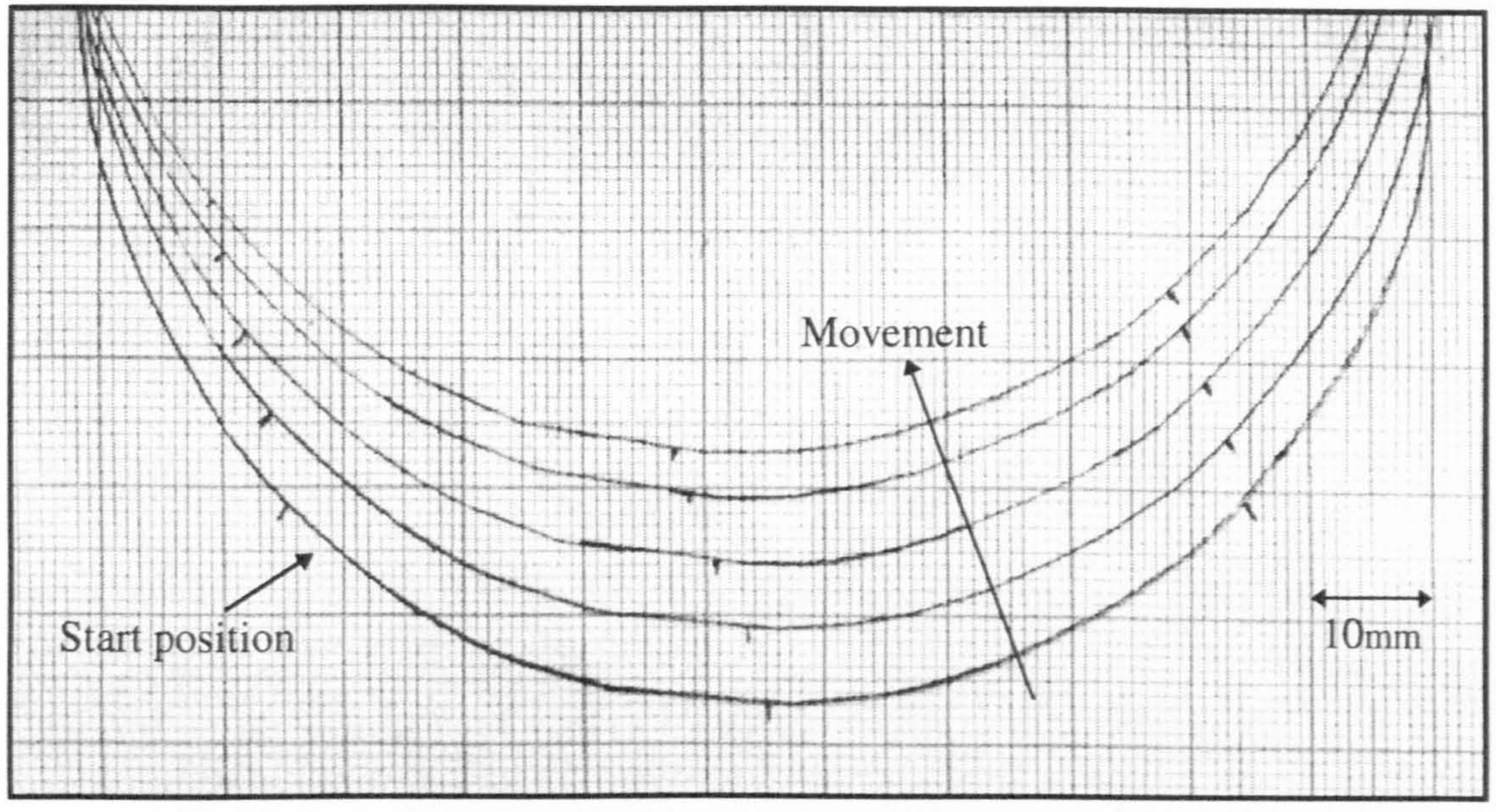

Figure F.5 Observed movement at 180°

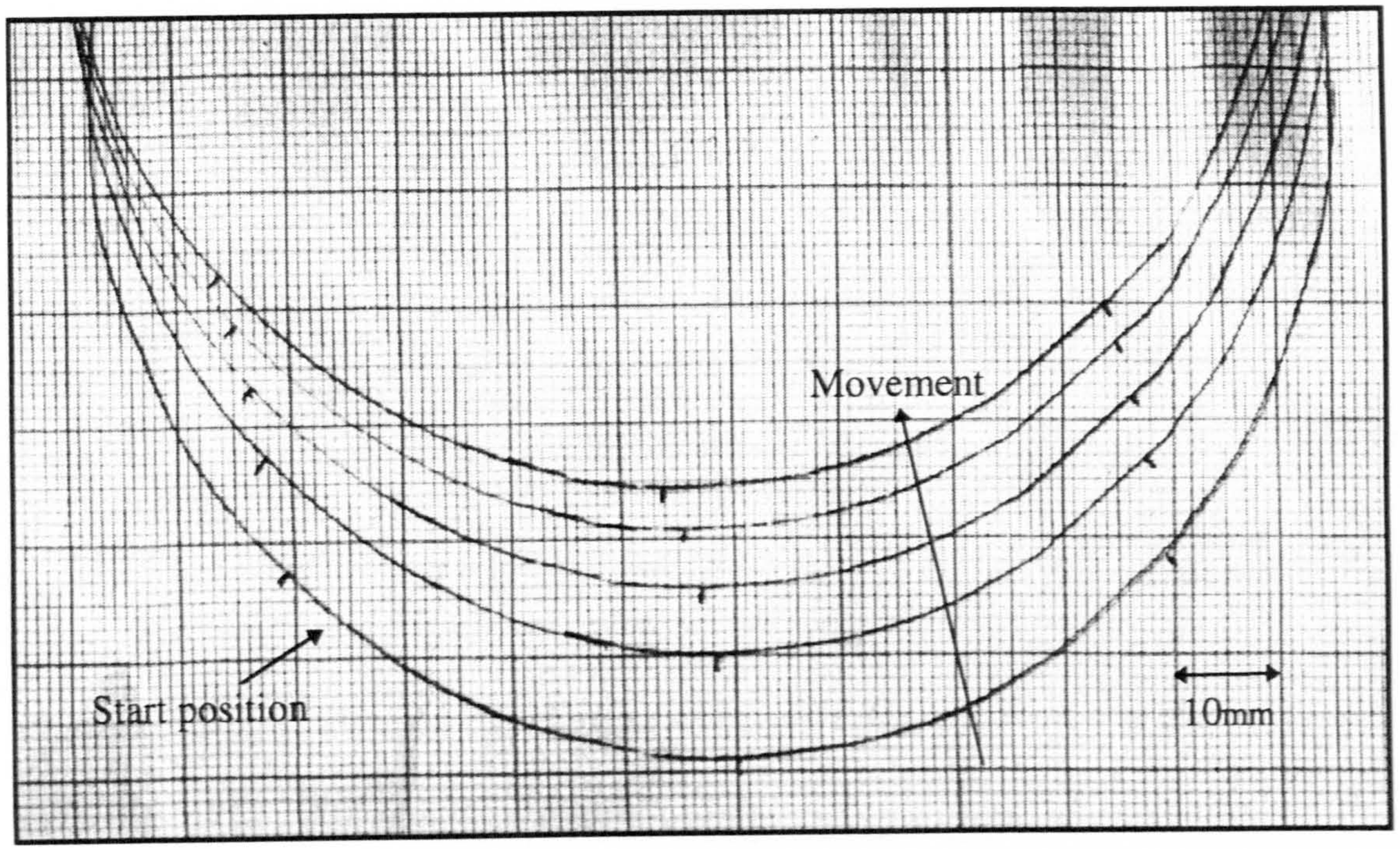

Figure F.6 Observed movement at 225°

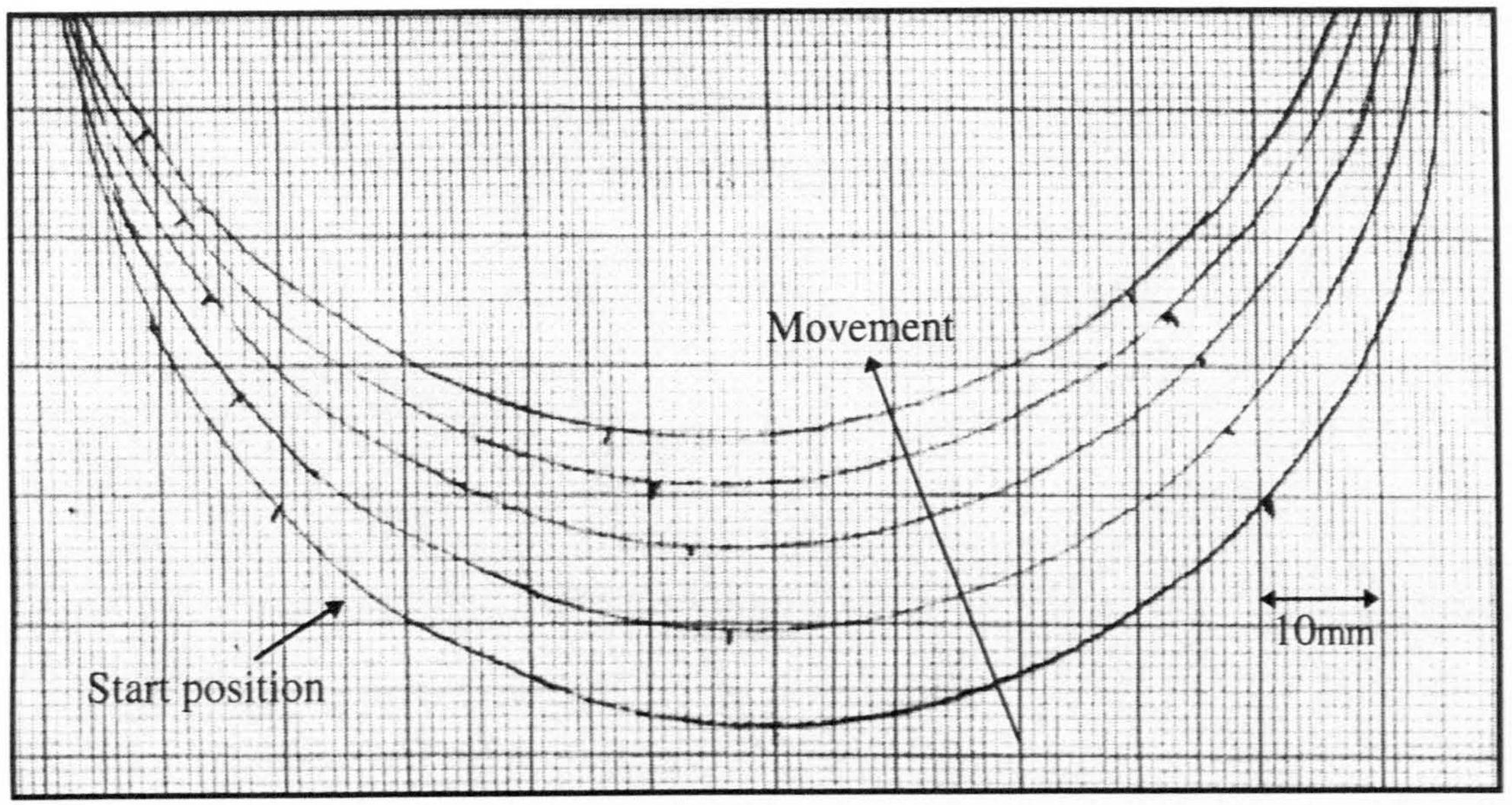

Figure F.7 Observed movement at 270°

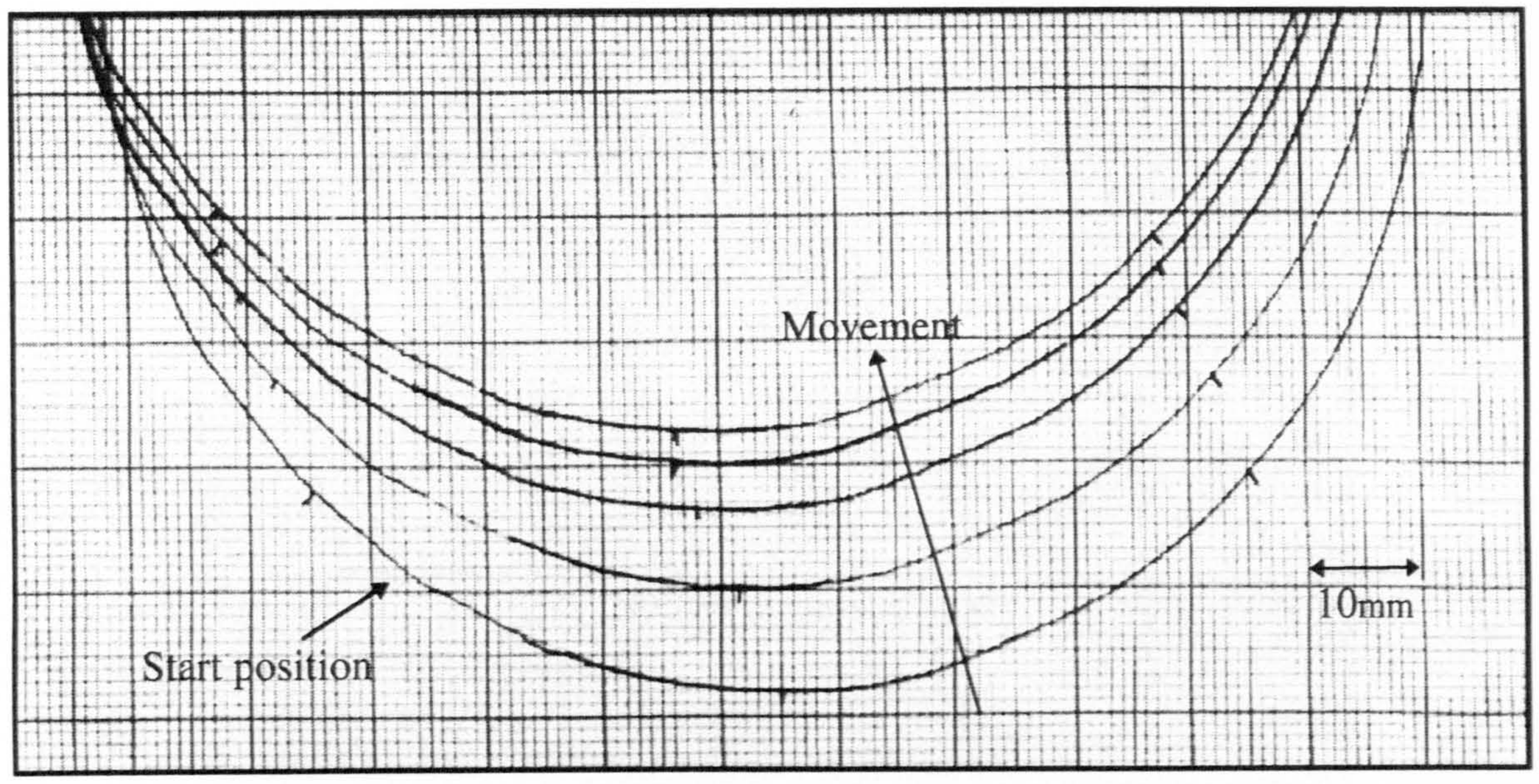

Figure F.8 Observed movement at 315°

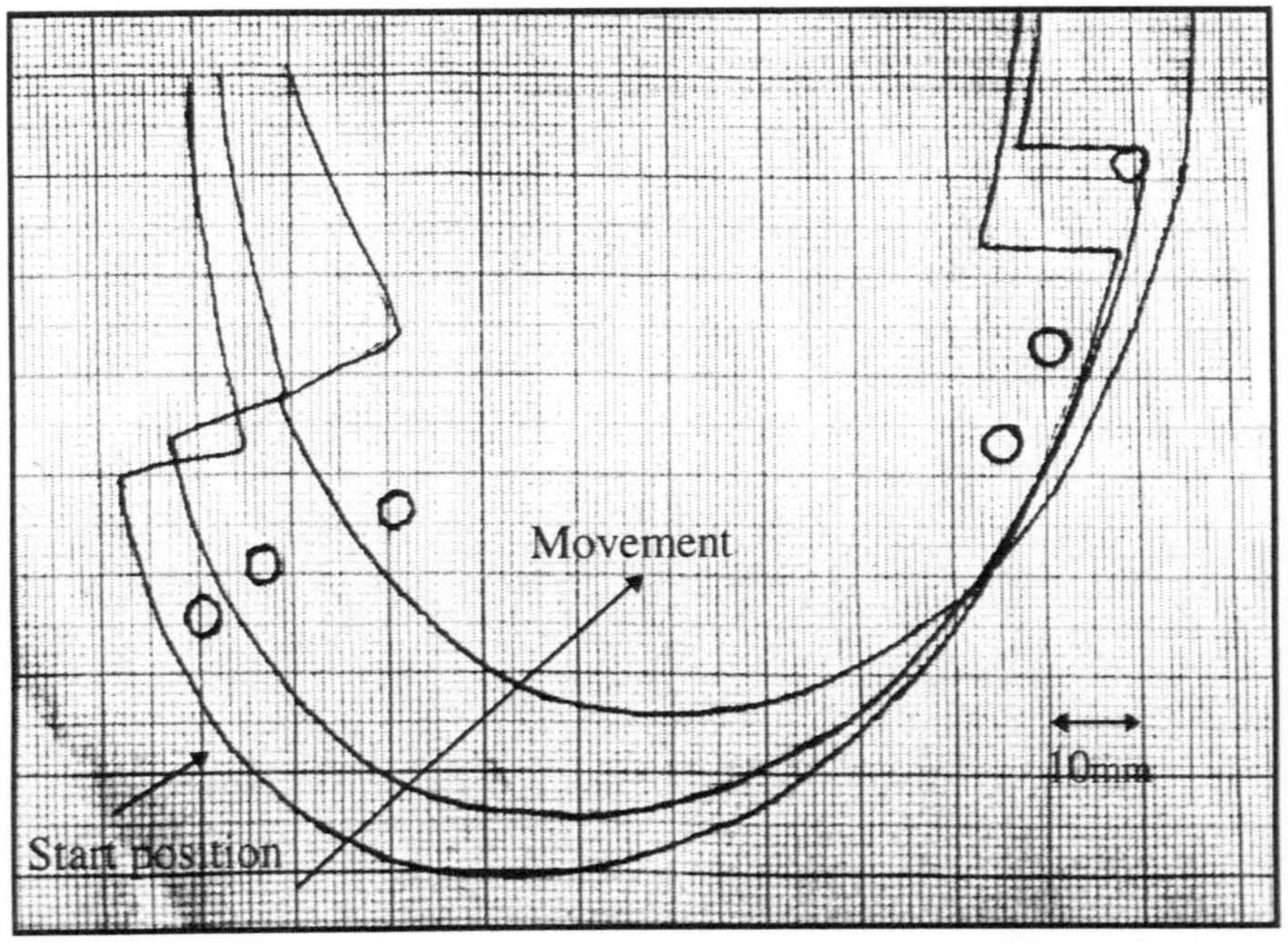

Figure F.9 Observed movement for a sample shoe insole component

Appendix G

Drift / Slip results for the Autoscan Flat components.

G.1 Introduction.

The results included in this section of workpiece movement are taken from a wide variety of flat samples and show a significant improvement over both the roller and carborundum belt handling mechanisms. Little or no movement occurs for the majority of samples tested, furthermore the sample orientation during each of the tests demonstrated no noticeable effect on the results. Consequently the samples were tested at random orientations reflecting how workpieces would be presented to a commercial machine.

G.2 Pinned belts on flat components.

Figures G.1-G.5, show an example result for each of the samples tested. Part (a) of the figures show the raw camera data extracted during the movement measurement tests. These show the trend of any movement that may be occurring, particularly in the case of the shoe insole component. Part (b), of the figures show the actual edge displacement as measured from one cycle to the next. Here a trend is evident showing that a movement in one direction is generally compensated for on the next cycle, resulting in no net effect. This can be best seen in Figure G.6.

Figure G.6 contains an analysis into the handling characteristics across the range of flat parts tested. The author believes this demonstrates the 'flapping' effects that could be observed at the edge of the samples as it changes direction between cycles. It should be noted that occasional deviations occur outside the range covered by Figure G.6,

however these are very rare, (Figure G.5) and could not be seen if included. These large losses of position occur invariably at the start of testing for, either the insole components or, the brogue shoe components that will be discussed in Appendix H. This, in the case of the insole components, is due to its limp nature which enables the part to drop between the front and rear belt sets at certain orientations putting an undue load onto the workpiece. Once the pins have bedded in however (5-10 cycles) no further net movement is evident.

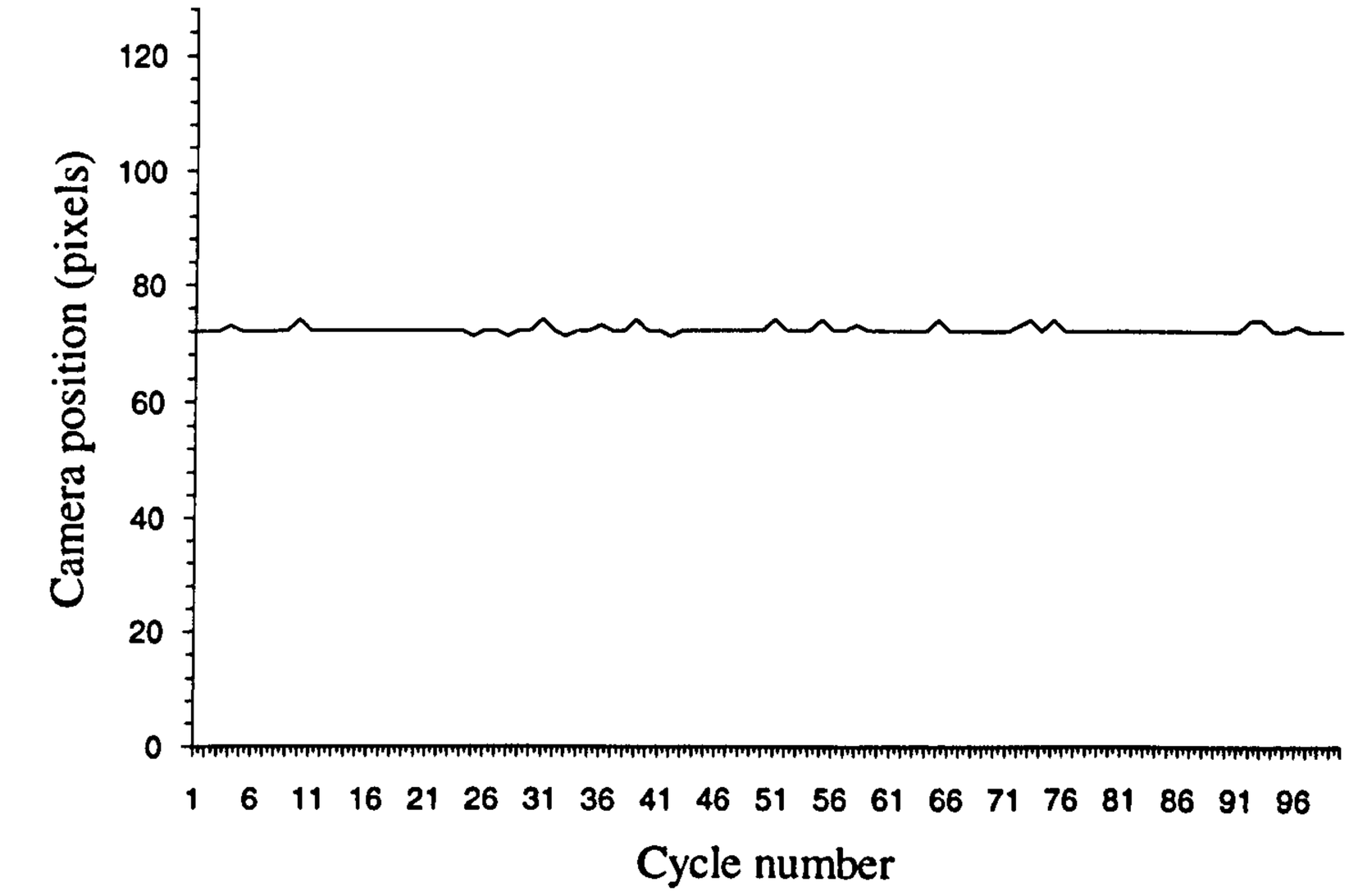

(a) Edge positional variation measured by the line-scan camera.

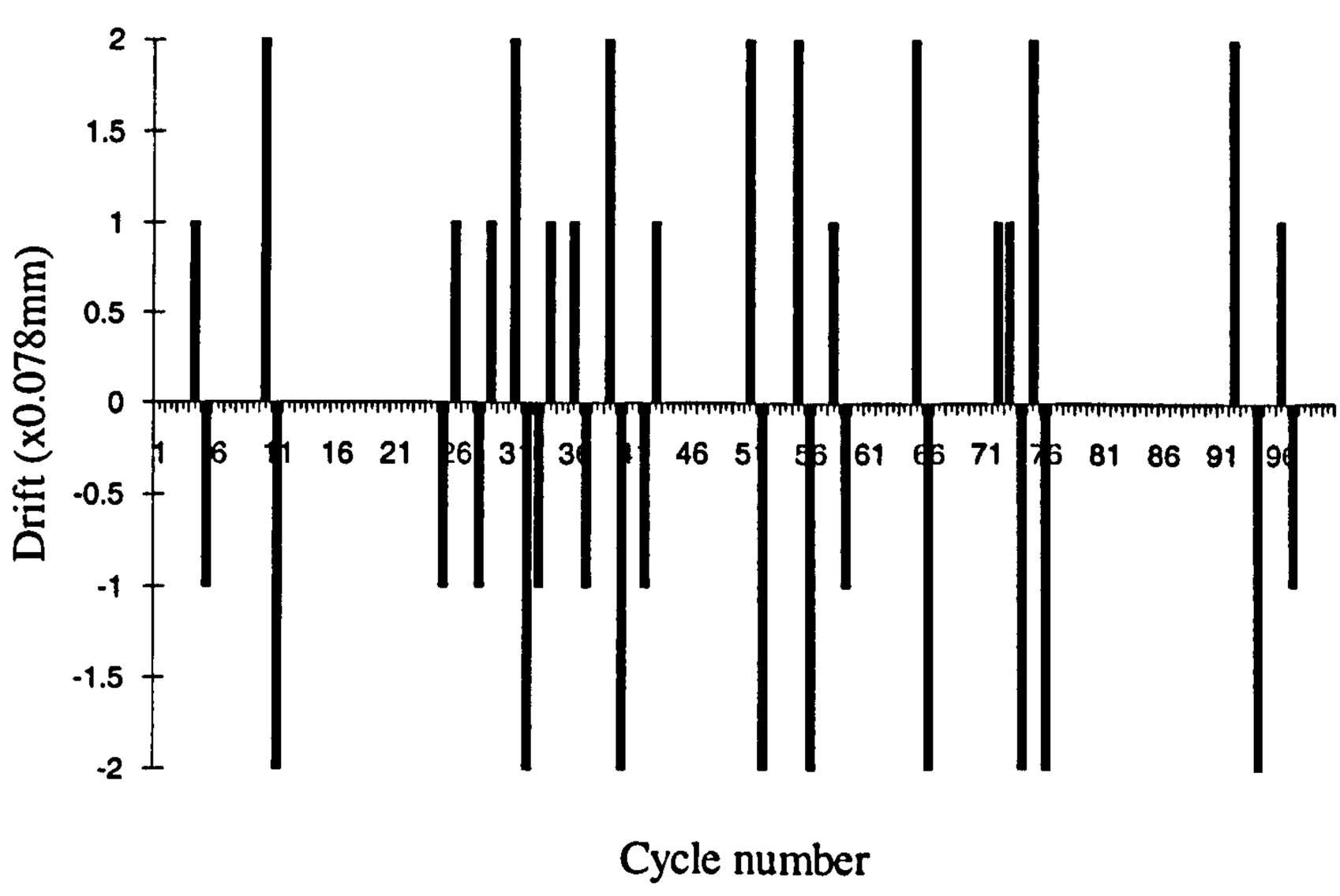

(b) Degree of movement measured per cycle.

Figure G.1 Movement measurements obtained for sample DWLF8

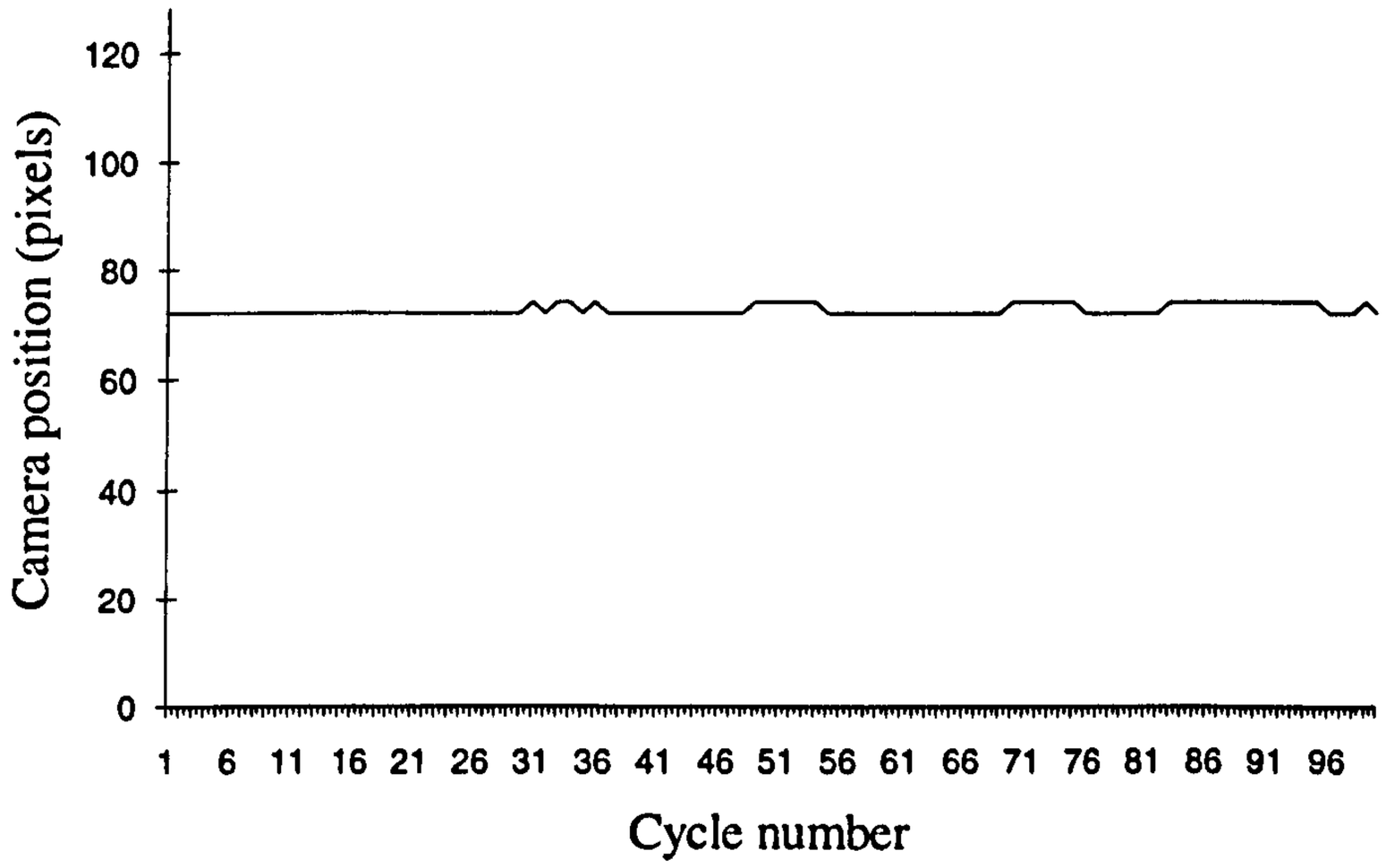

(a) Edge positional variation measured by the line-scan camera.

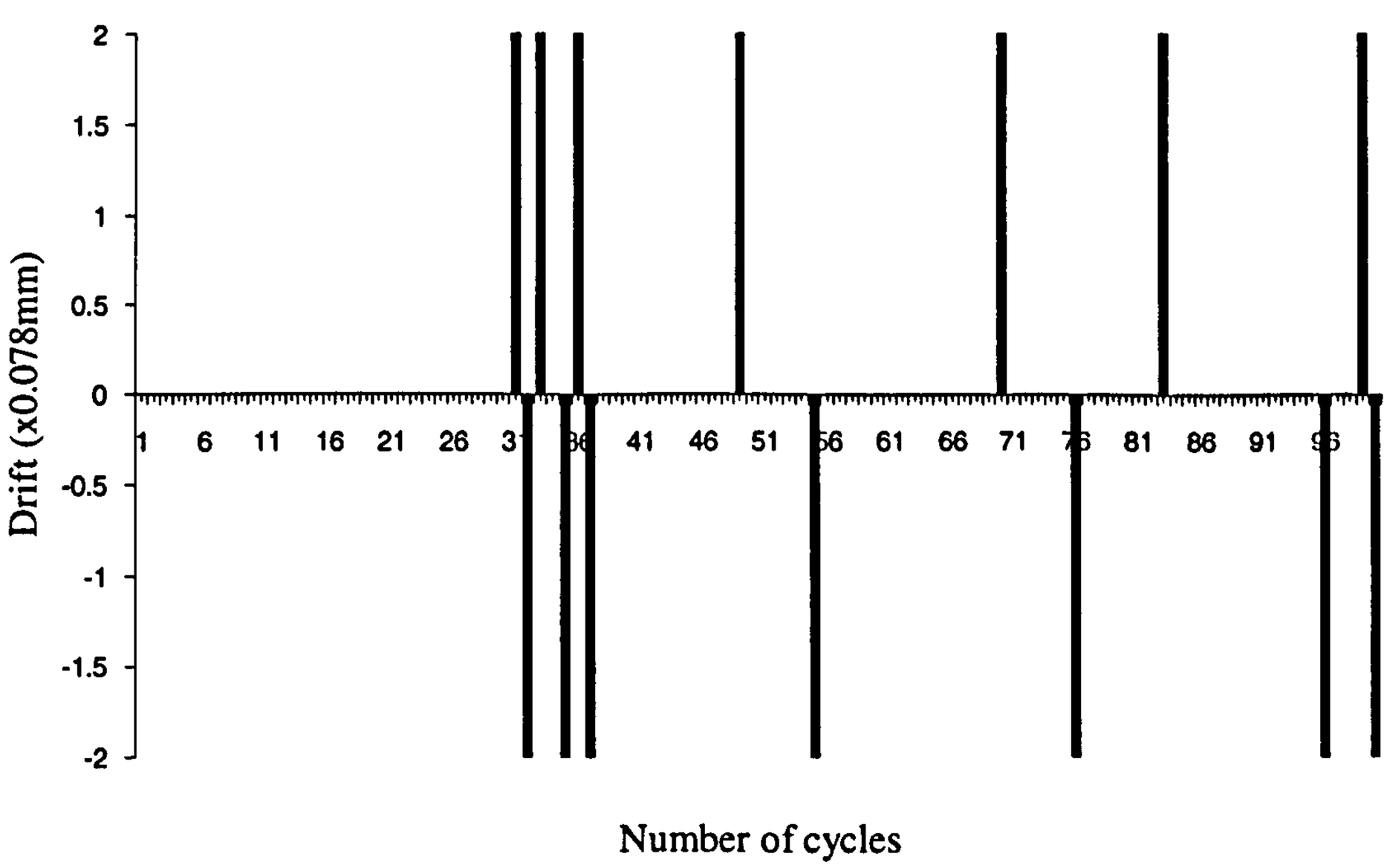

(b) Degree of movement measured per cycle.

Figure G.2 Movement measurements obtained for sample DWF7

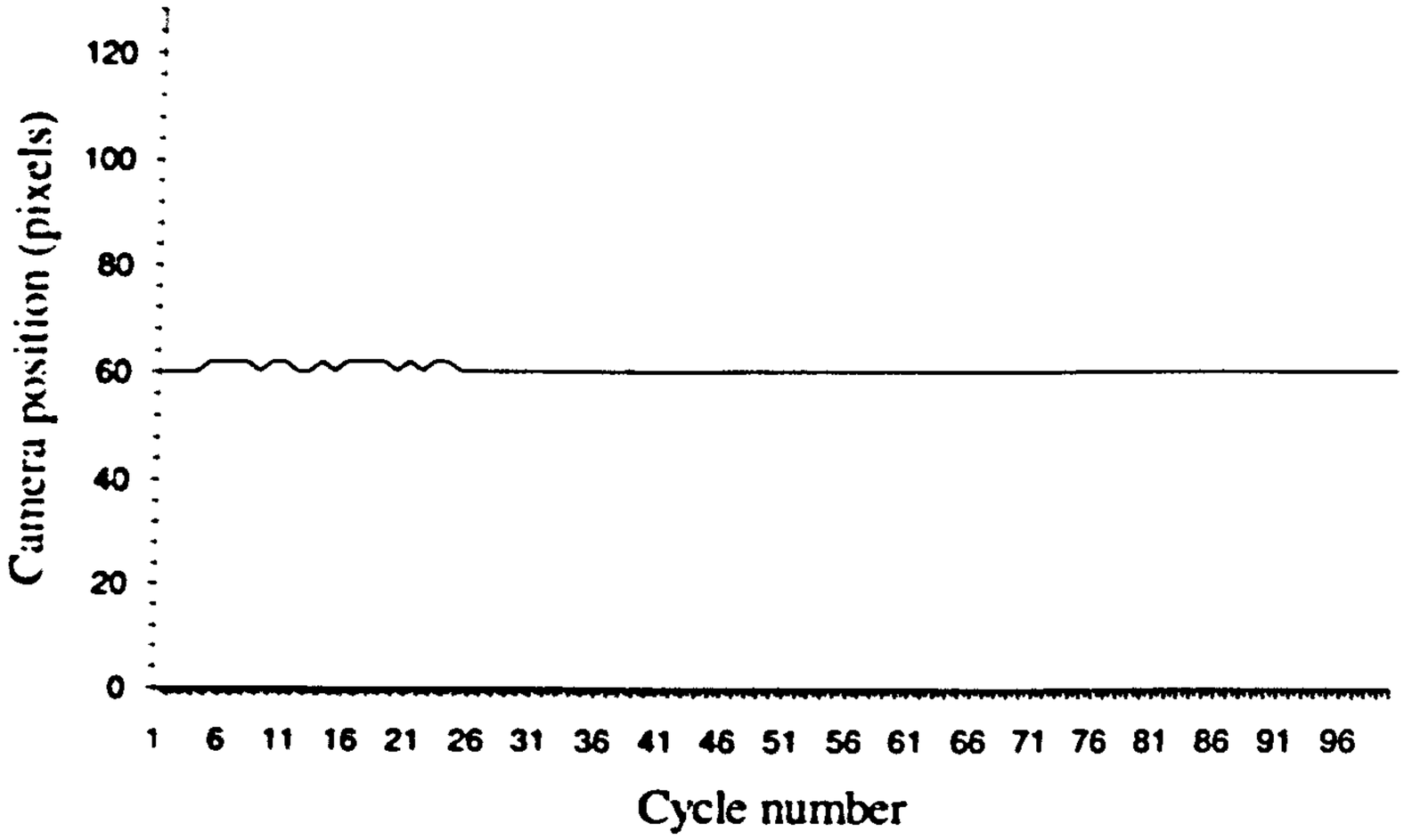

(a) Edge positional variation measured by the line-scan camera.

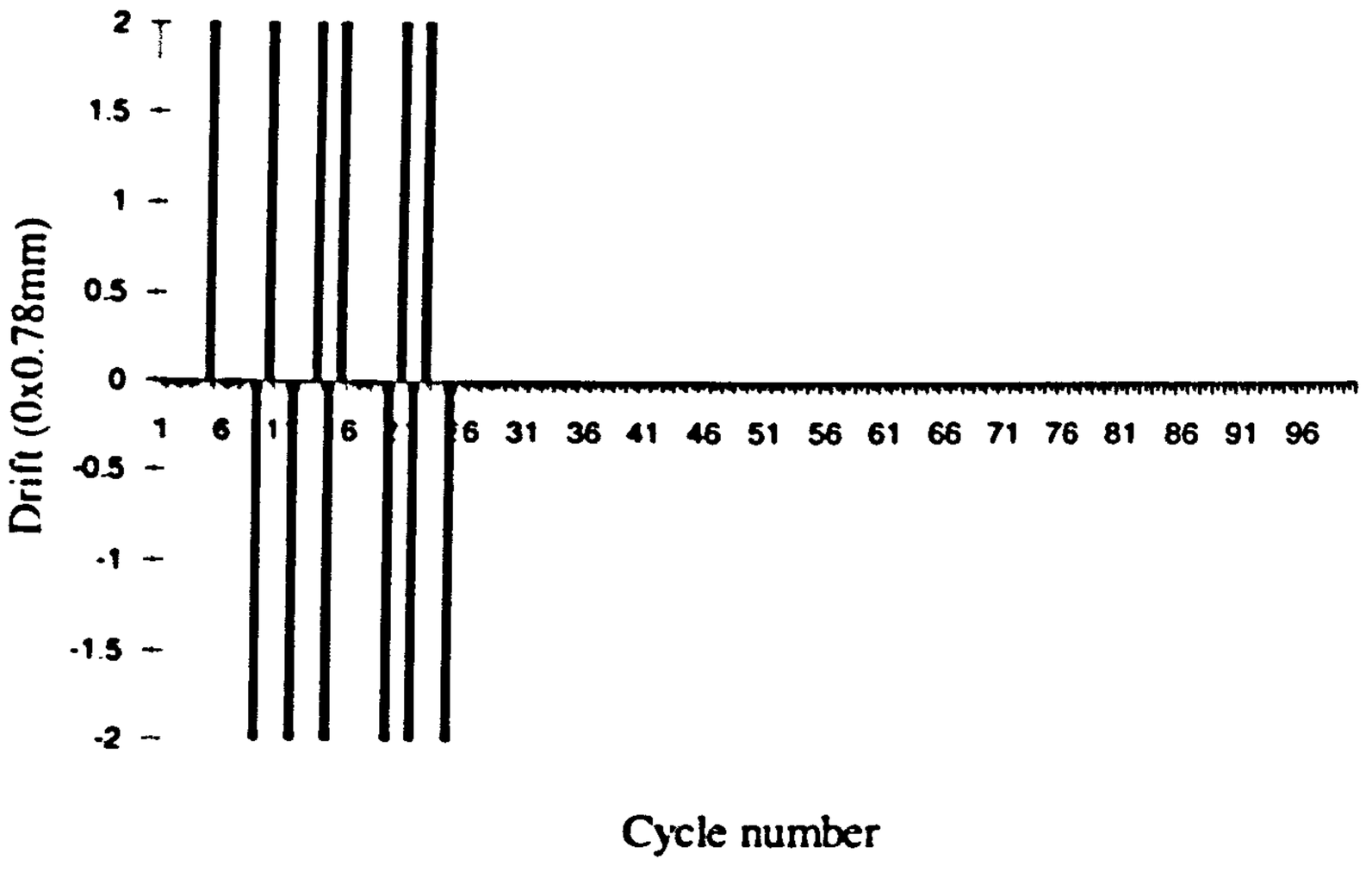

(b) Degree of movement measured per cycle.

Figure G.3 Movement measurements obtained for sample DWFI2

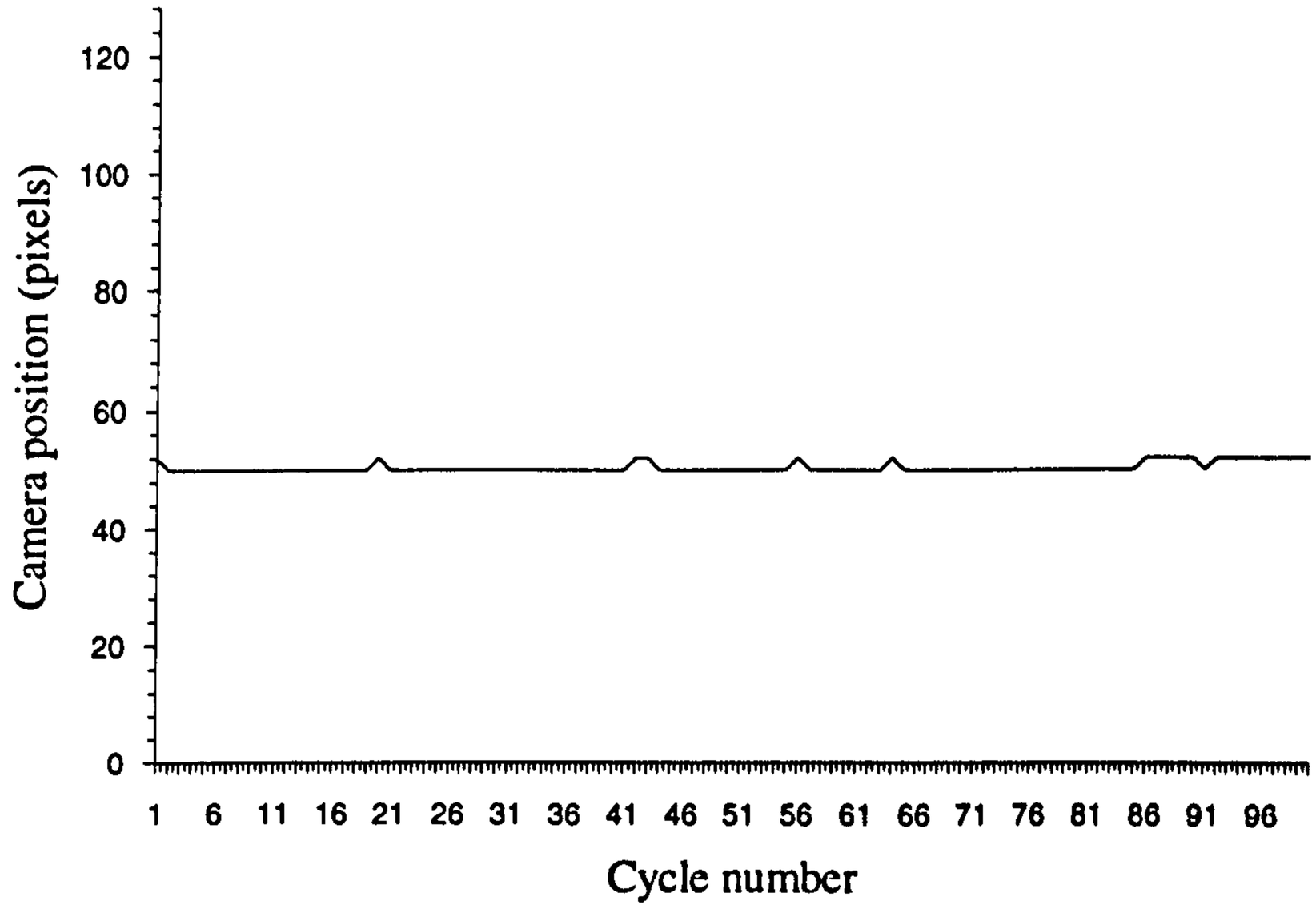

(a) Edge positional variation measured by the line-scan camera.

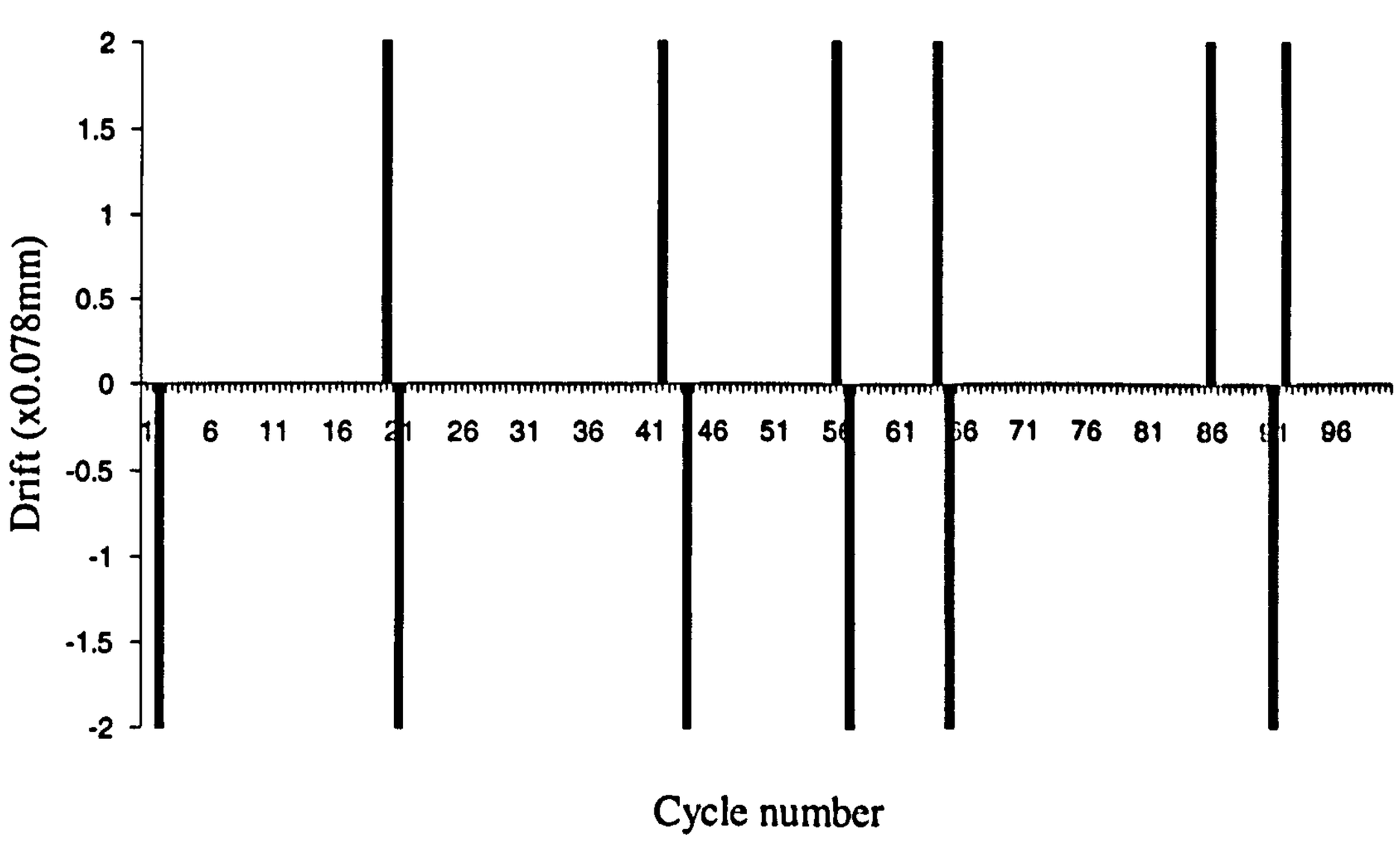

(b) Degree of movement measured per cycle.

Figure G.4 Movement measurements obtained for sample DWFS5

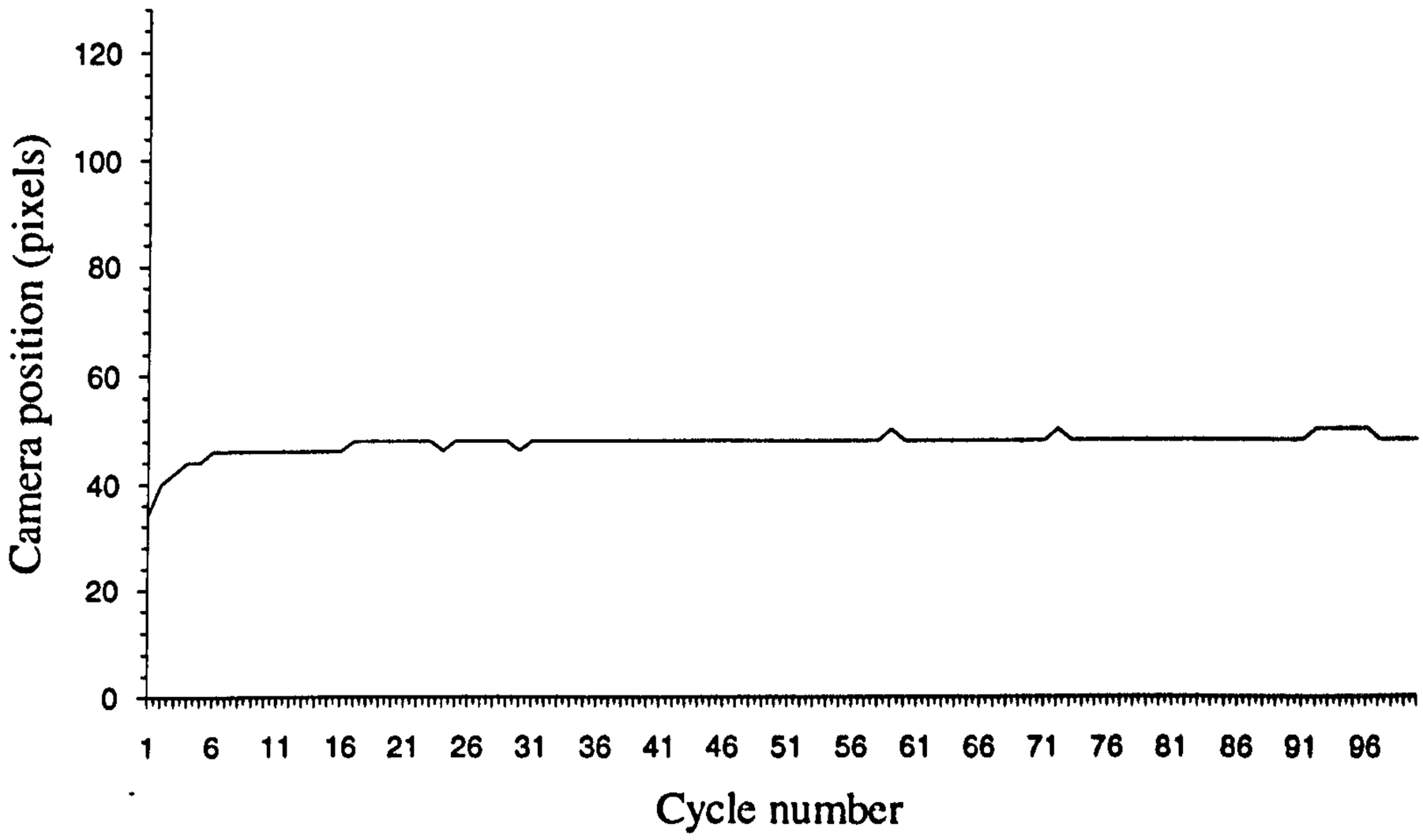

(a) Edge positional variation measured by the line-scan camera.

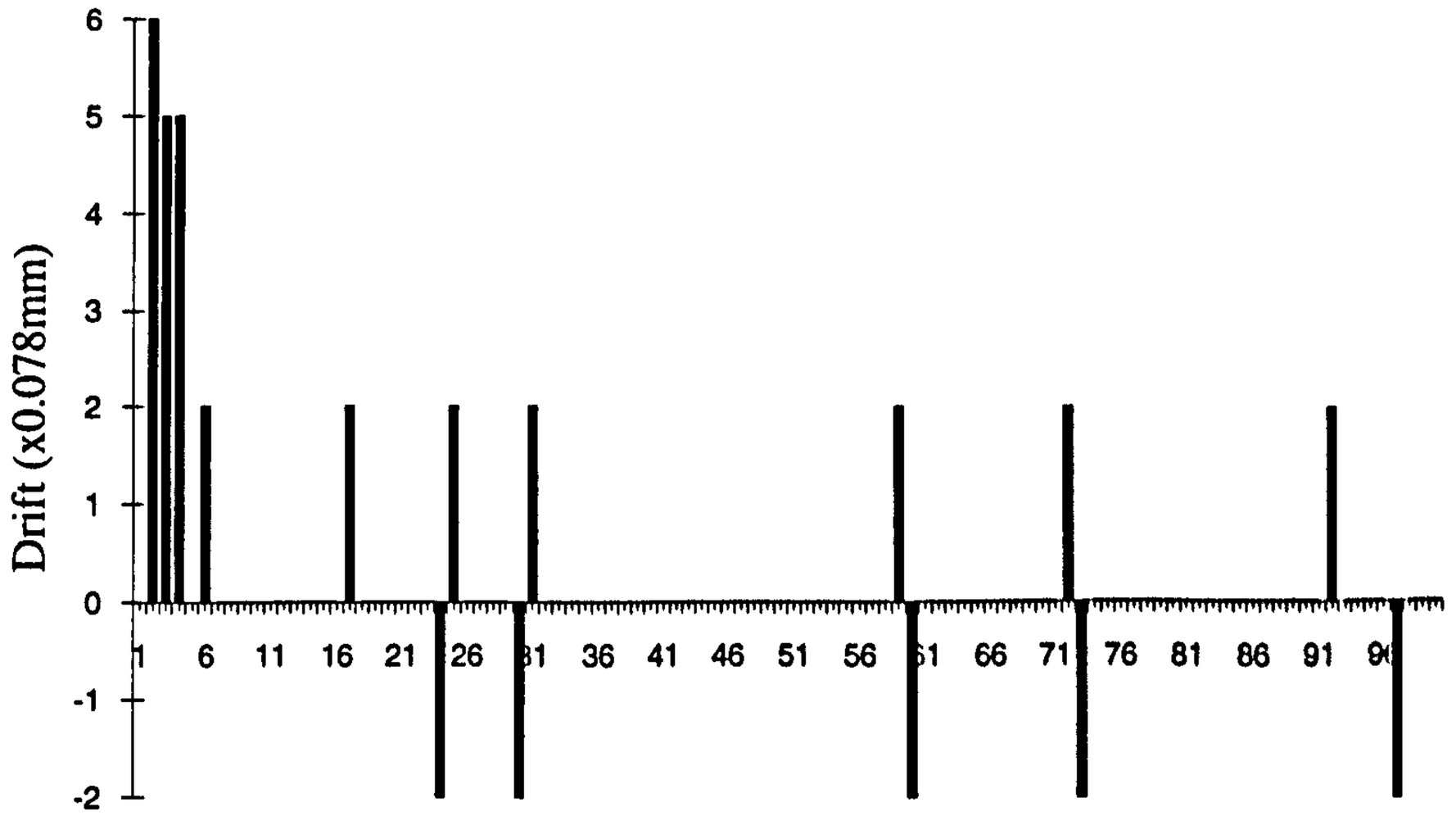

(b) Degree of movement measured per cycle.

Figure G.5 Movement measurements obtained for sample INSOLE6

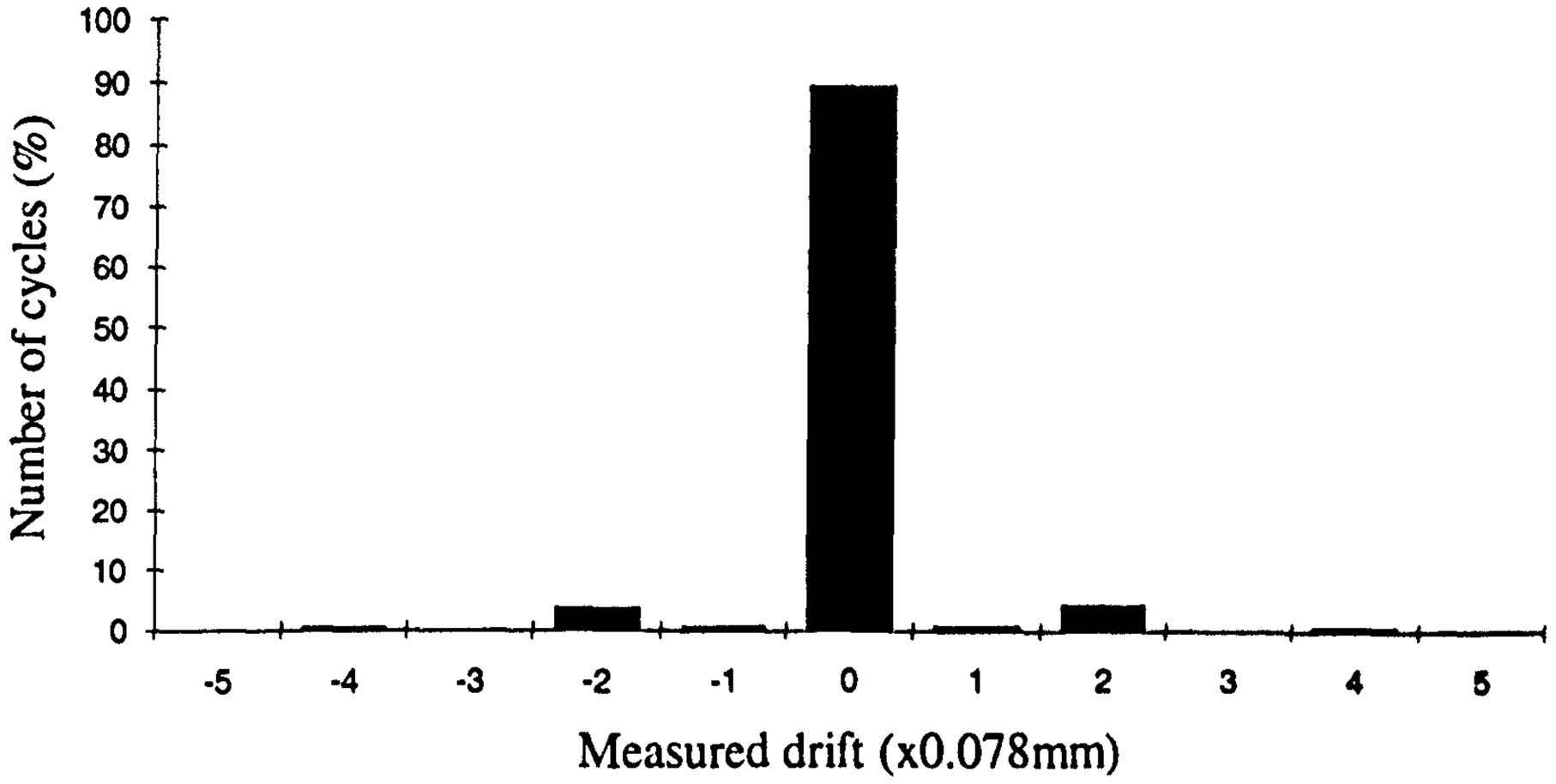

Figure G.6 Error distribution for Flat samples tested.

Appendix H

Drift / Slip results for the Autoscan Compound components.

H.1 Introduction.

The results included in this section on workpiece mvement, were observed for the samples described in Appendix D.2. In addition to these test samples, a brogue, upper component, was also tested. This workpiece represents a typical shoe part that may require structural stitching.

H.2 Pinned belts on compound components.

Figures H.1-H.4, show an example result for each of the compound samples tested. Similar to Appendix G, part (a) of the figures show the raw camera data extracted during the movement measurement tests. This shows the trend of any movement that may be occurring, particularly in the case of the brogue shoe upper component. Part (b), of the figures show the actual edge displacement as measured from one cycle to the next. Similar to the results for flat parts, a trend is evident showing that a displacement (movement), in one direction is generally compensated for on the next cycle, resulting in no net effect. Figure H.5 is a second example of results obtained for the brogue component. This result was taken with the part inserted at 90° to that shown in Figure H.4. The result shows an apparent high degree of movement during the initial cycles, before settling down to a steady, zero net movement, condition. These apparent large errors only occured at certain orientations where the part was able to catch on the edge of the feed table highlighting a limitation in the handling mechanism.

Figure H.6 contains an analysis into the drift / slip distribution across the range of compound parts tested.

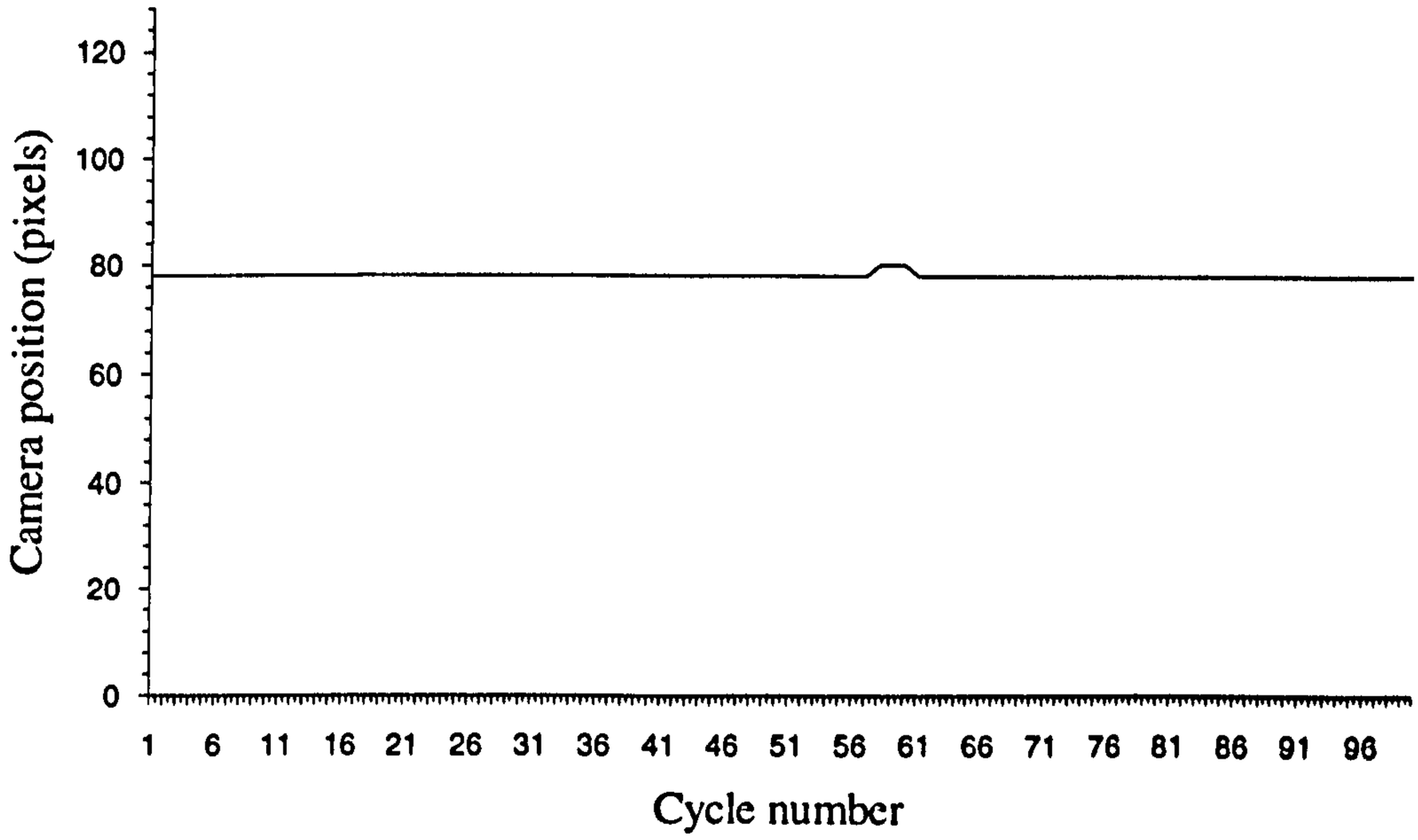

(a) Edge positional variation measured by the line-scan camera.

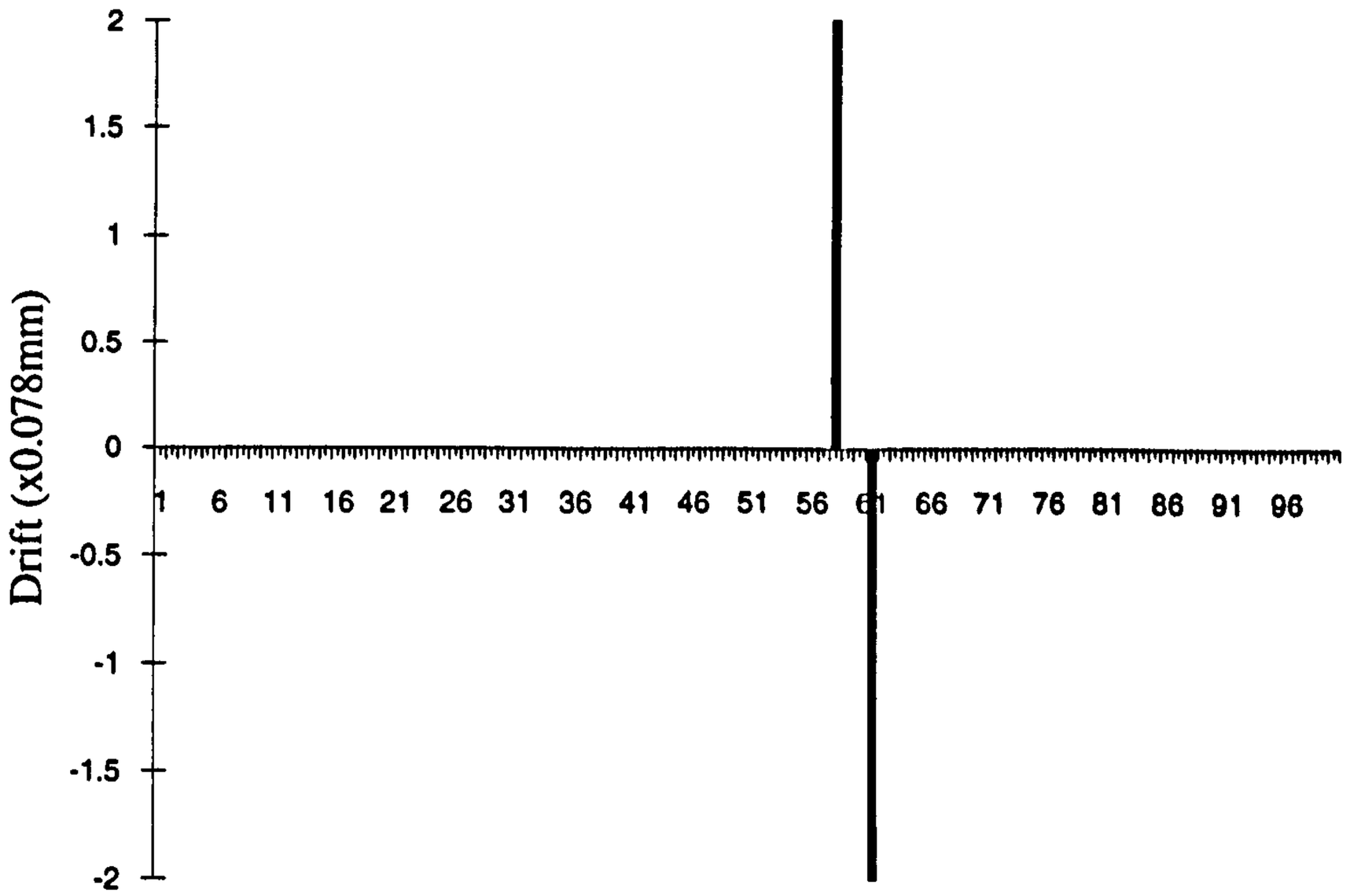

(b) Degree of movement measured per cycle.

Figure H.1 Movement measurements obtained for sample DWCC1

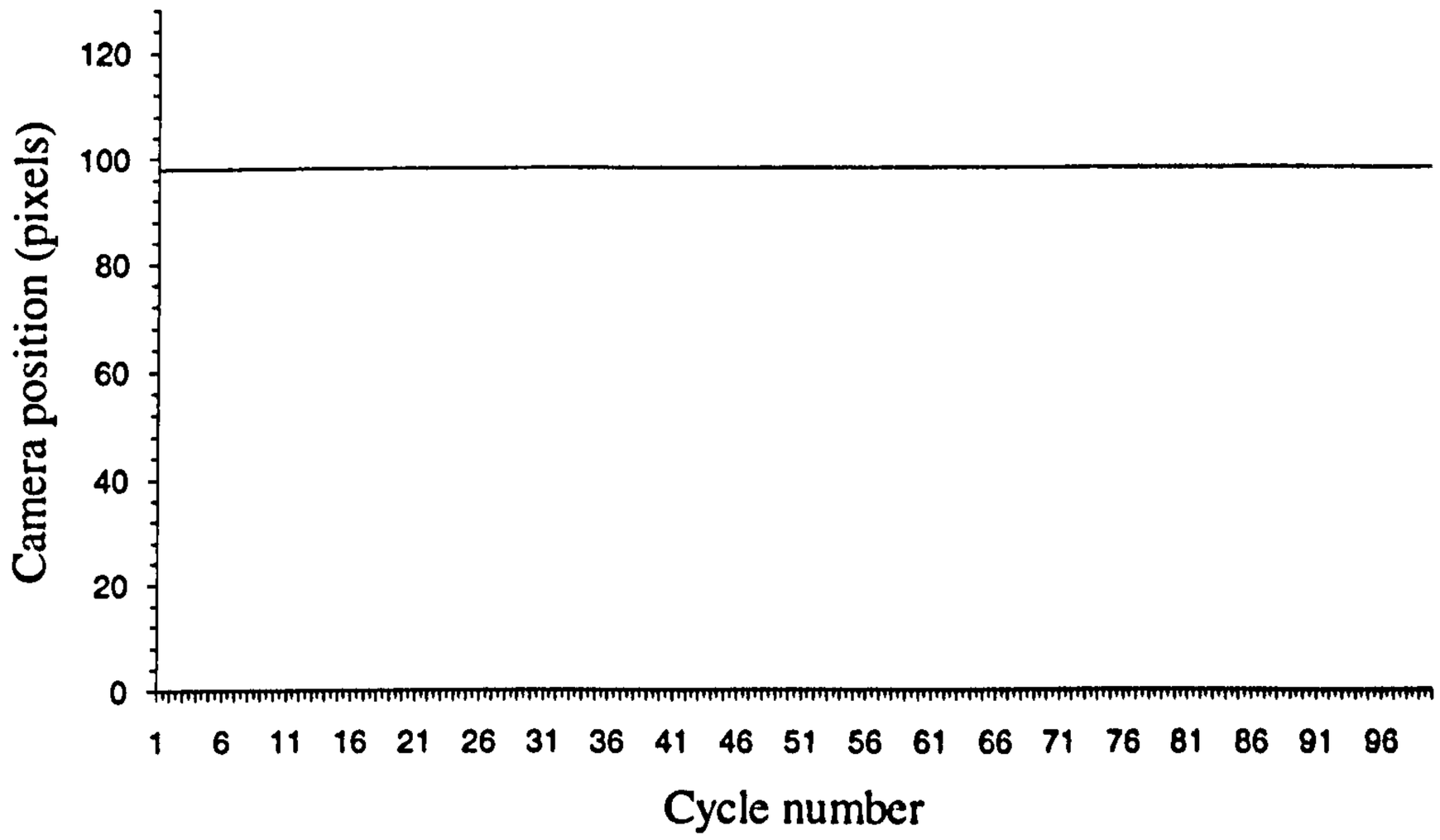

(a) Edge positional variation measured by the line-scan camera.

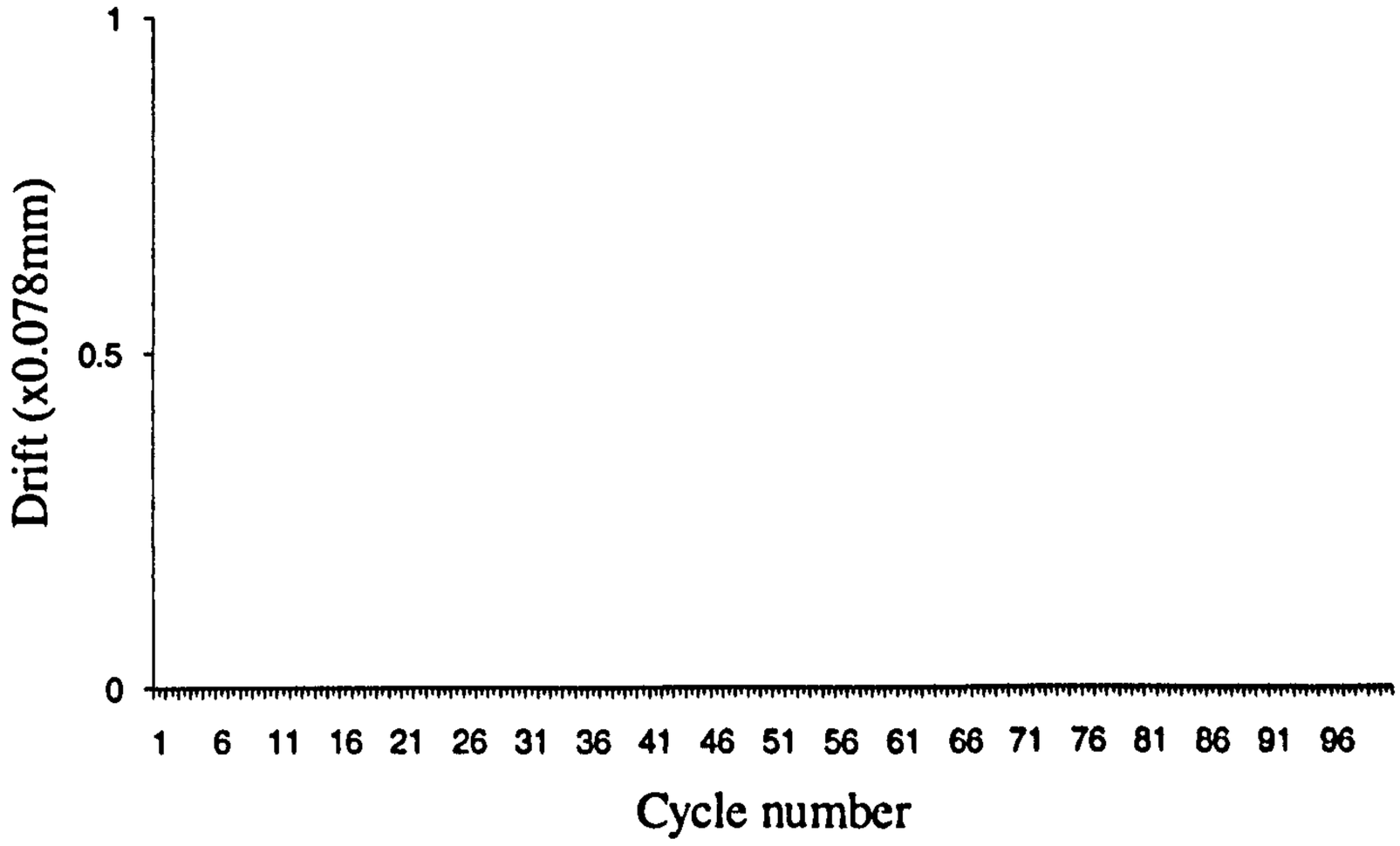

(b) Degree of movement measured per cycle.

Figure H.2 Movement measurements obtained for sample DWCR4

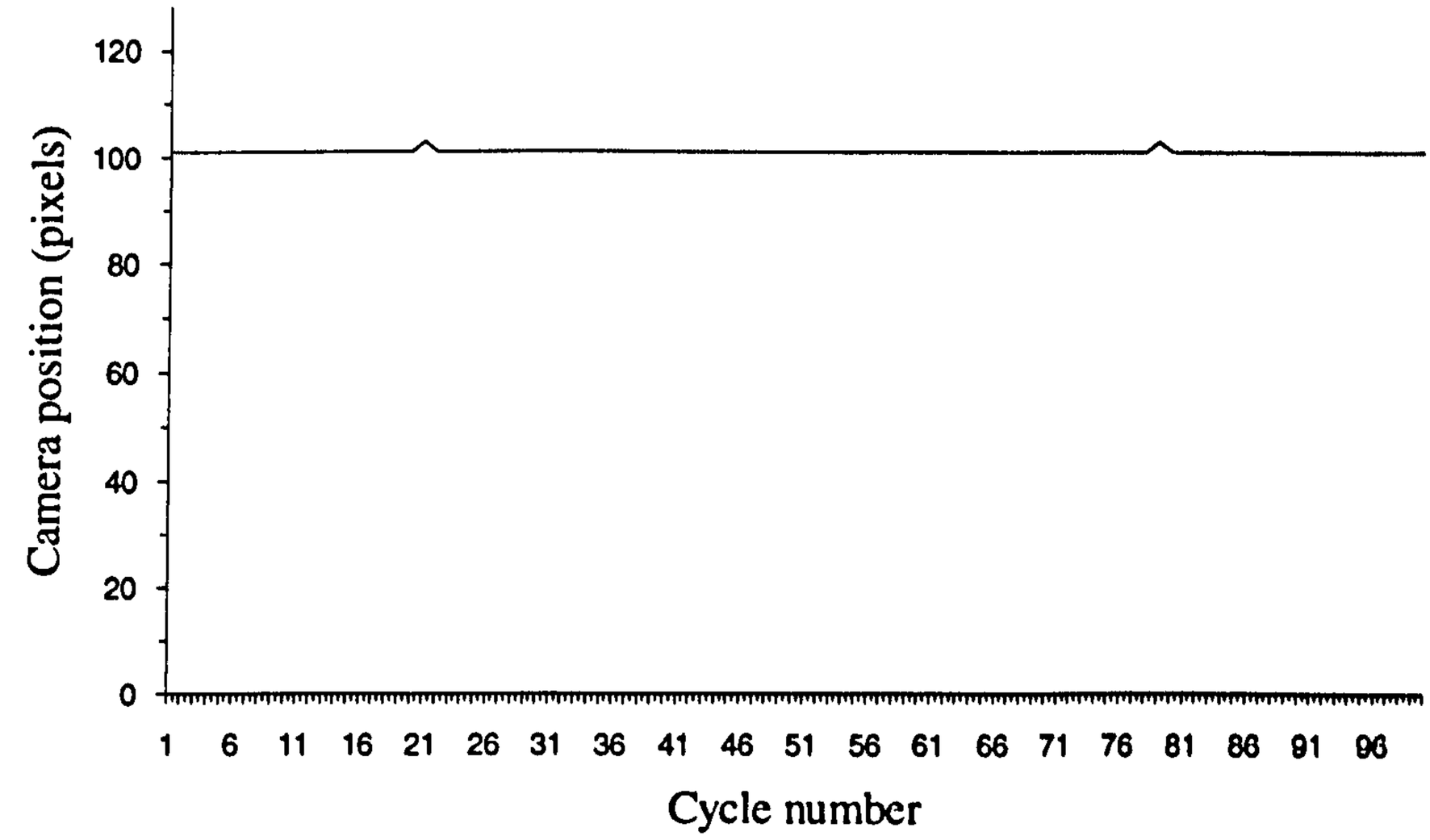

(a) Edge positional variation measured by the line-scan camera.

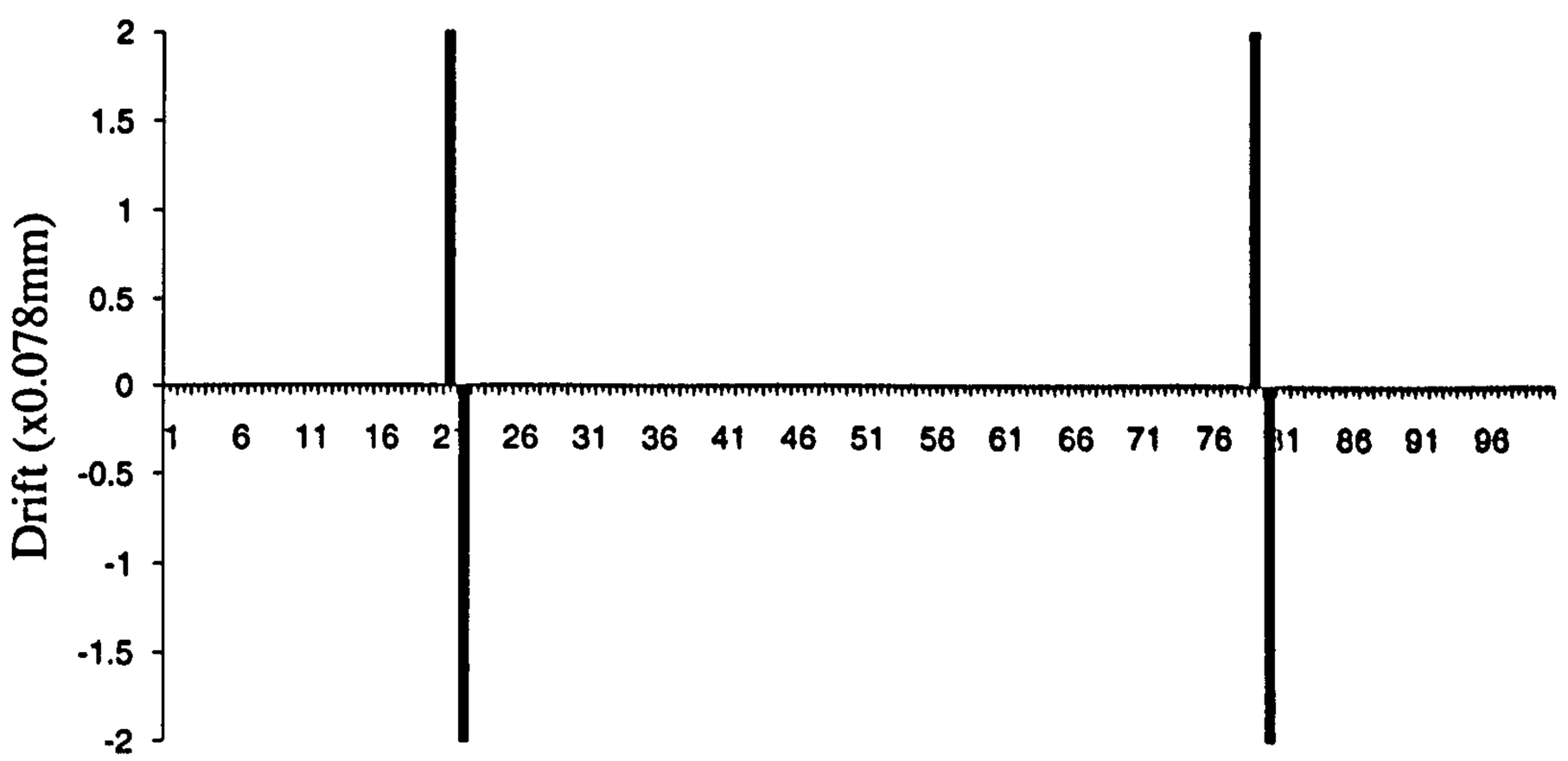

(b) Degree of movement measured per cycle.

Figure H.3 Movement measurements obtained for sample DWCS2

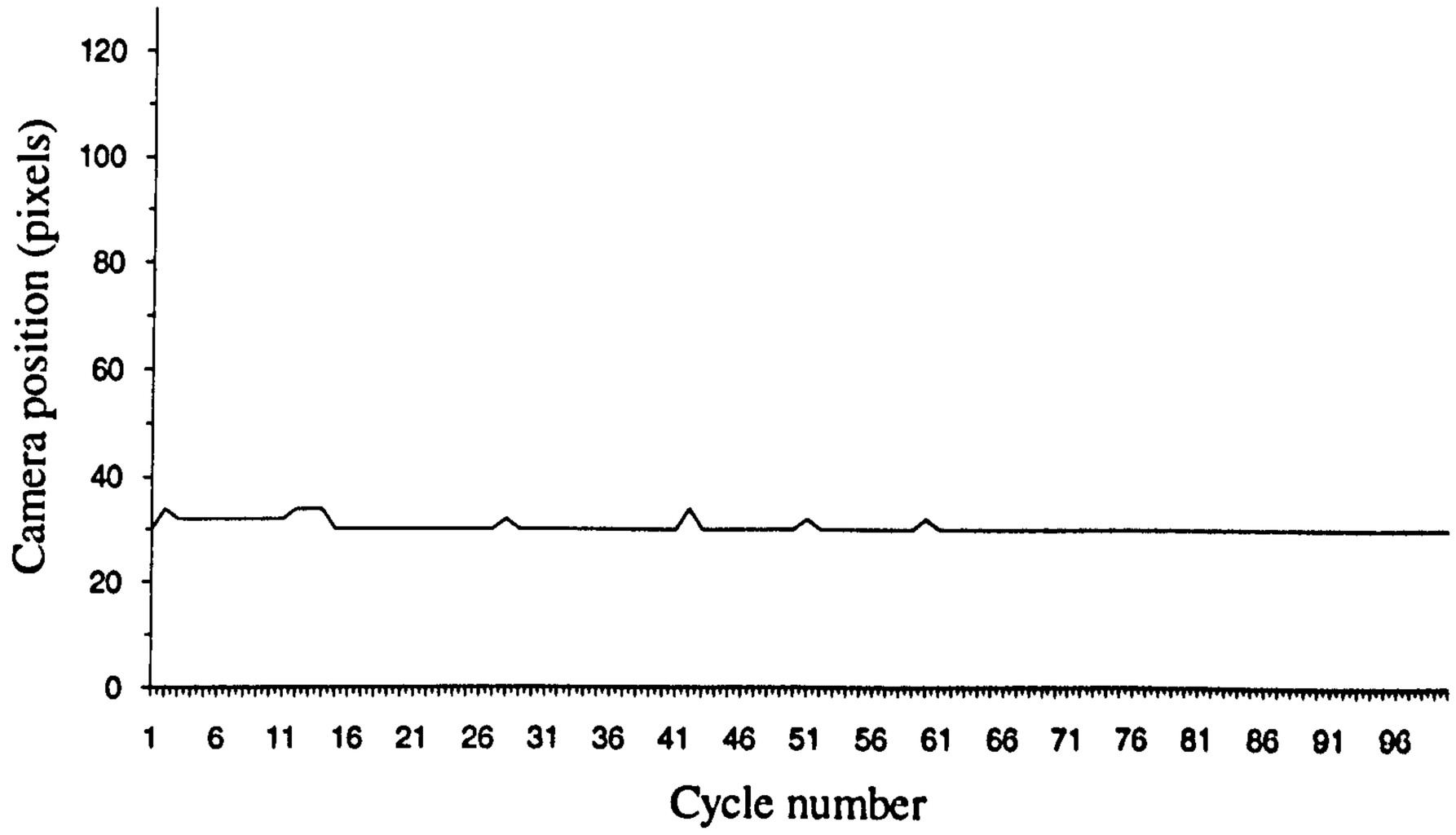

(a) Edge positional variation measured by the line-scan camera.

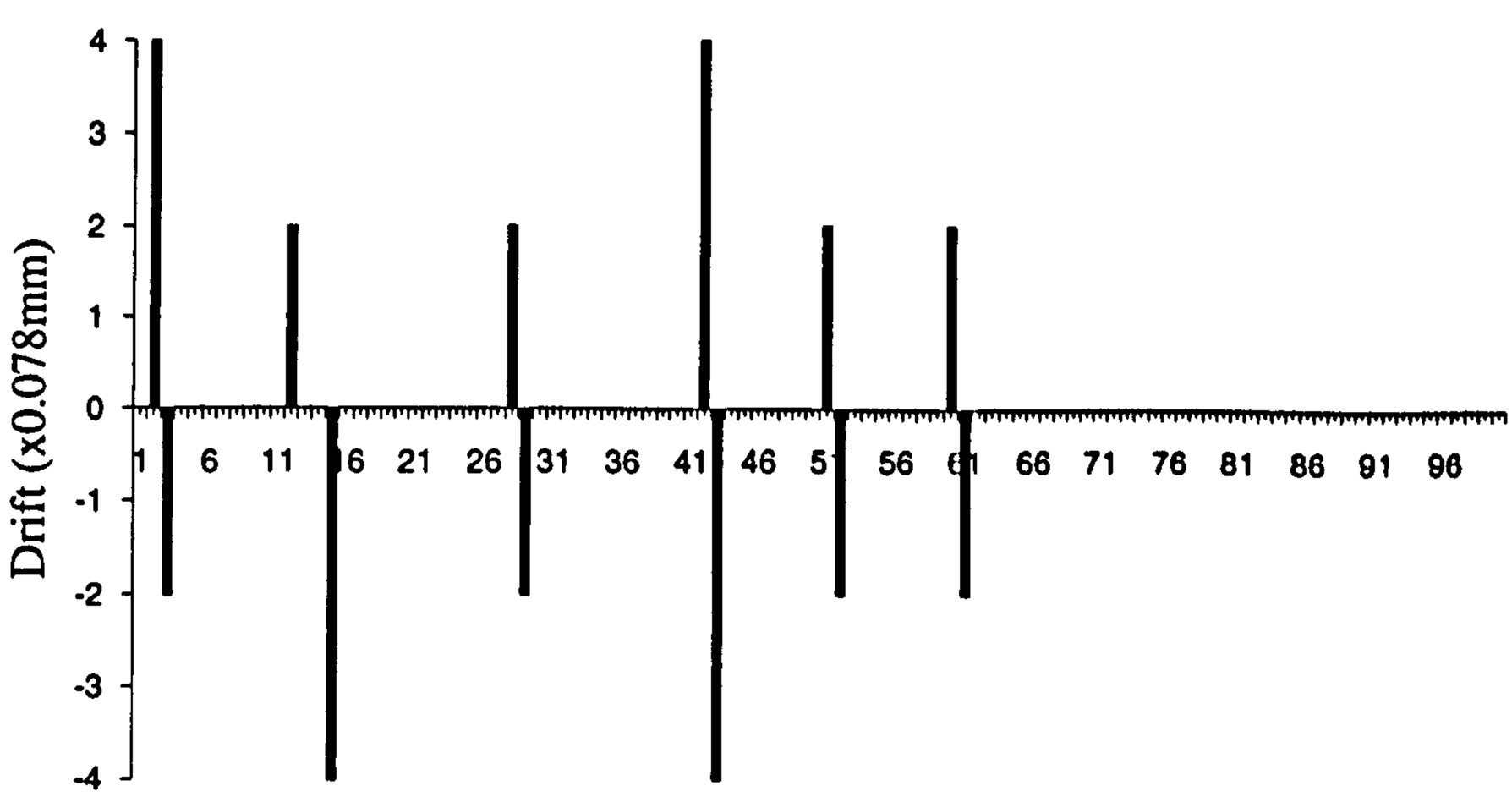

(b) Degree of movement measured per cycle.

Figure H.4 Movement measurements obtained for sample BROGUE (0°)

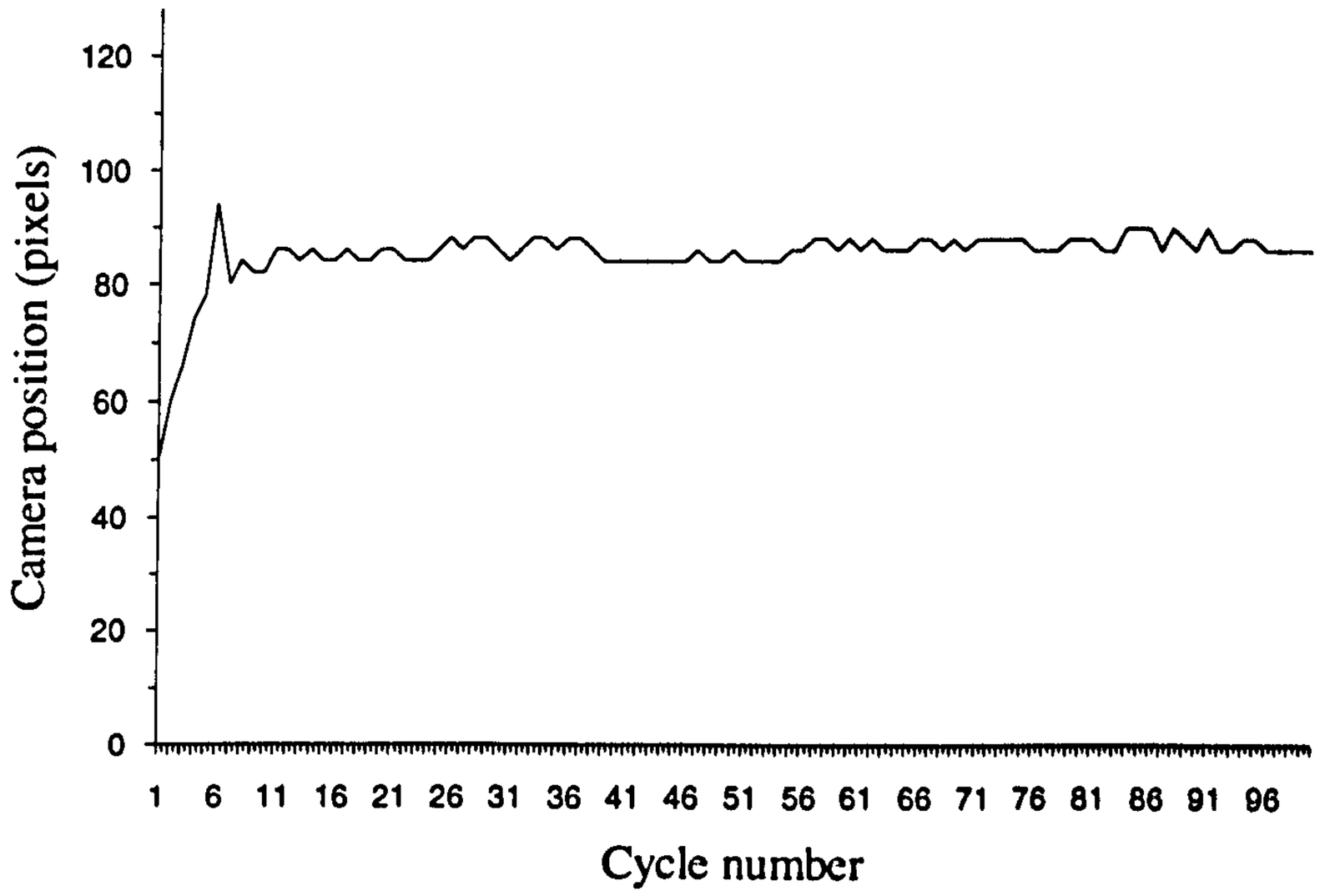

(a) Edge positional variation measured by the line-scan camera.

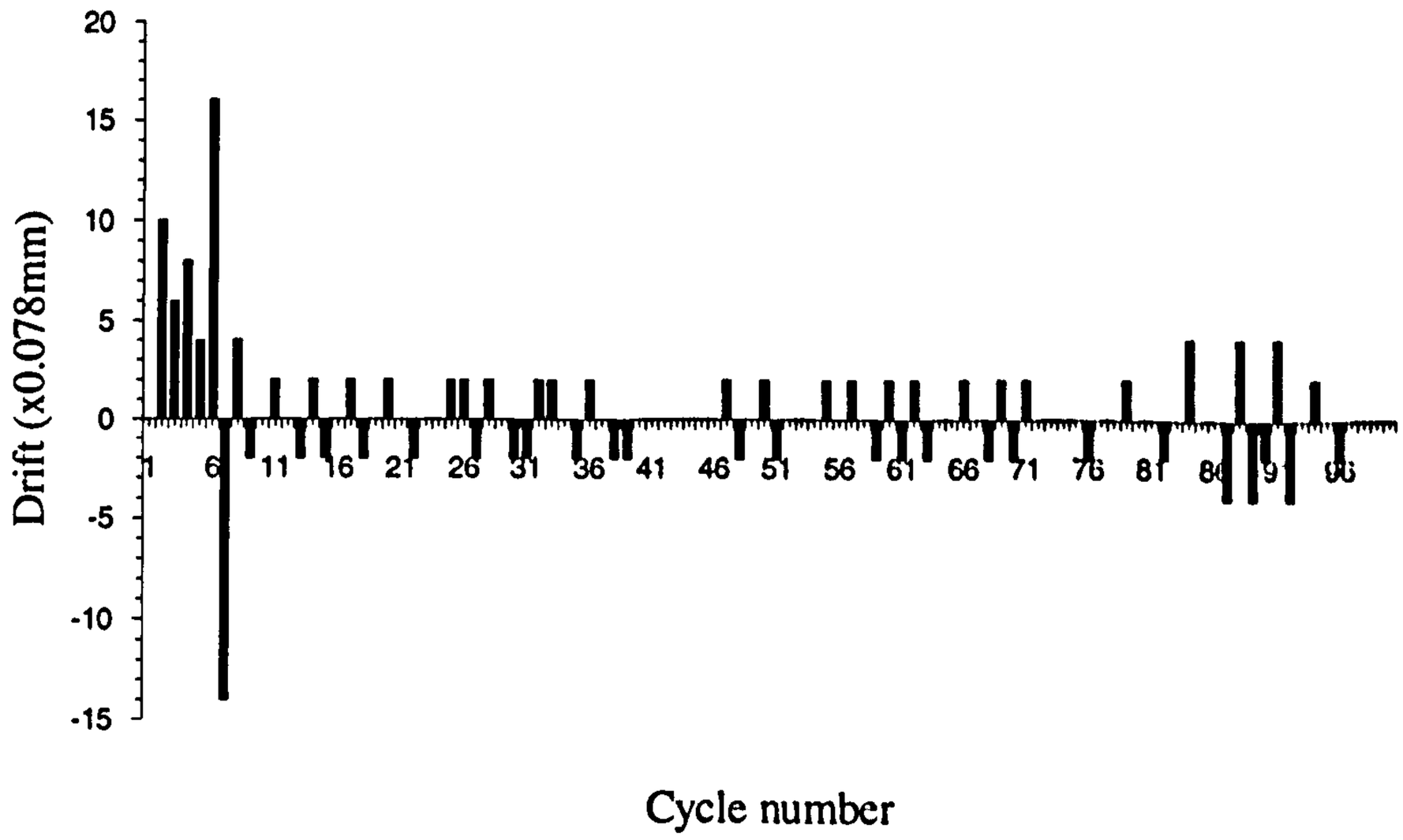

(b) Degree of movement measured per cycle.

Figure H.5 Movement measurements obtained for sample BROGUE (90°)

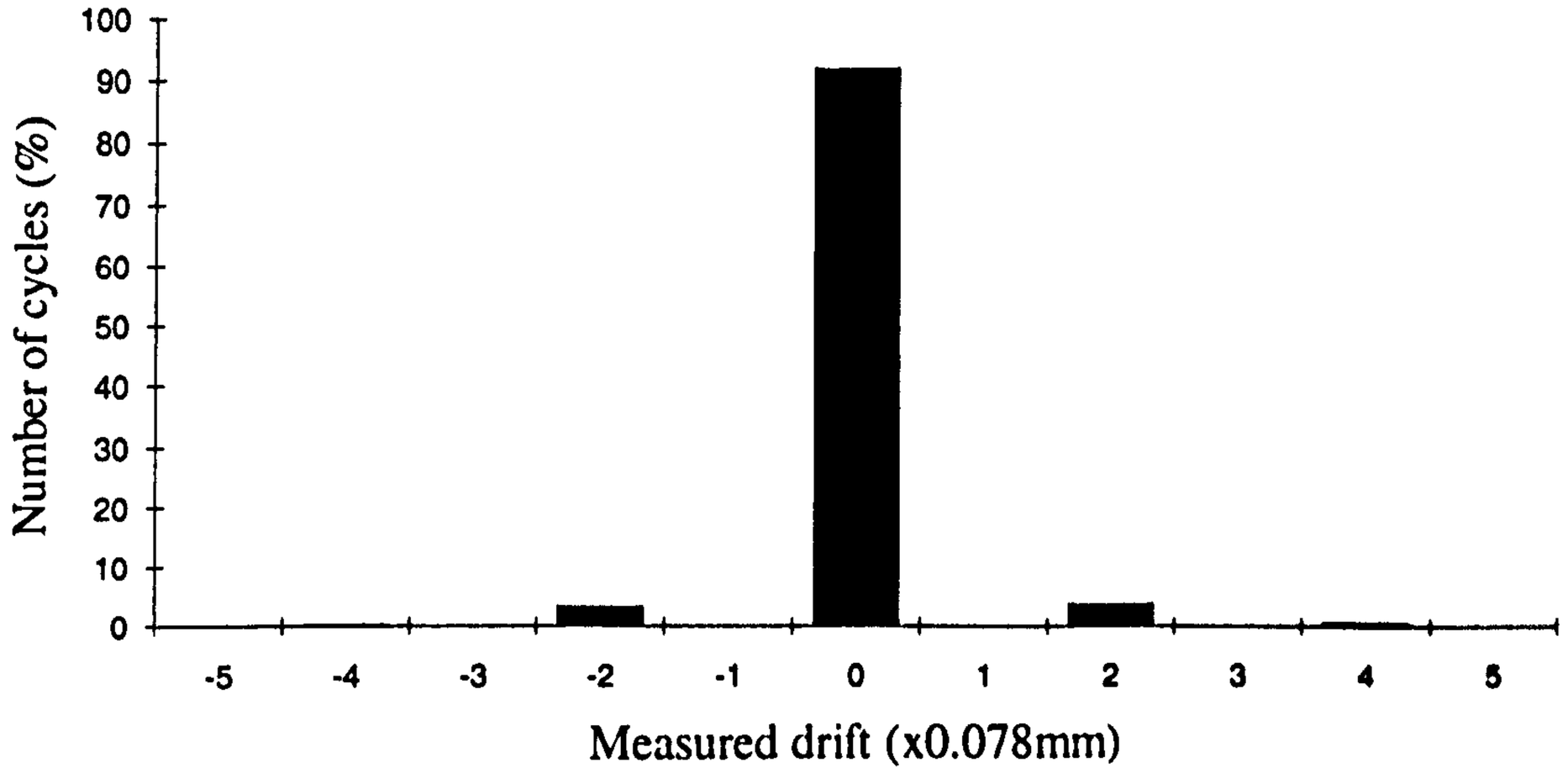

Figure H.6 Errror distribution for Compound samples tested.

Appendix I

Determination of required sample size

I.1 Determination of sample size required.

As the formulas for standard error and confidence intervals all involve knowing the number of samples tested during the experiment it is apparent that if the number of samples, (n), tested increases, the accuracy of such calculations similarly increases. However there comes a point when for a given degree of confidence the error bounds can be said to be within acceptable limits. Therefore there is little to be gained by taking far more samples than is required to reach this point. Here, with reference to Bhattacharyya and Johnson[48], we will determine the number of samples required to achieve a high degree of confidence within the given specification for parts tested using the pinned belt configuration.

I.2 Calculation of n.

Assume that a value for the population standard deviation, (σ), is known. Where the population is all leather and synthetic types used in shoemaking.

The formula for a 100(1-a)% error bound for the estimation of μ by $\overline{X}$ is given by,

$$Z_{a/2}\frac{\sigma}{\sqrt{n}} \quad \text{..... (1)}$$

In order to be 100(1-α)% sure that a degree of error d is not exceeded we now have,

$$Z_{\alpha/2}\frac{\sigma}{\sqrt{n}} = d \quad \ldots\ldots\ldots\ldots\ldots\ldots\ldots\ldots\ldots (2)$$

Solving for n, the number of samples required gives,

$$n = \left[\frac{Z_{\alpha/2}\sigma}{d}\right]^2 \quad \ldots\ldots\ldots\ldots\ldots\ldots\ldots\ldots\ldots (3)$$

This solution is valid if n is large or if the population distribution is normal. However where this is not the case a conservative estimate for n can be determined by implementing the Chebyshev inequality.

For a random number X with a mean μ, for every distribution we can obtain a probability bound that X is no more than d units from μ.

$$P\left[|X-\mu| > d\right] \leq \frac{Var(X)}{d^2} \quad \ldots\ldots\ldots\ldots\ldots\ldots\ldots (4)$$

Note,

$$Var(X) = \frac{\sigma^2}{n} \quad \ldots\ldots\ldots\ldots\ldots\ldots\ldots\ldots\ldots (5)$$

Hence,

$$P\left[\left|\overline{X} - \mu\right| \leq d\right] \geq 1 - \frac{\sigma^2}{nd^2} \quad \ldots\ldots\ldots\ldots\ldots\ldots\ldots (6)$$

so by equating $1-\frac{\sigma^2}{nd^2}$ to the desired assurance 1-α, the sample size n is given by,

$$n = \frac{\sigma^2}{\alpha d^2} \quad \ldots\ldots (7)$$

In summary,

To be 100(1-α)% sure that the error $|\overline{X}-\mu|$ does not exceed d, the required sample size is given by,

$$n = \left[\frac{Z_{\alpha/2}\sigma}{d}\right]^2 \quad \ldots\ldots (8)$$

However if n is small and the population is non-normal a conservative estimate of the upper bound for the sample size can be found using,

$$n = \frac{\sigma^2}{\alpha d^2} \quad \ldots\ldots (9)$$

with n being rounded up to the next highest integer.

I.3 Determination of confidence levels

As the materials that exist in shoe manufacturing as varied and often have inherently complex structures it is reasonable to assume that the population distribution

is non-normal. Consequently the second method for determining the sample size will be used in order to give a conservative estimate for n.

If the population is subdivided into two categories,

1. Flat components tested
2. Compound components tested

the number of samples required to give a sample mean no greater than 5 units, (d=2.5 is approximately 0.2mm), from the population mean with at least 95% probability, ($\alpha = 0.05$), can be determined.

Table J, contains the results obtained from the drift experiments taken using the pinned belts using the line-scan camera method.

	All Flat Parts	All Compound Parts
Mean ($\overline{X}$)	0.044	0.038
Standard deviation (σ)	0.871	0.910

Table I. Statistical results obtained for populations of flat and compound parts

Using the information contained in Table J and equation 9, the number of components, n_{flat} and $n_{compound}$ can be calculated,

$$n_{flat} = 2.79 \text{ , } n_{compound} = 2.65$$

Therefore, rounding up to the next highest integer gives,

$$n_{flat} = n_{compound} = 3 \qquad \text{(minimum)}$$

These values are exceedingly low, demonstrating the accuracy of the handling mechanism and the repeatibility of the results, regardless of component type, (flat or compound). The result also demonstrates that the number of samples actually taken, (46 flat, and 16 compound parts), was greater than actually required to achieve a 95% confidence limit for d=2.5.

Appendix J

Examples of pre-tacking various materials.

J.1. Pre-tack examples using the test component shape.

This section contains example results obtained by implementing the procedures outlined in Chapter 4. Figures J.1-J.4, show the measured edge positional discrepancies from the desired position after final stitching. In order to produce these samples the test pattern had to be photocopied onto thin cardboard to form a template. This was then placed on top of the sample material and drawn around to produce the cutting pattern. This resulted in large possible errors being introduced into the edge position even before pre-tacking and final stitching. Consequently these results are included in this appendix as additional information only as it is difficult to discriminate between the human and process errors.

The samples tested and shown here are;

Figure J.1, Paper, this has been included as a reference.

Figure J.2, Denim.

Figure J.3, Patent leather.

Figure J.4, Calf leather.

The figures show that the edges of the line of the edges for the non-paper samples are far more irregular than the paper sample(s). This is due to the difficulties in sample construction. However, the statistics for the three non-paper samples show that there is a strong trend for the edges to remain closely aligned after final stitching.

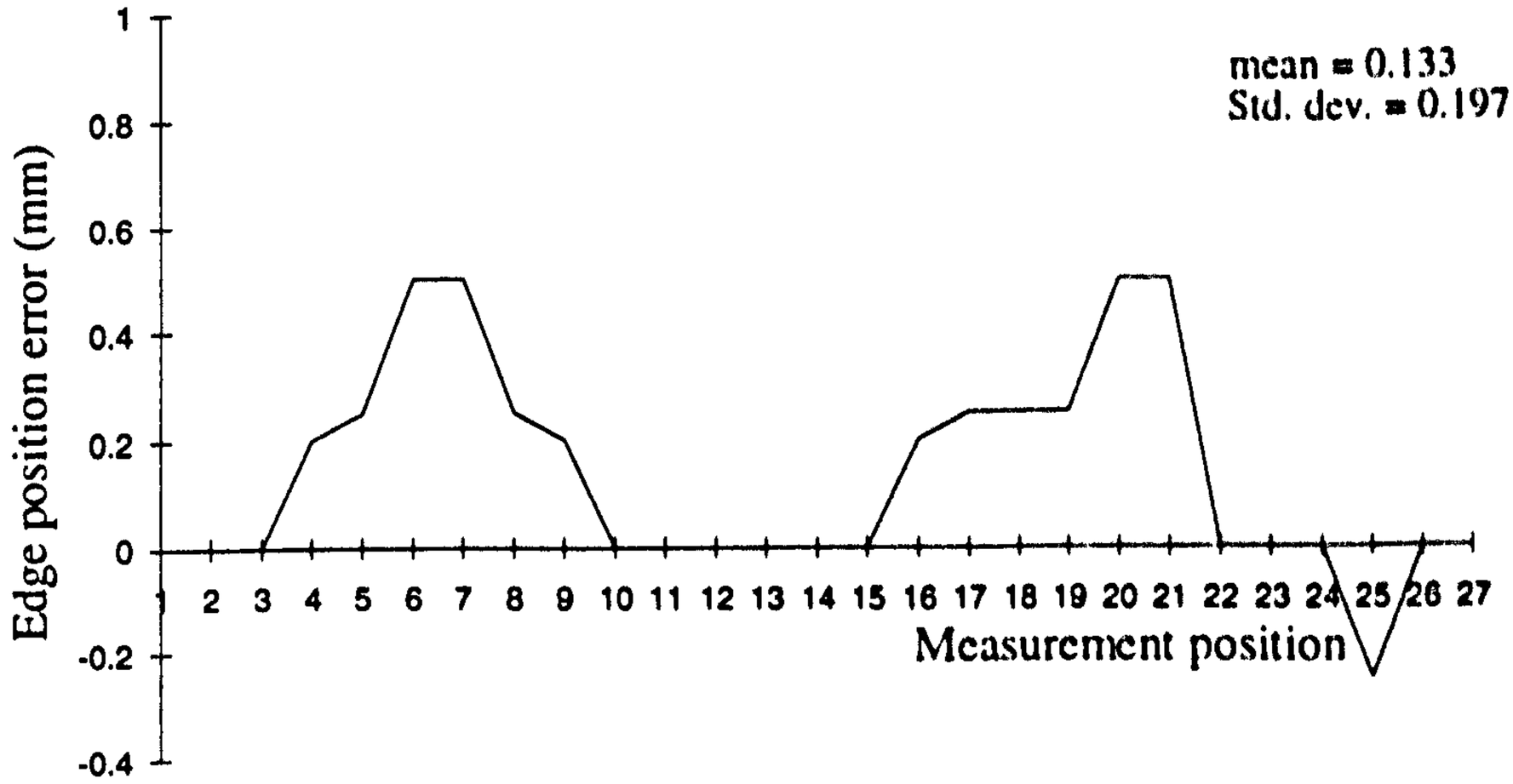

Figure J.1. Edge misalignment errors after final stitching for a paper sample

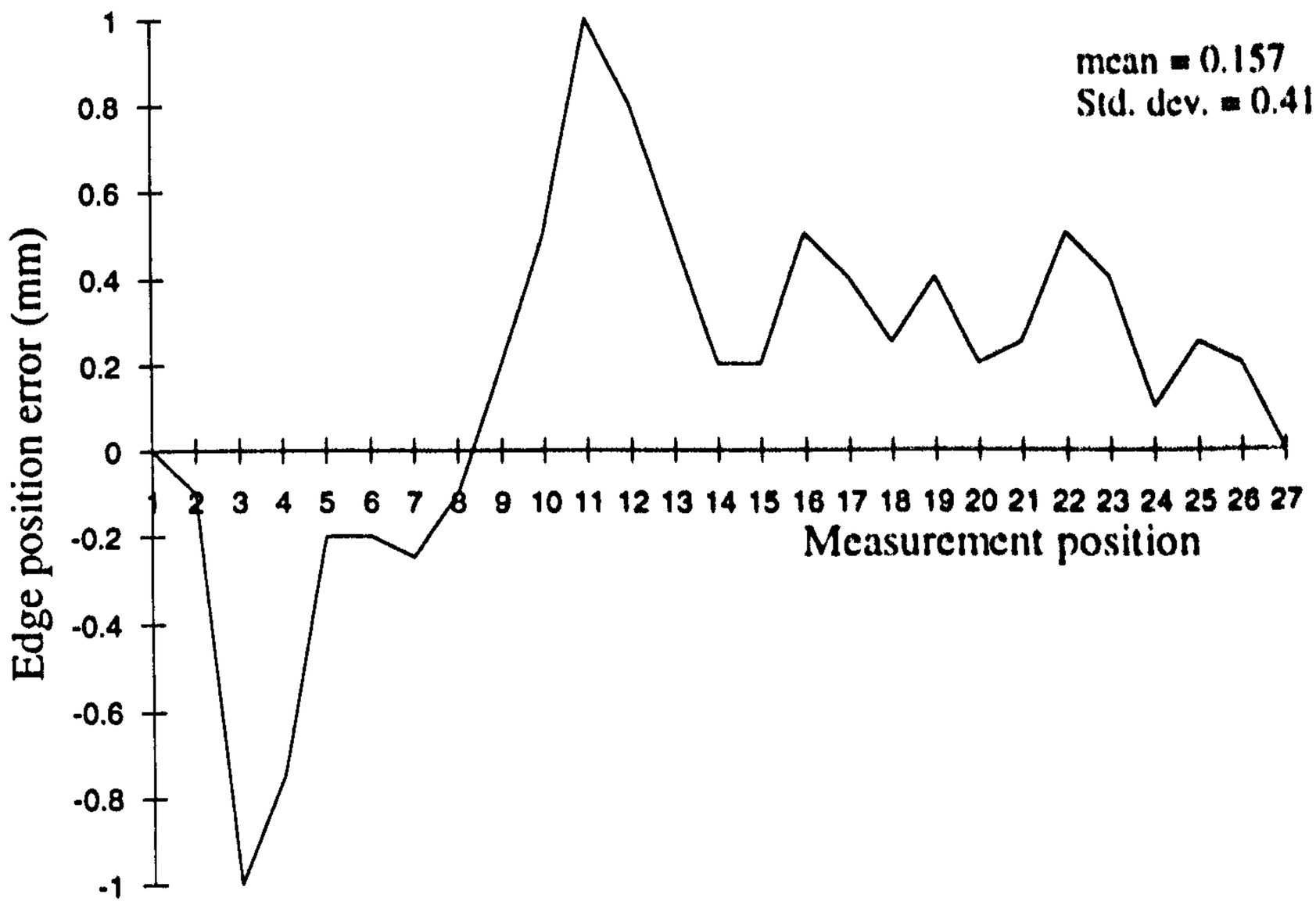

Figure J.2. Edge misalignment errors after final stitching for a Denim sample

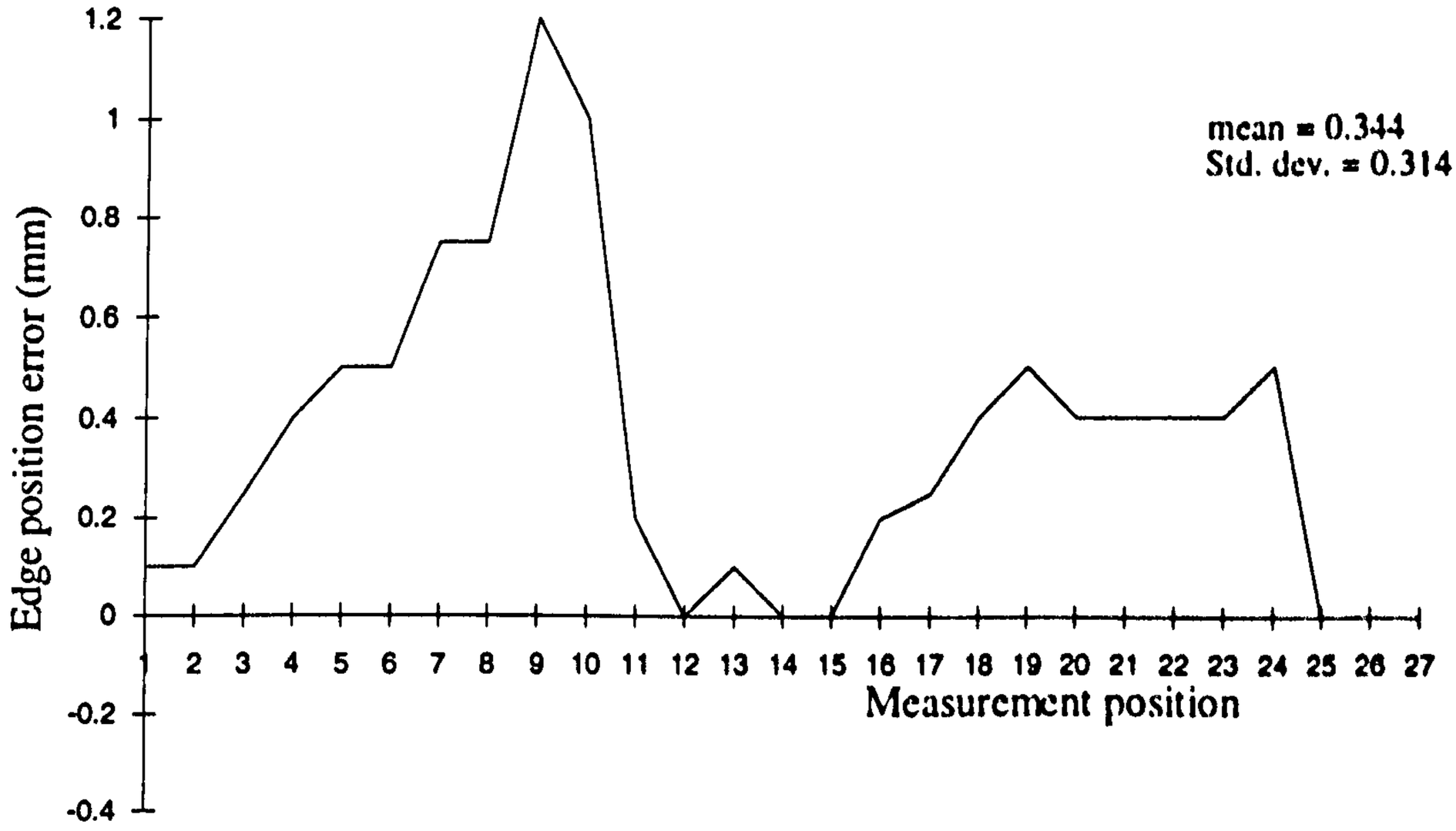

Figure J.3. Edge misalignment errors after final stitching for a patent leather sample

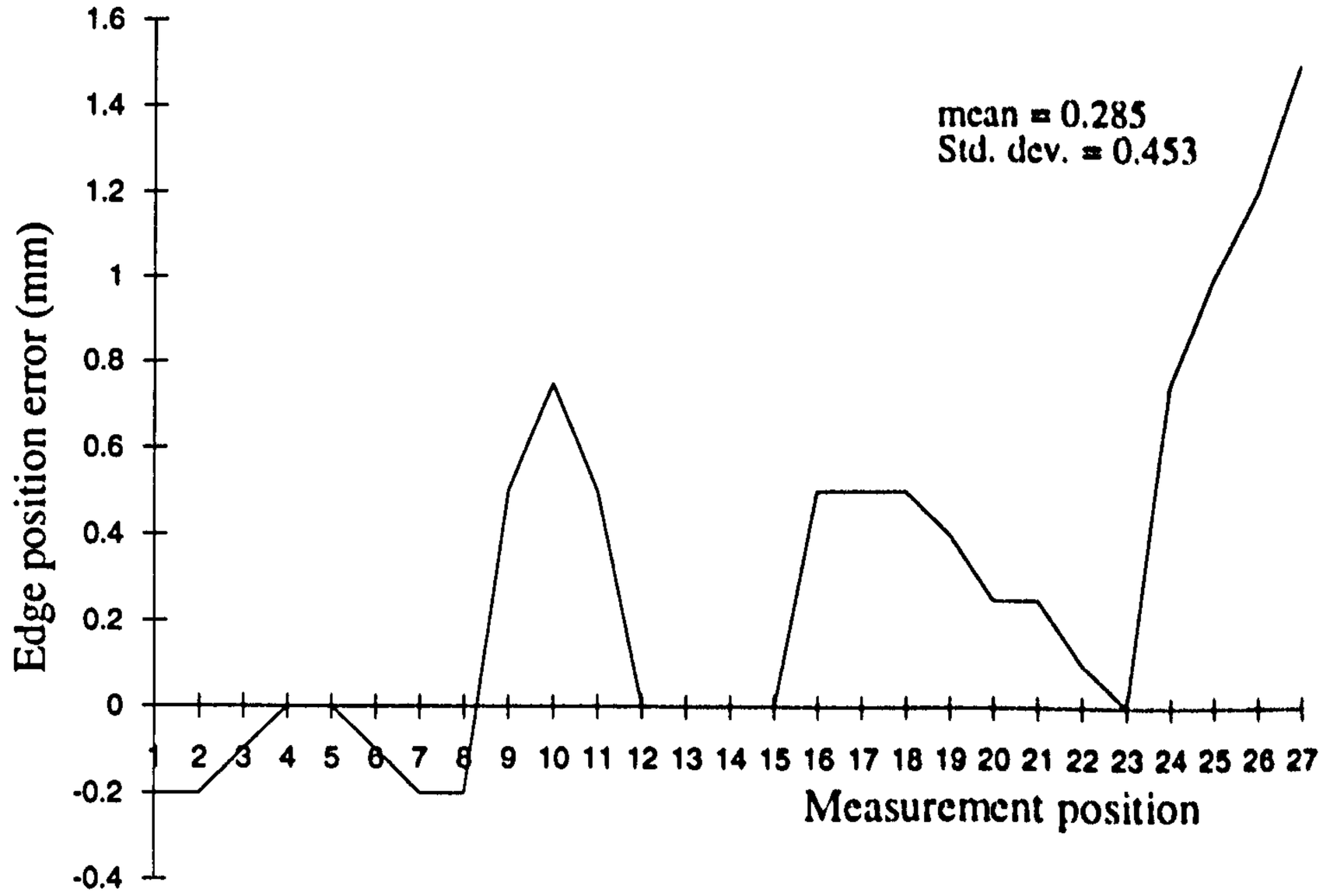

Figure J.4. Edge misalignment errors after final stitching for a calf leather sample

Appendix K

Laser line-stripe characteristics and example images.

K. Laser line-stripe investigations for edge following.

This appendix contains examples of images taken using an area camera of laser line-stripes incident on typical workpiece edges. The images have also been inverted to aid clarity.

K.1Gaussian distribution of light intensity over a laser line-stripe.

Figure K.1 shows histograms extracted from a complete line-stripe image. It can be seen from this image that the light intensity both along the length and across the width of the stripe vary according to the laws of Gausian distribution. This is a well understood effect, however there are now laser optics which compensate for this effect, giving an even intensity distribution. This figure has therefore been included to demonstrate the characteristics of the laser used during the investigations made in this thesis.

K.2 Examples of typical images obtained.

Figure K.2, shows a typical image extracted from a 'neat' square cut edge.

Figure K.3, shows a typical image extracted from a folded edge with a high degree of pear-shaping at the fold.

K.3 Examples of typical images obtained.

Figures K.4 and K.5 show examples of camera or laser misalignment.

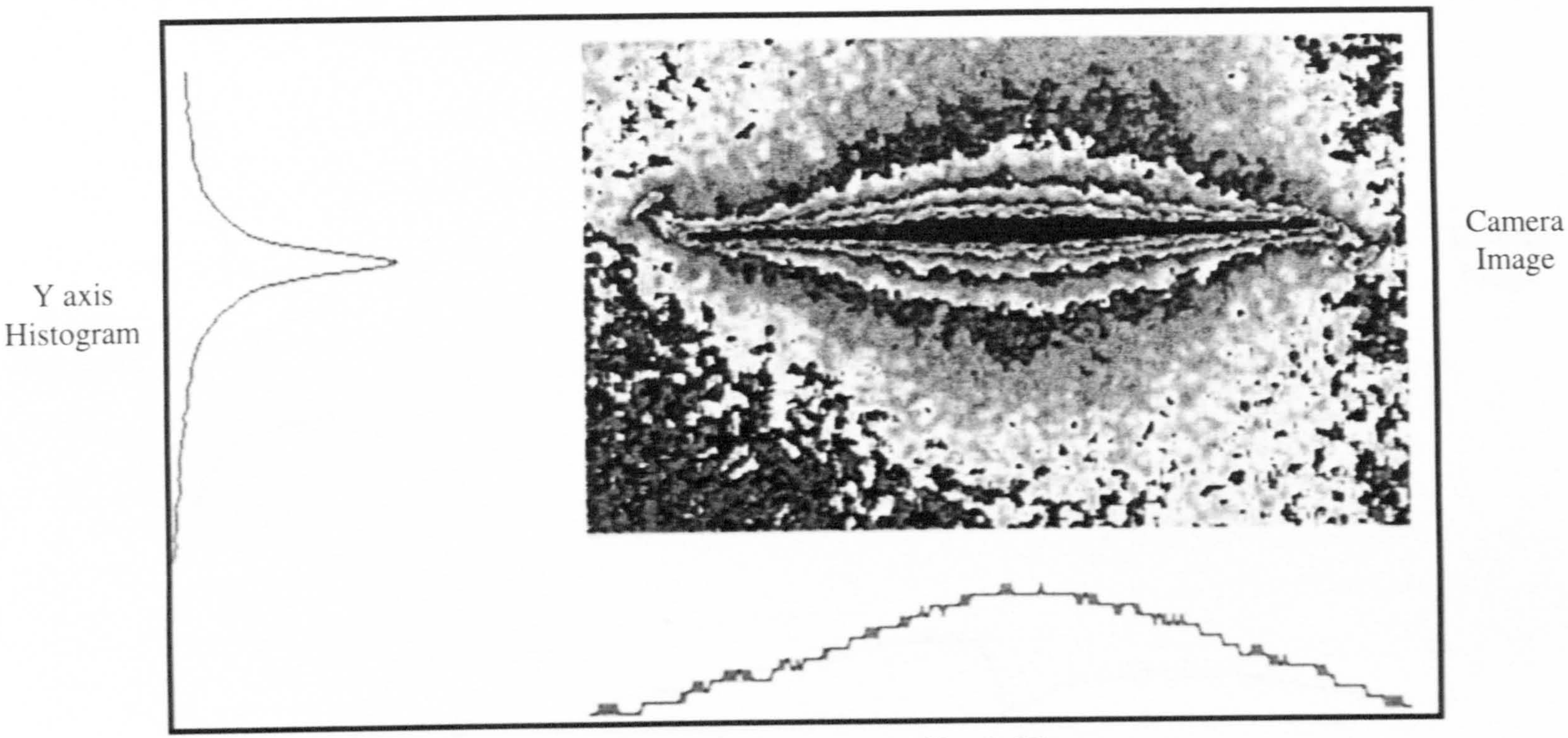

Figure K.1 Laser line-stripe characteristics.

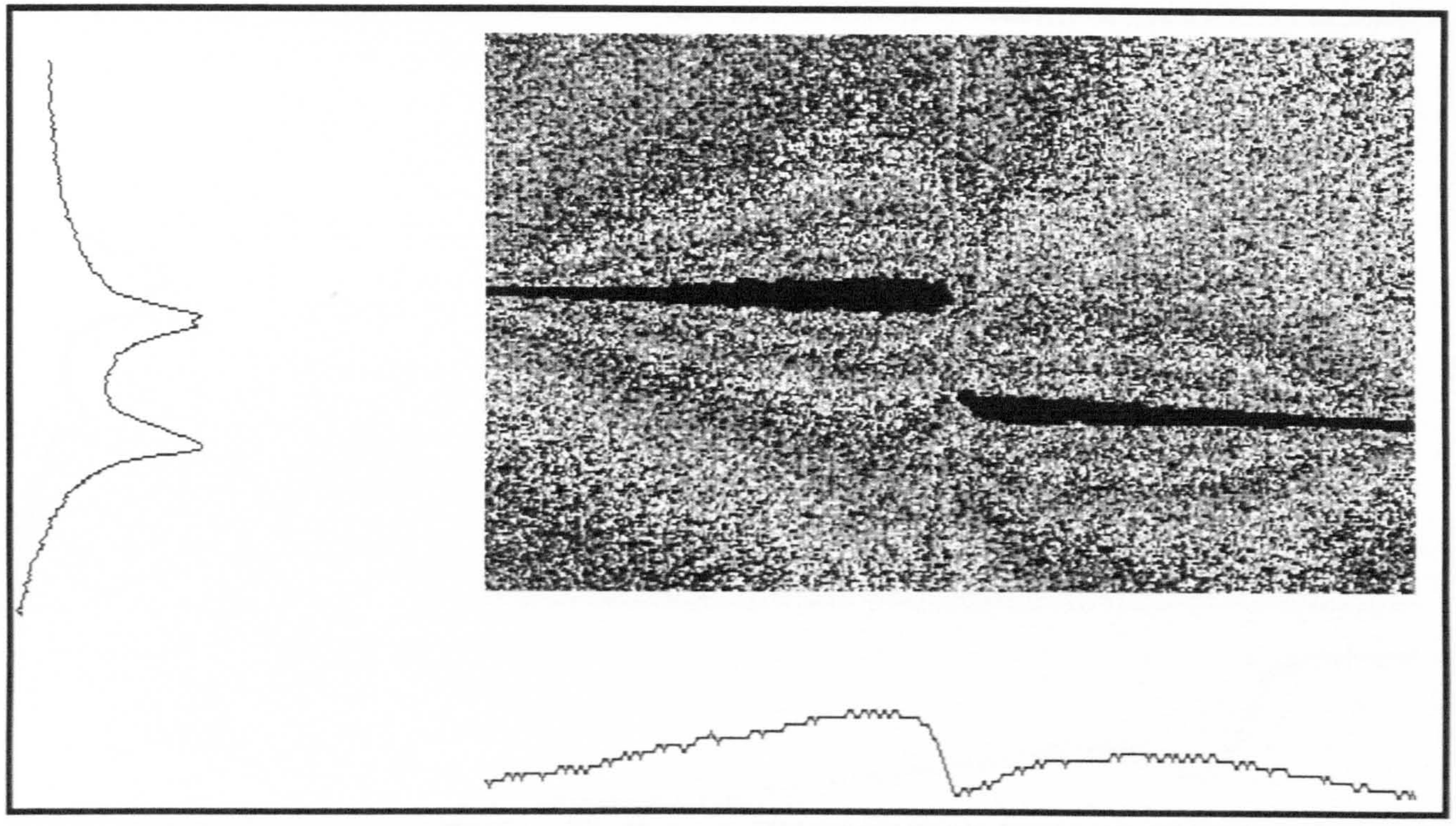

Figure K.2 Typical camera image obtained for a laser line-stripe on a square cut edge.

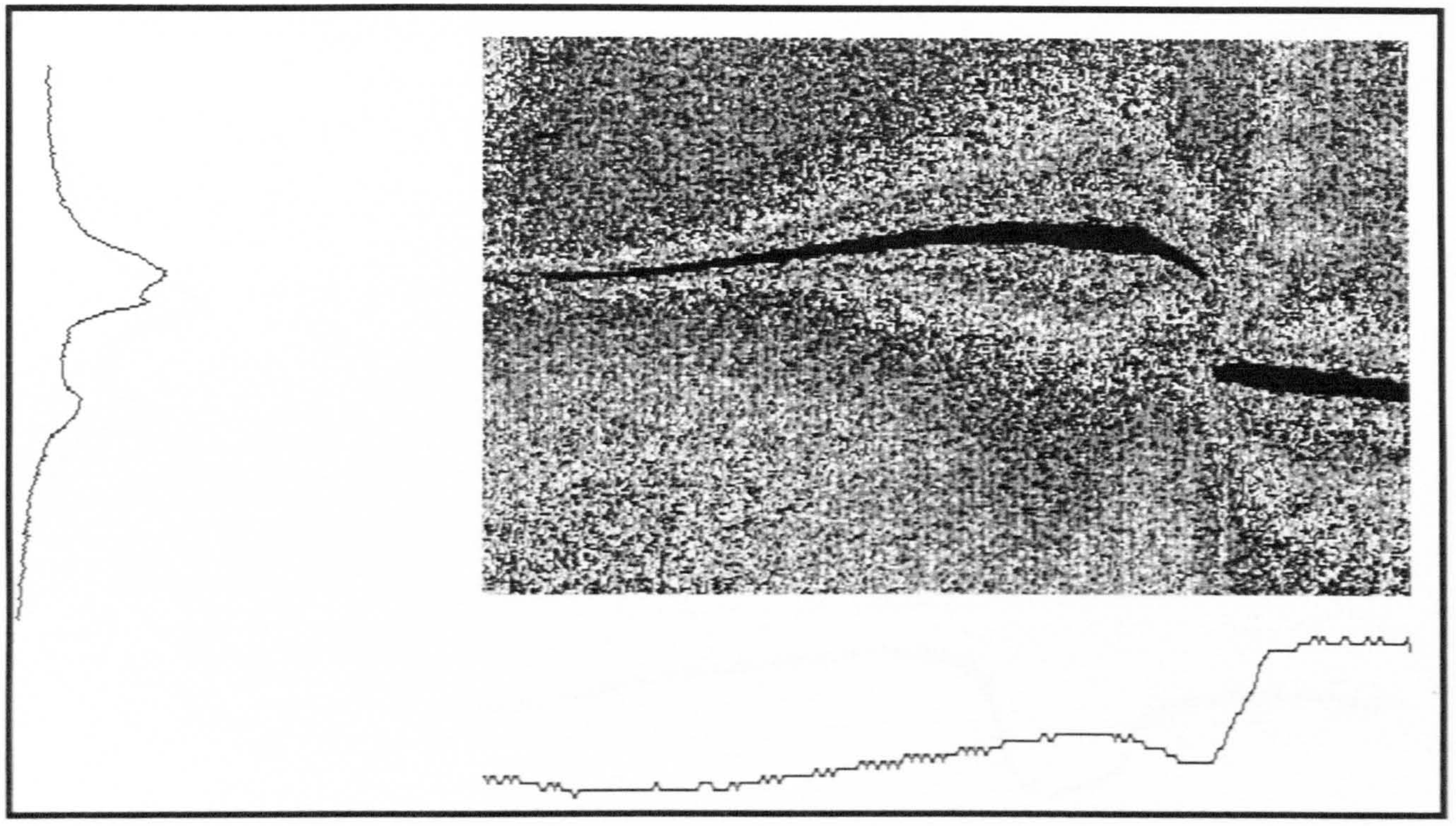

Figure K.3 Typical camera image obtained from a laser line-stripe on a folded edge.

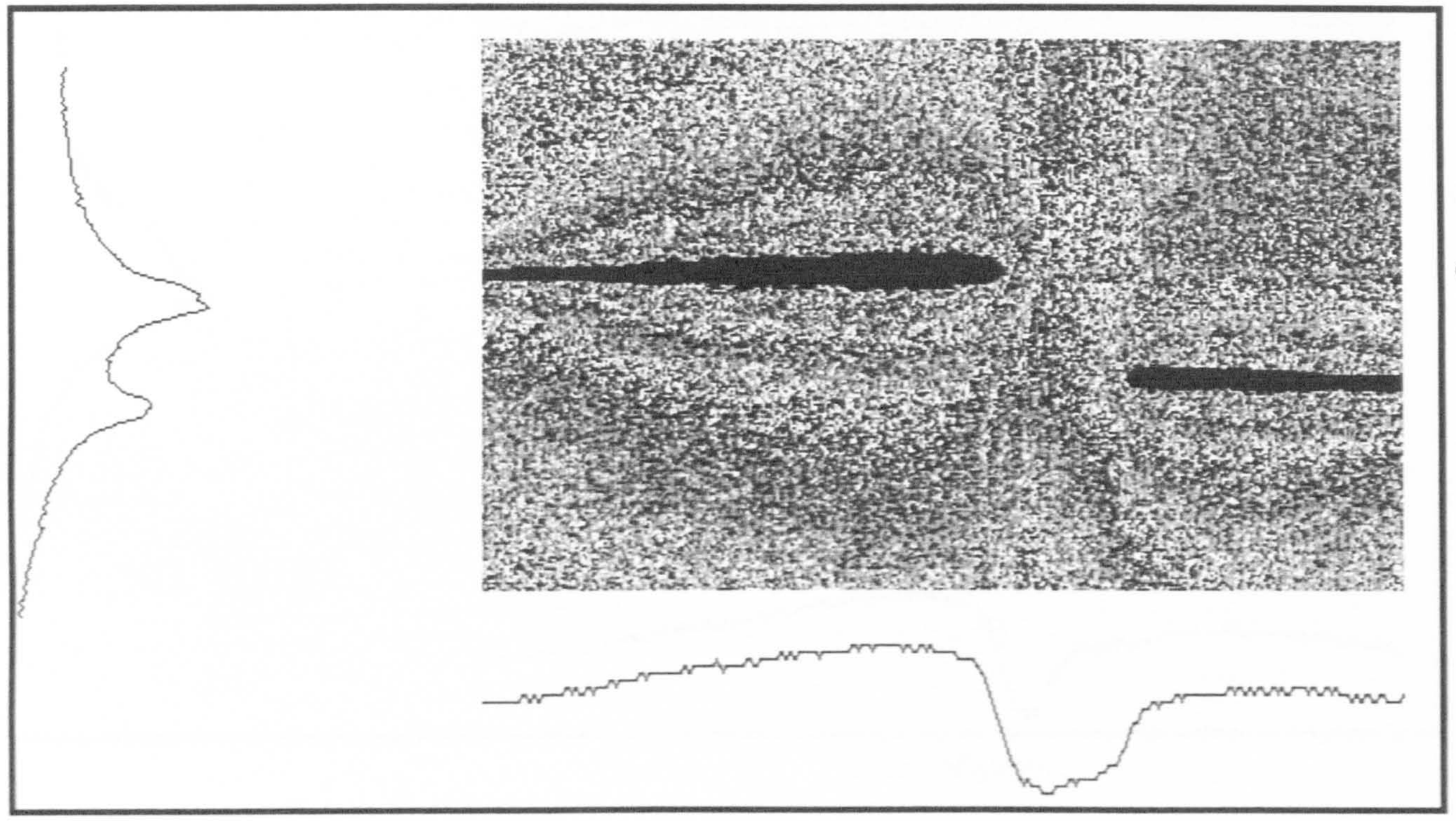

Figure K.4 An example of camera to laser misalignment. Laser crosses the edge from behind.

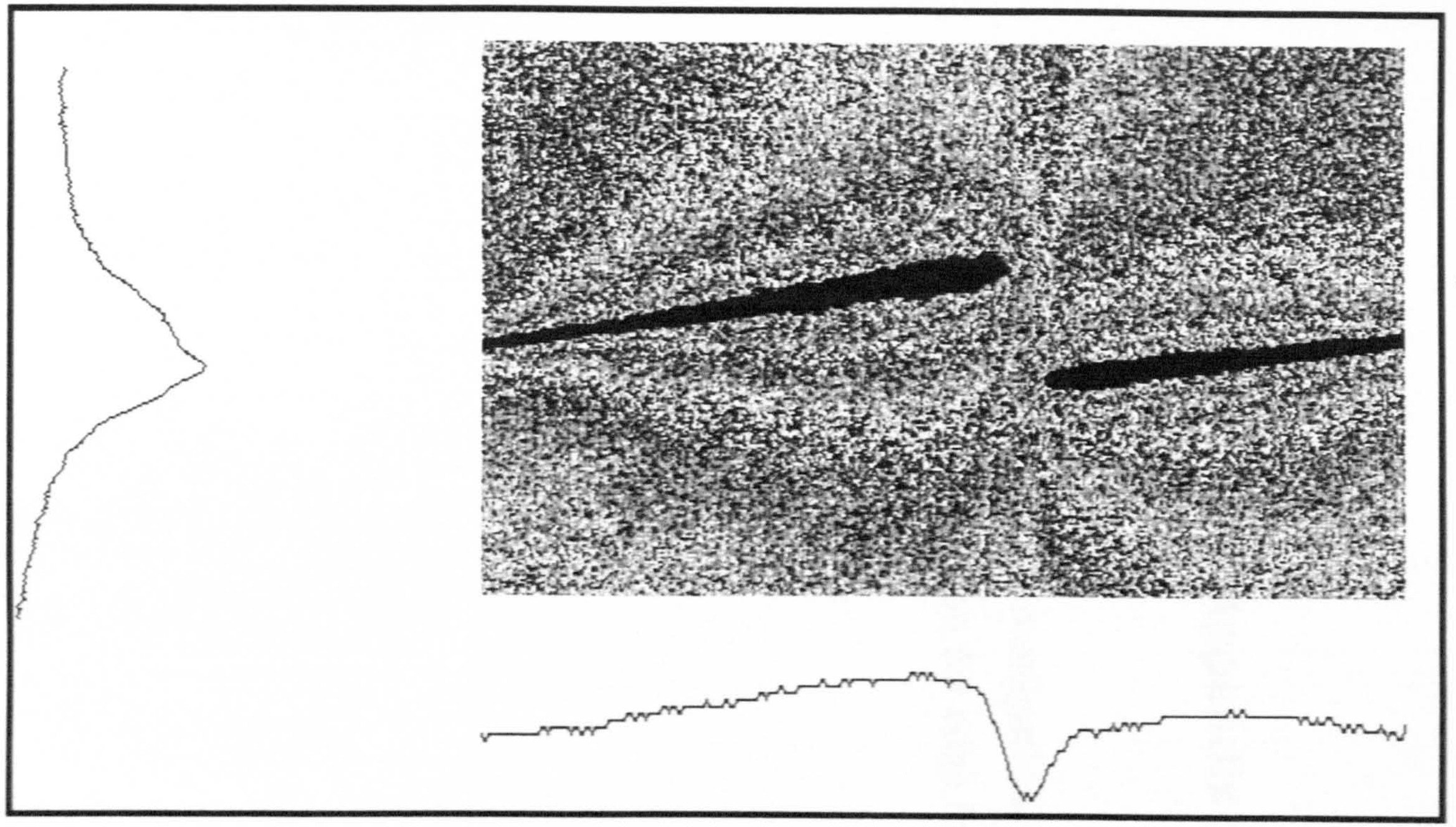

Figure K.5 An example of camera to laser misalignment. Laser and camera axis are not parallel.

Appendix L

Laser line-stripe investigations into characteristic extraction for edge following.

L. Laser line-stripe investigations for edge following.

This appendix contains the processed images of samples 1 to 5 referred to in Chapter 5, Section 5.5.5. These images were taken using screen capture techniques direct from the PC screen and includes the extracted values for :-

- Degree of fold, (pear-shaping)
- Perceived edge position
- True edge position
- Closed fold edge position
- Angle of light roll-off, (α)
- Component misalignment, (M)
- Calculated ellipse parameters (a and b)

All co-ordinate measurements are made with respect to an arbitrary reference position. This was taken for simplicity to be the screen origin, (top-left corner).

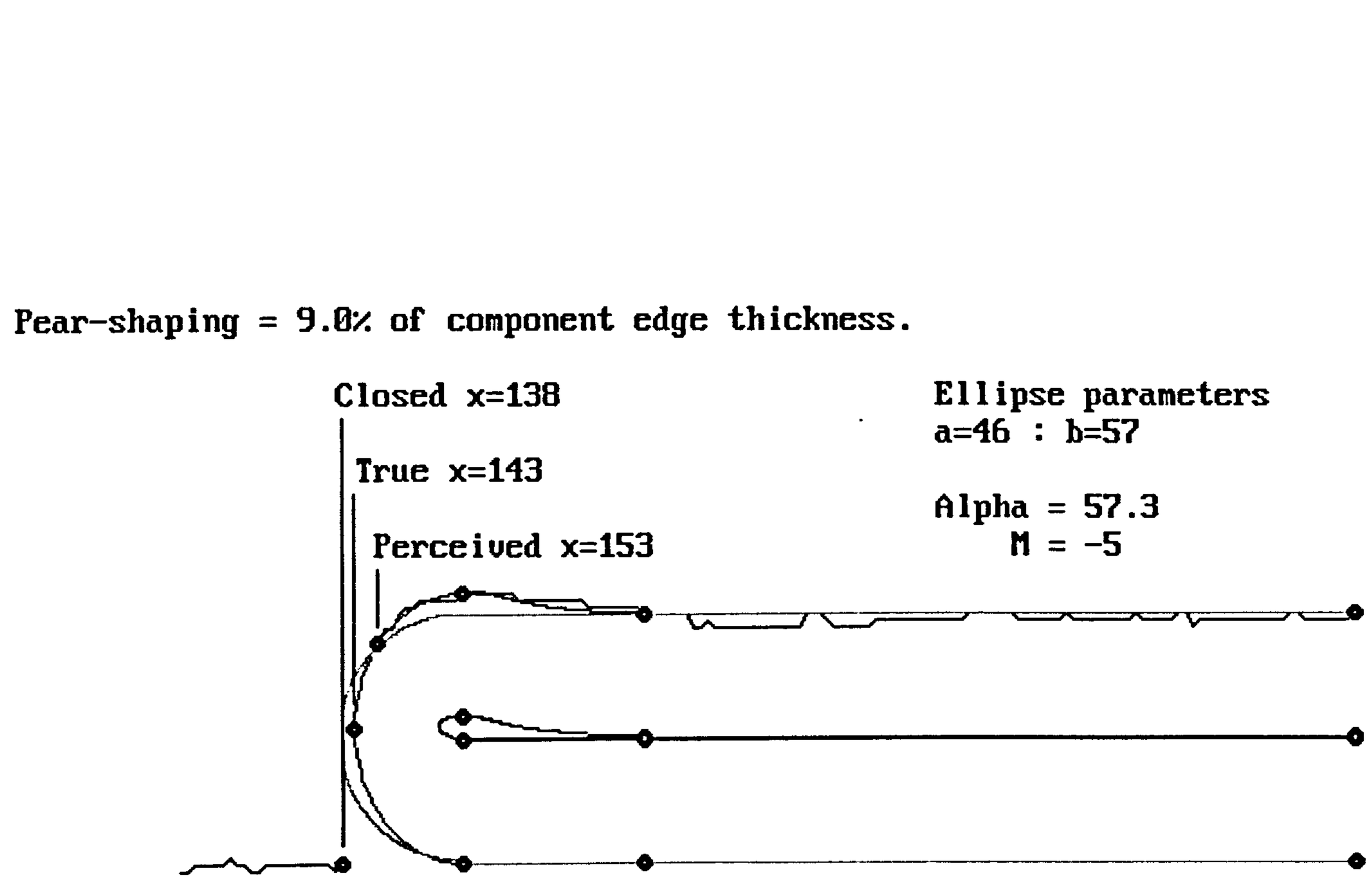

Figure L.1 Laser line-stripe characteristics for sample 1.

Pear-shaping = 15.0% of component edge thickness.

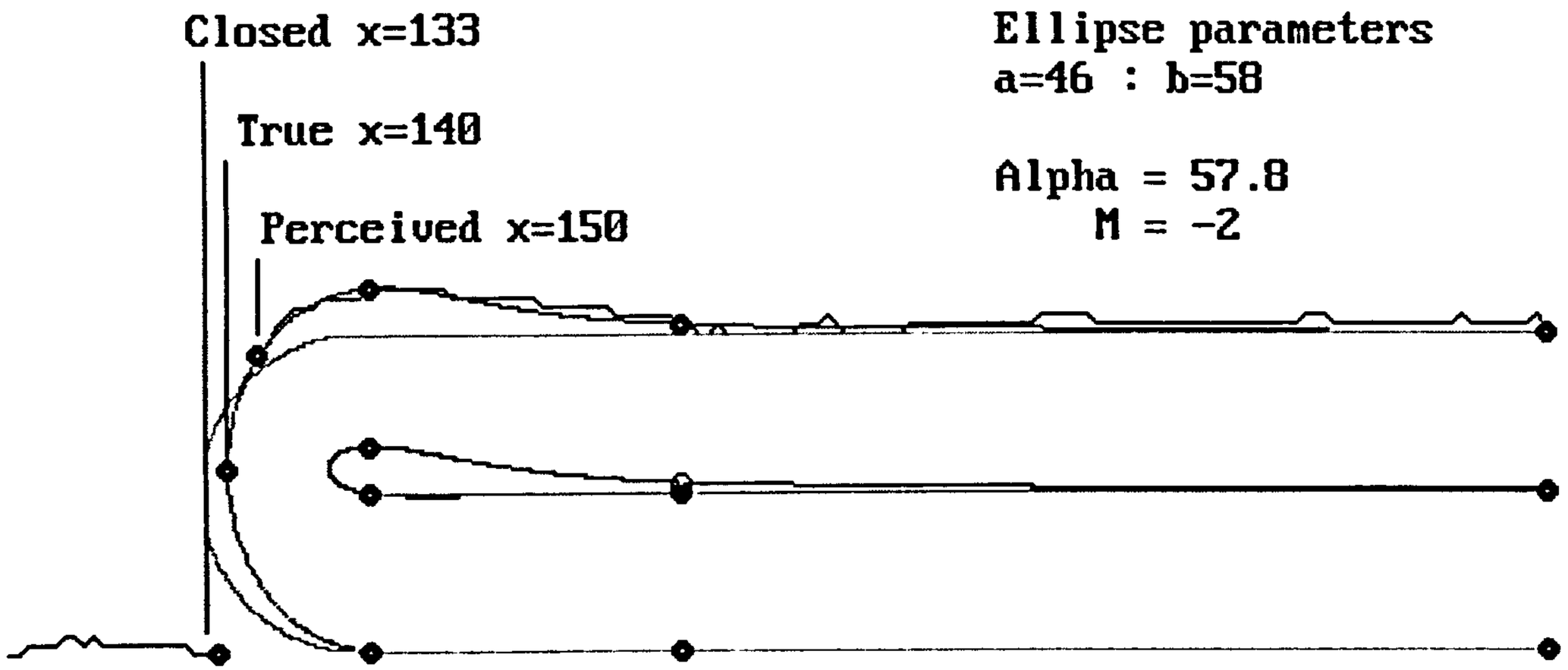

Figure L.2 Laser line-stripe characteristics for sample 2.

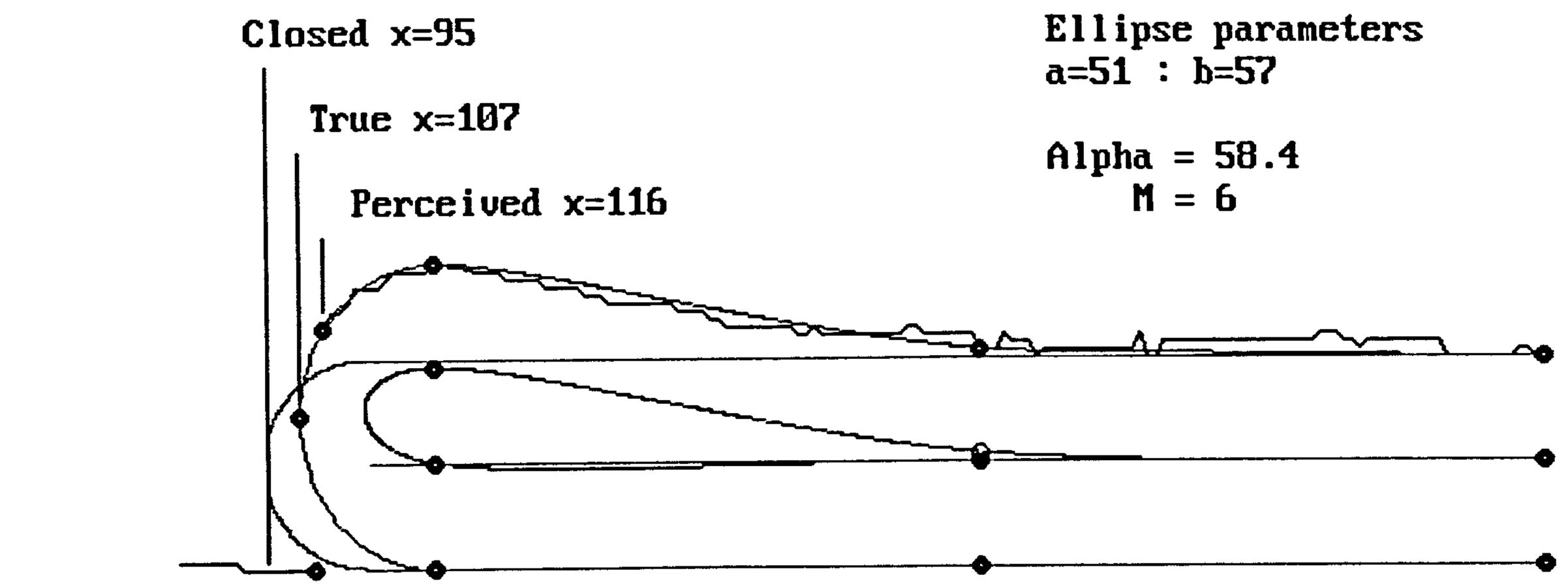

Figure L.3 Laser line-stripe characteristics for sample 3.

Pear-shaping = 15.0% of component edge thickness.

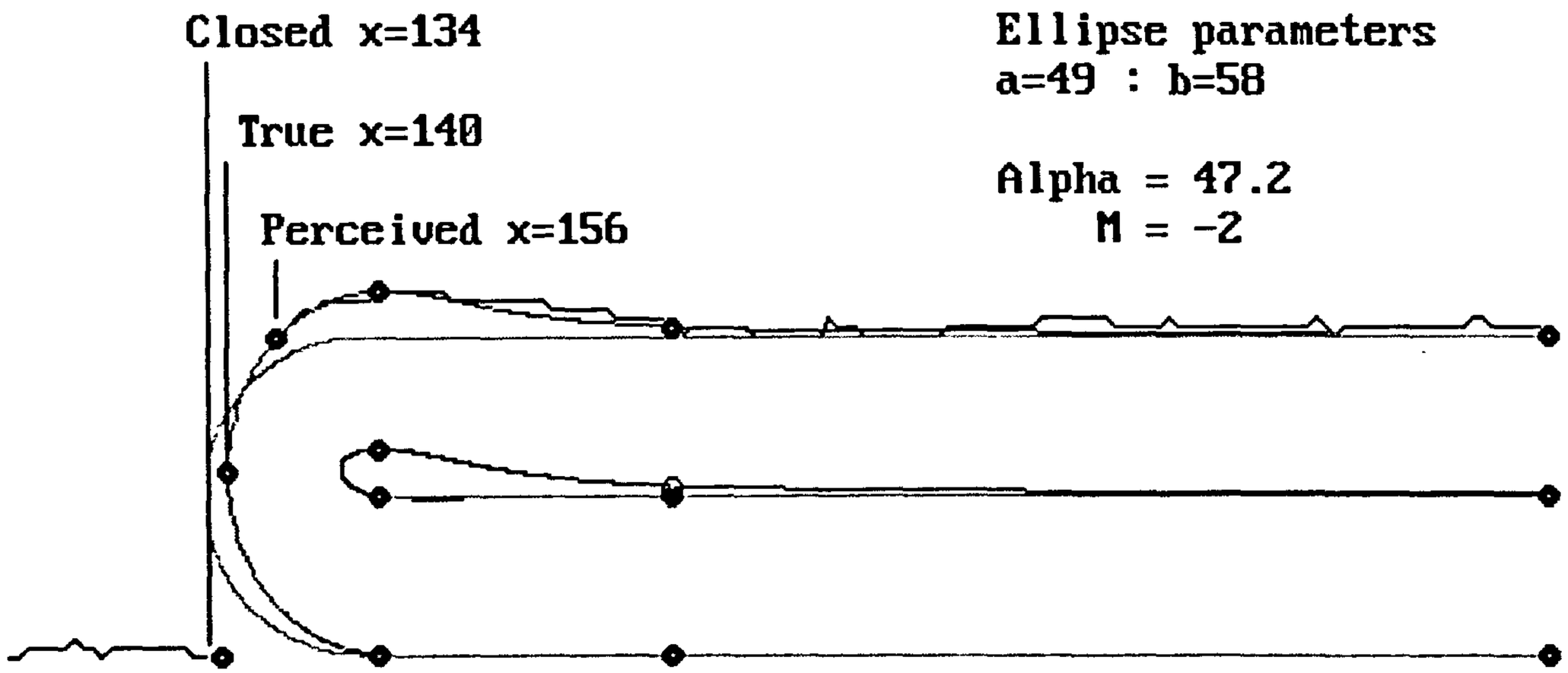

Figure L.4 Laser line-stripe characteristics for sample 4.

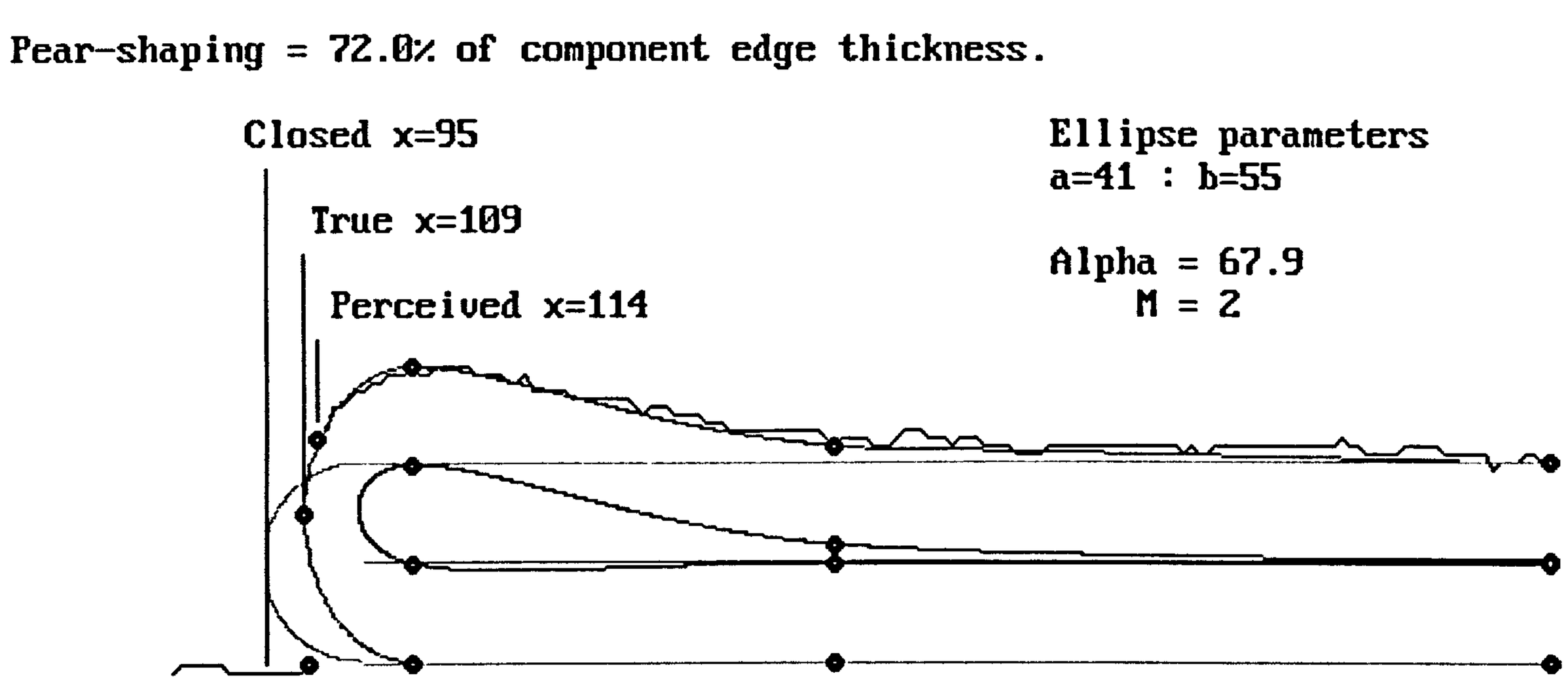

Figure L.5 Laser line-stripe characteristics for sample 5.

Appendix M

3-D Topography for Lasting.

Last alignment

Feature extraction

Profile matching

M.1 3-D Topography for Lasting.

This appendix contains images taken using screen capture techniques. Five samples were supplied by B.U.S.M so as to cover a cross-section of shoe types.

Sample 1: A gentleman's maroon brogue shoe.
Sample 2: A gentleman's black and brown 'slip on' shoe, with decorative tassels.
Sample 3: A gentleman's matt black moccasin style shoe.
Sample 4: A light blue maids sandal.
Sample 5: A youths black sports boot.

M.2 Angular correction for last misalignment.

This section contains results of angular correction discussed in Section 6.1.2 for samples 2-5. Sample 1 is included in Chapter 6, Figure 6.3, as the worked example.

Table M.1 contains a summary of the last angles measured before and after processing.

Sample	Perceived last angle	Corrected last angle
1	8.12°	0.00°
2	1.99°	0.00°
3	-0.74°	0.00°
4	3.27°	0.00°
5	6.91°	0.01°

Table M.1 Summary of results for angular correction. Samples 1-5.

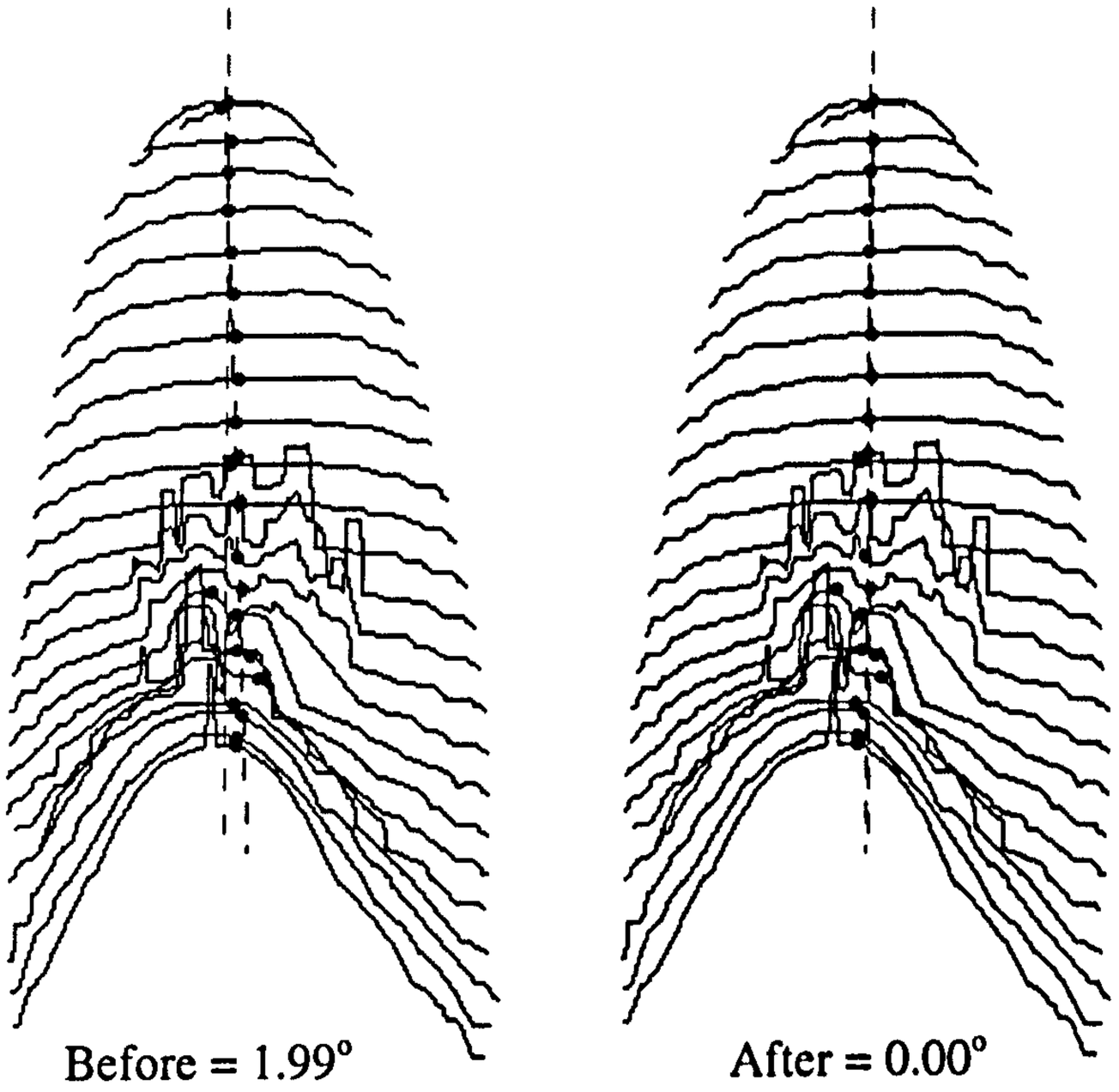

Figure M.1 Sample 2, before and after angular correction.

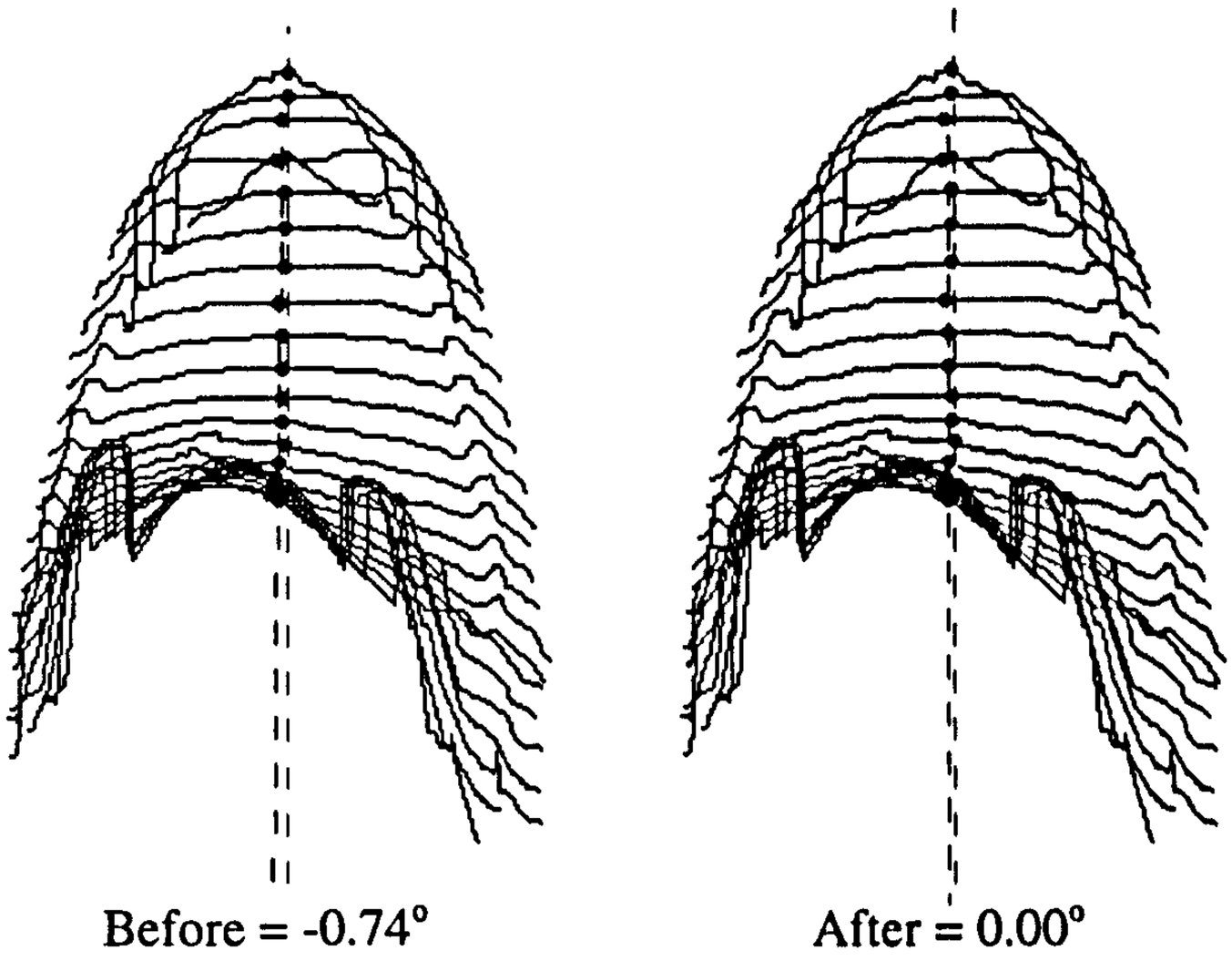

Figure M.2 Sample 3, before and after angular correction.

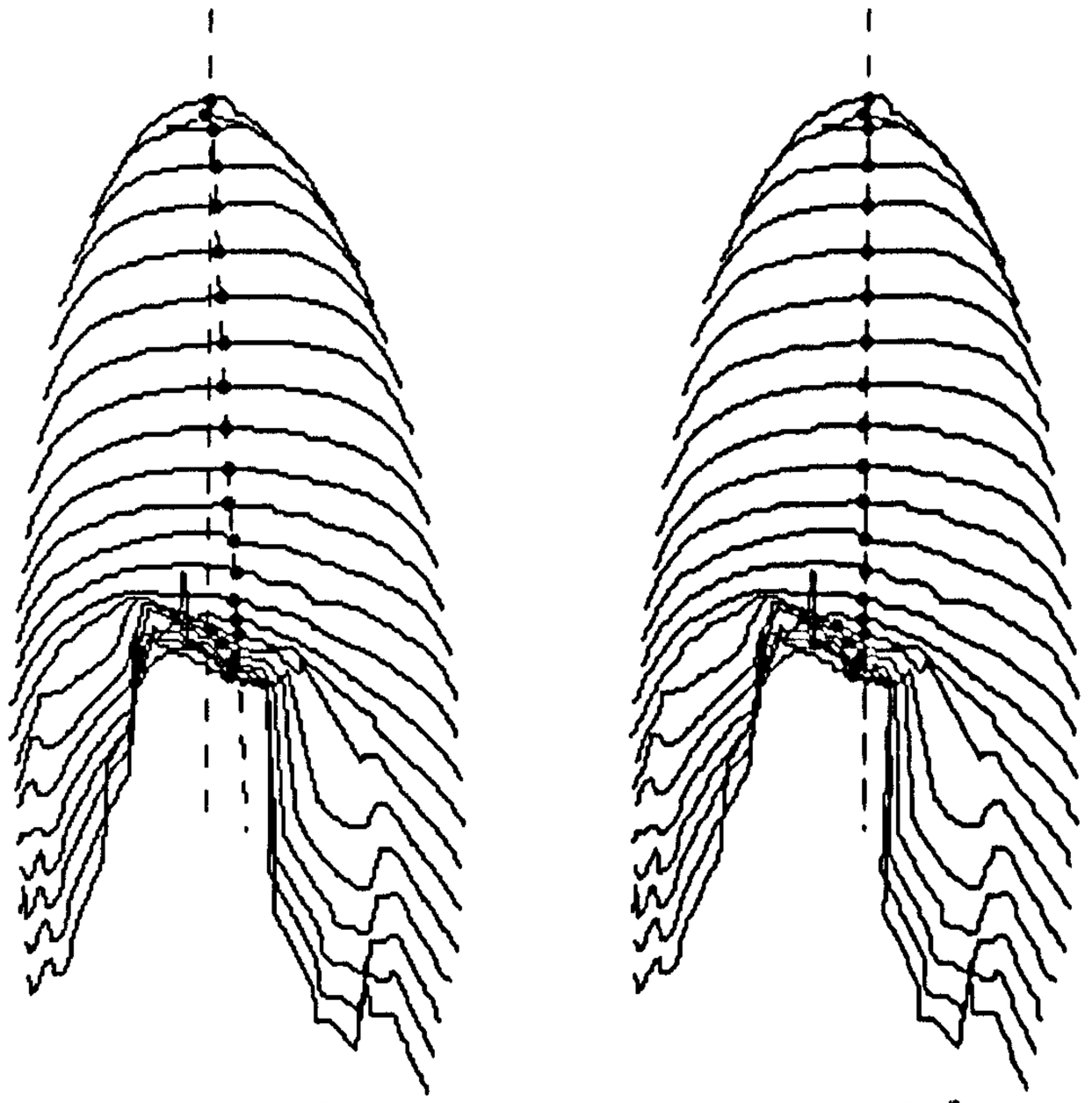

Figure M.3 Sample 4, before and after angular correction.

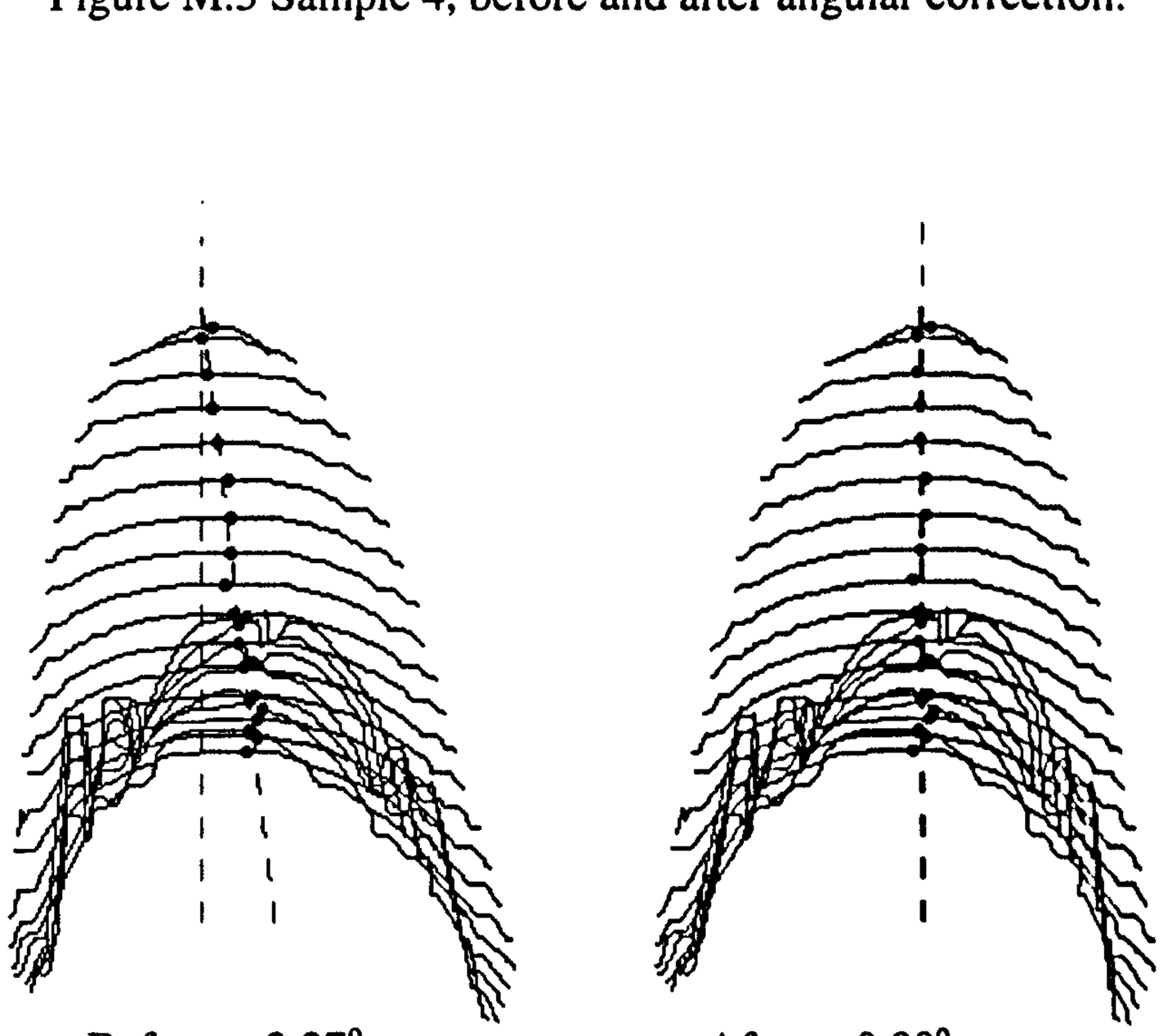

Figure M.4 Sample 4, before and after angular correction.

M.3 Feature extraction.

This section contains the results of performing full feature extraction, as discussed in Chapter 6, on shoe samples 1-5. (Sample 3, is included in Chapter 6 as Figure 6.5).

Sample 1, contains no features over the forepart of the upper, as shown by a score count of 1. The features that make a brougue style shoe can be seen by careful examination of the figure. However these features are too faint to be extracted by the processing methods implemented here. If the camera resolution was increase to, 2048 x 2048 pixels, it may be possible to produce algorithms capable of detecting these features.

Sample 2, demonstrates how decorative features can significantly effect obtainable results. The tassles are not well defined and can vary considerably in position from shoe to shoe. The score count indicates that this shoe is a 'slip on' in style by returning to 1 after line-stripe number 20.

Sample 3 provided the best results obtained using this form of processing. The ridge around the forepart of the shoe has been clearly extracted. It is the position of this ridge that would be used in lasting and as such the extracted information is of value.

Sample 4 also provides information that could be used to automate lasting of this kind of shoe. In contrast to sample 2, the ridge is created by the edge of the upper exposing the last below.

Sample 5, the sports boot, like that of the brogue sample provides very little information. The features extracted are those of the lacing wings and the padded tongue.

Scores

25) 3
24) 3
23) 3
22) 3
21) 3
20) 1
19) 1
18) 1
17) 1
16) 1
15) 1
14) 1
13) 1
12) 1
11) 1
10) 1
9) 1
8) 1
7) 1
6) 1
5) 1
4) 1
3) 1
2) 1
1) 1

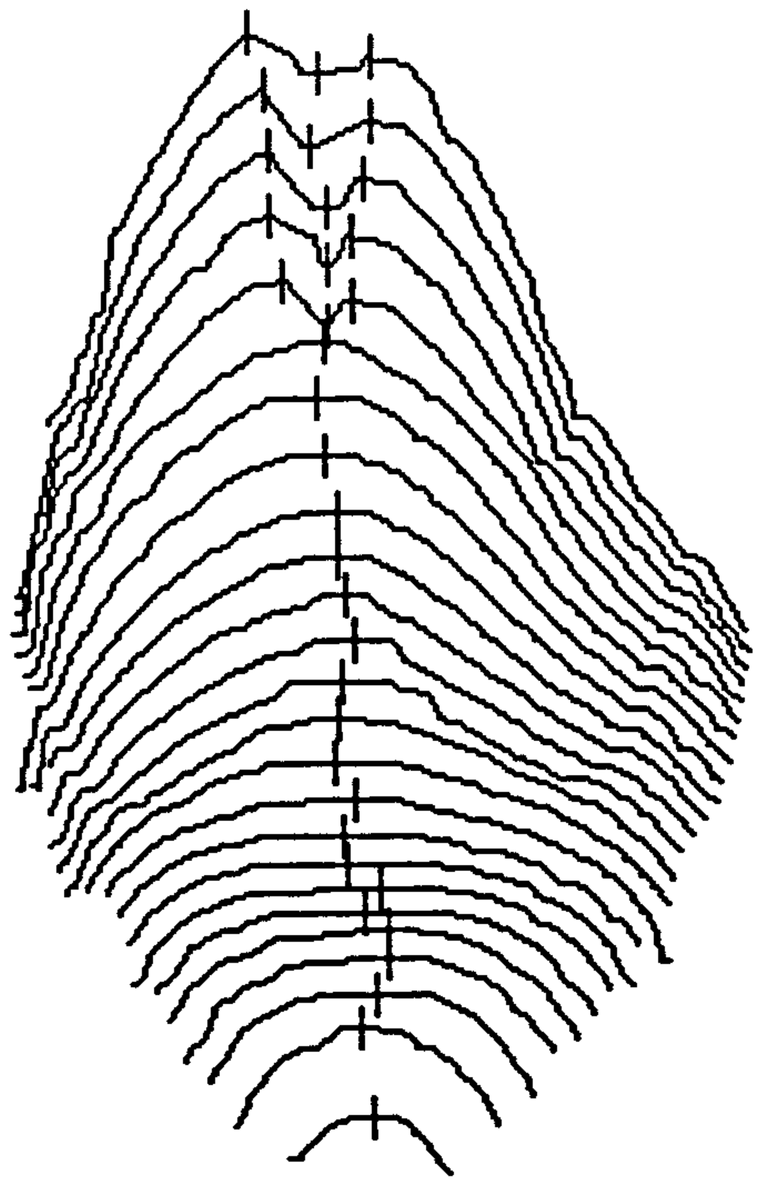

3-D view of upper

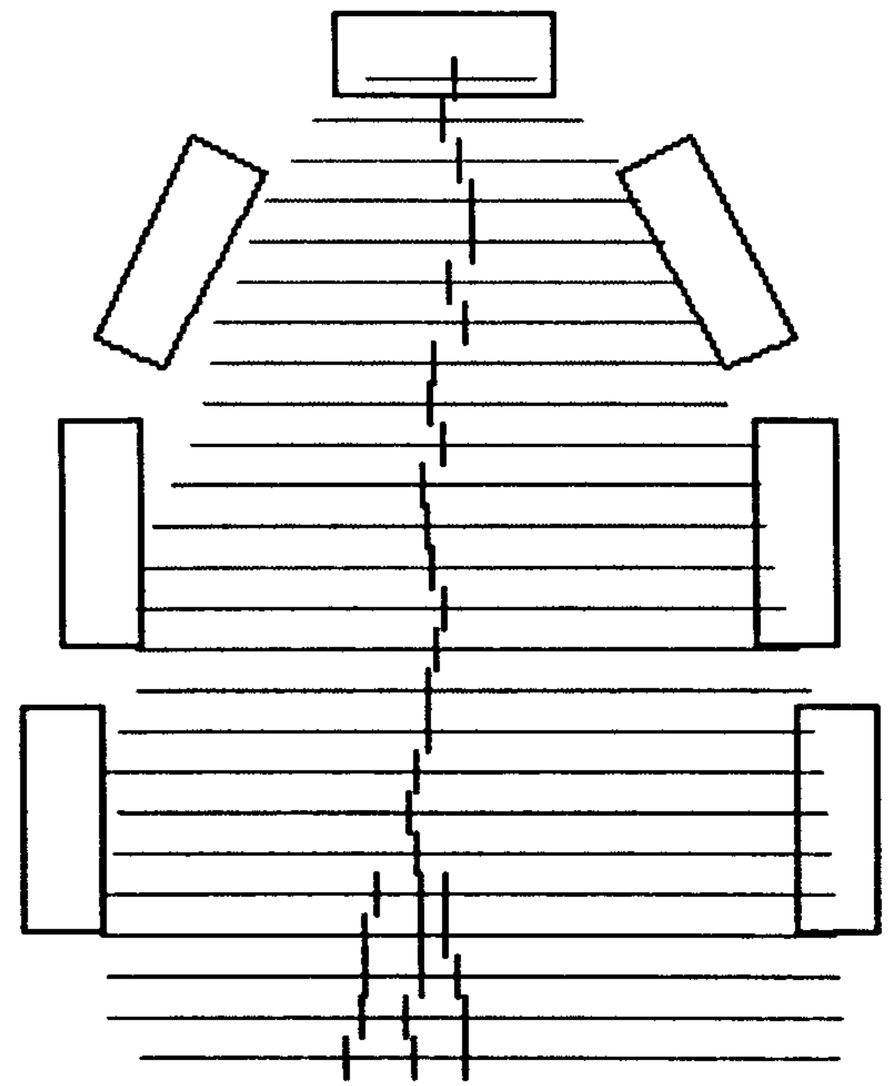

Lasting plan view

Figure M.5 Sample 1 with full feature extraction.

Scores

25) 1
24) 1
23) 1
22) 1
21) 1
20) 1
19) 3
18) 3
17) 3
16) 5
15) 7
14) 7
13) 5
12) 1
11) 1
10) 1
9) 1
8) 1
7) 1
6) 1
5) 1
4) 1
3) 1
2) 1
1) 0

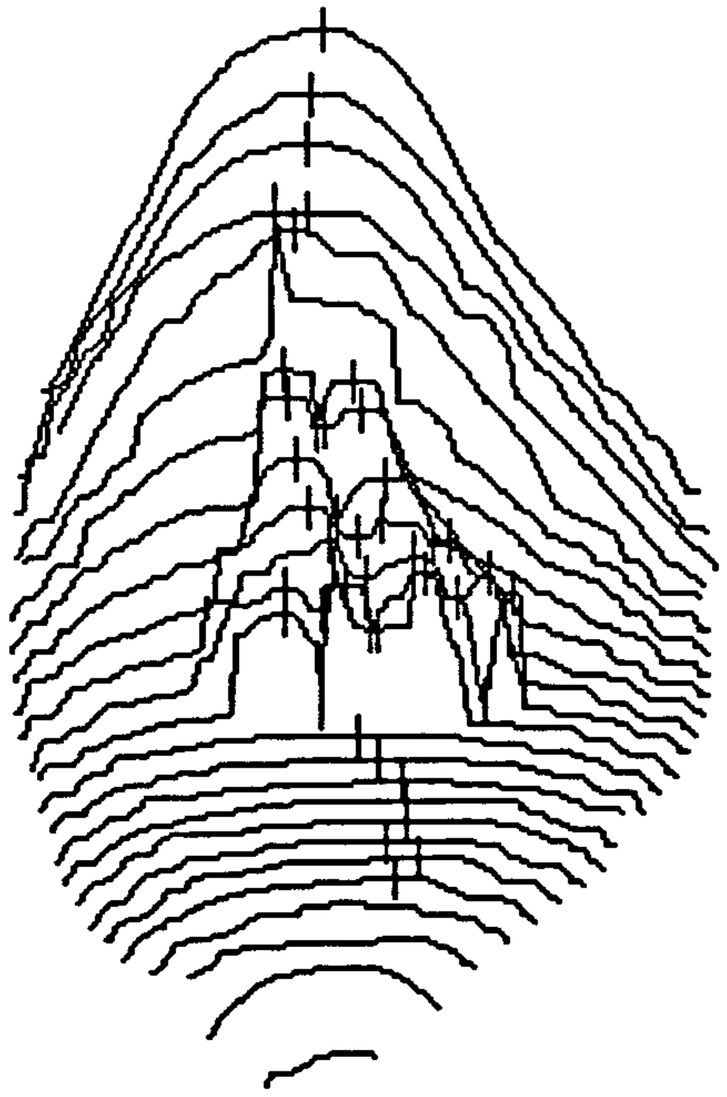

3-D view of upper

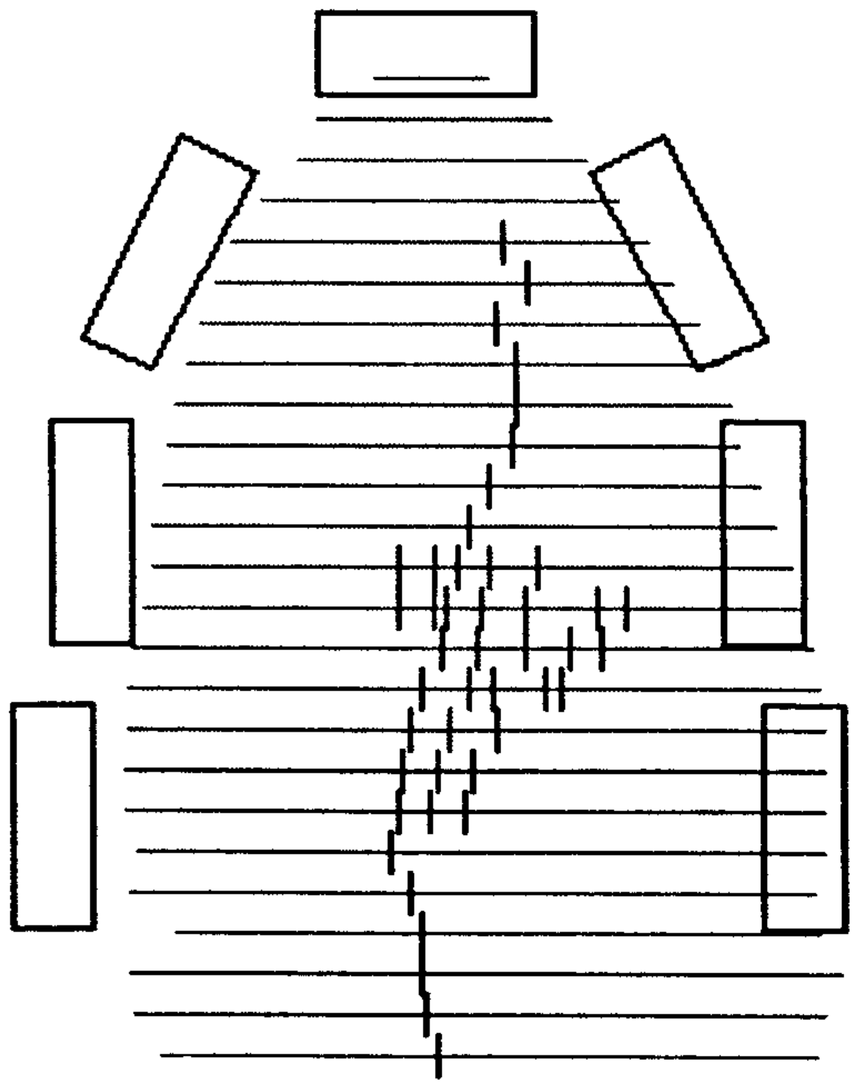

Lasting plan view

Figure M.6 Sample 2 with full feature extraction.

Scores

23) 6
22) 4
21) 6
20) 6
19) 4
18) 6
17) 2
16) 1
15) 1
14) 1
13) 3
12) 1
11) 1
10) 1
9) 1
8) 1
7) 1
6) 1
5) 1
4) 1
3) 1
2) 1
1) 1

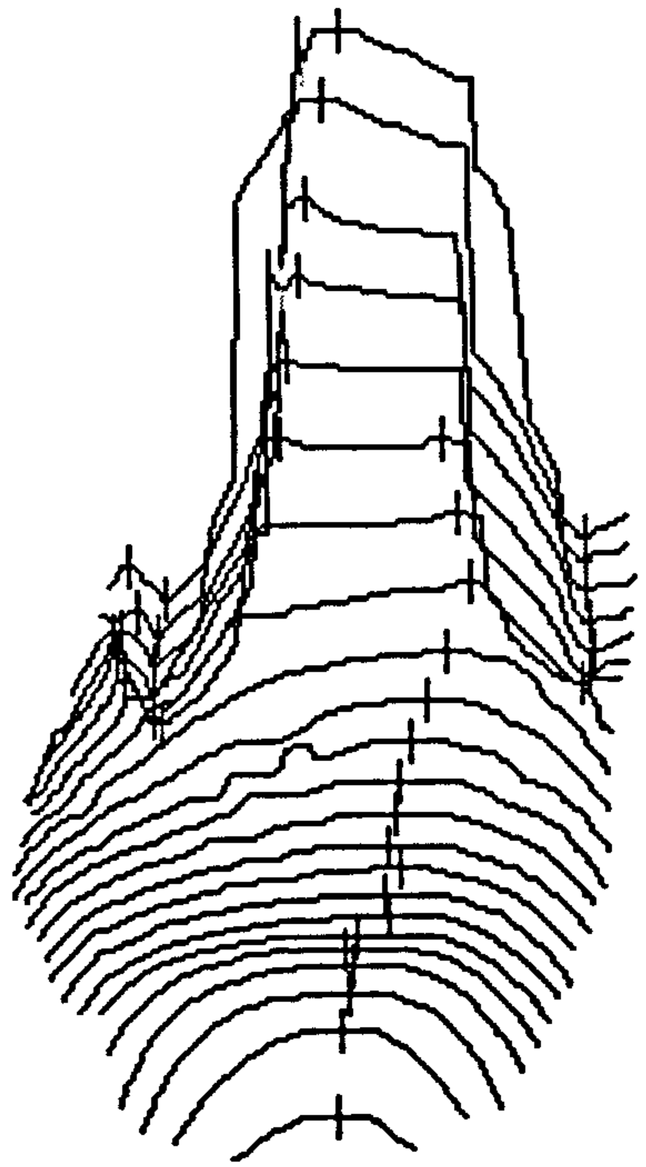

3-D view of upper

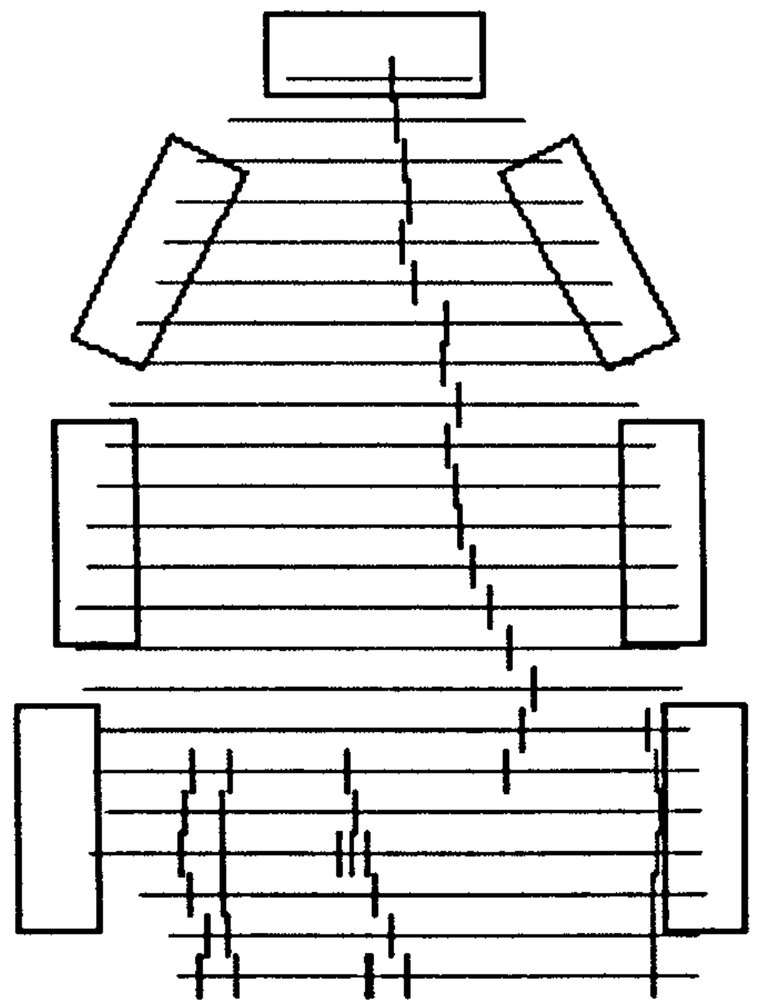

Lasting plan view

Figure M.7 Sample 4 with full feature extraction.

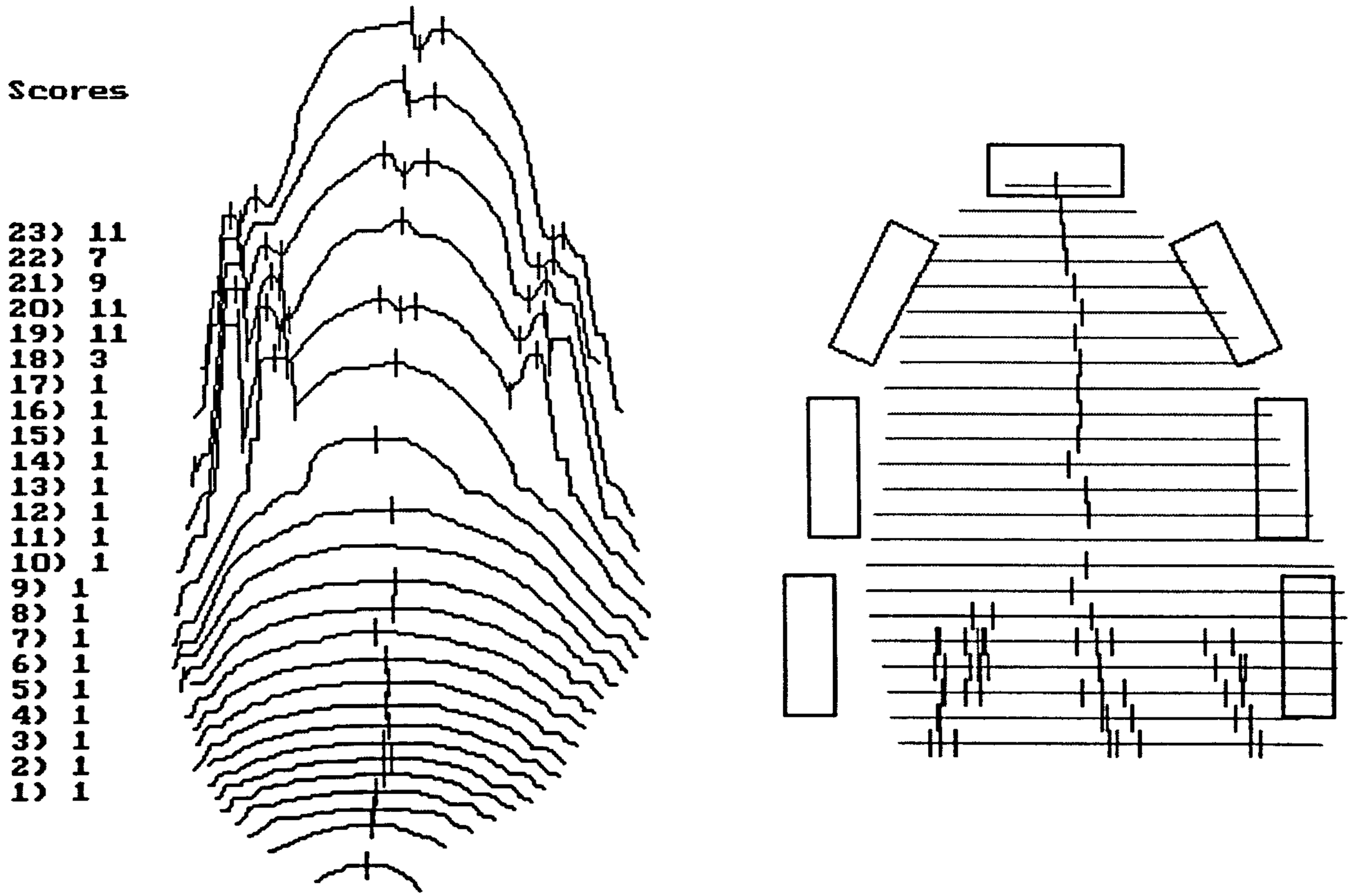

3-D view of upper

Lasting plan view

Figure M.8 Sample 5 with full feature extraction.

M.4 Profile matching.

This section contains the results of performing alignment matching on selected line-stripe images as discussed in Chapter 6. Four examples are included here to highlight the various effects observed when testing this method.

Figure M.9, shows a good match between the template data, (sample 2), and that of a second shoe of the same type. This result is as would be expected due to the same styles being compared.

Figure M.10, compares sample 2 with sample 3. Even though different shoe styles are used, there is still a strong match. The additional feature of the ridge in the specimen stripe, (sample 3), have been overpowered by their similarity in basic form.

Figure M.11, demonstrates the effects observed when similar styles of different feet are compared. Here there is little or no similarity as the form of the stripe is mirrored.

Figure M.12, shows the result of comparing sample 4 with sample 3, two very different shoe types. The results show no match between the samples

The use of characteristic matching as a mechanism for determining parameters to enable automated lasting is limited. This is shown by the effects demonstrated by Figures M.10 and discussed in Chapter 6. However, this method does appear to be able to differentiate between styles of differing types. As a result it may be of value in automating the selection of a template by matching a presented style with those already taught. It may therefore still have a value in the automation process.

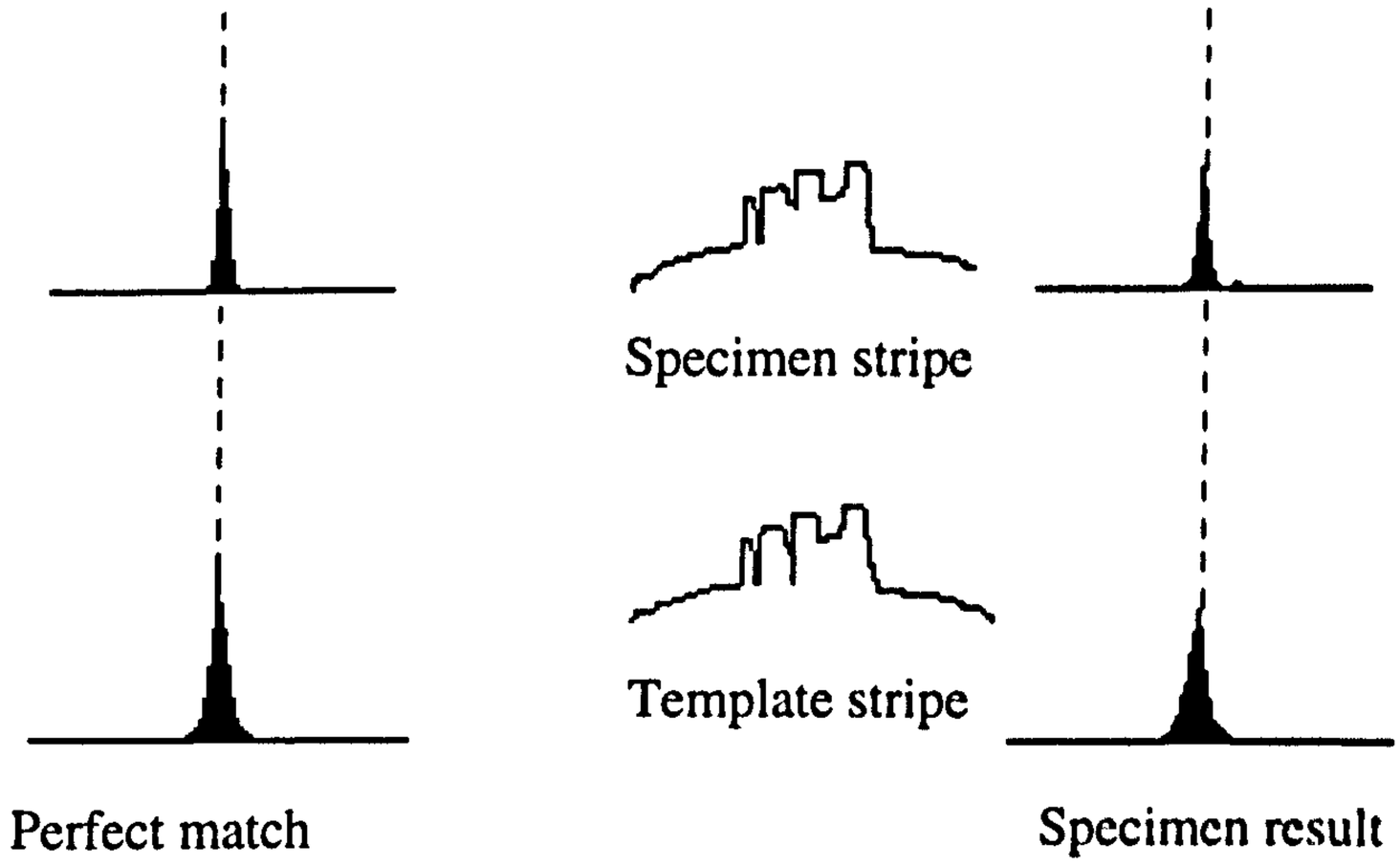

Figure M.9 Sample 2 compared with similar (stripe number 13)

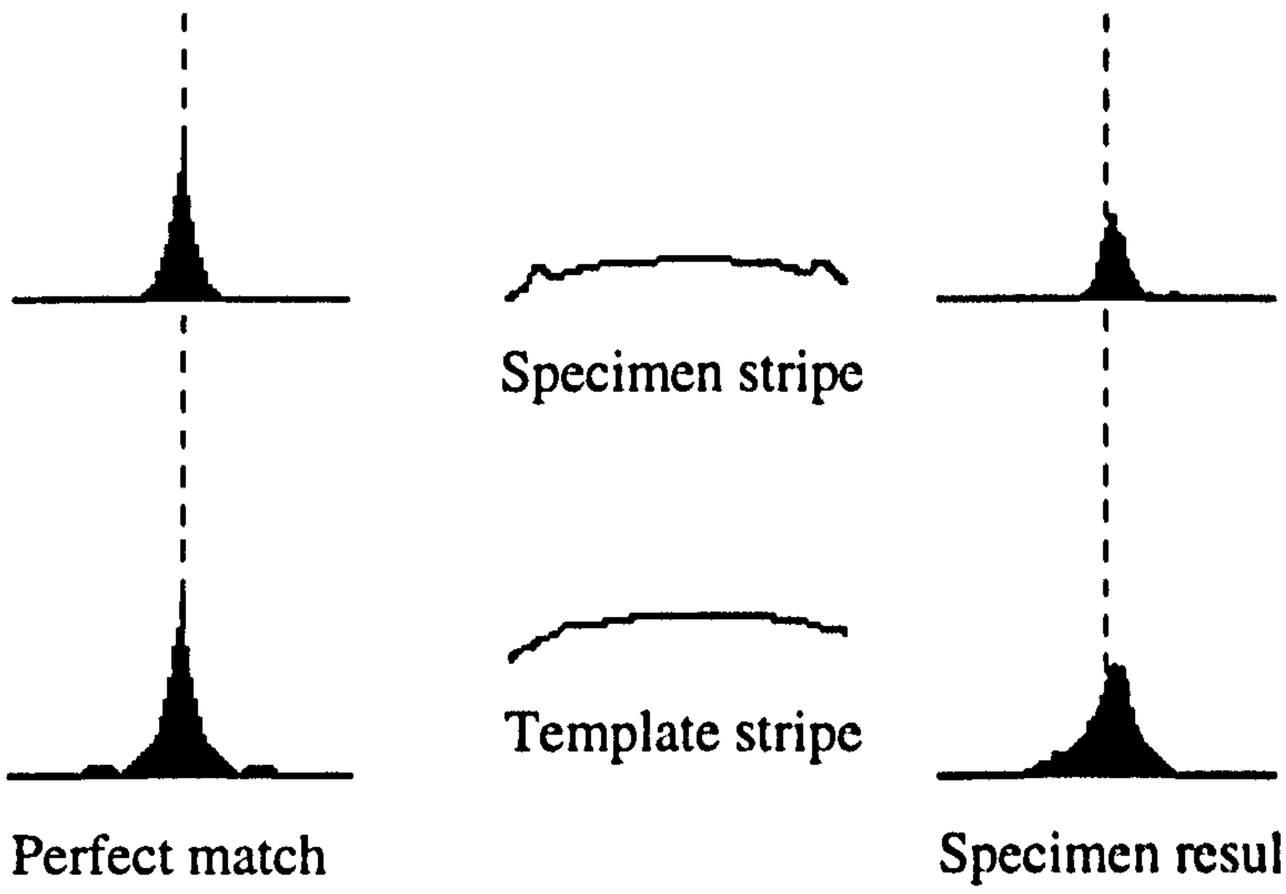

Figure M.10 Sample 3 compared with Sample 2, (stripe number 10).

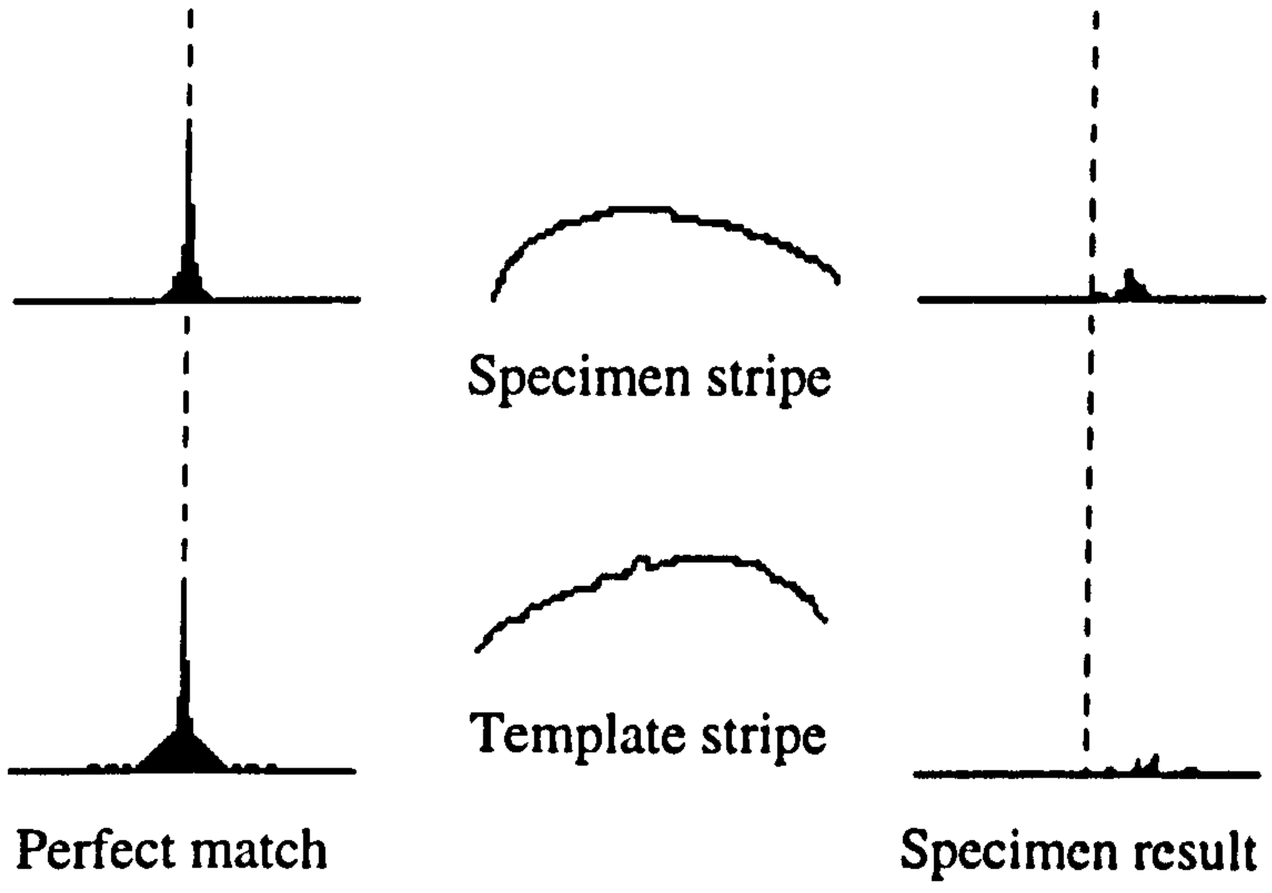

Figure M.11 Sample 4 compared with similar left foot (stripe number 13)

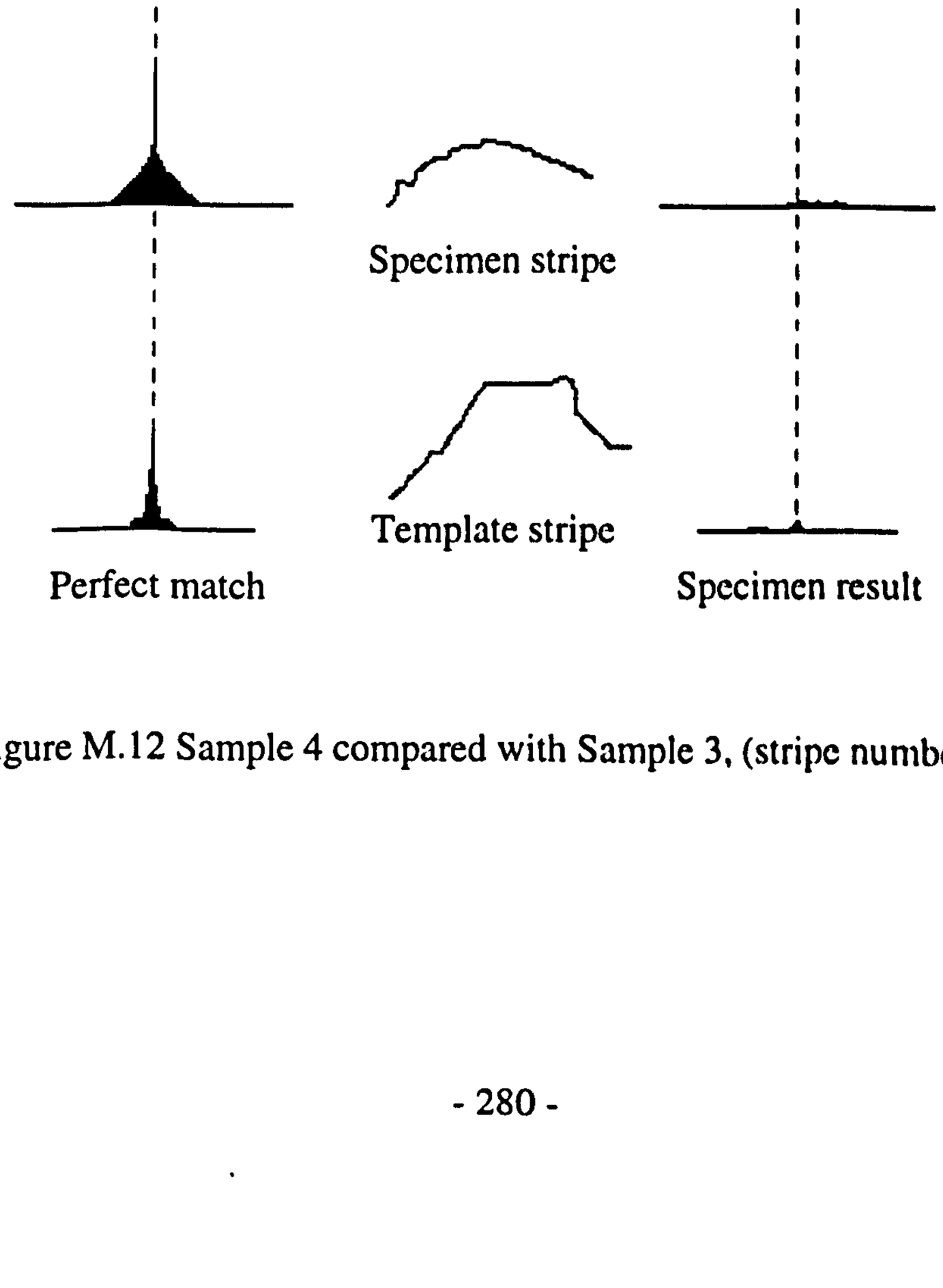

Figure M.12 Sample 4 compared with Sample 3, (stripe number 17).

Appendix N

3-D Topography.

Effects of point locking

Depth information extraction

Sole contour extraction

N.1 Effects of point locking.

This section contains examples of the results obtained whilst investigating the effects of point locking as described in Section 6.2.3. When the distance between and extracted point and its interpolated position, derived using cubic splines from the surrounding points, is within an experimentally determined tolerance then the point can be locked to ensure it is not moved by future iterations.

It can be seen from Figures N.1, 3, 5, where point locking is applied, that despite varying the degree of correction, how far an erroneous point is moved towards the its interpolated position, the processed result remains true to the original overall profile. However, in Figures N.2, 4 ,6 where point locking is disabled, as the degree by which an erroneous point is corrected increases so the overall profile becomes distorted. This is due to even correct points being moved to produce an ever increasingly smooth profile.

The best results seem to occur when point locking is implemented in conjunction with 50% error correction.

N.2 Depth information extraction.

This section contains example depth profiles extracted from samples supplied by B.U.S.M. Figures N.7-10 contain profiles extracted from the base of a lasted shoe, whilst Figures N.11-12 show examples of depth profiles extracted from soles.

The same mechanism for erroneous point correction has been applied to these images as that described for sole profile extracted. However, as the centre region of the

insole is fairly well defined no significant enhancements were obtained. Consequently for this type of measurement the raw extracted data may provide sufficient information for control purposes without the need for further processing.

N.3. Sole contour extraction.

This section contains examples of contour maps extracted for three styles of sole.

Figure N.13 shows a simple man's sole incorporating minimal grip and a significant heel height of approximately 25mm.

Figure N.14 contains an image of a lady's gym type sole. The sole is generally smooth with a slight heel.

Figure N.15 once again is of a man's sole. This time is has a high degree of grip in addition to a significant heel height 30mm. It can be seen from the image that the grip is restricted to the central region of the sole, the outer rim remaining smooth. In addition the heel support ridges can be seen.

Note.

All these images were obtained using screen capture techniques from the author's purpose written software.

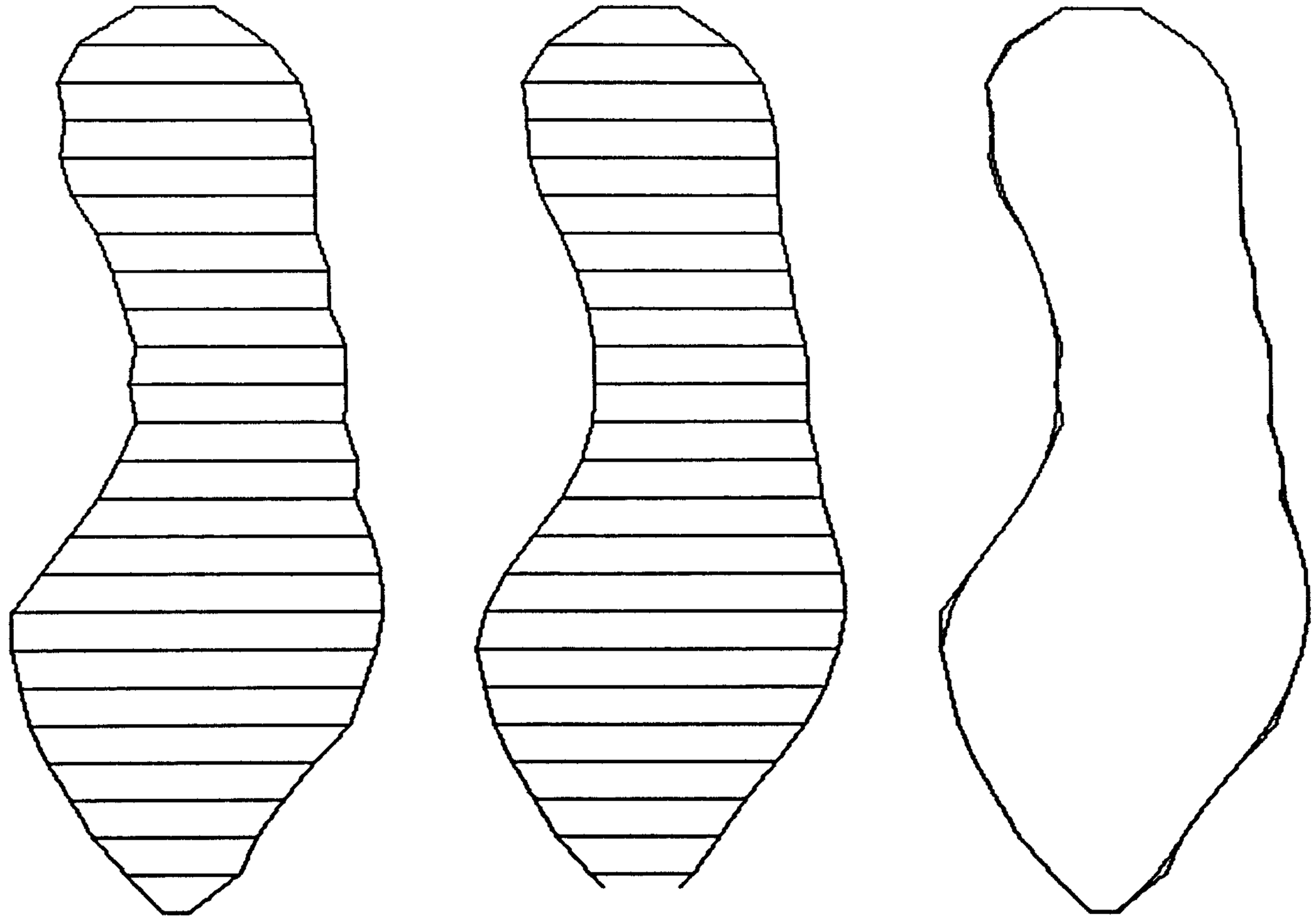

Before processing | After processing | Overlaid profiles

Figure N.1 Sample 1 with correction at 25% and Lock ON.

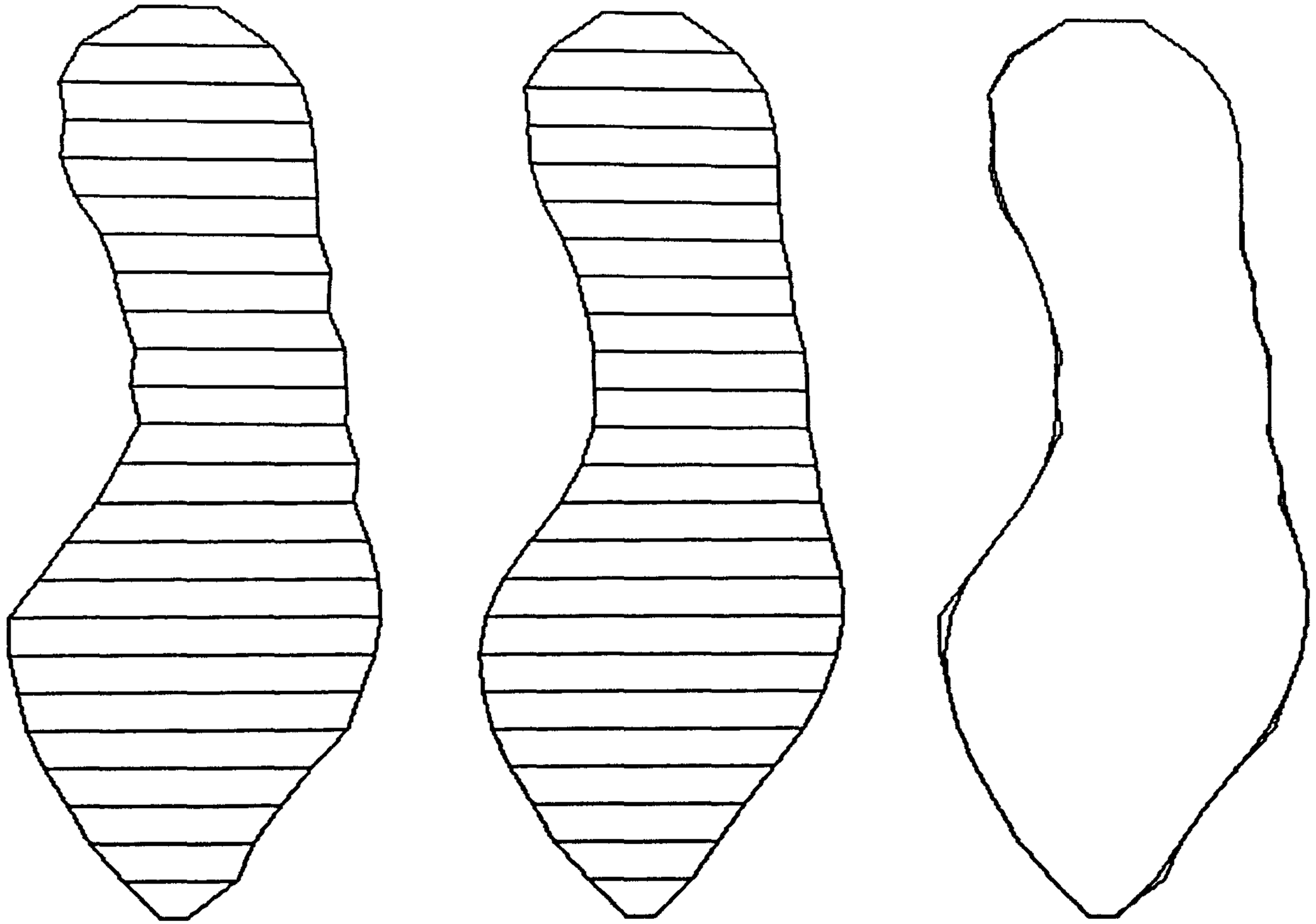

Before processing | After processing | Overlaid profiles

Figure N.2 Sample 1 with correction at 25% and Lock OFF.

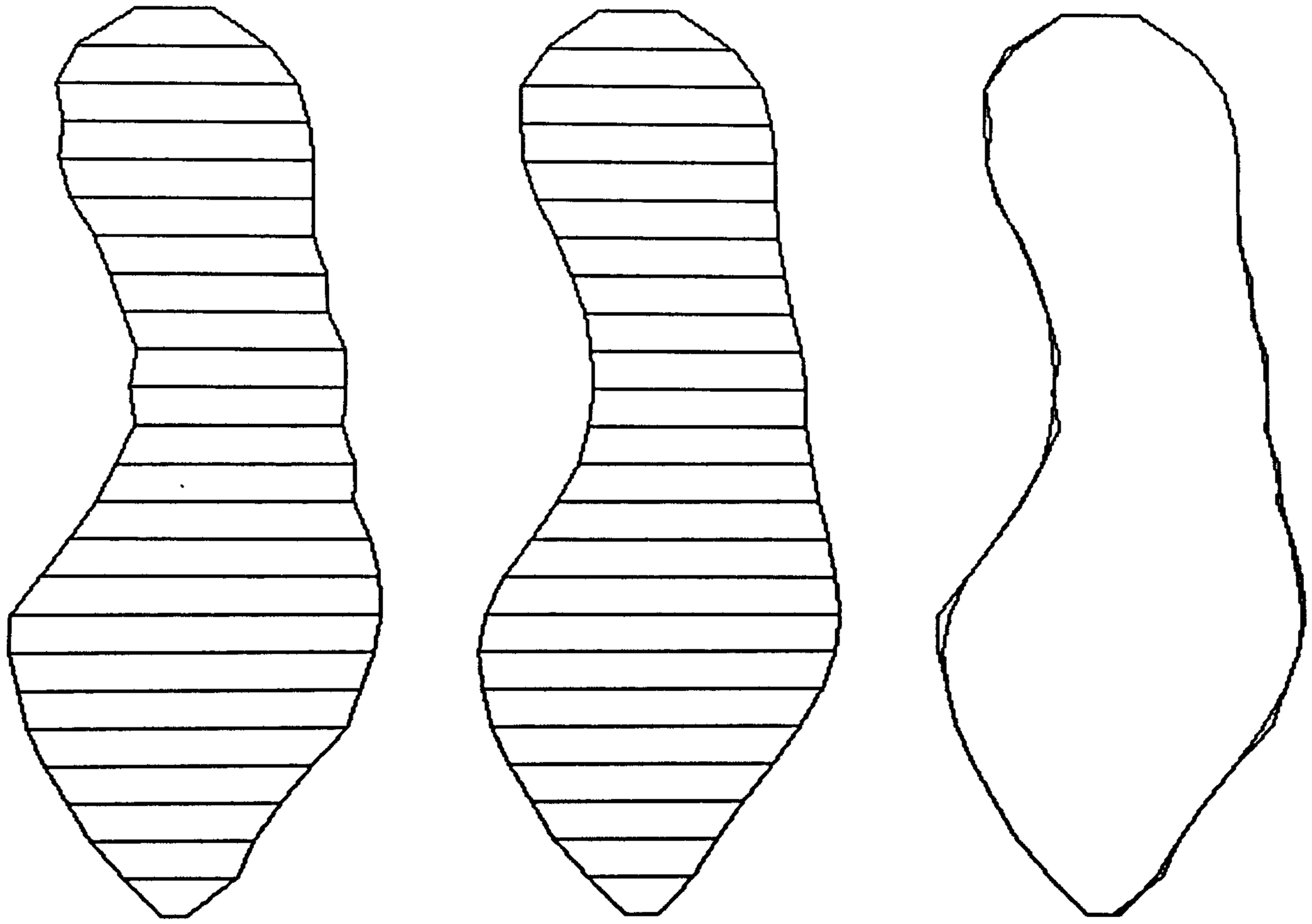

Before processing After processing Overlaid profiles

Figure N.3 Sample 1 with correction at 50% and Lock ON.

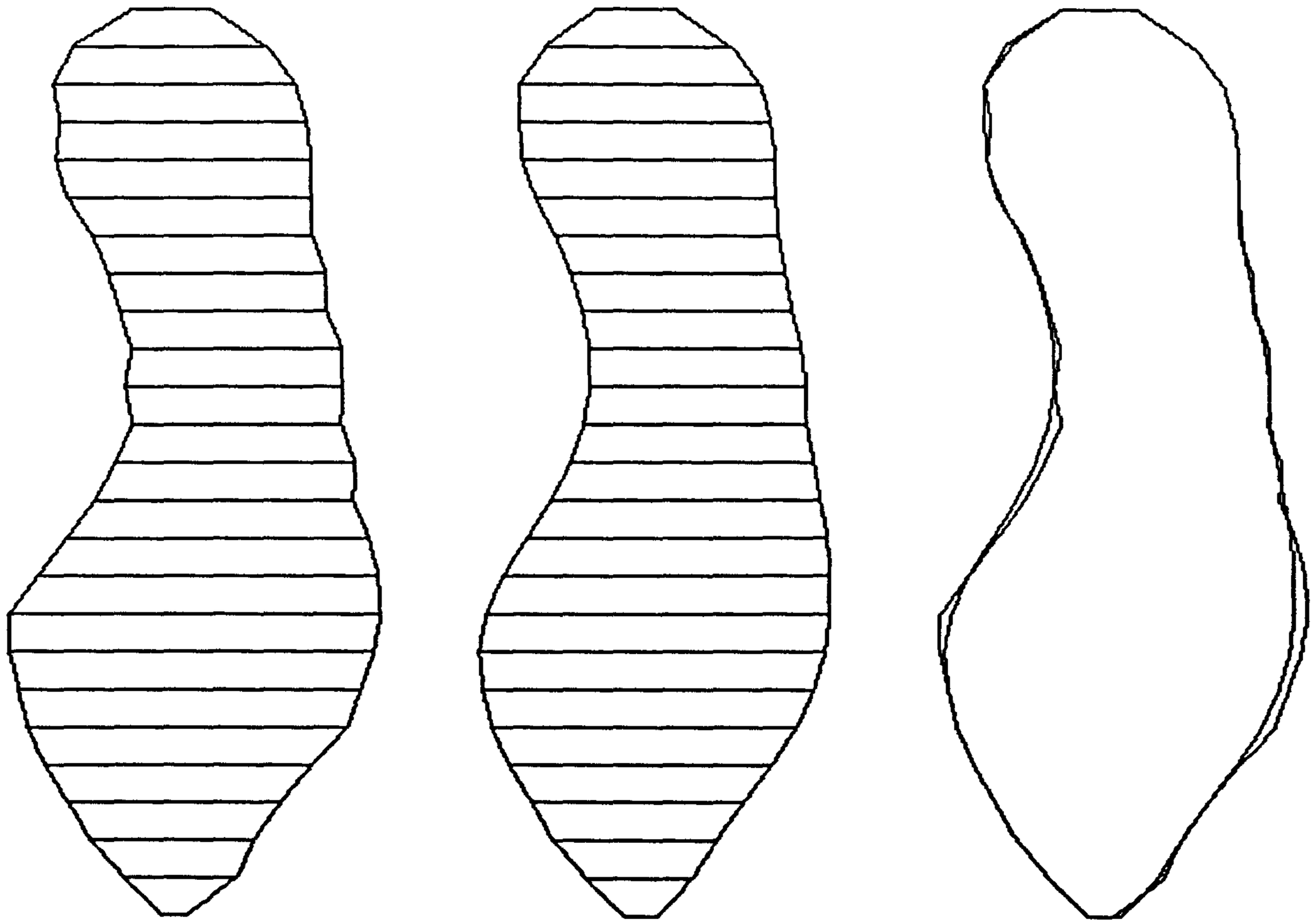

Before processing | After processing | Overlaid profiles

Figure N.4 Sample 1 with correction at 50% and Lock OFF.

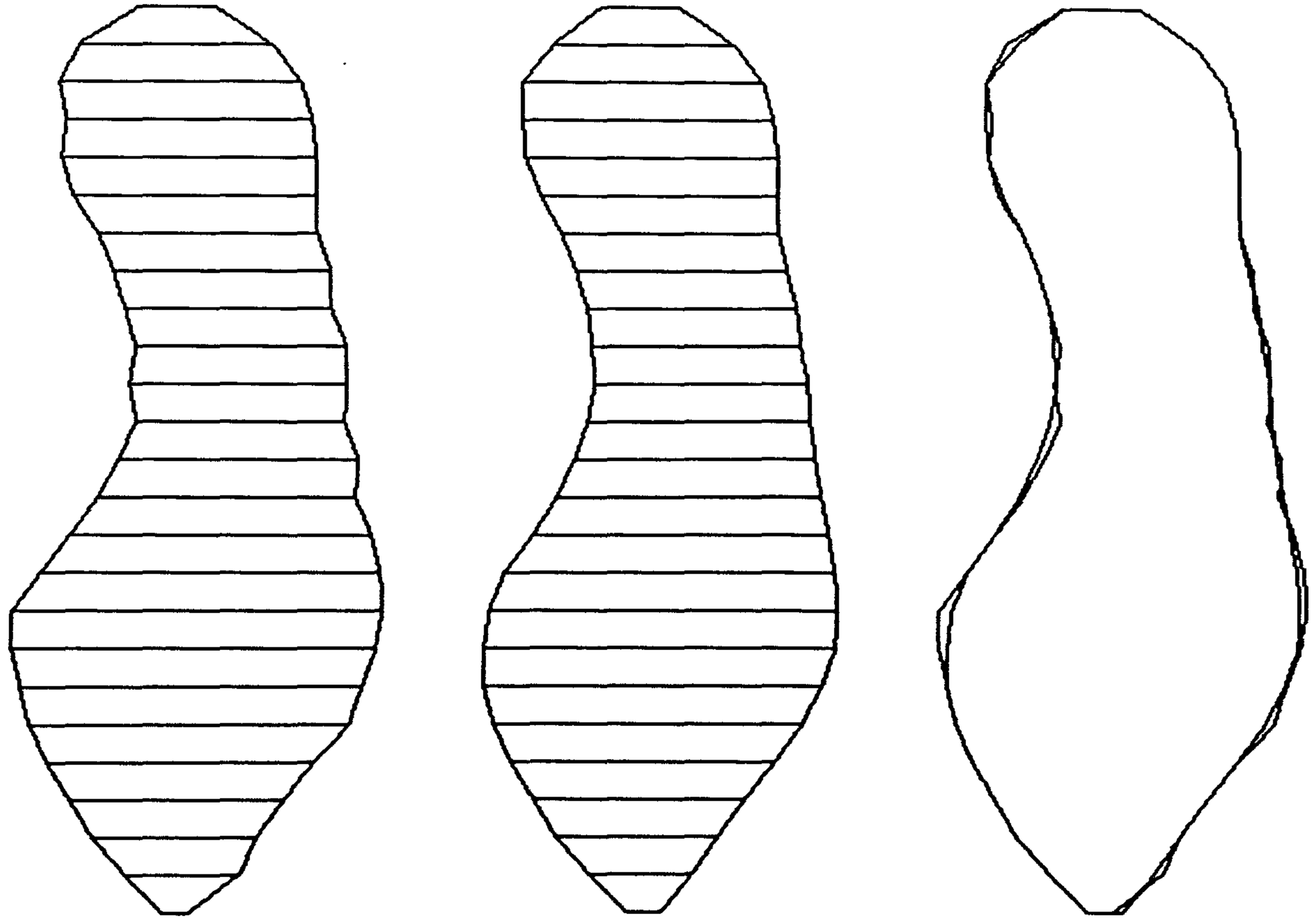

Before processing | After processing | Overlaid profiles

Figure N.5 Sample 1 with correction at 75% and Lock ON.

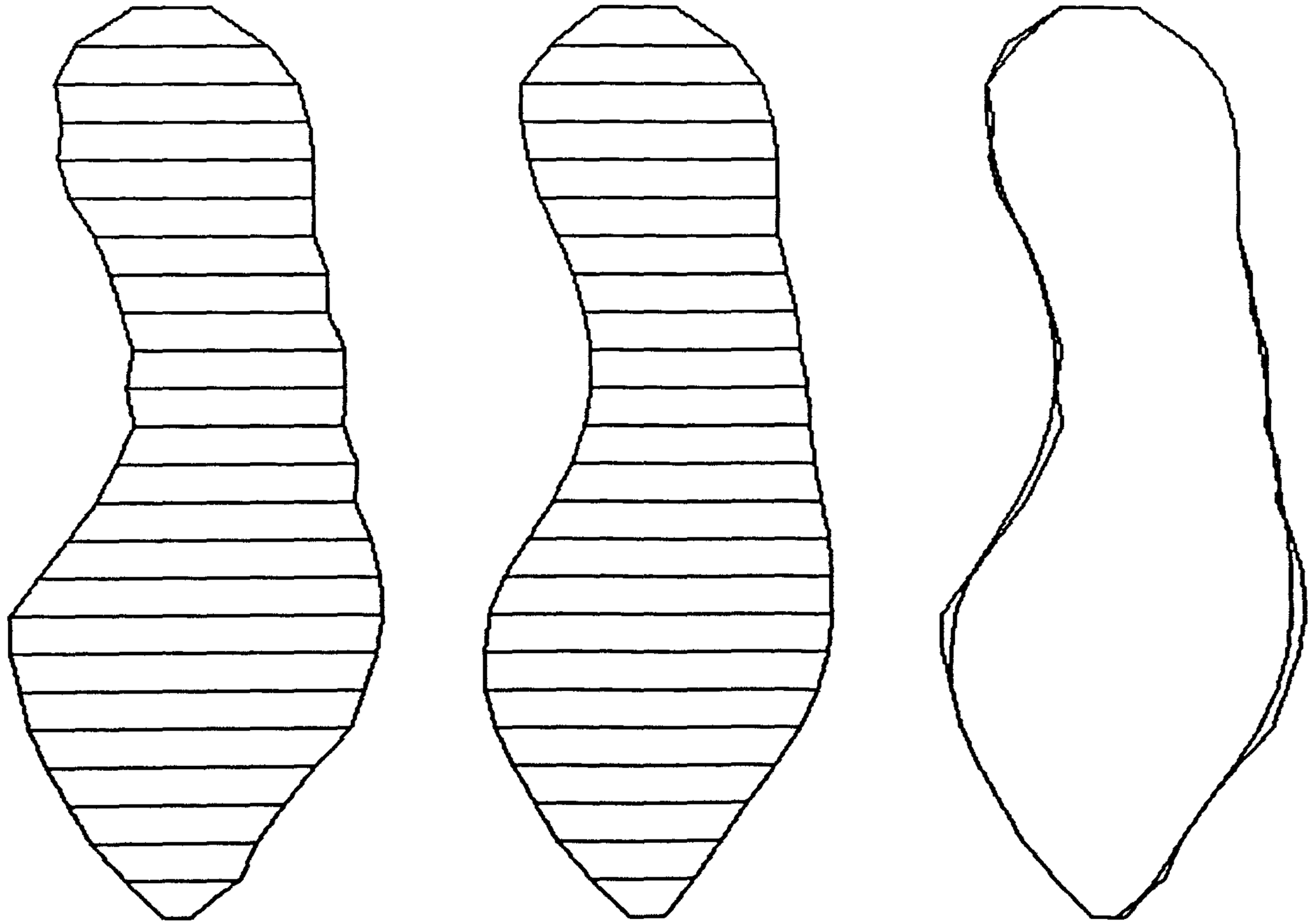

Before processing After processing Overlaid profiles

Figure N.6 Sample 1 with correction at 75% and Lock ON.

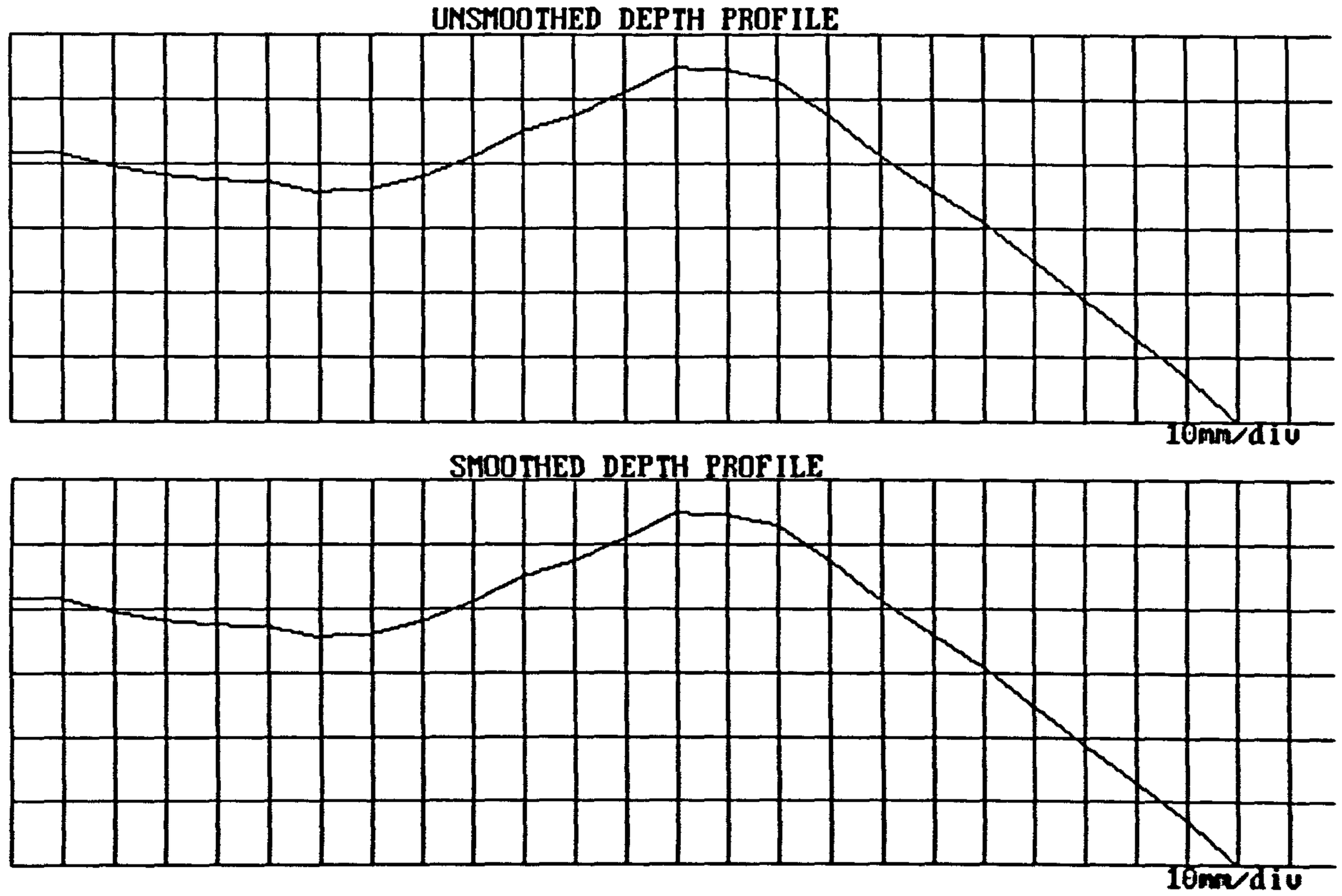

Figure N.7 Depth profile for Sample 1.

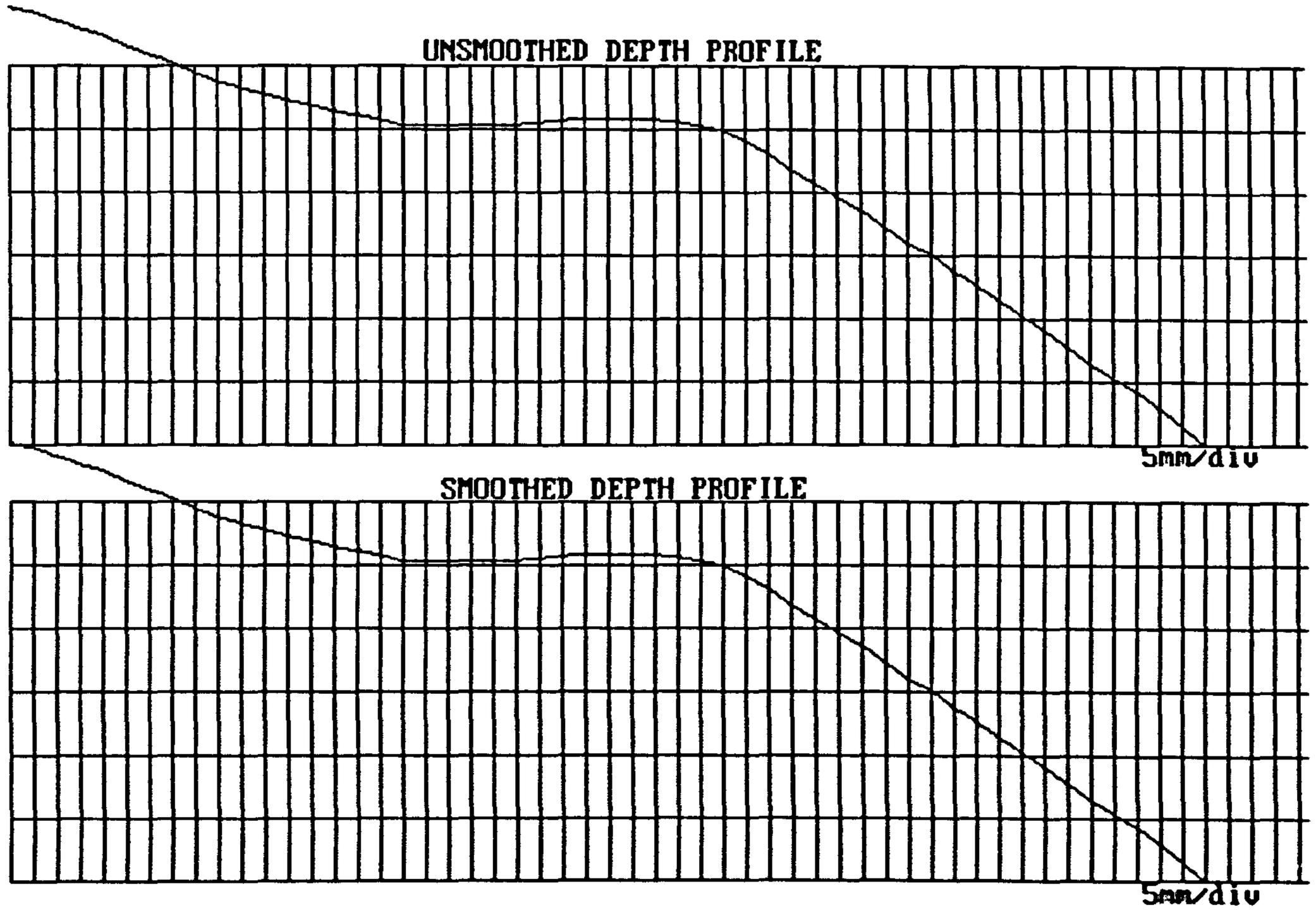

Figure N.8 Depth profile for Sample 3.

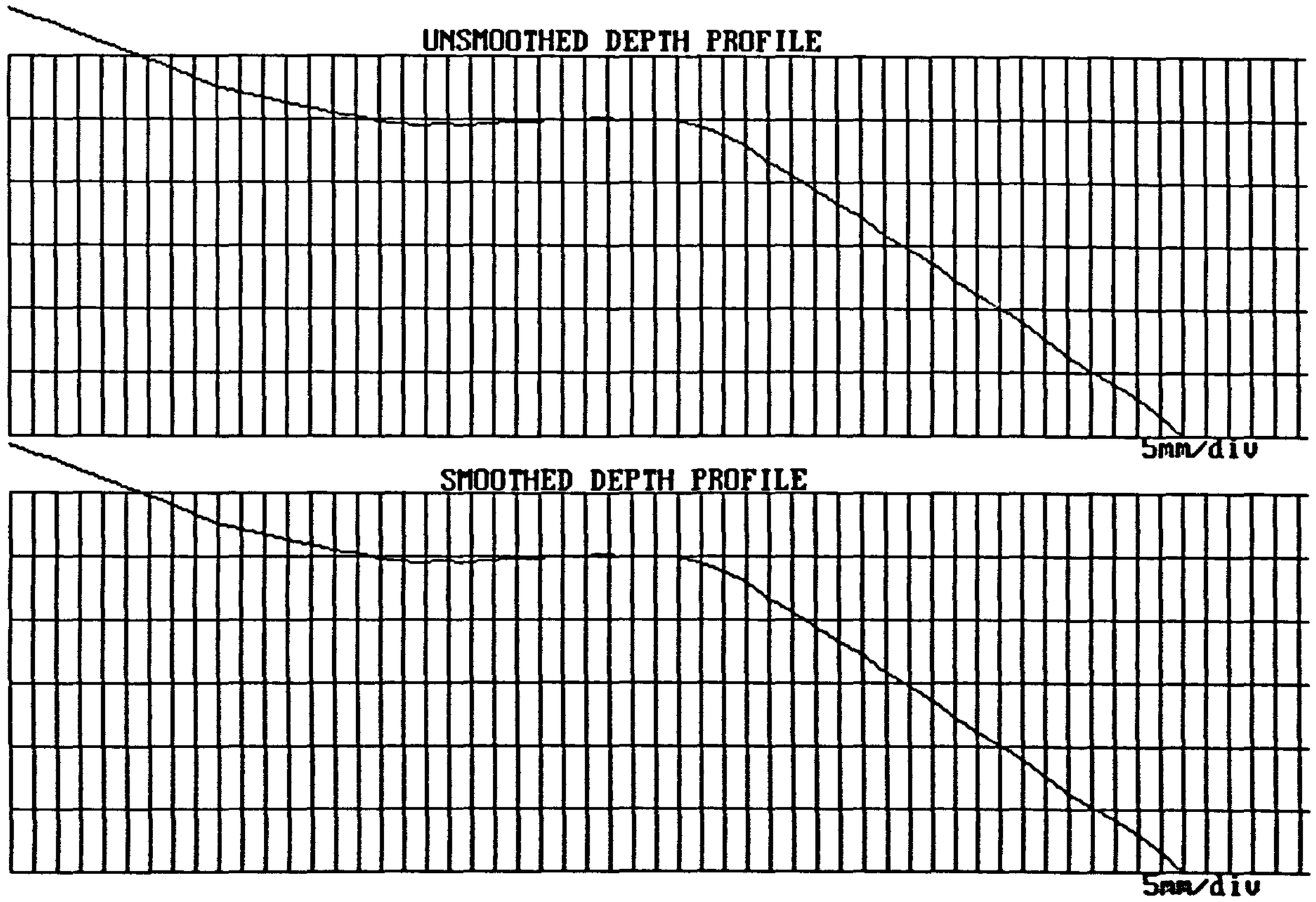

Figure N.9 Depth profile for Sample 5.

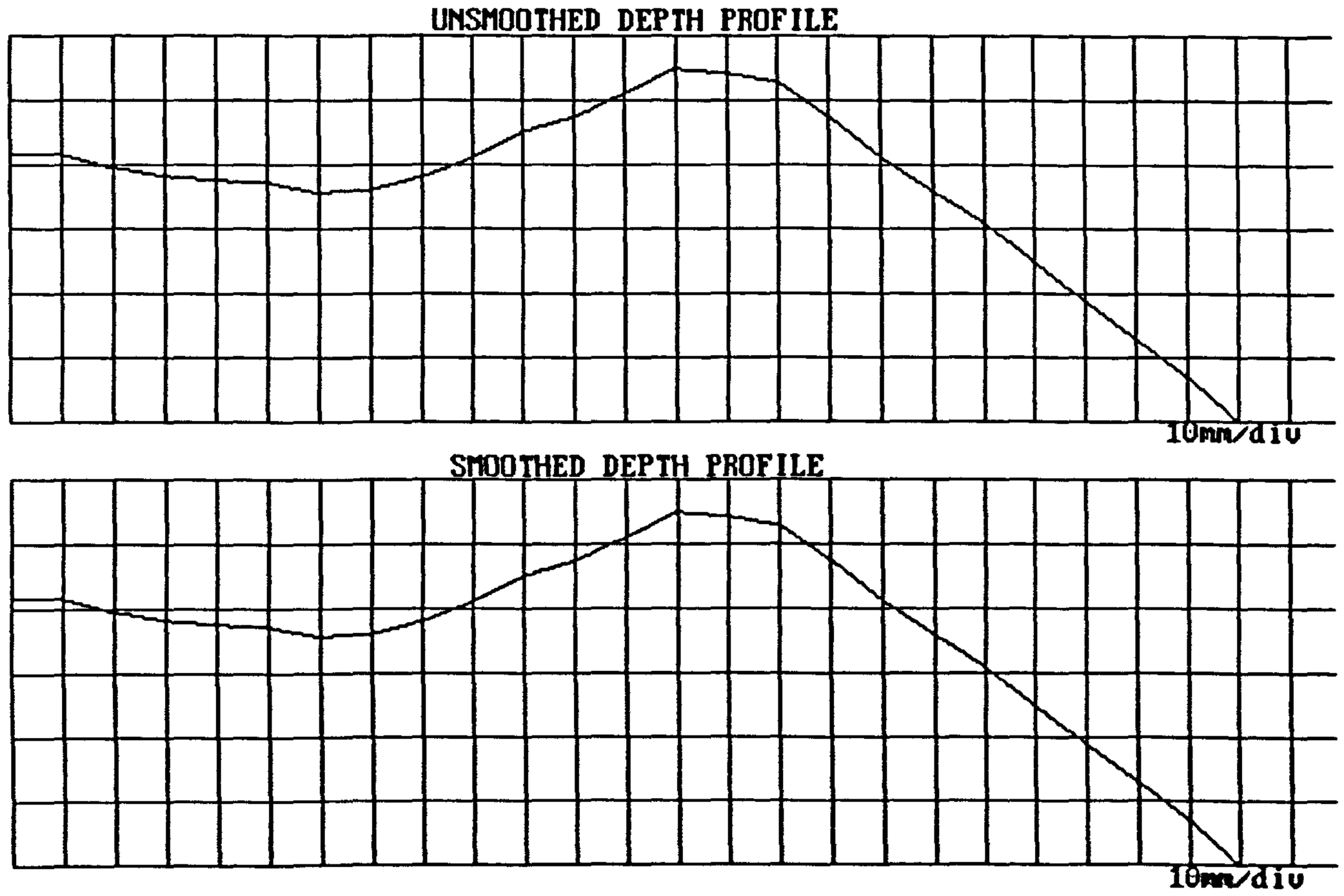

Figure N.10 Depth profile for Sample 8.

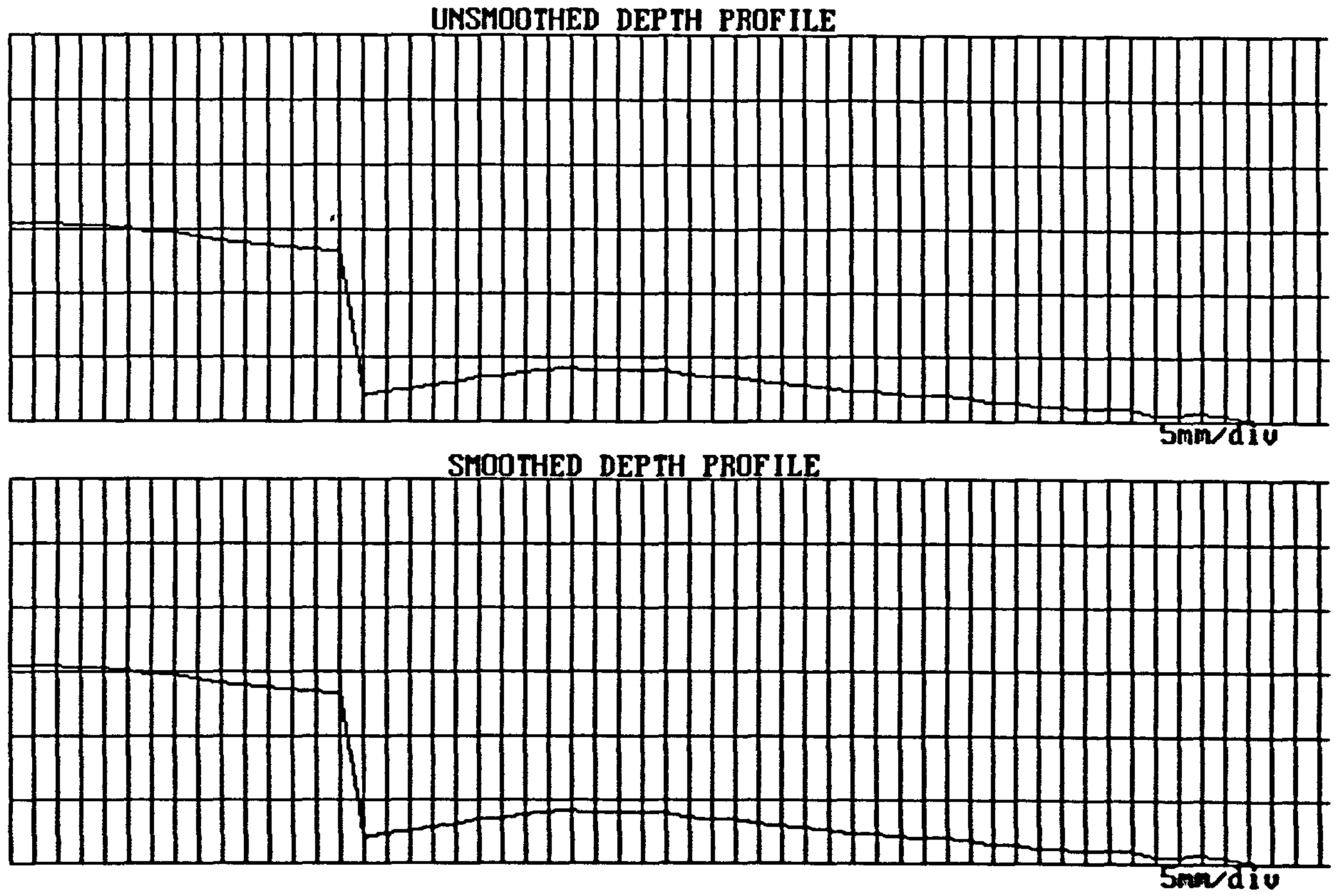

Figure N.11 Depth profile for sole Sample 1.

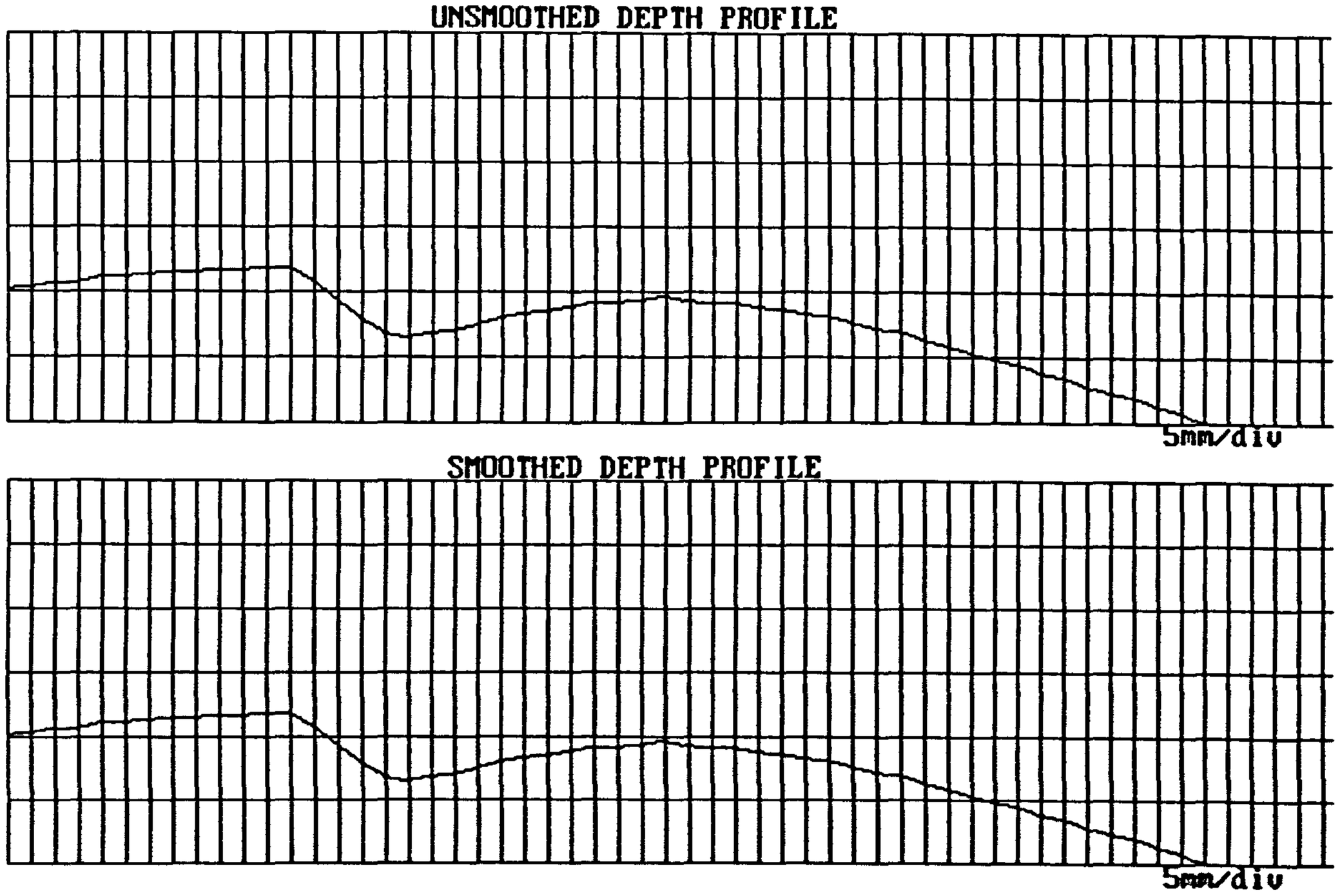

Figure N.12 Depth profile for Sample 6.

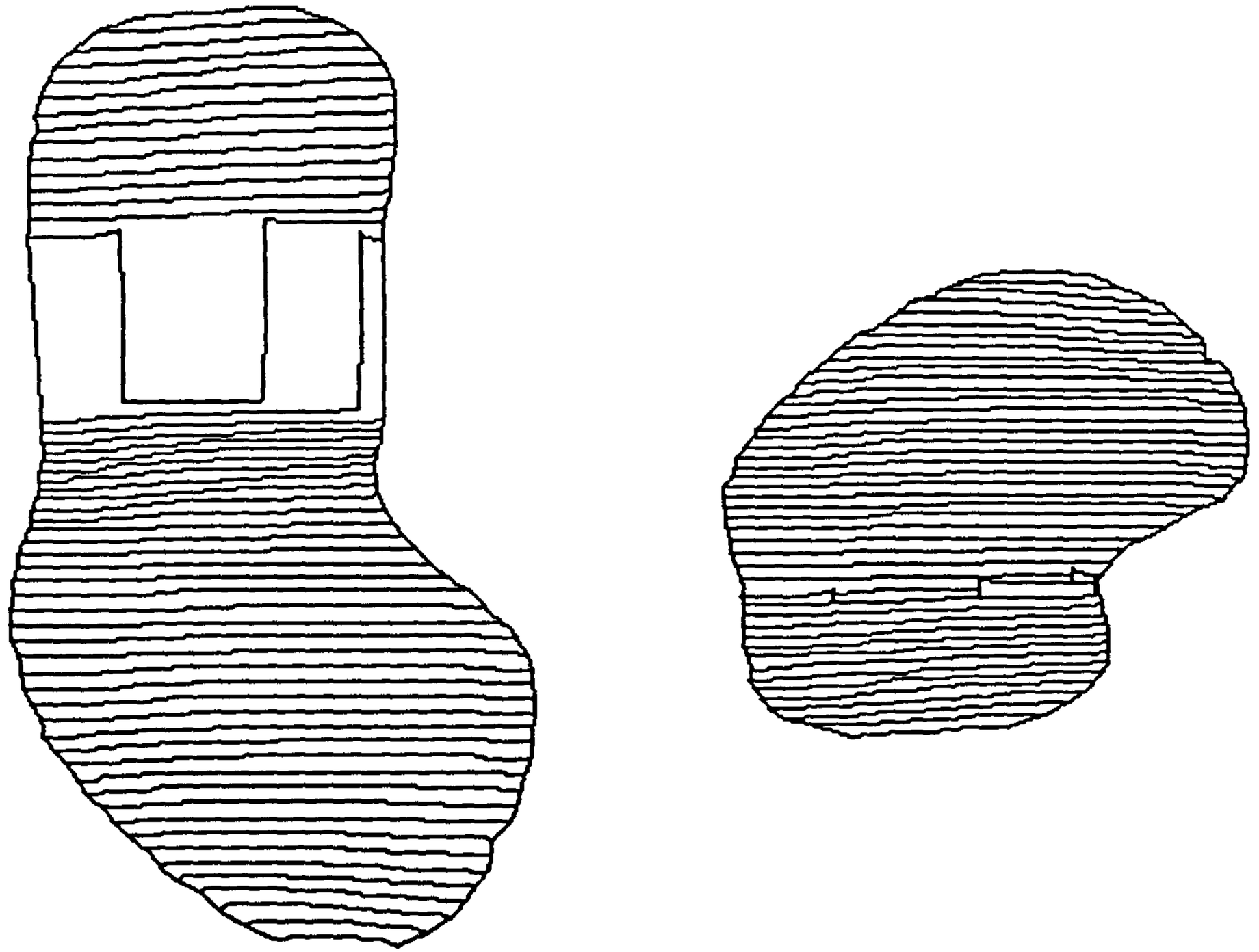

Figure N.13 Contour map for sole Sample 1.

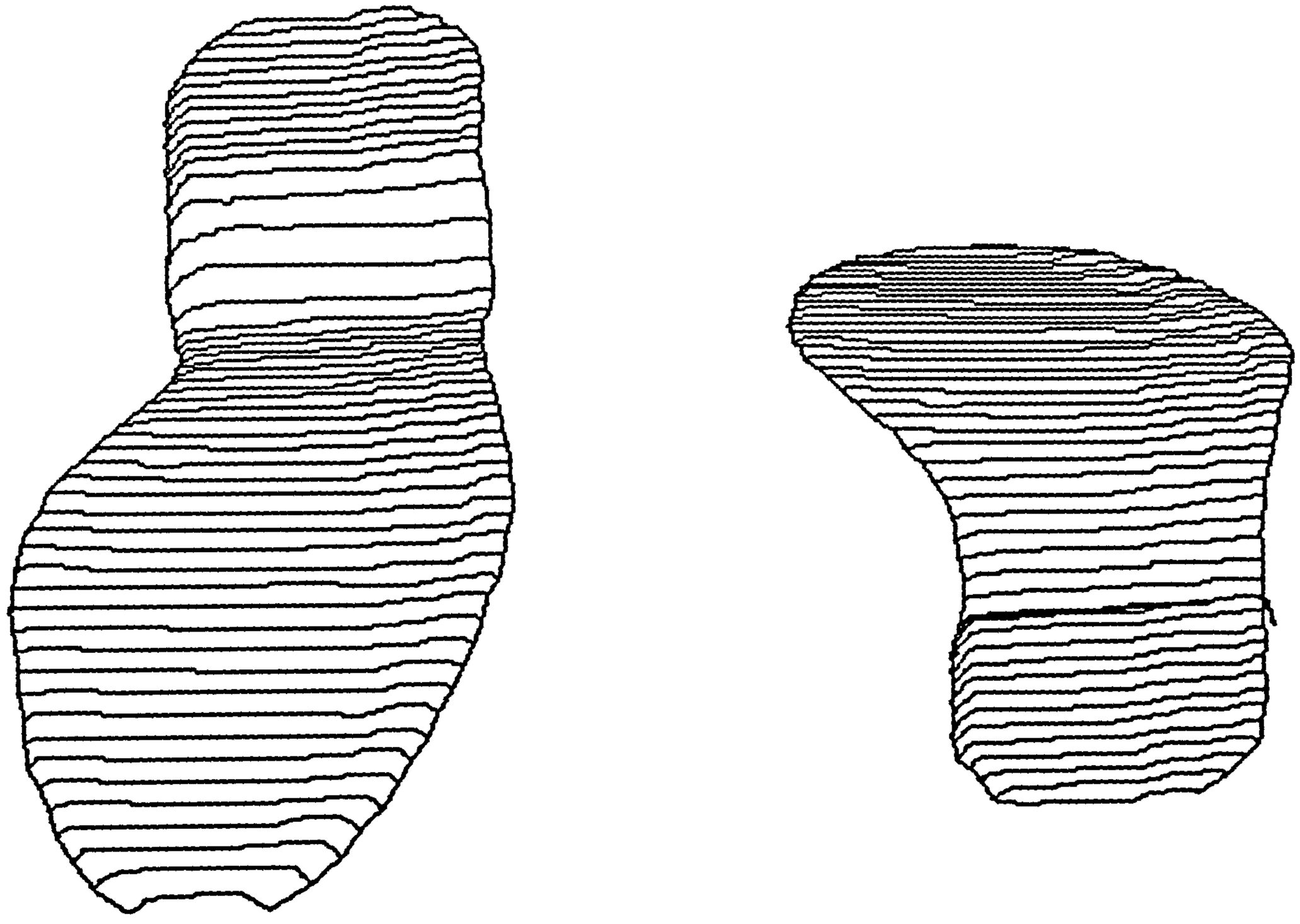

Figure N.14 Contour map for sole Sample 3.

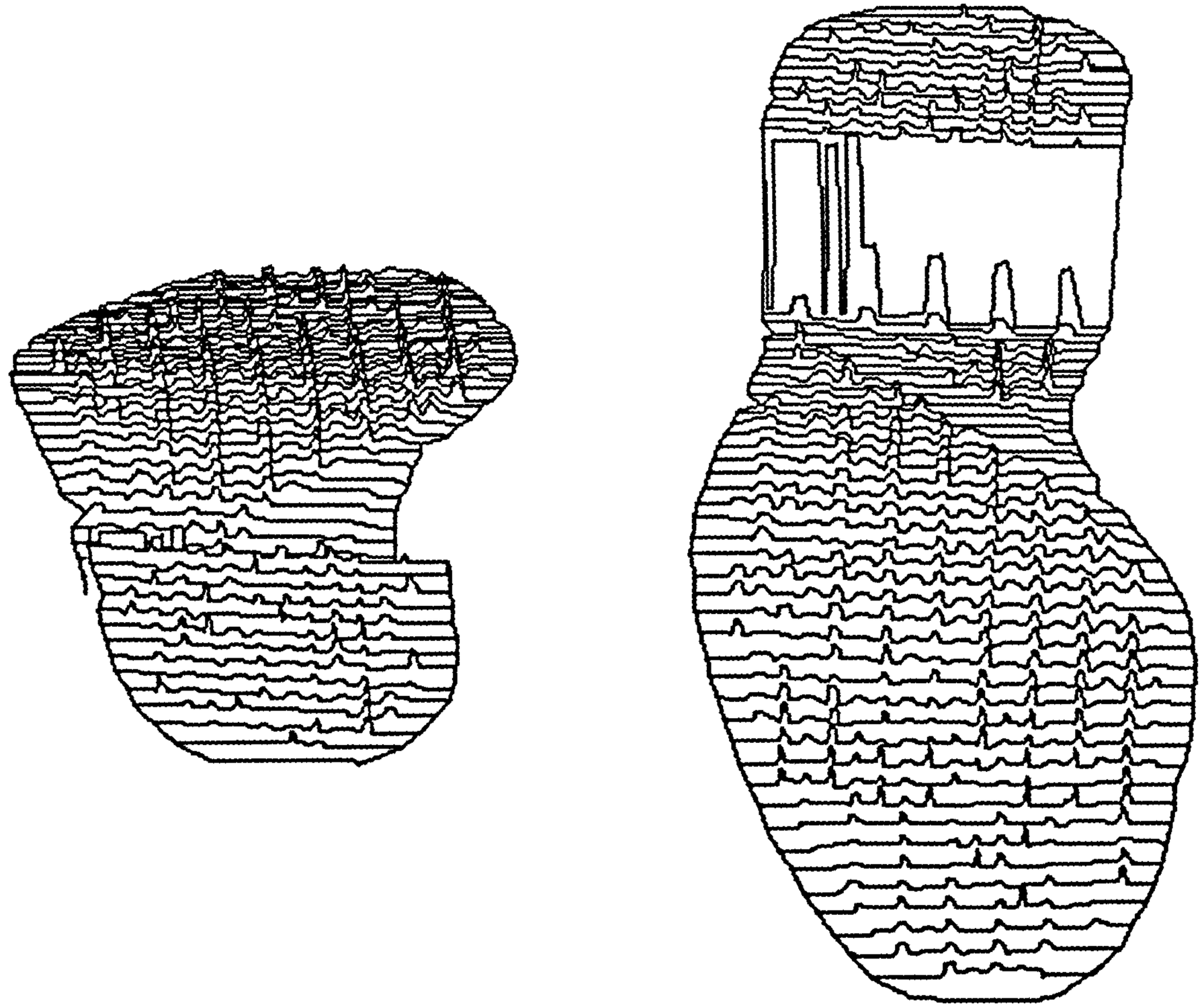

Figure N.15 Contour map for sole Sample 6.